No. 1 March 1, 1978 ISSN 0003-2670

NALYTICA CHIMICA ACTA

nternational journal devoted to all branches of analytical chemistry

ELSEVIER SCIENTIFIC PUBLISHING COMPANY

ANALYTICA CHIMICA ACTA

International journal devoted to all branches of analytical chemistry
Revue internationale consacrée à tous les domaines de la chimie analytique
Internationale Zeitschrift für alle Gebiete der analytischen Chemie

PUBLICATION SCHEDULE FOR 1978 (incorporating the section on Computer Techniques and Optimization).

	J	F	M	A	M	J	J	A	S	O	N	D
Analytica Chimica Acta	96/1	96/2	97/1	97/2	98/1	98/2	99/1	99/2	100	101/1	101/2	102
Section on Computer Techniques and Optimization			103/1			103/2			103/3			103/4

Scope. *Analytica Chimica Acta* publishes original papers, short communications, and reviews dealing with every aspect of modern chemical analysis, both fundamental and applied. The section on *Computer Techniques and Optimization* is devoted to new developments in chemical analysis by the application of computer techniques and by interdisciplinary approaches, including statistics, systems theory and operation research.

Submission of Papers. Manuscripts (three copies) should be submitted to:
for *Analytica Chimica Acta:* Dr. A. M. G. Macdonald, Department of Chemistry, The University, P.O. Box 363; Birmingham B15 2TT, England;
for the section on *Computer Techniques and Optimization:* Dr. J. T. Clerc, Laboratorium für Organische Chemie, Swiss Federal Institute of Technology, Universitätstrasse 16, CH-8092 Zürich, Switzerland.

Information for Authors. Papers in English, French and German are published. There are no page charges. Manuscripts should conform in layout and style to the papers published in this Volume. Authors should consult Vol. 93, p. 379 for details information. Reprints of this information are available from the Editors or from: Elsevier Editorial Services Ltd., Mayfield House, 256 Banbury Road, Oxford OX2 7DE (Great Britain).

Reprints. Fifty reprints will be supplied free of charge. Additional reprints (minimum 100) can be ordered. An order form containing price quotations will be sent to the authors together with the proofs of their article.

Advertisements. Advertisement rates are available from the publisher.

Subscriptions. Subscriptions should be sent to: Elsevier Scientific Publishing Company, P.O. Box 211, Amsterdam, The Netherlands. The section on *Computer Techniques and Optimization* can be subscribed to separately.

Publication. *Analytica Chimica Acta* (including the section on *Computer Techniques and Optimization*) appears in 8 volumes in 1978. The subscription for 1978 (Vols. 96–103) is Dfl. 1000.00 plus Dfl. 120.00 (postage) (Total approx. US $457.14). The subscription for the *Computer Techniques and Optimization* sections only (Vol. 103) is Dfl. 125 plus Dfl. 15.00 (postage) (Total approx. US $57.14). Journals are sent automatically by air mail to the U.S.A. and Canada at no extra cost and to Japan, Australia and New Zealand for a small additional postal charge. All earlier volumes (Vols. 1–87) are available at Dfl. 115.00 (plus postage).

Claims for issues not received should be made within three months of publication of the issue, otherwise they cannot be honoured free of charge.

ANALYTICA CHIMICA ACTA
VOL. 97 (1978)

ANALYTICA CHIMICA ACTA

International journal devoted to all branches of analytical chemistry

ELSEVIER SCIENTIFIC PUBLISHING COMPANY

Anal. Chim. Acta, Vol. 97 (1978)

Printed in The Netherlands

Analytica Chimica Acta, 97 (1978) 1—11

DUAL APPROACH TO THE EMISSION SPECTROGRAPHIC DETERMINATION OF ELEMENTS IN AIRBORNE PARTICULATE MATTER

AKIYOSHI SUGIMAE** and R. K. SKOGERBOE*

Department of Chemistry, Colorado State University, Fort Collins, Colorado 80523 (U.S.A.)

(Received 9th September 1977)

SUMMARY

A method is described in which atmospheric particulates are collected on high-purity graphite filter disks and analyzed initially by a point-to-plane spark excitation method and ultimately by d.c. arc excitation. The development of the methods is described and their capabilities are evaluated. The results indicate that 15—25 elements can be determined with accuracies within the ±10—15% precision limits. The methods involve direct analyses requiring minimal sample handling procedures to avoid contamination and loss problems.

Recent publications have emphasized the value of optical emission spectrometry (o.e.s.) for multielement analyses of atmospheric particulates [1—4]. The ability to determine several elements simultaneously is clearly advantageous from several viewpoints. The instrumentation costs required for such emission spectrometric analyses are approximately the same as those for modern x-ray fluorescence equipment [5, 6] but are much less than required for neutron activation analyses [7—9] or proton induced x-ray emission analysis [10]. Such factors coupled with reductions in time requirements emphasize the economic advantages of o.e.s. However, the sampling and analytical methods used should also satisfy other criteria [4]. The sample collection media (filters) should exhibit negligible or uniform impurity blanks; the method of sampling and analysis should require minimal handling and pretreatment operations to prevent analyte contamination or loss problems; and the procedures should provide accurate determinations of as many elements of interest as possible. Methods which satisfy these criteria approach the ideal.

An o.e.s. method based on the use of graphite cup filters to minimize blank and sample handling problems has been previously described [4]. While this method has proven extremely useful, a primary limitation was associated with the fact that the sampling rates were restricted to about

---

**Present address: Environmental Pollution Control Center, Osaka Prefecture, 1-chome, Nakamichi, Higashinari-ku, Osaka 537, Japan.

1 l min^{-1} so that sample volumes were relatively small unless inordinately long collection periods were used. Moreover, the method was such that only a single measurement could be made per sample. Precision estimates were thus based on collection of replicate samples at each site. The present report describes sampling and o.e.s. methods developed to eliminate these general problems. High-purity graphite filter disks having very minimal blanks and amenable to use at higher flow rates have been used for sample collection. These disks are analyzed first by a direct o.e.s. method involving a point-to-plane spark excitation technique and, subsequently, by a d.c. arc excitation technique which requires that the filter disk be reduced to a powder. This dual approach allows the simultaneous determination of 15—25 elements at levels representative of atmospheric concentrations. It also provides replicate analyses by each technique and redundant determinations on several elements. The latter are useful for quality assurance purposes since the two techniques are sufficiently different that they can be regarded as independent analyses.

EXPERIMENTAL

Apparatus and reagents

The spectrographic instrumentation and operating conditions are described in Table 1. Photographic plates were read on a densitometer, calibrated by the two-step method, and intensities were determined via standard procedures.

All reagents used were of AR grade or better.

Procedure

Each collection filter was treated with a 1:1 mixture of collodion and methanol, added dropwise, and air-dried to fix the aerosol collected to the surface. Replicate point-to-plane spark excitation analyses were run on each filter under the conditions given in Table 1. The surfaces (0.25 mm) of the filters were subsequently machined off with a tungsten carbide tool. The powder was collected; 100 mg was weighed; internal standard solution containing In and Pd was added; the solution was evaporated in an oven; and the dry sample was mixed 1:4 by weight with CaF_2 in a Wiggle-Bug. Three 30-mg samples from each collection were packed into the sample electrodes and analyzed by d.c. arc excitation as stipulated in Table 1. Powder standards were prepared as described below. Weighed amounts of these (usually 5 mg) were dispersed in 10 ml of a glycerol—ethanol mixture (1:1) and each suspension was transferred to a filtering funnel by washing with ethanol. The solution was drawn through a graphite filter under suction such that the standards were uniformly deposited. Each standard filter prepared in this manner was placed in a muffle furnace at 400°C for 30 min to burn off the excess of glycerol. Standard filters were treated and analyzed as above for calibration purposes. The analytical and internal standard wavelengths used are summarized in Table 2.

TABLE 1

Spectrographic instrumentation and operating conditions

Optical system	
Spectrograph	Baird-Atomic, 3-m (model 169)
Grating	21,000 lines/in. blazed for 270 nm first order
Wavelength range	220—420 nm
Slit width	25 μm
External optics	Single lens set to pass 2 mm of discharge
Step filter	Step factor of 2; 2 darkest steps used
Detector	Kodak EK-33 plates developed according to manufacturer's instructions
Excitation systems	
Source unit	Jarrell-Ash custom varisource (model 40-750)
D.c. discharge	28 A (shorted electrodes)
sample electrode	Ultra Carbon No. 202 (anode)
counter electrode	A.S.T.M., C-5
analytical gap	3 mm
electrode sheath	Device described by Margoshes and Scribner [11] with argon flow at 15 l min^{-1}
exposure time	30 s, no preburn
Spark discharge	
capacitance	0.0075 μF
inductance	310 microhenrys
resistance	Residual
breakdowns/half-cycle	6
counter electrode	Argon-sheathed Ag wire (Fig. 1)
electrode sheath	See Fig. 1, argon flow at 10 l min^{-1}
analytical gap	4 mm
exposure time	30 s, no preburn, triple exposure

Atmospheric samples were collected on 47-mm diameter graphite disk filters (Poco Graphite, No. 47-F). These were placed in filter holders (Gelman, No. 2220) connected to pumps (Gelman, No. 23000) and air was drawn through at constant rates for the required time periods.

RESULTS AND DISCUSSION

Previous experience with the use of graphite media for atmospheric particulate collection demonstrated the essentiality of using low blank filters for collections in clean atmospheres or for the short sampling periods required if the measurements were to reflect short-term meteorological changes [4]. Other research interests, however, are such that higher sample collection rates become desirable. Thus, when graphite disk filters (47-mm diameter) became available, efforts were devoted to the development of analytical o.e.s. methods amenable to collections on the disks. The initial emphasis was to develop direct high-voltage spark excitation methods which did not require utilization of the entire sample, so that other measurements,

TABLE 2

Analytical wavelengths and working concentration ranges for the spark and arc methods

Element	Spark method[a]		Arc method	
	Analytical wavelength, nm	Concentration range, $\mu g\ m^{-3}$ [b]	Analytical wavelength, nm	Concentration range, $\mu g\ m^{-3}$ [b]
Ag	—	—	328.1[c]	0.0008— 0.08
Al	309.3	0.25—35	308.2[d]	0.4 —40
Be	—	—	313.0[c]	0.0002— 0.02
Ca	317.9	0.25—35	—	—
Cd	—	—	326.1[c]	0.04— 5
Cr	284.3	0.08— 1	284.3[c]	0.02— 3
Fe	261.2	0.25—35	303.7[d]	0.4 — 40
Mg	285.2	0.25—35	278.0[d]	0.4 — 40
Mn	257.6	0.03— 1	260.6[d]	0.02— 2
Na	—	—	330.3[c]	0.4 — 40
Ni	341.5	0.08— 1	341.5[c]	0.02— 2
Pb	283.3	0.25—35	283.3[c]	0.4 — 40
Si	—	—	298.8[d]	2 —160
Sn	317.5	0.08— 1	317.5[c]	0.02— 2
Ti	334.9	0.25—10	337.2[d]	0.2 — 25
V	318.4	0.08— 1	318.4[c]	0.02— 2
Zn	334.5	0.8 —10	328.2[d]	0.2 — 25

[a]All analytical wavelengths were referenced to silver at the 272.2-nm wavelengths as an internal standard. [b]For 10-m^3 sample. [c]Indium emission at 303.9 nm was used as the internal standard reference for these wavelengths. [d]Palladium emission at 324.3 nm was used as the internal standard reference for these wavelengths.

if required, could be based on the unused portions. As the spark excitation method evolved, it became apparent that complementary analyses on the same filter samples by arc excitation would expand the analytical capabilities and provide analyses of several elements, already determined by the spark method, for cross-check purposes. For convenience, the two excitation methods are discussed separately below.

Spark excitation

Excitation conditions. The initial choice of spark excitation was based on the potential advantages associated with direct analyses of filter disks by point-to-plane methods with minimal sample preparation. To determine the best excitation conditions, several atmospheric sample collections were made and used for the initial studies described below.

The filters were mounted on a platform machined from aluminum with a post attached for direct mounting in the electrode clamps in the spark stand. The disks were held tightly in place on the platform with 3 small tantalum strips attached to the platform by screws and arranged to overlap the disks by approximately 2—3 mm at the point of contact. Relatively

large amounts of the particulates were blown off the surface during sparking. To prevent this, a mixture of collodion and methanol (1:1 v/v) was added dropwise to each filter and air-dried; sparking of filters in this manner did not result in sample loss.

Examination of spectra which were run in an air atmosphere indicated unfavorable line-to-background ratios as well as intense cyanogen bands. Consequently, the counter electrode sheath device illustrated in Fig. 1 was used to reduce the background emission problem as well as stabilize the dimensional wander of the spark over the sample surface. Measurements made with argon and argon—oxygen mixtures as sheath gases indicated that pure argon at a flow rate of 10 l min^{-1} produced the best signal-to-background ratios and discharge stability. It was also established that the use of a silver wire rather than graphite or tantalum for the counter electrode gave a significant increase in the line-to-background ratios. Placement of the wire inside the glass sheath system (Fig. 1) drastically reduces the wear rate, so that numerous analyses can be run without readjustment of the wire position. The silver emission observed proved useful for internal standard purposes (see Table 2). Optimization experiments also demonstrated that the spark control conditions given in Table 1 provided the best line-to-background ratios.

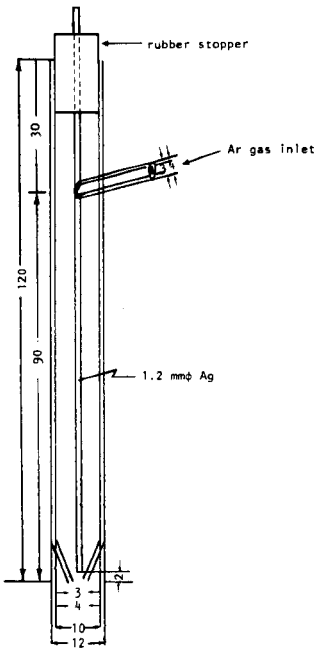

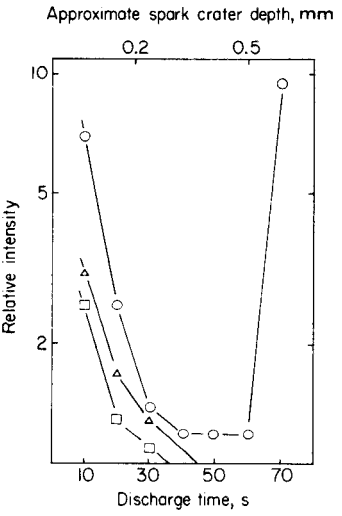

Fig. 1. Diagram of counter electrode sheath device for spark analysis. All dimensions in nm.

Fig. 2. Spark discharge time required for vaporization of atmospheric particulates. ○ Al; △ Si; □ Pb.

The conditions described above were used to determine the discharge times required for removal of all particulates collected by the filters. Moving plate measurements were used to determine the degree of penetration of particulates into the filters and thus the exposure times required. Typical results (Fig. 2) illustrate that the majority of the particles are retained at or near the filter surface even though the aerodynamic diameters of the particles containing the different elements may vary over an order of magnitude or more. In each instance, the emission intensity was reduced to an insignificant or a graphite blank level after 30—40 s. This coincides with spark crater depths visually estimated with a microscope of approximately 0.2—0.3 mm. The sudden rise in Al emission after 60 s corresponded with the spark breaking through the 0.5-mm thickness filter to the aluminum holder.

Calibration standards. Two general approaches to the preparation of particulate filter standards were examined: solution doping and deposition of powder standards on the filters. Moving plate studies on filters on which standard aqueous solutions were deposited and dried indicated that the analytical elements were distributed quite uniformly through the entire thickness of the filters. This approach was abandoned because the concentration versus depth profiles did not coincide with those for actual particulate samples (Fig. 2).

Powder standards containing the elements listed at the concentrations indicated in Table 3 were prepared by mixing the Specpure oxides, except for CaF_2 and $MnCO_3$, with graphite (National carbon, SP-2) as the diluent in a ball mill. The ranges given in Table 3 were selected to be generally representative of the compositional variability of atmospheric particulates. Standard filters were prepared by the procedures outlined in the experimental section. Since each disc has an active filtration area of 38—40 mm diameter and the spark craters have nominally 3—4 mm diameter, each standard or sample filter may be used for 18—30 replicate runs.

Moving plate studies on these powder standards verified that the vaporization vs. time curves closely paralleled those for actual samples (Fig. 2). Studies were also carried out to establish whether chemical form or particle size significantly affected the vaporization—excitation processes. The results

TABLE 3

Concentrations ($\mu g\ g^{-1}$) of individual elements in synthetically prepared powder standards

Standard No.	Elements and concentration		
	Al, Ca, Fe Mg, Pb	Ti, Zn	Cr, Mn, Ni Sn, V
1	500	500	50
2	1700	1700	170
3	5500	5500	550
4	1.8%	1.8%	1800
5	7.0%		

summarized in Fig. 3 illustrate that particle diameters of 20 μm or less are vaporized at rates comparable to those observed with actual samples (compare Figs. 2 and 3A). When the particles were considerably larger, the rate of vaporization decreased. The data summarized in Fig. 3B further illustrate that salts such as iron nitrate or chloride, which are partially soluble in the glycerol—methanol mixture used for powder deposition penetrate the filter to greater depths with a concomitant effect on the apparent vaporization rates. Insoluble compounds (e.g. Fe_2O_3 and FeS) do not penetrate and are vaporized at rates comparable to each other and actual atmospheric samples. Since atmospheric aerosols are generally much smaller than 20 μm and relatively insoluble, these observations support the general validity of this means of standard preparation.

The particle size effect observed suggested that the actual amount of material deposited might also prove limiting. To check this, varying weights of NBS fly ash (SRM 1633) were deposited on filters and analyzed for iron by the spark procedure; the calibration curves developed with the synthetic powder standards were used. The summarized results in Table 4 verify that

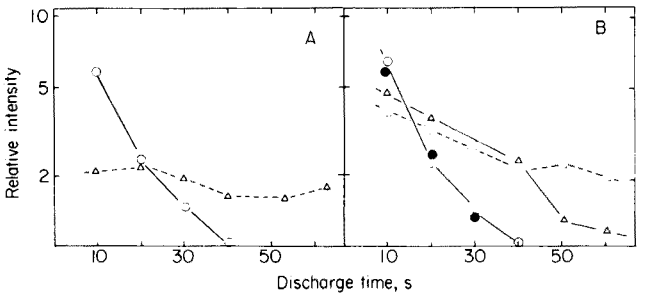

Fig. 3. Effects of particle size and composition on vaporization and excitation. A. Particle diameter of Fe_2O_3; ○ less than 20 μm; △ 60—90 μm. B. Chemical composition (all less than 20 μm): ○ Fe_2O_3; ● FeS; △ $Fe(NO_3)_2$; □ $FeCl_3$.

TABLE 4

Effects of the amount of sample deposited on analytical accuracy

Wt. of NBS fly ash deposited, mg	Amount iron, μg		Error (%)
	Present[a]	Determined	
0.30	2.5	2.2	−12.0
0.85	7.1	7.0	−14.1
2.5	21	25	+19.0
5.0	42	41	−2.4
10.0	84	64	−23.8
50.0	210	95	−54.8
100.0	420	130	−69.0

[a]Calculated from the NBS specified concentration.

the determination is accurate within experimental error (±10—20%) for sample deposits of less than approximately 10 mg but a negative systematic departure occurs for large sample sizes. Since few actual sample collections would result in the deposition of more than 10 mg of total particulate material, this limitation should not be considered serious.

Analytical range and precision. The conditions outlined in Table 1 were used with powder deposition standards for calibration and definition of the analytical ranges. The analytical curves were linear over at least two orders of magnitude but attempts were not made to determine the upper limits of linearity since they were generally beyond the levels expected in typical atmospheres. The ranges given in Table 2 were based on collection of a 10-m^3 sample; this collection volume is generally representative of a 24-h sampling period at flow rates of 6—8 l min^{-1} which can be drawn through the graphite filters. These data indicate the elements which can be determined by the spark method at levels generally expected in urban and some rural atmospheres.

Extensive evaluations of the analytical precision over wide concentration ranges on both standard and actual samples were also carried out. Relative standard deviations observed for 3—6 replicate measurements typically ranged from 2 to 18% with most values falling in the 6—12% range. Although the non-uniform distribution of powders or aerosol across the filter surfaces may account for some loss in precision, these data indicate that this is not a serious problem. Further data on precision and analytical accuracy are presented below.

Arc excitation

As indicated above, appreciable portions of the filter samples were available for further analyses after completion of the spark analyses. Consequently, an arc-excitation method was developed to extend the analytical capabilities and provide cross-check information on some elements.

Excitation conditions. Previous reports [4, 12] have shown that the use of a high-current d.c. arc in an argon atmosphere provides a particularly sensitive means for vaporization and excitation of impurities in numerous materials. Thus, the excitation conditions summarized in Table 1 are those which have been used extensively in this laboratory for several years.

Sample preparation. The spark penetration studies (Fig. 2) indicated collection of most of the aerosol at or near the filter surfaces. To confirm this, collection filters were placed in a nylon holder which permitted the filter faces to be machined off in a lathe with a tungsten carbide tool while the powder was caught in a plastic bag. By removing the collection surface in increments of 0.04 mm and analyzing these, it was confirmed that all elements collected were restricted to penetration depths of less than 0.25 mm. To avoid dilution of the aerosol with the portion of the graphite filters having no aerosol present, filters were machined to the 0.25-mm depth over the effective collection diameter (ca. 38 mm). Filters previously analyzed

by the spark method have spark craters of comparable or greater depths. Thus, only the filter surface unsampled by the spark analysis is eventually included in the powder sample obtained and this practice reduces the dilution of the powder sample concentration by a factor of 3 or more. The subsequent steps in sample preparation have been given above.

Standardization. Standards prepared by the powder deposition method described above were treated as samples for calibration purposes. The analytical ranges determined are listed with the spark results in Table 2 for convenience in making comparisons. The method clearly extends the analytical sensitivity for several elements. The precision of replicate analyses by the arc method also lies in the range 5—20% with most values occurring in the 8—15% range.

Comparisons of analytical results

To illustrate the general capabilities of the methods and obtain cross-check analytical information, three different airborne particulate samples were collected and analyzed by the present methods. In addition, 100 mg of the graphite—aerosol powder obtained from each sample was digested in hot nitric acid, evaporated to near dryness, taken up in (1 + 1) HCl, and analyzed with a d.c. plasma—Echelle spectrometer system. The results obtained by these three independent methods are summarized in Table 5. These demonstrate the analytical capabilities and indicate that the results are generally consistent within the precision limits of the methods.

To characterize the accuracy of the results, 5 mg of NBS fly ash (SRM 1633) was deposited on a filter and submitted to the analytical procedure. The results are compared with reported values in Table 6. Again, the agree-

TABLE 5

Comparisons of analyses by three independent methods

Element	Concentrations determined, $\mu g\ m^{-3}$								
	Sample 1			Sample 2			Sample 3		
	Spark	Arc	Plasma	Spark	Arc	Plasma	Spark	Arc	Plasma
Al	2.5	1.6	2.2	3.1	3.0	2.8	3.2	2.9	2.5
Be	—	0.00011	—	—	0.00014	—	—	0.00014	—
Ca	1.0	—	0.9	2.1	—	1.9	0.9	—	0.9
Fe	0.76	0.70	0.88	2.3	1.9	2.3	0.79	0.75	0.88
Mn	0.017	0.015	—	0.036	0.032	—	0.013	0.019	—
Mg	0.71	0.60	0.68	1.3	1.1	1.7	0.66	0.73	0.83
Na	—	0.75	0.70	—	1.4	1.2	—	1.3	1.2
Ni	—	0.012	—	—	<0.006	—	—	0.014	—
Pb	0.83	1.1	—	0.81	0.65	—	0.46	0.61	—
Si	—	2.9	—	—	5.2	—	—	4.0	—
Ti	0.09	0.10	—	0.49	0.49	—	0.12	0.14	—
V	—	0.04	—	—	0.03	—	—	0.01	—
Zn	—	0.26	—	—	0.13	—	—	0.33	—

TABLE 6

Comparison of results on SRM 1633 (Fly Ash)

Element	Concentration[a]		
	NBS values	Ref. [13] values	This work
Al	—	12.7 ± 0.5%	14%
Be	12[b]	—	11
Cr	131 ± 2	127 ± 6	120
Fe	—	6.2 ± 0.3%	5.8%
Mn	493 ± 7	496 ± 19	500
Mg	—	1.8 ± 0.4%	1.4%
Na	—	3200 ± 400	2900
Ni	98 ± 3	98 ± 9	120
Si	—	21 ± 2%	16%
Ti	—	7400 ± 300	6100
V	214 ± 8	235 ± 13	210
Zn	210 ± 20	216 ± 25	210

[a]Given in $\mu g\ g^{-1}$ unless designated as wt. %. [b]Information value only.

ment between results is within the precision limits; the methods are clearly capable of producing accurate analyses.

Few atmospheric collection media offer the general capabilities of the graphite filters used herein. The blank levels are generally negligible; the highest impurity levels are for those elements (e.g. Fe and Si) consistently found to be at high concentrations in the atmosphere. The retention of the aerosol collected at the filter surfaces makes them nearly ideal for x-ray fluorescence as well as spark excitation analyses. The methods described herein are advantageous from several viewpoints and add to the battery of techniques useful for atmospheric monitoring. The use of complementary but essentially independent methods in a mode of operation which conserves sample, such as that described, provides quality assurance that can prove extremely valuable.

This research was supported in part by National Science Foundation grant No. MPS 73-05082A01.

REFERENCES

1 D. R. Scott, W. A. Loseke, L. E. Halbake, and R. J. Thompson, Appl. Spectrosc., 30 (1976) 392.
2 R. G. Keenan and D. H. Byers, Arch. Ind. Hyg. Occup. Med., 6 (1952) 226.
3 A. Sugimae, Anal. Chem., 46 (1974) 1123.
4 J. L. Seeley and R. K. Skogerboe, Anal. Chem., 46 (1974) 415.
5 T. G. Dzubay and R. K. Stevens, Environ. Sci. Technol., 9 (1975) 663.
6 L. S. Birks, Anal. Chem., 44 (1972) 557R.
7 W. H. Zoller and G. E. Gordon, Anal. Chem., 42 (1970) 257.

8 N. K. Aras, W. H. Zoller, G. E. Gordon, and G. J. Lutz, Anal. Chem., 45 (1973) 1481.
9 I. Olmez, N. K. Aras, G. E. Gordon, and W. H. Zoller, Anal. Chem., 46 (1974) 935.
10 K. A. Hardy, R. Akselson, J. W. Nelson, and J. W. Winchester, Environ. Sci. Technol., 10 (1976) 176.
11 M. Margoshes and B. F. Scribner, Appl. Spectrosc., 18 (1964) 154.
12 A. J. Bedrosian, R. K. Skogerboe and G. H. Morrison, Anal. Chem., 40 (1968) 854.
13 J. M. Andov, W. H. Zoller, I. Almey, N. K. Aras, G. E. Gordon, L. A. Rancitelli, K. H. Abel, R. H. Filby, K. R. Shah, and R. C. Ragaini, Anal. Chem., 47 (1975) 1102.

Analytica Chimica Acta, 97 (1978) 13—19

DETERMINATION OF BENZO[a]PYRENE IN SHALE OIL BY SOLID-SURFACE FLUORESCENCE

R. J. HURTUBISE* and G. T. SKAR

Department of Chemistry, University of Wyoming, Laramie, Wyo. 82071 (U.S.A.)

R. E. POULSON

Laramie Energy Research Center, United States Energy Research and Development Administration, Laramie, Wyo. 82071 (U.S.A.)

(Received 5th October 1977)

SUMMARY

A method has been developed for determining benzo[a]pyrene in shale oil by combining dry-column chromatography, thin-layer chromatography and fluorescence spectrometry. A two-step separation method was employed to isolate benzo[a]pyrene from shale oil. Benzo[a]pyrene was identified and determined by detecting its fluorescence directly from chromatoplates; as little as 0.06 ng can be detected. The limit of detection of benzo[a]pyrene in shale oil is ca. 1.2 ppm and the reproducibility of the method is ±2.6 ppm.

Because of their occurrence in sources such as automobile exhaust, coal tars, processed foods, and high-boiling petroleum, polynuclear aromatic hydrocarbons (PAH) have been investigated extensively in recent years. Many PAH are carcinogenic to animals and probably to man [1]. There have been several publications on the separation, characterization, identification and determination of PAH in complex samples [2—10]. Many of the methods involve relatively sophisticated techniques and instruments. Recently, relatively simple methods for the separation, fluorescence characterization and identification of polynuclear aromatic hydrocarbons in shale oil were reported [11]. This report describes a quantitative method which is inexpensive, rapid and sensitive for the determination of benzo[a]pyrene (BaP) in shale oil.

EXPERIMENTAL

Apparatus

BaP was determined with a Kontes K-495000 Densitometer in the fluorescence mode with the "read" head. The excitation source was a K-495000-0823 long wave u.v. lamp filtered to exclude wavelengths greater than 400 nm. A No. 843 photodetector filter supplied with the instrument was employed with a peak transmission at 425 nm.

Fluorescence emission spectra were recorded with a Schoeffel SD 3000 spectrodensitometer in the reflection mode, with a grating emission monochromator.

Materials

The dry column consisted of a 33-cm section of polyethylene tubing (0.375 in i.d., Curtin Matheson Scientific, Inc.), 30 cm of which was packed with aluminum oxide, activity II to III according to Brockman (ICN Life Sciences Group, Cleveland, Ohio). The bottom of the column was plugged with glass wool. All solvents used were reagent grade. Precoated, 20 × 20 cm 30% acetylated cellulose chromatoplates were used for thin-layer chromatography (t.l.c.) work (Cel 300 AC/30-22 Brinkmann Instruments, Inc., Westbury, New York). The 99 + % BaP was obtained from Aldrich Chemical Co., Milwaukee, Wis. A 10-μl Hamilton syringe was used in spotting the chromatoplates. A Selectasol chromatography chamber (Schleicher and Schuell, Inc., Keene, New Hampshire) was employed in determining the eluants to be used in the t.l.c. work. The shale oil samples were obtained from the Laramie Energy Research Center, United States Energy Research and Development Administration, Laramie, Wyoming.

Procedures

A 0.1 g ± 0.005 g shale oil sample, weighed accurately, was dissolved in 2.5 ml of n-hexane. The solution was placed quantitatively on top of the aluminum oxide column and developed with n-hexane/ether (19:1). Solvent was added until the leading fluorescent band reached about 2 cm from the bottom of the column. The column was then observed with a u.v. handlamp and the purple fluorescent band located at about half the migration distance of the leading fluorescent band was sliced with a razor blade from the column to give a 6-cm section. If the purple band was not observable, a 6-cm section, centered around a point 0.45 times the migration distance of the leading fluorescent band, was cut out. Most of the shale oil samples consistently gave five major distinct fluorescent bands, each ca. 5 cm in length when viewed under u.v. radiation. The colors of each band, from top to bottom of the column, were bright blue, blue, violet, bluish-green and violet. Some samples showed a blue fluorescent streak throughout the column but this caused no serious problems in isolating BaP.

The aluminum oxide from the sliced section was stirred for 30 min with 20 ml of 1,2-dichloroethane. After decanting the solvent, the aluminum oxide was washed twice with 10-ml aliquots of 1,2-dichloroethane, with the last wash filtered rather than decanted. The combined extracts were evaporated to dryness under vacuum at room temperature and the residue was dissolved in 1 ml of n-hexane.

This solution (5 μl) was spotted in duplicate on a 30% acetylated cellulose chromatoplate. Standard solutions of BaP in n-hexane at concentrations of 2, 6, and 10 ng μl^{-1} were also spotted in 5-μl amounts in duplicate. The plate

was developed for 1 h with methanol—n-hexane—acetone (7:3:2, v/v). The plate was then air-dried and the fluorescence intensity of each BaP spot was recorded with the Kontes densitometer. Each spot was scanned perpendicular to the direction of development. Recorded peak heights corresponding to fluorescence intensity of the standards were plotted versus nanograms of BaP. The unknown amount of BaP on the chromatoplate was obtained from the calibration curve and the amount of BaP in the sample was calculated as micrograms BaP per gram of shale oil (ppm).

The fluorescence emission spectra of each BaP oil spot measured directly on the chromatoplate were obtained by following procedures previously described [11].

RESULTS AND DISCUSSION

Separation of benzo[a]pyrene from shale oil

Of the several column and t.l.c. systems tested, the Al_2O_3 dry-column chromatography—30% acetylated cellulose combination gave the best separation. Previously ethanol/n-hexane/acetone (2:1:1) was used to separate BaP on the acetylated cellulose chromatoplates [11]. However, further work with other shale oil samples showed some streaking of components and BaP on chromatoplates. Experiments showed that the combination of methanol/n-hexane/acetone (7:3:2) could be used for all shale oil samples; BaP was completely resolved from the other components and was devoid of streaking.

It was shown previously [11] that, with the initial dry-column separation, BaP in shale oil migrated at a rate based on the number of aromatic rings, and the reversed-phase partition t.l.c. system used separated ring isomeric PAH. Other workers have reported similar results for PAH in other samples [12, 13]. Fluorescence emission spectra were obtained for BaP on the acetylated chromatoplates, after the initial dry-column separation, to confirm that it had been isolated. Figure 1(A, B) shows the fluorescence emission spectra for a suspect BaP spot and a standard spot from a shale oil sample that contained a relatively large amount of BaP. Figure 1(C, D) shows emission spectra for a sample containing a relatively small amount of BaP, with 5 ng of standard BaP on the chromatoplate; although the fluorescence of BaP can be distinguished, better-defined spectra were obtained (Fig. 1, E, F) when the BaP sample size was increased to 100 ng.

There is the possibility that methyl or dimethyl derivatives of BaP could migrate at the same rate as BaP in the t.l.c. system employed. Commercial standards of these derivatives are not available and it was not possible to investigate this aspect. However, naphthalene, 2-methylnaphthalene and 2,3-dimethylnaphthalene gave R_F values of 0.52, 0.74 and 0.77, respectively, in the t.l.c. system used; these values suggest that it may be possible to resolve methyl or dimethyl derivatives of BaP.

Determination of benzo[a]pyrene

Table 1 shows recovery data for BaP in three shale oil samples; the accuracy of the method is good over a wide range of concentrations. Sample 5 was the

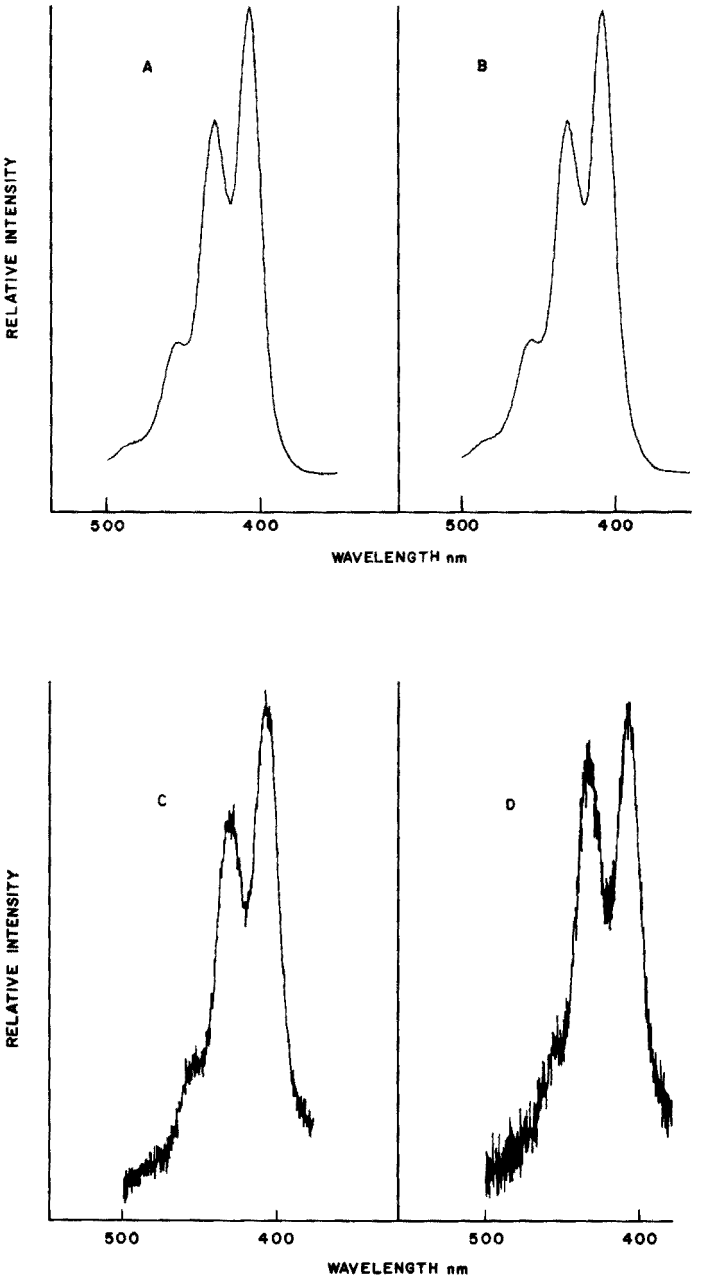

Fig. 1. Fluorescence emission spectra of BaP on a 30% acetylated cellulose chromatoplate. (There is no correlation between relative fluorescence intensity for the emission spectra.) A. 100 ng of BaP standard. B. Approximately 200 ng of BaP from Sample 4. C. 5 ng of BaP standard. D. Approximately 5 ng of BaP from Sample 7. E. 50 ng of BaP standard. F. Approximately 100 ng of BaP from Sample 7.

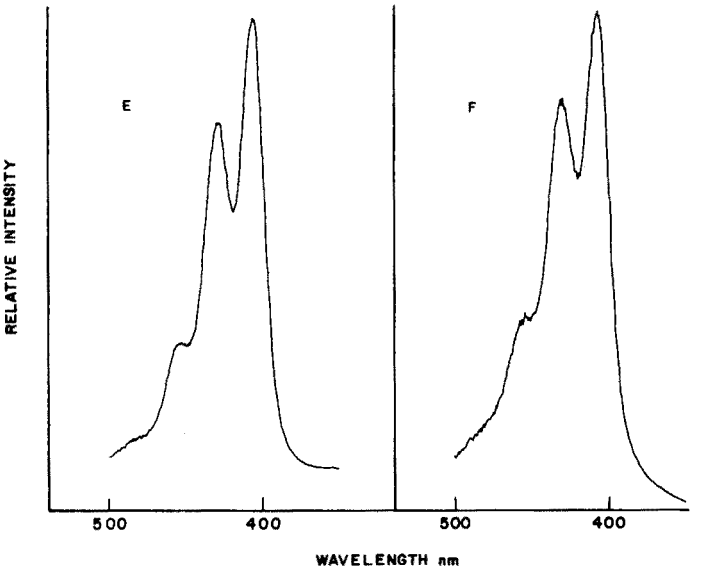

Fig. 1 (continued).

TABLE 1

Percentage benzo[a]pyrene recovery in spiked shale oil samples

Sample	ppm BaP present[a]	ppm BaP added	ppm BaP found[b]	Recovery (%)
1	23.3	10.0	32.2	89.0
		100	117	93.7
2	8.2	10.0	17.6	94.0
		100	97.6	89.4
5	9.1	10.0	20.1	110
		100	94.2	85.1

[a]Average value from Table 2. [b]Average of duplicate determinations.

most difficult sample to work with, because of streaking on the dry column, but reasonable results were obtained.

The precision of the method (Table 2) was obtained from replicate determinations on samples 1, 2 and 5; sample 5, which gave the most streaking on the dry column, gave the best precision of the three samples.

Samples 3 and 4 were used in experiments to investigate the sample size dependency of the method. The results in Table 3 show a sample size dependency at larger sample sizes. Streaking on the column and on the thin-layer chromatoplate was a problem with large samples and this probably accounts for the low values obtained. The highest values were obtained for 0.050 g of samples 3 and 4. Assuming the values for 0.100 g to be accurate

TABLE 2

Reproducibility of the method and amount of benzo[a]pyrene in shale oil samples

Sample	Benzo[a]pyrene[a] Average ± ppm	Number of detms.
1	23.3 ± 3.0	8
2	8.2 ± 3.3	6
3	35.0	2
4	39.5[b]	2
5	9.1 ± 1.4	9
6	none detected	2
7	11.3	2

[a]Determined at the 95% confidence level. [b]Two t.l.c. developments.

because well-defined spots were obtained without streaking, the value for 0.050 g lies within the reproducibility of the method for sample 3 but lies 0.2 ppm outside the reproducibility of the method for sample 4. More work is required to test if this is significant. Samples of 0.100 g were used in the development of the method because a low limit of detection, no streaking and well-defined spots were obtained. The results in Table 3 show the importance of using the optimum sample size. Sample 4 was unique because an unknown fluorescent component was present immediately above BaP on the 30% acetylated cellulose chromatoplate. Experiments with the Kontes units showed that at least 3.3 mm of space was necessary between the spots for no interference from the unknown fluorescent component to result. The interference problem was eliminated by carrying out two t.l.c. developments with the 30% acetylated cellulose chromatoplate. With the two developments sample 4 yielded an average value from duplicate determinations of 39.5 ppm BaP. With one t.l.c. development an average value of 44.4 ppm BaP (Table 3) was obtained, indicating that the unknown fluorescent component interfered. Sample size variation experiments did not detect this error.

TABLE 3

Variation of sample size

Weight (g)	Sample 3 BaP, ppm[a]	Sample 4 BaP, ppm[a]
0.050	36.8	46.8
0.100	35.0	44.0[b]
0.150	25.5[c]	44.4
0.200	26.0	39.2

[a]Average of 2 determinations. [b]Average of 4 determinations. [c]Average of 5 determinations.

Limit of detection

The limit of detection (ppm) for BaP in shale oil was calculated from the amount of BaP on a chromatoplate that would give a signal equal to twice the background signal, which was considered to consist of fluorescence from the chromatoplate, residual fluorescence from the shale oil, and recorder and densitometer noise. A comparison was made between the Schoeffel unit and the Kontes unit in determining the limit of detection. Because no BaP was detected in Sample 6 (Table 2), the background signal from this sample on 30% acetylated cellulose chromatoplates was considered to be representative of shale oil samples. The limit of detection of BaP was then calculated to be 1.2 ppm (Schoeffel unit) and 2.2 ppm (Kontes unit). The Schoeffel unit, a research spectrodensitometer with a high intensity xenon lamp source, is expected to have better performance characteristics than the Kontes densitometer, which was designed for routine analysis.

In additional experiments, the relative fluorescence intensities of BaP standards were measured on 30% acetylated cellulose, aluminum oxide and silica gel chromatoplates in the reflection mode and transmission mode with the Schoeffel unit; the best limit of detection was obtained for BaP on 30% acetylated cellulose chromatoplates with the fluorescence measured in the reflection mode. The smallest amount of BaP detected in the fluorescence reflection mode on 30% acetylated cellulose was 0.06 ng. On both silica gel and aluminum oxide the smallest amount of BaP detected was 1.6 ng.

Shale oil samples

Table 2 shows the results for the BaP content of several shale oil samples. The amount of BaP was well above the limit of detection of the method for most of the samples. With samples in which no BaP is detected, larger samples can be used with a dry column of correspondingly larger diameter; a larger diameter column could also be employed for samples with 1 ppm or less of BaP. The method was also applied to two petroleum products; no BaP was detected.

REFERENCES

1 J. B. Andelman and J. E. Snodgrass, CRC Crit. Rev. Environ. Control, 4 (1974) 69.
2 G. F. Kirkbright and C. G. de Lima, Analyst, 99 (1974) 338.
3 W. Giger and M. Blumer, Anal. Chem., 46 (1974) 1663.
4 G. M. Janini, K. Johnston and W. L. Zielinki, Anal. Chem., 47 (1975) 670.
5 R. C. Pierce and M. Katz, Anal. Chem., 47 (1975) 1743.
6 K. Potthast and G. Eigner, J. Chromatogr., 103 (1975) 173.
7 M. L. Lee, M. Novotny and K. D. Bartle, Anal. Chem., 48 (1976) 405.
8 R. E. Tentoft and T. H. Gouw, Anal. Chem., 48 (1976) 2195.
9 R. F. Severson, M. E. Snook, R. F. Arrendale and O. T. Chortyk, Anal. Chem., 48 (1976) 1866.
10 L. Zoccolillo, J. Chromatogr., 120 (1976) 485.
11 R. J. Hurtubise, J. F. Schabron, J. D. Feaster, D. H. Therkildsen and R. E. Poulson, Anal. Chim. Acta, 89 (1977) 377.
12 L. R. Snyder, Principles of Adsorption Chromatography, Dekker, New York, 1968.
13 R. G. Pierce and M. Katz, Anal. Chem., 47 (1975) 1743.

Analytica Chimica Acta, 97 (1978) 21—27

ANALYTICAL APPLICATIONS OF PEROXYOXALATE CHEMILUMINESCENCE

P. A. SHERMAN, J. HOLZBECHER and D. E. RYAN*

Trace Analysis Research Centre, Chemistry Department, Life Sciences, Dalhousie University, Halifax, N.S. B3H 4J1 (Canada)

(Received 14th September 1977)

SUMMARY

Peroxyoxalate chemiluminescence can be applied to the determination of hydrogen peroxide and aromatic hydrocarbon fluorophores in a static system. Hydrogen peroxide causes a linear response in the range 10^{-6}—10^{-1} M when bis(2,4,6-trichlorophenyl) oxalate is used with perylene as the fluorophore. As the intensity of chemiluminescence from different aromatic hydrocarbons varies substantially, there is a degree of selectivity in their determination. If metal chelates are employed as fluorophores, trace metal analysis is possible.

In luminescence, an external light source is used to raise a molecule to an excited electronic state and light is emitted when the molecule returns to the ground state. In chemiluminescence the process is identical but the energy necessary for excitation is provided by a chemical reaction. The energy required for visible light emission is in the range 40—70 kcal mol^{-1}.

An efficient chemiluminescent reaction requires an efficient chemical pathway leading to the excited state of the product molecule and this excited product molecule must be capable of emitting energy as light (direct chemiluminescence) or be able to transfer its energy to another molecule that has this potential (sensitized chemiluminescence). Most chemiluminescence reactions have a low efficiency with quantum yields of the order of 1%. Classical examples of non-biological chemiluminescence include lophin (imidazole derivative), lucigenin (biacridinium salt) and luminol (phthalhydrazide derivative). To date, most of the work in solution has been done with luminol; analytical methods for the determination of both the metal catalyst (Co(II), Cu(II), Cr(III), Fe(II), Ni(II), Mn(II)) and the oxidant (H_2O_2, OCl^-, I_2, MnO_4^-) have been developed [1—5].

In the late 1960's there were several reports on the chemiluminescence from reactions of hydrogen peroxide with oxalyl chloride [6, 7], oxalic anhydrides [8], oxalic esters [9, 10] and oxalic amides [11] in the presence of fluorescent organic compounds. These reactions were substantially more efficient than those previously reported and, since they appeared to constitute a general class of reactions involving peroxyoxalate intermediates, the term *peroxyoxalate luminescence* has been used as a generic name.

Peroxyoxalate luminescence is sensitized chemiluminescence, and decomposition of the 1,2-dioxetane (I) intermediate may provide the chemical

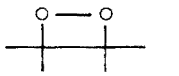
(I)


(II)

energy required for excitation and sensitized chemiluminescence [12—14] but the mechanism is still not well understood [13—18]; for oxalic esters, Rauhut and co-workers [9, 10] have proposed that C_2O_4 (II) is the decomposable intermediate providing the transferrable excitation energy for the luminescence. It is a general chemiluminescence system, because energy is produced (by reaction of an oxalate derivative with hydrogen peroxide) which can excite (and thus serve as a "source" for) various fluorescent compounds (fluorophores) such as polynuclear aromatics, metal chelates, uranyl salts, etc. The system can be used analytically for the determination of hydrogen peroxide or a variety of potential fluorophores.

Reaction with hydrogen peroxide in the presence of a fluorophore is very selective and a linear range of at least four orders of magnitude has been reported (10^{-7}—10^{-3} M). Its usefulness was extended by coupling the detection of chemiluminescence to enzymatic analysis; in particular, glucose in urine may be determined by using glucose oxidase to convert glucose to gluconic acid and hydrogen peroxide [19]. The advantage of peroxyoxalate luminescence over luminol chemiluminescence is that the analysis can be done at pH 6 and glucose can be determined without removing uric acid which interferes seriously at the more basic pH required for luminol chemiluminescence. In a similar manner, peroxyoxalate luminescence can be used to determine the reduced form of nicotinamide adenine dinucleotide (NADH) which, in the presence of methylene blue, reduces oxygen to hydrogen peroxide. A linear range of 2×10^{-7} to 1×10^{-4} M NADH was reported [20].

Methods for the determination of fluorophores, on the other hand, cannot be expected to be very selective. The peroxyoxalate luminescence reaction is capable of exciting any compound which fluoresces in the visible or infrared region of the spectrum, although there is a considerable variation in quantum yield [21]. Lechtken and Turro have shown [22] that chemiluminescent efficiency decreases steadily with increasing singlet excitation energy. It would, therefore, seem desirable to couple the method with a separation technique when applying peroxyoxalate luminescence to fluorophore determinations. Curtis and Seitz [23] have successfully combined peroxyoxalate luminescence with thin-layer chromatography of dansyl derivatives.

Determinations of hydrogen peroxide in solution by peroxyoxalate luminescence used flow systems [19, 20]. A simple static system was adopted in the present study.

EXPERIMENTAL

Apparatus, reagents, solutions

All chemiluminescence measurements were made with an Aminco Chem-Glow Photometer (photomultiplier tube type 931-VA, S-4 response). The injection port provided with the instrument was not used, to avoid possible contamination from the rubber septum. The signal was recorded with a Bausch and Lomb V.O.M.-5 Strip Chart Recorder.

Bis(2,4,6-trichlorophenyl) oxalate (TCPO) was chosen as the aromatic oxalate ester because of its ease of preparation, relative stability and the high quantum yields obtained with its use. It was prepared by the method of Mohan and Turro [24]. The white, finely crystalline, purified product (from chloroform) melted sharply at 189°C. Hydrogen peroxide (30%) and methyl acetate were Fisher Certified ACS. Stock solutions (10^{-3} M) of aromatic hydrocarbons (Aldrich, highest purity available) were prepared in methyl acetate; lower concentrations were prepared daily by dilution.

RESULTS AND DISCUSSION

Polynuclear aromatic hydrocarbons

The peroxyoxalate luminescent system was applied to the determination of eleven polynuclear aromatics (Table 1). Methyl acetate was used as the reaction solvent since the highest quantum yields with peroxyoxalate luminescence have been observed in ester and ether solvents [6, 9]. The oxalate esters are, however, unstable in ether solutions (dioxane, dimethoxyethane); presumably they react with the organic peroxides that tend to form in these solvents. TCPO was relatively stable in methyl acetate solution. Methyl acetate is fairly miscible with water, which overcomes problems of irreproducibility resulting from inhomogeneity of the reaction mixture (hydrogen peroxide is added as an aqueous solution).

The chemiluminescence signal intensity for constant fluorophore concentration increases with the concentration of both TCPO and H_2O_2. For example, for 0.2 ml of 10^{-6} M 9,10-diphenylanthracene (DPA) and 0.2 ml of 10^{-3} M TCPO, signals of 29, 69 and 117 were obtained on the addition of 0.1 ml of 3%, 30%, and 50% peroxide, respectively; similarly with 0.2 ml of 10^{-6} M DPA and 0.1 ml of 30% H_2O_2, signals of 27, 84, and 277 were observed on the addition of 0.2 ml of 0.5×10^{-3}, 1×10^{-3} and 5×10^{-3} M TCPO, respectively. Thirty percent hydrogen peroxide and 10^{-3} M TCPO were used in further experiments (30% peroxide is readily available and 10^{-3} M solutions of TCPO in methyl acetate are easily prepared).

In the initial experiments (with DPA as the fluorophore) the signal reached a maximum after ca. 40 s and then formed a stable plateau lasting for ca. 5 min followed by a slow decline. This type of behaviour can be rationalized by the formation of a chemiluminescence intermediate at a constant rate following a short induction period. In later experiments, in which a different batch of methyl acetate was used, the signal immediately peaked and then declined rapidly. Addition of acetic acid, however, restored the signal to its

TABLE 1

Data on polynuclear aromatic hydrocarbons

Fluorophore	Structure	Chemiluminescence response at 10^{-6} M	Fluorescence quantum yield	E_s (kcal mol^{-1})	λ_{em} (nm)
Perylene	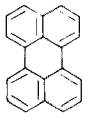	900+	0.94	66	470
9,10-DPA	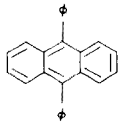	123	1.00	73	430
Anthracene	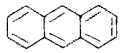	42.3	0.36	76	400
1,2-Benzanthracene	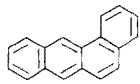	4.2	—[a]	74	382
Coronene	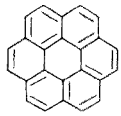	3.6	—[a]	68	450
Chrysene	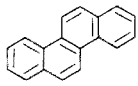	1.8	0.14	79	380
Pyrene	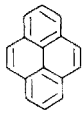	1.6	0.32	77	385
Phenanthrene	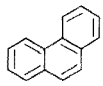	1.4	0.13	83	365
Fluorene	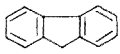	1.35	0.80	95	310
Fluoranthene	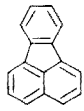	0.33	0.30	~72	460
m-Terphenyl	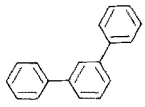	—[a]	0.29	—[a]	340

[a]Data not available.

original form; although acetic acid is a common impurity in methyl acetate, the batch of methyl acetate used in the later studies probably contained little or no acetic acid.

Investigation of the effect of acetic acid on the chemiluminescence reaction showed that an increase in the acetic acid concentration (0.1 ml of 0.002 to 2 M acetic acid in methyl acetate added to the sample cuvette after TCPO) resulted in progressively slower chemiluminescence reaction. A signal that reached a constant plateau in approximately 40 s was obtained by the addition of either 0.1 ml of 0.2 M acetic acid in methyl acetate, or 1 drop of aqueous 2 M acetic acid. This type of signal was suitable for analytical purposes. An acidic medium is necessary to establish a plateau type of signal. Above ca. pH 3 (aqueous 0.2 M acetic acid) the signal exhibits peaking and rapid decline.

The response to eleven different polynuclear aromatic hydrocarbons was examined. In these studies 10^{-3} M TCPO solutions in methyl acetate were freshly prepared on the day of analysis. Data for 0.2 ml of TCPO solution + 0.2 ml of hydrocarbon + 0.1 ml of 30% H_2O_2, given in Table 2 and Fig. 1, show that the intensity of the chemiluminescence signal varies considerably with the fluorophore employed in the reaction. Several factors, including chemiluminescence quantum yield, fluorescence quantum yield, and photomultiplier tube response, contribute to the results. The structures, fluorescence quantum yields [25] and spectral characteristics of the compounds investigated are given in Table 1. The values given for E_s represent the energy of the first excited singlet state relative to the ground state [26]. The wavelength of maximum emission in the fluorescence spectrum is denoted as λ_{em}. The photomultiplier tube employed responded to wavelengths in the range 350—600 nm, with a maximum at ca. 470 nm (S-4 response). The results, in general, agree with those obtained by Lechtken and Turro [22]; as the singlet excitation energy of the fluorophore increases, the chemiluminescence response decreases. Perylene has the lowest excitation energy and exhibits the strongest chemilumi-

TABLE 2

Response of different fluorophores (in arbitrary units)

Fluorophore	Concentration (M)				
	10^{-7}	10^{-6}	10^{-5}	10^{-4}	10^{-3}
Perylene	96	900+	—	—	—
9,10-Diphenylanthracene	12.9	123	—	—	—
Anthracene	—	42.3	105	—	—
1,2-Benzanthracene	—	4.2	36	320	—
Coronene	—	3.6	37	340	—
Chrysene	—	1.8	14	123	—
Pyrene	—	1.6	6.0	57	—
Phenanthrene	—	1.4	11.7	18	—
Fluorene	—	1.35	9.6	96	—
Fluoranthene	—	0.33	0.9	6	63
m-Terphenyl	—	—	0.36	0.96	3.9

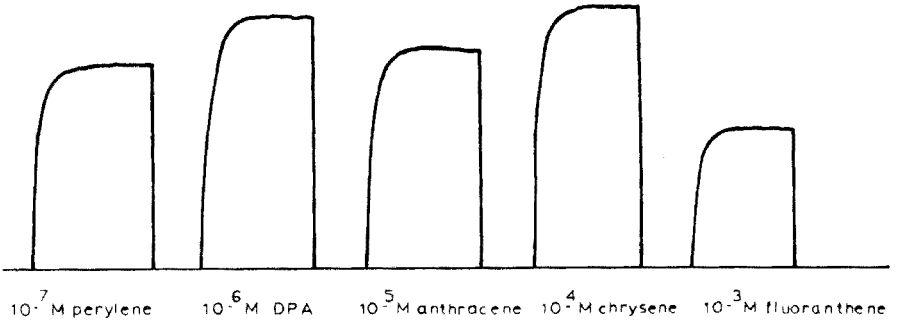

Fig. 1. Response of some polynuclear aromatics. The same photomultiplier sensitivity was used throughout.

nescence response; it also has a high fluorescence quantum yield and λ_{em} is at the maximum of the photomultiplier tube response.

Hydrogen peroxide

Peroxyoxalate luminescence has been applied to the determination of hydrogen peroxide in a static system. Perylene was chosen as a fluorophore because it exhibited the highest response of the aromatic hydrocarbons investigated. In a typical procedure, 0.2 ml of 10^{-3} M perylene was added to 0.2 ml of 10^{-3} M TCPO in the sample cuvette followed by 0.1 ml of hydrogen peroxide solution (all solutions were in methyl acetate). A linear response to hydrogen peroxide was observed over 5 orders of magnitude (10^{-6} to 10^{-1} M final concentration); sensitive determinations of hydrogen peroxide (with a linear calibration curve over a wide range of concentrations) are possible in a static system.

Metal chelates

Preliminary experiments showed that peroxyoxalate luminescence can be applied to the determination of metal chelates which can be excited in the near u.v. and visible regions of the spectrum. The practical determination of trace metal ions with peroxyoxalate luminescence is highly dependent on the selectivity of the chelation reaction involved. Further studies are in progress.

This work is taken, in part, from the M.Sc. thesis of Paula A. Sherman and was supported by a grant from the National Research Council of Canada.

REFERENCES

1 W. R. Seitz, W. W. Suydam and D. M. Hercules, Anal. Chem., 44 (1972) 957.
2 W. R. Seitz and D. M. Hercules, Anal. Chem., 44 (1972) 2143.
3 D. T. Bostick and D. M. Hercules, Anal. Chem., 47 (1975) 447.
4 A. K. Babko and N. M. Lukovskaya, J. Anal. Chem. U.S.S.R., 20 (1965) 1153.
5 A. K. Babko and L. I. Dubovenko, Z. Anal. Chem., 200 (1964) 428.
6 M. M. Rauhut, B. G. Roberts and A. M. Semsel, J. Am. Chem. Soc., 88 (1966) 3604.

7 E. A. Chandross, Tetrahedron Lett., (1963) 761.
8 L. J. Bollyky, R. H. Whitman, B. G. Roberts and M. M. Rauhut, J. Am. Chem. Soc., 89 (1967) 6523.
9 M. M. Rauhut, L. J. Bollyky, B. G. Roberts, M. Loy, R. H. Whitman, A. V. Iannotta, A. M. Semsel and R. A. Clarke, J. Am. Chem. Soc., 89 (1967) 6515.
10 M. M. Rauhut, Acc. Chem. Res., 2 (1969) 80.
11 D. R. Maulding, R. A. Clarke, B. G. Roberts and M. M. Rauhut, J. Org. Chem., 33 (1968) 250.
12 F. McCapra, Chem. Commun., (1968) 155.
13 H. E. O'Neal and W. H. Richardson, J. Am. Chem. Soc., 92 (1970) 6553.
14 W. H. Richardson, J. Am. Chem. Soc., 94 (1972) 1619.
15 F. McCapra, Pure Appl. Chem., 24 (1970) 611.
16 D. R. Kearns, Chem. Rev., 71 (1971) 395.
17 E. H. White, J. D. Miano, C. J. Watkins and E. J. Breaux, Angew. Chem., 13 (1974) 229.
18 N. J. Turro and P. Lechtken, J. Am. Chem. Soc., 95 (1973) 264.
19 D. C. Williams, G. F. Huff and W. R. Seitz, Anal. Chem., 48 (1976) 1003.
20 D. C. Williams and W. R. Seitz, Anal. Chem., 48 (1976) 1478.
21 M. M. Rauhut, B. G. Roberts, D. R. Maulding, W. Bergmark and R. Coleman, J. Org. Chem., 40 (1975) 330.
22 P. Lechtken and N. J. Turro, Mol. Photochem., 6 (1974) 95.
23 T. G. Curtis and W. R. Seitz, J. Chromatogr., 134 (1977) 343.
24 A. G. Mohan and N. J. Turro, J. Chem. Ed., 51 (1974) 528.
25 I. B. Berlman, Handbook of Fluorescence Spectra of Aromatic Molecules, Academic Press, New York (1971).
26 J. B. Birks, Photophysics of Aromatic Molecules, Wiley-Interscience, London (1970).

Analytica Chimica Acta, 97 (1978) 29—35

A COATED PIEZOELECTRIC CRYSTAL DETECTOR FOR THE SELECTIVE DETECTION AND DETERMINATION OF HYDROGEN SULFIDE IN THE ATMOSPHERE

L. M. WEBBER, K. H. KARMARKAR and G. G. GUILBAULT*

Department of Chemistry, University of New Orleans, New Orleans, Louisana 70122 (U.S.A.)

(Received 12th September 1977)

SUMMARY

A method for the selective detection and determination of hydrogen sulfide in the atmosphere is presented. This method utilizes the reversible adsorption of H_2S on a piezoelectric quartz crystal coated with an acetone extract of soots resulting from the burning of organochlorine compounds. The extract of a soot prepared from chlorobenzoic acid provided the best substrate. The method is useful in the concentration range 1—60 ppm.

It is now recognized that even trace amounts of noxious gases have an adverse effect on ecological systems. Such recognition has dramatized the need to develop increasingly more sensitive devices to measure such low concentrations. Piezoelectric crystals, with active coatings which will selectively adsorb gaseous pollutants, have been shown to be useful in the detection of trace pollutants [1—3]. Many coatings are not selective, so that a method to separate individual components is necessary. A gas chromatographic method has been developed for this purpose [4, 5].

A piezoelectric device is most useful when it can be used to detect a specific component only. A number of methods for the selective detection of specific gases have been developed. The detection of SO_2 has received the most attention and a number of selective coatings have been found [6]. The detection of SO_2 under various conditions has been investigated [7—9], as has the use of a coated piezoelectric crystal for the continuous monitoring of SO_2 [10, 11]. The specific detection of ammonia has also received some attention, and a method for the detection of this gas, using a dry nitrogen carrier gas, has been developed. A similar method was developed for NO_2 [12]. A method for the detection of ammonia in air has also been developed [13].

Hydrogen sulfide is a toxic gas which has caused atmospheric pollution problems and is detrimental to industrial health and safety. Various methods for the detection of H_2S in low concentrations have been developed [14, 15], but most of these are time-consuming or require bulky instrumentation.

A piezoelectric device can be quite portable and takes little time for a measurement. This paper reports the development of a new coating for a piezoelectric crystal which is sensitive toward H_2S in the concentration range 1—60 ppm.

EXPERIMENTAL

The apparatus and instrumentation were identical with those reported previously [13], except for the oscillator. An OT-03 oscillator circuit from International Crystal Mfg. Co. was used. The crystal was a general-purpose crystal with silver electrodes (Jan Crystals, Fort Myers, Fla.). Some particular experiments, which will be discussed later, used a gold electrode crystal (International Crystal Mfg. Co.). All crystals were of the smaller size, HC25/U, and had a resonant frequency of 9 MHz.

Briefly, the procedure was as follows. A 5-ml sample of test gas containing H_2S diluted by air was injected into a stream of air, the carrier gas, at a flow rate of 30 ml min^{-1}; nitrogen was not used as carrier gas. When the H_2S strikes the coated piezoelectric crystal surface, it is adsorbed and the weight change caused by that adsorption is observed as a change in frequency of the crystal. This change is related to the concentration of H_2S in the test sample. The change in frequency was measured by a frequency counter which was adapted for use with a chart recorder.

The coating for the crystal was prepared by burning several substances in air over a bunsen flame and collecting the soot residue. The compounds burned to obtain soots are listed in Table 1. Soots were obtained by repeatedly dipping a spatula into the particular compound, placing the spatula near the bunsen flame to ignite it and collecting the black residue. The soot residue was then placed in acetone, the extract was placed onto the crystal, and the acetone was allowed to evaporate leaving a film residue. The extract solution was applied to the electrode of the piezoelectric device (see Fig. 1). Care was taken to ensure that carbon particles were not applied to the crystal at the same time as the extracts since particles can stop the resonance of the crystal.

TABLE 1

Frequency changes produced by H_2S in reaction with various soot extracts

Soot extract	Frequency change	Soot extract	Frequency change
Benzene	0	Chlorobenzoic acid	85
Toluene	0	Benzyl chloride	8
Xylene	0	Chloroaniline	24
Carbon tetrachloride	0	Benzoyl chloride	0
Chloroform		Chloroacetic acid	70
Chloroform extract	10		
Acetone extract	30		

Test gas solutions were prepared by the syringe dilution method [5]. Chemically pure anhydrous H_2S was diluted with room air to the desired concentration by successive dilutions in a 10 ml syringe.

RESULTS

Choice of soot

Acetone extracts of certain soots showed a strong reaction with H_2S when applied to the quartz piezoelectric crystal. This reaction was indicated by the decrease in resonant frequency of the crystal; the amount of decrease was related to the concentration of H_2S in a mixture with air (Fig 2).

The acetone extracts of soots prepared from various compounds were tested as coatings. About 10,000-Hz change in frequency was observed for each coating substrate. In this coating procedure, the observation of change in frequency is the only way to know the quantity of the coating material. The compounds tested are listed in Table 1, along with the resultant frequency change observed for a 10-ppm sample. The soots of the first four compounds were extracted by the parent compound rather than acetone. Chloroform soot was extracted by chloroform as well as acetone, and the frequency changes exhibited by both extracts as a coating are shown for comparison.

Table 1 shows that the acetone extract of chlorobenzoic acid made the best coating. Chloroacetic acid coatings produced a frequency change that was almost as high, but those coatings saturated easily and were useful for

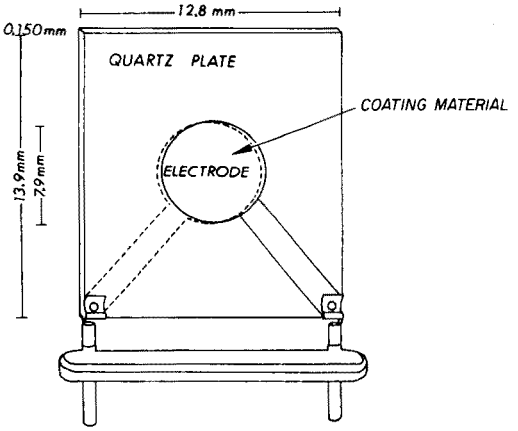

Fig. 1. Typical piezoelectric crystal.

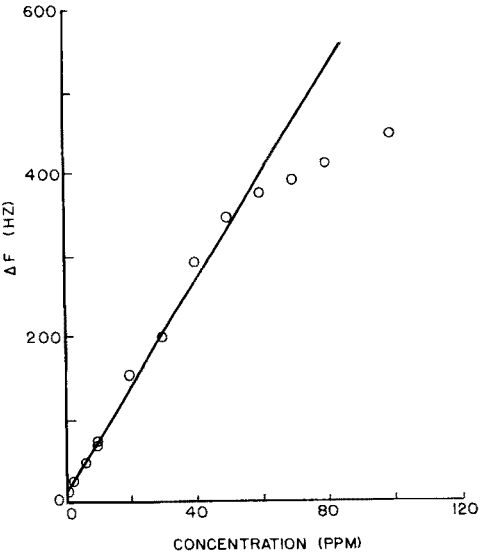

Fig. 2. Concentration vs. frequency change plot for chlorobenzoic acid soot extract.

only two or three days. The chloroform soot acetone extract was useful as a coating but its response to H_2S was much less than the chlorobenzoic acid soot extract; the same is true of other chlorine-containing compounds. Organic compounds without chlorine substituents proved inactive.

Linear range and precision

The usefulness of the acetone extract of the chlorobenzoic acid soot as a coating for a piezoelectric crystal for the determination of H_2S is demonstrated by Fig. 2, which shows a typical concentration vs. frequency change calibration plot. The plot is linear from 1 to 50 ppm with a correlation coefficient of 0.993. After 50 ppm the curve levels off, probably because of saturation of the coating by H_2S. The lower concentrations were the first measured, so that by the time the higher concentrations were determined the coating had been exposed to a number of samples. When the higher concentrations were measured first, a linear relationship was observed up to concentrations over 100 ppm. However, under such conditions of measurement, the recovery time was so slow that the coating was not as useful.

Figure 3 illustrates the effect of recovery time. When the injected H_2S test sample strikes the crystal surface and is adsorbed, the frequency change reaches a peak in less than 1 min. However, desorption is slower, and the time necessary for the frequency to regain a constant level is the recovery time. Figure 3 shows the relationship between the recovery time and the concentration tested. At low concentrations, the recovery time is reasonable being about 15 min for 10 ppm. At higher concentrations, recovery is much slower (about 30 min at 60 ppm). This should not be a problem in atmospheric

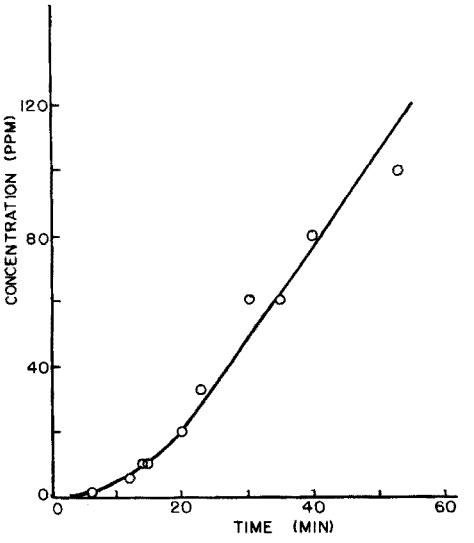

Fig. 3. Recovery time experiments. Time is that required for the crystal to return to its original base line.

measurements, however, because the higher concentrations should be found only in extreme cases.

Pure chlorobenzoic acid was also tried as a coating to ensure that the parent compound was not the active component of the coating. A coating made from that compound was inactive toward H_2S, and rapidly evaporated from the crystal surface.

The precision of the experimental data was demonstrated by a series of 10 consecutive measurements at 10 ppm. Of the 10, two measurements were significantly low and were eliminated. The mean reading for the remaining 8 was 64.13 with a standard deviation of 2.36 (r.s.d. = 3.6%). In another series of 6 consecutive measurements, the standard deviation was 3.97 (r.s.d. = 6.1%). Precisions of this order are adequate for measurements in this low range. Errors can be caused by not waiting long enough for recovery; this was the cause of the two low measurements mentioned above. The syringe dilution method for the preparation of the test gases also gives rise to measurement errors (ca. 3% uncertainty). However, this type of error should not be a factor in the measurement of unknown atmospheric samples, and an accurate assay should result. Day-to-day precision was not as good, and daily calibration would probably be necessary in the utilization of this method. All of the many calibration curves measured were linear in the same concentration range as reported above, and thus only one or two calibration points would be necessary. Least-squares correlation coefficients of 0.996, 0.993, 0.973 and 0.989 were obtained on four different days.

Sensitivity also varied from day to day, being especially good immediately after preparation of a fresh coating. For example, a frequency change of around 900 Hz was obtained for a concentration of 100 ppm on the day of preparation. Concentrations as low as 0.1 ppm could be detected within 3 days of initial crystal preparation. A more realistically useful range (after a few days of use) is, however, 1—60 ppm.

The useful lifetime of a single crystal preparation was not established. However, one crystal was still sensitive in the useful concentration range after 3 months of constant use.

Atmospheric humidity had negligible effects. Frequency changes caused by the injection of room air (blank measurement) was approximately 6 or 7 Hz, and were important only at very low concentrations of H_2S.

Studies of the reaction mechanism

Some attempts were made to characterize the reaction of H_2S with the chlorobenzoic acid soot coating. Gas chromatographic measurements with a flame ionization detector showed that the soot extract was composed of 3 or 4 major components and 10—15 minor ones. The last observed major component emerged from the column only when the column temperature reached 200°C. This peak was reduced in size by the addition of H_2S to the extract solution. Three to four major peaks were also observed when an electron capture detector was employed, indicating that chlorine (or perhaps

oxygen) was present in the compound. Elemental analysis of the chloroform soot showed 24.54% chlorine and 46.26% oxygen. Infrared spectra of the soot extracts were not changed by H_2S adsorption, and there were no dominant peaks which could help characterize the soot extract.

The results reported above were performed with soot extracts coated on a crystal which had silver electrodes. A crystal with gold electrodes was also coated with the chlorobenzoic acid soot extract; no reaction with H_2S was observed. However, there was a reaction when silver nitrate was applied along with the soot extract. A nickel-plated gold electrode was also tried with some success, but the activity was not as high as with the silver electrode. Crystals without coatings were not active. Since the metal of the electrode is involved in the reaction of H_2S with the soot extract coating as is the chlorine of the organic molecule, perhaps some type of Ag (or Ni)—RCl—H_2S complex is the reactive intermediate. Since the complex is readily reversible, it is not likely that a direct sulfide of silver or nickel is formed.

Clearly, there is not sufficient information to determine a reaction mechanism or to characterize the soot extract coating. It is believed that the coating provides a medium where the H_2S gas is adsorbed and reacts with the metal electrode to form a sulfide on the electrode surface. This reaction is completely reversible. Further research is necessary to determine a more lucid mechanism and to characterize the coating.

Some gases other than H_2S were injected into the system to test the selectivity of the chlorobenzoic acid soot coating. Carbon monoxide, chloroform, benzene, toluene and hexane all produced peaks that were nearly the same as the blank, and thus would not interfere with H_2S measurements. The signals produced by 1000 ppm of SO_2 and NH_3 were equivalent to 10 ppm H_2S; thus these gases would interfere when present at very high concentrations not normally present in air. NO_2 at 1000 ppm showed a very strong irreversible reaction. Since H_2S reacts with SO_2, NH_3 and NO_2, mixtures of these gases were not tested. Because of the reaction between those gases and H_2S, it is doubtful that concentrations in atmospheric samples would be sufficiently high to cause an interference when atmospheric H_2S is measured.

Conclusions

The coated piezoelectric quartz crystals can be used to determine H_2S at concentrations up to 60 ppm. Since the Occupational Safety and Health Administration (OSHA) lists 20 ppm as a ceiling value for H_2S, this type of coated crystal provides a measurement within the range of interest.

A piezoelectric detection system has as its greatest advantages simplicity and compactness. Most accepted methods [14, 15] for the determination of H_2S tend to be time-consuming or costly, or both. Even some recently reported methods fall into one of these categories [16—18]. Two commercial devices are available which measure and monitor H_2S concentrations within the range of interest; although they are reasonably simple in design [19, 20], they lack the simplicity and portability of the piezoelectric crystal device.

The financial assistance of the Army Research Office, Grant No. DAAG29-76-G-0215, is gratefully acknowledged.

REFERENCES

1 W. H. King, Jr., Anal. Chem., 36 (1964) 1735.
2 W. H. King, Jr. and L. W. Corbett, Anal. Chem., 41 (1969) 580.
3 W. H. King, Jr., Environ. Sci. Technol., 4 (1970) 1136.
4 F. W. Karasek and K. R. Gibbins, J. Chromatogr. Sci., 9 (1971) 535.
5 F. W. Karasek and J. M. Tiernay, J. Chromatogr., 89 (1974) 31.
6 M. W. Frechette and J. L. Fasching, Environ. Sci. Technol., 7 (1973) 1135.
7 K. H. Karmarkar and G. G. Guilbault, Anal. Chim. Acta, 71 (1974) 419.
8 K. H. Karmarkar, L. M. Webber and G. G. Guilbault, Environ. Lett., 8 (1975) 345.
9 K. H. Karmarkar, L. M. Webber and G. G. Guilbault, Anal. Chim. Acta, 81 (1976) 265.
10 J. L. Cheney and J. B. Homolya, Anal. Lett., 8 (1976) 175.
11 J. L. Cheney, T. Norwood and J. Homolya, Anal. Lett., 9 (1976) 361.
12 K. H. Karmarkar and G. G. Guilbault, Anal. Chim. Acta, 75 (1976) 111.
13 L. M. Webber and G. G. Guilbault, Anal. Chem., 48 (1976) 2244.
14 W. E. Ruch, The Analysis of Gaseous Pollutants, Ann Arbor-Humphrey, Ann Arbor, Michigan, 1970, p. 131.
15 M. B. Jacobs, The Analytical Toxicology of Industrial Inorganic Poisons, Interscience, New York, 1967, p. 540.
16 T. L. C. De Souza and S. P. Bhatia, Anal. Chem., 48 (1976) 2234.
17 D. L. Ehman, Anal. Chem., 48 (1976) 918.
18 A. R. Blanchette and A. D. Cooper, Anal. Chem., 48 (1976) 729.
19 Technical Bulletin, General Monitors, Inc., Costa Mesa, Calif.
20 Technical Bulletin, Energetics Science, Inc., Elmsford, N.Y.

Analytica Chimica Acta, 97 (1978) 37—42

RAPID DETERMINATION OF LEAD IN BIOLOGICAL TISSUES BY MICROSAMPLING-CUP ATOMIC ABSORPTION SPECTROMETRY

KENNETH W. JACKSON*, ERIC MARCZAK and DOUGLAS G. MITCHELL

Division of Laboratories and Research, New York State Department of Health, Albany, New York 12201 (U.S.A.)

(Received 30th September 1977)

SUMMARY

Lead can be determined in kidney, liver, and lung tissues by a rapid technique which does not require ashing or acid digestion of the sample. The tissue is homogenized with water, an aliquot of the homogenate is pipetted into a microsampling cup, and lead is determined directly by atomic absorption spectrometry. Calibration is by lead standards in a whole blood matrix. Results correlate well with those obtained by a wet-ashing procedure. The sensitivity (0.01 μg Pb g^{-1} wet tissue) permits the analysis of typical tissues with good precision. The procedure is rapid, and its simplicity minimizes the risk of contamination by extraneous lead during sample preparation.

Human exposure to environmental lead is generally monitored by blood lead [1, 2] and erythrocyte protoporphyrin [3, 4] determinations. Of the several workers who have examined tissue burdens of lead, almost all have used wet or dry ashing of the tissue and atomic absorption spectrometry (a.a.s.). Schroeder and Tipton [5], however, used dry ashing followed by emission spectrography for a detailed study of lead distribution. They found that lead accumulates principally in the bones, with most of the remaining burden distributed through eight other organs, including liver, kidneys, and lungs. Piscator and Lind [6], using dry ashing, dissolution of the ash in nitric acid, and a.a.s. found high lead concentrations in kidneys.

The direct analysis of solid tissue samples has been described by Langmyhr and Aamodt [7], who used graphite furnace a.a.s. Their method is faster than the classical ashing methods but requires grinding the dry tissue and weighing each sample aliquot into the furnace. A 2-min dry-ash-atomize cycle is then required.

A rapid procedure for the determination of cadmium in biological tissues has been described [8]. Briefly, the tissue is homogenized with deionized water, and the homogenate is aliquoted into nickel cups for direct determination by microsampling-cup a.a.s. Sample pretreatment is simpler than with earlier methods, resulting in rapid analysis and minimal risk of contamination. This procedure has now been adapted to the determination of lead in human kidney, liver, and lung tissues.

EXPERIMENTAL

Instrumentation

The computer-controlled microsampling-cup atomic absorption spectrometer has been described [8]. Although this instrument is more sophisticated than commercially available atomic absorption spectrometers, any instrument with a Delves microsampling-cup accessory should be suitable.

Sample preparation

Whole organs (kidney, liver, and lung), which had been individually packed into polyethylene bags and frozen at autopsy, were prepared in the same manner as for the cadmium procedure [8]. Cross-sectioning, cubing, and weighing were performed on the unthawed sample so that lead could not be lost through drainage of tissue fluids, and the weight of the tissue used was the wet weight without loss of any liquid. The tissue was then homogenized in four times its weight of water.

Possible sources of lead contamination during this sample preparation were the stirrer and chamber of the laboratory mixer and the surgical knife blade. The original brass bush on the stirrer was replaced with a Teflon bush; all other parts of the mixer were stainless steel. The mixer and knife blade were soaked for 24 h in (1 + 1) nitric acid, and the acid solutions were analyzed for lead by the microsampling-cup method. No atomic absorption signal was detected at 217.0 nm, confirming the absence of lead contamination.

Preparation of standards

Lead standards in a whole blood matrix were used. A vial of lyophilized blood (Tox-El, A. R. Smith, Los Angeles, Calif.) was reconstituted with exactly 5 ml of deionized water. The manufacturers' stated concentration of 0.65 μg Pb ml^{-1} on this standard was verified by the method of Hessel [2], which involves chelation of lead with ammonium pyrrolidine dithiocarbamate (APDC), extraction into methyl isobutyl ketone (MIBK), and a.a.s. at 217.0 nm. The same method showed a lead concentration of 0.06 μg ml^{-1} in a blood sample drawn from a cow into sodium heparin anticoagulant (0.05 g l^{-1} blood). The reconstituted Tox-El blood and the cow blood were mixed to produce calibration standards of 0.06, 0.26, 0.45, and 0.65 μg Pb ml^{-1}.

Procedure

Aliquots (50 μl) of the (1 + 4) tissue homogenates were pipetted in triplicate into nickel microsampling cups. Each whole blood standard was diluted (1 + 4) and aliquots (50 μl) were pipetted in duplicate into identical cups. After oven-drying at 60°C for 15 min, the cups containing the calibration standards were injected into a stoichiometric air-acetylene flame. Integrated absorbances were measured at 217.0 nm, and a least-squares

regression was calculated. As a quality control check, any line with a coefficent of correlation less than 0.995 was automatically rejected, and recalibration was required. After calibration, the cups containing the oven-dried sample homogenates were injected into the flame. The lead concentration of each sample was calculated from the mean absorbance of the triplicate measurements.

RESULTS AND DISCUSSION

Examination for matrix interferences

A common interference during micro a.a.s. occurs when incomplete combustion of the matrix results in obstruction of the light path by particulate matter (non-specific absorption). This interference did not occur during cadmium determinations because of the high tissue dilutions involved (1 + 4999 and 1 + 1249). However, the sensitivity of this method for lead is approximately 10 times lower than that for cadmium. This, together with the generally lower concentrations of lead in tissues, necessitates the use of far more concentrated homogenates. At the concentration used (1 + 4), non-specific absorption was seen. At the lead resonance wavelength, 217.0 nm, 50 μl of a (1 + 4) liver homogenate containing 0.232 μg Pb ml^{-1} (1.16 μg Pb g^{-1} liver) produced two completely resolved peaks, the first appearing almost immediately after the cup was injected into the flame, and the other appearing after 4 s (Fig. 1). At a non-absorbing cadmium ion line (214.4 nm), only the first peak was seen, with no absorption from 4 to 10 s after injection. Therefore the second peak at 217.0 nm is due completely to lead atomic absorption without interference by non-specific absorption. The two peaks can be completely resolved by adjusting the height of the absorption tube above the microsampling cup. If the cup is too close to the tube the peaks overlap, while loss of sensitivity occurs if the cup is moved too far away.

Interferences may be shown by enhancement or suppression of the atomic absorption signal; these may be caused by chemical interference or occlusion of analyte atoms by concomitant species. Such interferences are generally compensated for by matching the matrix in the calibration standards. Such a matrix effect did not occur during the determination of cadmium, and aqueous calibration standards were suitable. However, a tissue matrix enhances the volatility of lead. A 0.232 μg Pb ml^{-1} solution of a (1 + 4) liver homogenate (1.16 μg Pb g^{-1} liver) gave an absorption peak height more than double that of an aqueous solution containing the same concentration of lead, and its peak area was 1.3 times as large (Fig. 2).

Commercial whole blood standards, when volatilized, gave non-specific and atomic absorption peaks similar to those of tissue homogenates, both in time after cup injection and in duration. This indication that use of blood standards would compensate for this matrix interference was tested in two ways.

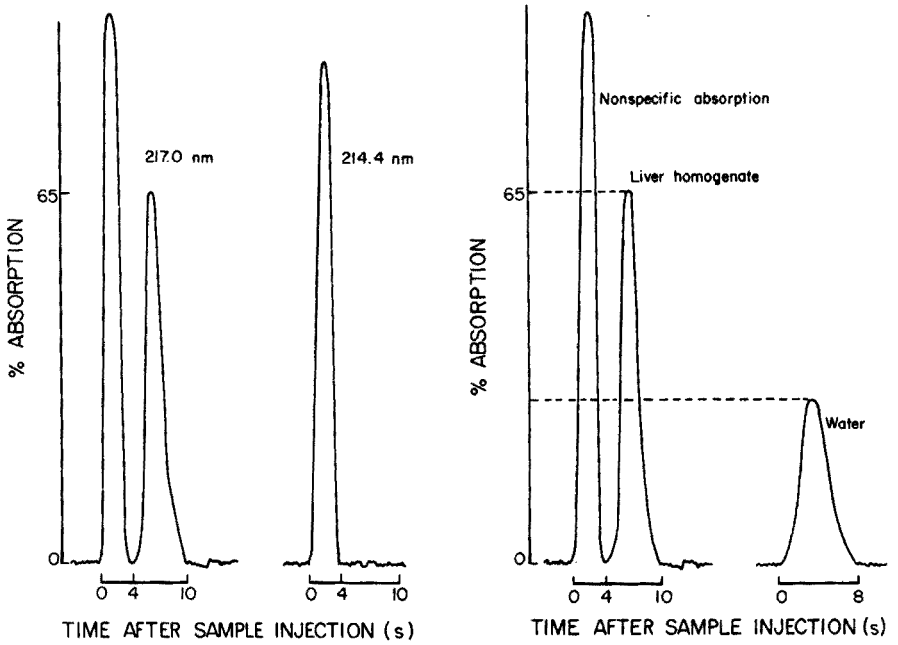

Fig. 1. Absorption signals from a (1 + 4) liver homogenate (50 μl) at the lead resonance wavelength (217.0 nm) and a non-atomic absorption wavelength (214.4 nm).

Fig. 2. Atomic absorption signals at 217.0 nm for 0.23 μg Pb ml^{-1} in two matrices: liver homogenate and water.

(a) Ten tissue homogenates were analyzed by the method of standard additions, each being spiked with blood at five concentrations from 0 to 0.65 μg Pb ml^{-1}. They were then analyzed against a curve derived from the blood calibration standards. Comparative results by the two methods are given in Table 1.

(b) Four tissue samples were analyzed by the method in this paper and by a conventional wet-ashing procedure [9] involving digestion with nitric acid and repeated evaporation almost to dryness until total destruction of the organic matter was evidenced by a clear, almost colorless solution. The digestates were then analyzed by a.a.s. against a calibration curve derived from solutions of an inorganic lead salt in nitric acid. Results are given in Table 2.

The generally good agreement of the microsampling cup method with the standard additions and wet-ashing procedure confirms that the commercial blood lead standards are suitable and that sample pretreatment (e.g., ashing) and background correction are not required to correct for matrix effects.

Precision, sensitivity, and detection limit

Precision data for typical kidney, liver, and lung tissues are shown in Table 3. Relative standard deviations were calculated from 10 determinations,

TABLE 1

Results obtained from a whole blood calibration curve and by standard additions (All results are μg Pb g^{-1} wet tissue)

Liver					
Whole blood curve	0.38	0.42	1.97	2.20	0.48
Std. addn.	0.39	0.41	1.94	2.00	0.54
Kidney					
Whole blood curve	0.42	0.31	0.54		
Std. addn.	0.43	0.30	0.51		
Lung					
Whole blood curve	0.59	0.68			
Std. addn.	0.65	0.72			

TABLE 2

Results obtained on kidney samples by microsampling-cup a.a.s. and by a wet-ashing/a.a.s. technique
(All results are μg Pb g^{-1} wet tissue)

Microsampling cup	0.30	0.48	0.47	0.31
Wet ashing	0.31	0.49	0.48	0.21

each being the average of three absorbance measurements by the homogenization—micro a.a.s. method. For cadmium a significant improvement in precision was obtained when integrated absorbance was used rather than peak height. In the case of lead, however, peak height measurement leads to approximately comparable precision, and so an instrument with signal integration is unnecessary.

The detection limit (S/N = 2) and sensitivity (1% absorption) of the method are both 0.01 μg Pb g^{-1} wet tissue. The linear range could not be determined because the highest calibration standard available was 0.65 μg Pb ml^{-1} blood. However, the accuracy of determinations in Table 1 indicates linearity at least as high as 2.0 μg Pb g^{-1} wet tissue. Typical concentrations of lead in kidneys, livers, and lungs are given in Table 4, and the linear range should permit the direct analysis of most typical tissues.

TABLE 3

Relative standard deviations for typical tissues

Tissue	Wet tissue (μg Pb g^{-1})	s_r[a]	
		Peak absorbance	Integrated absorbance
Kidney	0.42	2.8	3.0
Liver	0.42	2.5	3.7
Lung	0.68	2.2	2.6

[a] n = 10, each an average of three replicates.

TABLE 4

Typical concentrations of lead in wet tissues from three organs[a]
(All concentrations are μg Pb g^{-1})

	Mean	90% Range
Kidney	1.2	0.28—2.5
Liver	1.7	0.52—3.3
Lung	0.52	0.11—1.6

[a]See Reference 10.

If dilution is necessary to bring the lead concentration into the known linear range, homogenate concentration must be maintained at (1 + 4) to prevent interference. Therefore, a suitable diluent is blood of known low lead concentration.

Conclusions

The homogenization—micro a.a.s. procedure is precise and its sensitivity is more than adequate for the tissues tested.

One difficulty of the commonly used wet- or dry-ashing procedures is the likelihood of sample contamination by environmental lead during the time-consuming sample pretreatment stage. In this microsampling cup procedure no reagents are required, and sample pretreatment is rapid and simple. No contamination problems have been encountered. Typical dry ashing times for tissues are 24 h or more. Wet ashing is faster but still generally takes several hours. In contrast, the recommended procedure requires a total elapsed time of less than 30 min for the analysis of a single tissue sample: a 10-min homogenization followed by the pipetting of three aliquots, drying for 15 min, and an a.a.s. determination taking only 1 min per sample. If several tissues are to be analyzed, the time per tissue is further reduced, since all samples are oven-dried in the microsampling cups simultaneously.

We are grateful to Theodore J. Kneip for providing comparative analytical results by the wet-ashing procedure.

REFERENCES

1 H. T. Delves, Analyst (London), 95 (1970) 431.
2 D. W. Hessel, At. Absorpt. Newsl., 7 (1968) 55.
3 S. Piomelli, J. Lab. Clin. Med., 81 (1973) 932.
4 J. J. Chisolm and D. H. Brown, Clin. Chem., 21 (1975) 1669.
5 H. A. Schroeder and I. H. Tipton, Arch. Environ. Health, 17 (1968) 965.
6 M. Piscator and B. Lind, Arch. Environ. Health, 24 (1972) 426.
7 F. J. Langmyhr and J. Aamodt, Anal. Chim. Acta, 87 (1976) 483.
8 K. W. Jackson and D. G. Mitchell, Anal. Chim. Acta, 80 (1975) 39.
9 M. Eisenbud and T. J. Kneip, Trace Metals in Urban Aerosols, Final Report to Electric Power Research Institute, No. EPRI 117 (1976).
10 I. H. Tipton, in M. H. Seven and L. A. Johnson (Eds.), Metal Binding in Medicine, Lippincott, Philadelphia, 1960, p. 27.

Analytica Chimica Acta, 97 (1978) 43—49

ATOMIC FLUORESCENCE SPECTROMETRY OF THALLIUM WITH A FREQUENCY-DOUBLED DYE LASER AND VITREOUS CARBON ATOMIZER

J. P. HOHIMER* and P. J. HARGIS, Jr.

Sandia Laboratories, Albuquerque, New Mexico 87115 (U.S.A.)

(Received 7th September 1977)

SUMMARY

A vitreous carbon atomizer is described for use in laser-excited atomic fluorescence spectrometry and is applied to the determination of thallium in aqueous solution. When a frequency-doubled N_2 laser-pumped dye laser is used to excite the atomic thallium at 276.8 nm and the combined direct-line fluorescence and stepwise-line fluorescence are detected at 352.9 and 351.9 nm, respectively, the limit of detection is 2.5×10^{-14} g in a 0.5-pg ml^{-1} sample solution. The calibration curve for thallium has a linear range extending over six orders of magnitude.

In recent years, tunable dye lasers have been studied as excitation sources for atomic fluorescence spectrometry (a.f.s.) [1—6]. Dye lasers are ideal excitation sources for a.f.s. because of their high spectral power density which allows the saturation of atomic transitions thereby attaining the maximum possible fluorescence signal while minimizing the effects of source instabilities. In addition, dye lasers may be operated at any wavelength in the visible and near-infrared regions and can be frequency-doubled to extend their operation to the ultraviolet [7—10] where the strongest lines of most elements lie. However, with all the advantages inherent in dye lasers the early analytical results [1—3] were disappointing, and the limits of detection with laser-excited a.f.s. were in most cases no lower than those which could be obtained with atomic absorption or atomic emission spectrometry with conventional excitation sources. There are several reasons for this: (1) the detection of resonance fluorescence was severely limited by the strong Rayleigh and Mie scattering of the intense laser beam in the atomization system; (2) the most sensitive lines of most elements lie in the ultraviolet and were not excited in these studies; and (3) flame atomizers were used although non-flame atomizers have proven superior in obtaining lower limits of detection for most elements.

In this paper, the construction of a vitreous carbon atomizer designed expressly for laser-excited a.f.s. is reported. This atomizer has been used to detect cesium in aqueous solutions with a detection limit of 1.2×10^{-12} g in a 20-pg ml^{-1} solution [6]. A N_2 laser-pumped dye laser tuned to 455.5 nm

excites the cesium and the stepwise-line fluorescence at 852.1 nm is detected. Black-body emission from the atomizer determined the lower limit for the detection of cesium. In the present study, the dye laser was frequency-doubled to excite thallium at 276.8 nm, and the combined direct-line fluorescence emitted at 352.9 nm and the thermally-assisted stepwise-line fluorescence emitted at 351.9 nm were detected. At this detection wavelength, the black-body emission from the vitreous carbon atomizer was greatly reduced, and thallium could be measured with a detection limit of 2.5×10^{-14} g in a 0.5-pg ml^{-1} solution.

A flameless atomizer was chosen for these studies because flameless atomizers have proven superior to the conventional flame atomizers in many respects. They produce a denser atomic vapor with increased sample residence time, and are free from the chemiluminescence and thermal emission found in the flame gases. Their atomization efficiency approaches 100%. They can be operated in an inert gas environment to reduce fluorescence quenching and metal-oxide formation, and they have lower levels of ionization for the alkali metals. Finally, small sample sizes (including solid samples) can be used [11—13]. As a result of these factors, much lower limits of detection have been obtained for most metals with flameless atomizers.

EXPERIMENTAL

Vitreous carbon atomizer

Figure 1 shows the design of the vitreous carbon atomizer. The atomizer uses an electrically heated slotted evaporation boat made of vitreous carbon, which has a liquid sample capacity of about 60 μl (Beckwith Carbon Co., Cat. No. V-21). Vitreous carbon was chosen because of its extremely low porosity and high purity [14]. The use of vitreous carbon atomizers for a.f.s. with conventional excitation sources has been reported previously [15].

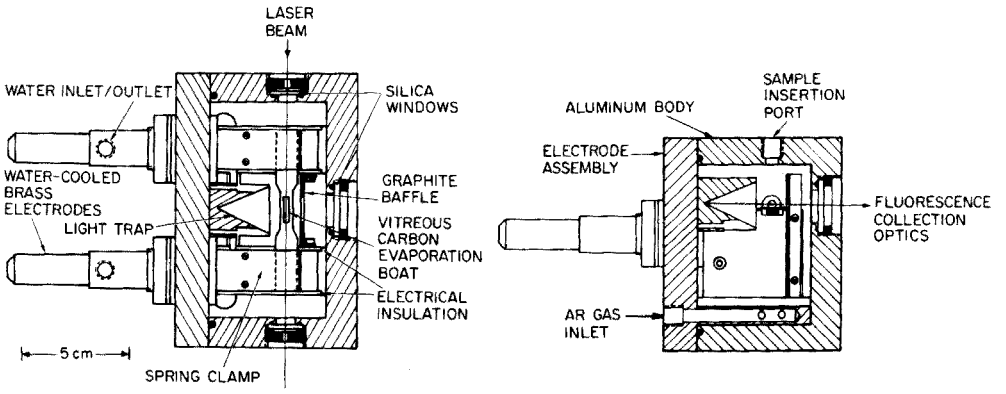

Fig. 1. Vitreous carbon atomizer for laser-excited a.f.s.

The evaporation boat is held firmly in contact with two water-cooled brass electrodes by beryllium-copper spring clamps. Apertures at either end of the atomizer housing maintain the alignment of the unfocused laser beam along the axis of the evaporation boat at 2 mm above the surface of the boat. The electrode assembly can be removed from the atomizer housing for replacement of the boat, without affecting the alignment of the laser beam or collection optics. An optical system based on narrow-band interference filters is used to collect the fluorescence emitted normal to the exciting laser beam. A graphite baffle (with 0.32 × 1.3 cm slit) and a blackened conical light trap were incorporated into the atomizer assembly to reduce the level of continuum radiation reaching the collection optics. In addition, the center of the observed region in the atomizer was imaged onto an adjustable slit to filter the fluorescence spatially, thereby restricting the field of view of the photomultiplier tube (PMT) and further reducing the noise level (continuum radiation) from the atomizer.

A programmable high-current power supply (Perkin-Elmer, Model HGA-2100) is used to heat the vitreous carbon atomizer. The necessary adaptation of this commercial power supply — to increase its output voltage to about 12 V r.m.s. a.c. — was accomplished by replacing the high-current transformer in the power supply (Signal Transformer Co., Cat. No. 24-100, wired for 12 V operation). This power supply controller permits automated temperature programming of the drying, ashing and atomizing stages. It also controls the flow of argon gas (>99.995% purity) which removes sample vapors from the atomizer during the drying and ashing stages and which minimizes fluorescence quenching and oxide formation of the atomized species. Fused silica windows and O-ring seals are incorporated into the atomizer so that it may be operated under static atmospheric conditions or under inert gas flow conditions at reduced, standard, or positive pressures.

Figure 2 shows the temperature—voltage characteristics of this atomizer. The color temperature over a spot of about 0.6-mm diameter located at the center of the sample cavity was measured as a function of the r.m.s. a.c. voltage applied to the evaporation boat. Measurements were made at the end of a 15-s heating cycle with an automatic optical pyrometer (Pyrometer Instrument Co., "Photomatic" Photo I); the temperatures were determined from the output voltage and the calibration tables supplied. Measurements were also made with a thermocouple (W-5%Re—W-26%Re, 3 mil wires) fitted into a small cavity drilled into the center of the boat; the data obtained are also shown in Fig. 2. The lower temperatures measured with the thermocouple are probably due to poor thermal contact with the evaporation boat.

Apparatus

A schematic diagram of the arrangement used for the laser-excited a.f.s. is shown in Fig. 3. A 250-kW nitrogen laser (Avco-Everett, Model C950B) was used to pump a tunable dye laser of the Hänsch design [16]. The dye laser was operated at 553.6 nm with a 5.0×10^{-3} M solution of the organic

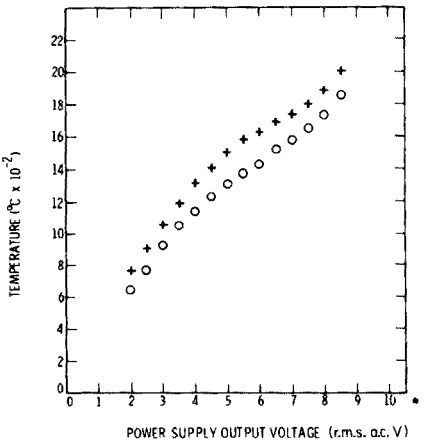

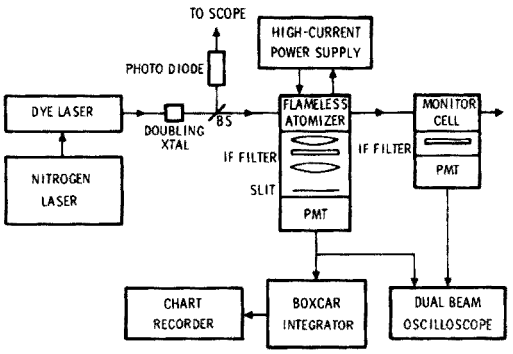

Fig. 2. Temperature-voltage characteristics of the vitreous carbon atomizer. + Pyrometer. ○ Thermocouple.

Fig. 3. Experimental arrangement for laser-excited a.f.s. with the flameless atomizer.

dye Pilot 495 in ethanol. The unfocused dye laser output was frequency-doubled to 276.8 nm in a 2.5-cm long, angle-tuned KDP (potassium dihydrogenphosphate) crystal (Cleveland Crystals, Inc.) and was tuned to excite the $6^2P_{1/2} \rightarrow 6^2D_{3/2}$ transition of atomic thallium. A color filter (Corning, 3-144) was used before the doubling crystal to prevent scattered N_2 laser light from reaching the atomizer. A second color filter (Corning, 7-54) was used after the doubling crystal to block the fundamental dye laser light at 553.6 nm and transmit the second harmonic light at 276.8 nm. The transmission of this filter at 276.8 nm was approximately 60%.

The second harmonic lasing energy reaching the atomizer was typically 0.15 μJ in a 5-ns pulse with the laser operating at a pulse repetition rate of 50 pulses/s. The spectral bandwidth of the u.v. light was about 0.03 nm. No attempt was made to increase the doubling efficiency by focusing the laser output into the KDP crystal. A biplanar photodiode (Korad, Model K-D1 with S5 response) was used to monitor the u.v. output energy from the doubling crystal. For this series of measurements, the atomizer was operated at atmospheric pressure with the quartz windows removed.

An uncoated quartz lens (85 mm focal length, $f/2.8$) was used to collect the thallium direct-line fluorescence from the $6^2D_{3/2} \rightarrow 6^2P_{3/2}$ transition at 352.9 nm and the stepwise-line fluorescence from the $6^2D_{5/2} \rightarrow 6^2P_{3/2}$ transition at 351.9 nm. The collimated fluorescence was passed through an interference filter (10 nm FWHM, 26% transmission at 352.5 nm) and was imaged by a second lens onto a variable slit (1.5 mm × 8 mm) to restrict the field of view of the detector to the region directly above the evaporation boat. The non-resonant fluorescence signal was detected by a PMT (RCA 8850) cooled to −50°C. The PMT signal was amplified (× 10 by a LeCroy Research

Systems Model 133B pulse amplifier), averaged by a boxcar integrator (Princeton Applied Research, Model 162), and recorded on a strip-chart recorder.

The detection of non-resonant fluorescence (e.g., direct-line and/or stepwise-line fluorescence) in laser-excited a.f.s. measurements eliminates the strong Rayleigh and Mie scattering of the laser light which otherwise limits the detection to relatively high concentrations. This non-resonant detection also eliminates self-absorption and increases the analytically useful concentration range over which measurements can be made [17].

The frequency-doubled laser was tuned to the thallium transition at 276.8 nm by monitoring the non-resonant fluorescence signal from thallium in an evacuated quartz vapor cell heated in a temperature-stabilized oven to approximately 350°C. This fluorescence signal was used to adjust the boxcar integrator for optimum sampling gate widths (50 ns) and position. It was also processed by a second channel of the boxcar integrator and used to monitor the laser amplitude and frequency stability. The average value of the signal changed by less than 7% during 2 h.

Reagents

A 1000-μg ml^{-1} thallium standard solution was serially diluted with deionized water (>18 MΩ-cm resistivity) to obtain sample concentrations down to 0.5 pg ml^{-1}. The accuracy of these serial dilutions was checked at concentrations of 0.1, 1.0, 10.0 μg ml^{-1} with a conventional flame atomic absorption spectrometer [18]. Sample solutions containing less than 1.0 ng ml^{-1} Tl were prepared immediately before use. All solutions were stored in polyethylene bottles.

Measurement techniques

Initial measurements of thallium were made with 50-μl samples of 1.0 ng ml^{-1} concentration to establish the optimum temperatures and timing for the atomization cycle. The samples were inserted into the cavity in the evaporation boat with a 50-μl micropipette (Variable Volumetrics, Inc., Finpipette 11) with disposable polypropylene tips. The following atomization conditions were found to be optimum: dry for 120 s at $\geqslant$100°C, ash for 90 s at ca. 400°C, and atomize for 7—15 s at ca. 1400°C (color temperature) with the argon flow interrupted. The non-resonant fluorescence signal which occurred during the atomization time was recorded with a 1-s time constant.

RESULTS AND DISCUSSION

Figure 4A shows the fluorescence signal from a series of five samples (10 pg ml^{-1}) under the above conditions; the standard deviation of these samples was 9% and improved with increased sample concentration (6% at 0.1 ng ml^{-1}; 4% at 1.0 ng ml^{-1}). The peak value of each signal was used in establishing the precision of the measurement and in defining the limit of detection and linearity of the measurements. After each sample, a blank

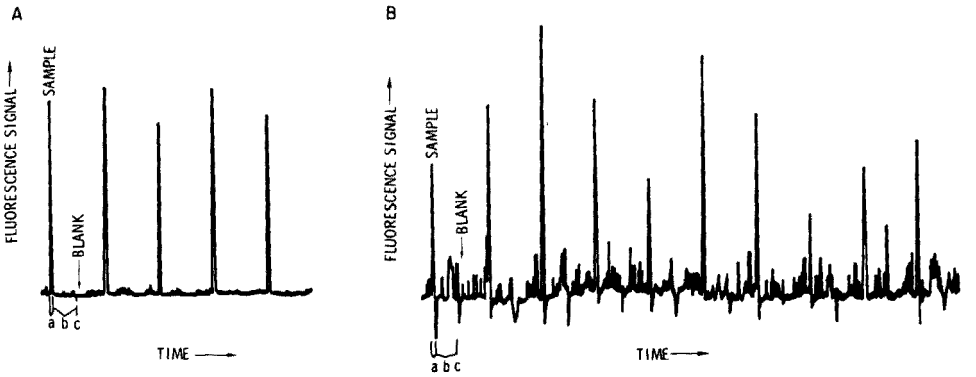

Fig. 4. Non-resonant-fluorescence signals from (A) 5 successive determinations of 50-μl thallium samples at 10 pg ml^{-1}, and (B) 10 successive determinations of 50-μl thallium samples at 0.5 pg ml^{-1}. Time scale: (a) sample atomization, 7 s; (b) chart recorder continues to run after atomization completed (ca. 30 s); (c) chart recorder off during evaporation cool-down period (ca. 60 s), blank insertion, dry and ash cycles.

was run as an indication of the background noise level and as a check for memory effects.

The lowest concentration measured was 0.5 pg ml^{-1}; the signal-to-noise ratio was then approximately 3:1. Figure 4B shows a series of ten samples at this level. The calculated amount of thallium present in each sample was 7.4×10^7 atoms; this resulted in a mean signal level of 0.47 V at the output of the boxcar integrator. The primary sources of noise at the detection limit are the dark current in the photomultiplier and noise internal to the boxcar integrator and associated electronics, rather than continuum radiation from the atomizer. This is evidenced by the fact that the noise level is not significantly increased during atomization of the blank samples (Fig. 4B).

For the thallium calibration curve (Fig. 5), calibrated neutral density filters were used to attenuate the fluorescence signals reaching the PMT for sample concentrations above 10 pg ml^{-1}. This was necessary to prevent the PMT from being saturated by the strong fluorescence at high concentrations. The measured calibration factors for the neutral density filters and the mean fluorescence signal levels were used to construct the calibration curve. This curve is linear over more than six orders of magnitude with an analytically useful range extending from 5.0 pg ml^{-1} to 10 μg ml^{-1} (2.5×10^{-13}—5.0×10^{-7} g).

The limit of detection reported here — 2.5×10^{-14} g in a 0.5-pg ml^{-1} solution — is more than four orders of magnitude lower than that previously reported for thallium by laser-excited a.f.s. [2], and is two orders of magnitude lower than the best value for thallium reported by atomic absorption spectrometry [11]. This lower detection limit can be attributed to several factors: (1) laser excitation of the most sensitive thallium transition at 276.8 nm; (2) the use of a flameless atomizer and fast collection optics; and (3) the detection of non-resonant fluorescence in the ultraviolet which eliminates scattered laser light and greatly reduces the background noise level arising from continuum radiation from the atomizer.

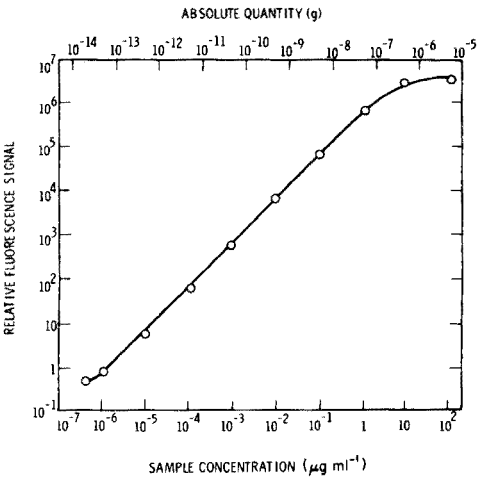

Fig. 5. Calibration curve for thallium. (Error bars are smaller than the symbols used to indicate the data points.)

The authors express their appreciation to M. E. Wilkins for technical assistance, E. A. Igel for use of the automatic optical pyrometer, M. H. Robertson for preparation of the thallium monitor cell, D. I. Miller for independently checking the accuracy of the diluted standard solutions, and G. W. Gobeli for encouragement and useful discussions. This work was supported by the U.S. Energy Research and Development Administration.

REFERENCES

1 M. B. Denton and H. V. Malmstadt, Appl. Phys. Lett., 18 (1971) 485.
2 L. M. Fraser and J. D. Winefordner, Anal. Chem., 43 (1971) 1693; 44 (1972) 1444.
3 N. Omenetto, N. N. Hatch, L. M. Fraser and J. D. Winefordner, Anal. Chem., 45 (1973) 195; Spectrochim. Acta Part B, 28 (1973) 65.
4 J. Kuhl and H. Spitschan, Opt. Commun., 7 (1973) 256.
5 S. Neumann and M. Kriese, Spectrochim. Acta Part B, 29 (1974) 127.
6 J. P. Hohimer and P. J. Hargis, Jr., Appl. Phys. Lett., 30 (1977) 344.
7 R. S. Adhav and R. W. Wallace, IEEE J. Quantum Electron., QE-9 (1973) 855.
8 F. B. Dunning, E. D. Stokes, and R. F. Stebbings, Opt. Commun., 6 (1972) 63.
9 F. B. Dunning, F. K. Tittel, and R. F. Stebbings, Opt. Commun., 7 (1973) 181.
10 C. F. Dewey, Jr., W. R. Cook, Jr., R. T. Hodgson, and J. J. Wynne, Appl. Phys. Lett., 26 (1975) 714.
11 B. V. L'Vov, Atomic Absorption Spectrochemical Analysis, Adam Hilger, London, 1970,
12 G. F. Kirkbright, Analyst, 96 (1971) 609.
13 R. F. Browner, Analyst, 99 (1974) 617.
14 F. C. Cowlard and J. C. Lewis, J. Mater. Sci., 2 (1967) 507.
15 C. J. Molnar and J. D. Winefordner, Anal. Chem., 46 (1974) 1419, 1807.
16 T. W. Hansch, Appl. Opt., 11 (1972) 895.
17 V. Svoboda, R. F. Browner, and J. D. Winefordner, Appl. Spectrosc., 26 (1972) 505.
18 D. Miller, private communication.

Analytica Chimica Acta, 97 (1978) 51—57

IMPROVEMENTS IN THE NON-DISPERSIVE ATOMIC FLUORESCENCE SPECTROMETRIC DETERMINATION OF ARSENIC AND ANTIMONY BY A HYDRIDE GENERATION TECHNIQUE§

KANJI TSUJII* and KAZUO KUGA

Central Research Laboratory, Hitachi Ltd., Kokubunji, Tokyo (Japan)

(Received 12th July 1977)

SUMMARY

A sodium borohydride reduction, with subsequent atomization in a small argon—hydrogen—entrained air flame has been developed for the determination of arsenic and antimony by non-dispersive atomic fluorescence spectrometry. The proposed method increases the signal level and decreases the noise level in the system. The detection limits for arsenic and antimony are 0.05 ng and 0.1 ng, respectively. The analytical working curves are linear over about four decades of concentration from the detection limits. The consumption rates of hydrogen and argon are comparatively low, while the speed of hydride evolution is improved; a peak measurement requires less than 40 s. The technique has been applied to the determination of arsenic in steel samples.

The advantages and disadvantages of a non-dispersive system for atomic fluorescence spectrometry (a.f.s.) have been discussed in a number of publications [1—10]. This system offers improved signal levels, because of the large optical aperture and simultaneous detection of multiple lines for the element of interest. However, the noise level is likely to increase depending on the background radiation levels from the atom reservoir. For non-dispersive systems employing flame atomizers, the noise limitations are due to the background radiation from the flame [5—10].

Hydride generation is now well known as a sensitive pretreatment technique for the determination of arsenic, antimony, selenium, tellurium etc. by atomic spectrometry [11—28].

As reported previously [29, 30], this technique can be applied effectively to non-dispersive systems for a.f.s. for the following reasons: (1) hydride compounds are easily decomposed in a cool flame, e.g. an argon—hydrogen—entrained air flame which emits very low background radiation; (2) the elements of interest are converted to hydrides and isolated from the matrix elements which occasionally cause severe light scattering effects; and (3) most of the elements known to form volatile hydrides have multiple fluores-

§This paper was presented at the 28th Pittsburgh Conference on Analytical Chemistry and Applied Spectroscopy, Cleveland, March 1977.

cence spectral lines within the spectral response range of a solar-blind photomultiplier, which is often used in non-dispersive a.f.s. For example, arsenic and antimony have 12[31] and 9[32] atomic fluorescence spectral lines in the u.v. region.

In previous work [29, 30] the liberated hydrides and hydrogen were stored for a fixed time prior to introduction into the flame atomizer. These studies indicated (1) that the noise level decreases with decreasing hydrogen flow-rates; (2) that the hydrogen flow-rate has a lower limit with the hydride generation method described previously, because the pressure increase in the vessel during reduction extinguishes the flame; and (3) that the system noise limitations are caused by OH band emission spectra (280—320 nm) emitted by the flame, and the noise is decreased by about 90% when a screen is placed between the burner and the detector.

To overcome these limitations, a hydride generation method similar to that reported by Thompson and Thomerson [24] is coupled with a small argon—hydrogen—entrained air flame.

EXPERIMENTAL

Apparatus

Schematic diagrams of the apparatus and the specially manufactured two-slot burner are shown in Figs. 1 and 2. The burner head is situated so that the incident beam from the light source passes parallel to the burner slots. The sources used were Perkin-Elmer electrodeless discharge lamps operated at 10 W (As) and 5 W (Sb), as recommended, by a Perkin-Elmer Model 185-120 power supply. The light beam was focused by a quartz lens (34 mm diam., 60 mm focal length) and refocused by a concave mirror (65 mm diam., 55 mm focal length) just above the burner. The fluorescent radiation was detected directly by a solar-blind photomultiplier (HTV R166). A John Fluke power supply

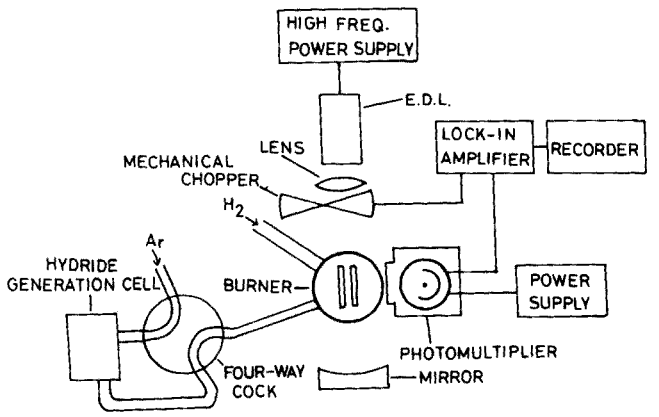

Fig. 1. Schematic diagram of the apparatus.

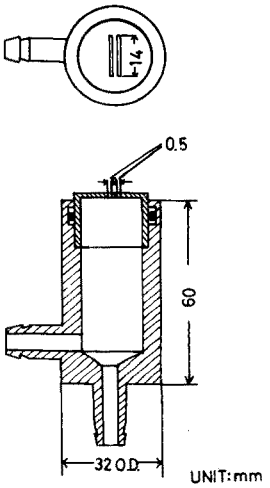

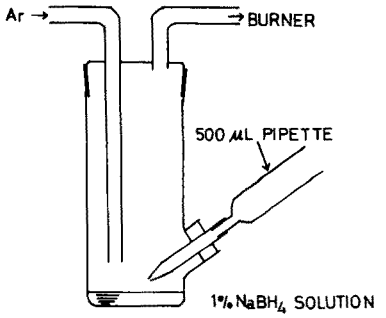

Fig. 2. Two-slot burner.

Fig. 3. Hydride generation cell.

(Model 412B) was used to provide high voltage (550 V) for the photomultiplier. The signals from the photomultiplier were fed into a lock-in amplifier (Princeton Applied Research Corp., Model HR-8) which was phased with a reference signal from a mechanical light chopper (Princeton Applied Research Corp., Model 125, chopping frequency: 27 Hz). The distance from the burner top to the center of the light beam was 1 cm and from the center of the burner slots to the photomultiplier was about 9 cm. The hydride generation cell (capacity, 90 ml), constructed from borosilicate glass, is shown in Fig. 3.

Reagents

Commercially available arsenic(III) and antimony(III) 1000-ppm standard solutions (Kanto Chemical Corp.), made from sodium arsenite and antimony trichloride, respectively, were used. An arsenic(V) 1000-ppm standard solution, prepared by dissolving sodium arsenate, was used when this technique was applied to the determination of arsenic in steel samples. Sodium borohydride solution (1%) was prepared, just before use, by dissolving sodium borohydride pellets (>98% pure; Alfa Inorganics). All other reagents were of analytical-reagent grade.

Procedure

The four-way stopcock was initially set for argon to pass through the bypass tube. Sodium borohydride solution (1%, 2 ml) was transferred to the hydride generation cell. A sample solution was taken by an Eppendorf 500-μl pipette, which was then set as shown in Fig. 3. Next, the four-way stopcock was set to allow argon to pass through the cell. The sample solution was injected into

the cell and the reduction products were supplied continuously to the flame by a constant flow of argon gas. The atomic fluorescence signals were recorded, and the peak heights were measured.

RESULTS AND DISCUSSION

The response to arsenic and antimony was independent of the hydrochloric acid concentration from 1 to 8 M; this is similar to the results reported earlier [13, 24].

To minimize the pressure increase in the cell and to prevent reagent contamination, all measurements were made with 1 M hydrochloric acid.

Effect of hydrogen flow rate

The effect of the hydrogen flow-rate on the noise level and signal intensity was measured. The argon flow-rate was kept constant at 1.0 l min^{-1}. The noise level dependence on the hydrogen flow-rate is shown in Fig. 4. The noise

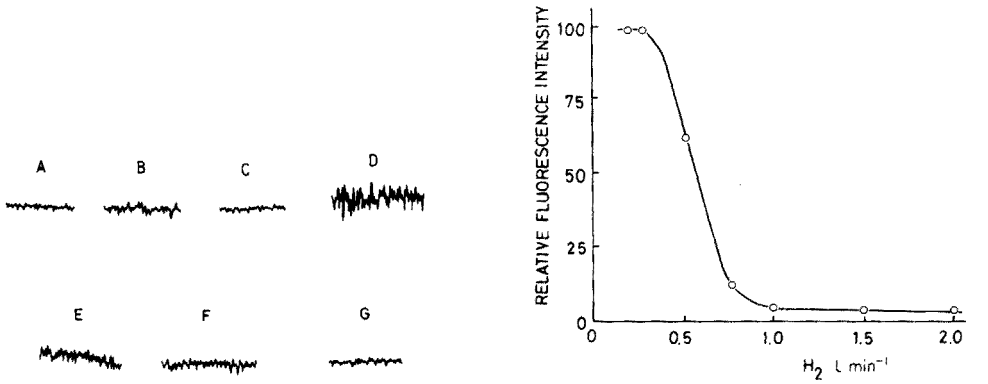

Fig. 4. Noise level dependence on the hydrogen flow-rate. Argon flow-rate, 1.0 l min^{-1}. A, detector box shutter closed. B, detector box shutter open. C, outdoor light cut off. Hydrogen flow-rates: D, 2.0 l min^{-1}; E, 1.0 l min^{-1}; F, 0.5 l min^{-1}; G, 0.25 l min^{-1}.

Fig. 5. Effect of the hydrogen flow-rate on arsenic fluorescence intensity. Argon flow-rate, 1.0 l min^{-1}.

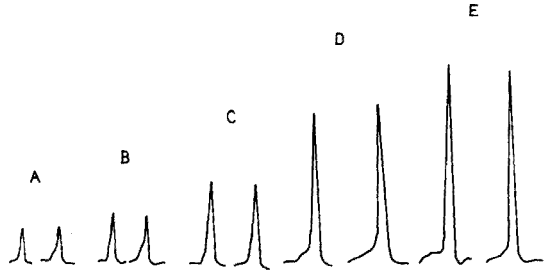

Fig. 6. Effect of the hydrogen flow-rate on antimony fluorescence signal. Argon flow-rate, 1.0 l min^{-1}. Hydrogen flow-rates: A, 0.7 l min^{-1}; B, 0.6 l min^{-1}; C, 0.45 l min^{-1}; D, 0.35 l min^{-1}; E, 0.25 l min^{-1}.

level increases slightly when the shutter of the detector box is opened but decreases to the initial level when outdoor light is cut off. The noise level suddenly increases when the flame is lit, but gradually decreases with decreasing hydrogen flow-rates. The noise level continues to decrease until it reaches the same level as that when the shutter of the detector box is closed. This occurs when the flow-rate decreases to 0.25 l min^{-1}. As reported previously [29], the decrease in noise level is closely related to decreasing OH band (280—320 nm) emission intensities.

The visible portion of the flame also decreased with decreasing hydrogen flow-rates. It was about 1 cm when the tip of a metallic wire dipped in a sodium chloride solution was placed in the flame (hydrogen flow-rate, 0.25 l min^{-1}). The flame, however, expanded slightly when the sample solution was injected into the cell.

The effects of the hydrogen flow-rate on arsenic and antimony fluorescence intensities are shown in Figs. 5 and 6, respectively. The signal intensity for each element increases with decreasing hydrogen flow rates. This phenomenon was not observed previously [29, 30], because the hydrogen flow-rate could not be decreased below 1.7 l min^{-1}, when the earlier hydride generation facility was used. This signal increase is probably caused by an increasing atom residence time in the light path and restriction of atoms in the small flame region.

The following measurements were made at flow rates of 0.25 l min^{-1} of hydrogen and 1.0 l min^{-1} of argon.

Detection limit and analytical working curve

The detection limits ($S:N = 2$) and reagent blanks for arsenic and antimony are shown in Table 1. The detection limits obtained with the former hydride generation cell are also given in Table 1. The improvement factors are 40 for arsenic and 30 for antimony. The detection limits obtained in this study cannot be compared directly with those reported previously because the light sources, the burner head, and the optical alignment are different. However, the small argon—hydrogen—entrained air flame plays an important role in improving the signal-to-noise ratio.

The analytical working curves for arsenic and antimony are shown in Fig. 7. The linear range covers four concentration decades from the detection limit;

TABLE 1

Detection limits and reagent blanks for As and Sb

Element	Detection limit (ng)		Reagent blank (ng)	
	Present	Previous	Present	Previous
As	0.05	2[29]	1	25[29]
Sb	0.1	3[30]	0.5	—

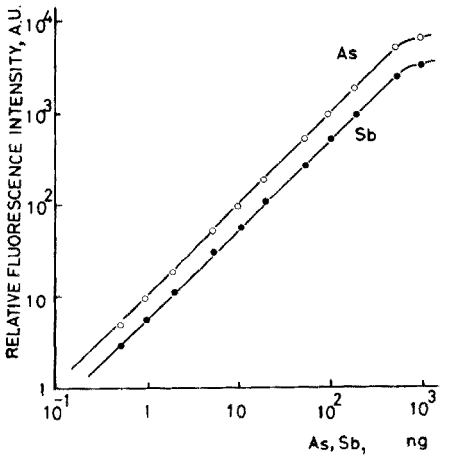

Fig. 7. Analytical working curves for arsenic and antimony.

this is about one decade superior to previous data [29, 30]. The relative standard deviation calculated from 7 peak-height measurements for 0.1 ppm arsenic solution(III) is 1.7%.

Determination of arsenic in steel samples

This technique was applied to the determination of arsenic in steel samples weighing ca. 0.1 g. The sample was weighed exactly and dissolved in 10 ml of aqua regia; 5 ml of perchloric acid was added and the solution was heated until white perchloric acid fumes were observed. To eliminate any interfering effects of co-existing elements, known to occur in the formation and evolution of arsine [25], a standard addition method was employed with 1000-ppm arsenic(V) solution as the standard. The results, shown in Table 2, are in good agreement with the certified values.

This technique is also applicable to other elements which form volatile hydrides, e.g. bismuth, germanium, lead, selenium, tin, and tellurium.

TABLE 2

Determination of arsenic in carbon steel samples (Japanese Standards of Iron and Steel)

Sample	Arsenic content (%)	
	Certified	Found[a]
No. 156-1	0.009	0.0093 (± 0.0003)
No. 157-1	0.020	0.019 (± 0.001)
No. 158-1	0.092	0.093 (± 0.003)

[a]Average of 4 determinations (± standard deviation).

REFERENCES

1 P. L. Larkins, R. M. Lowe, J. V. Sullivan and A. Walsh, Spectrochim. Acta, Part B, 24 (1969) 187.
2 T. J. Vickers and R. M. Vaught, Anal. Chem., 41 (1969) 175.
3 P. D. Warr, Talanta, 17 (1970) 543.
4 D. G. Mitchell and A. Johansson, Spectrochim. Acta, Part B, 25 (1970) 175.
5 P. L. Larkins, Spectrochim. Acta, Part B, 26 (1971) 477.
6 P. L. Larkins and J. B. Willis, Spectrochim. Acta, Part B, 26 (1971) 491.
7 R. C. Elser and J. D. Winefordner, Appl. Spectrosc., 25 (1971) 345.
8 T. J. Vickers, P. J. Slevin, V. I. Muscat and L. T. Farias, Anal. Chem., 44 (1972) 930.
9 V. I. Muscat, T. J. Vickers, W. E. Rippetoe and E. R. Johnson, Appl. Spectrosc., 29 (1975) 52.
10 E. F. Palermo, A. Montaser and S, R. Crouch, Anal. Chem., 46 (1974) 2154.
11 W. Holak, Anal. Chem., 41 (1969) 1712.
12 E. F. Dalton and A. J. Malonoski, At. Absorpt. Newsl., 10 (1971) 92.
13 F. J. Fernandez and D. C. Manning, At. Absorpt. Newsl., 10 (1971) 36.
14 R. C. Chu, G. P. Barron and P. A. W. Baumgarner, Anal. Chem., 44 (1972) 1476.
15 F. E. Lichte and R. K. Skogerboe, Anal. Chem., 44 (1972) 1480.
16 R. S. Braman, L. L. Justen and C. C. Foreback, Anal. Chem., 44 (1972) 2195.
17 Y. Yamamoto, T. Kumamaru, Y. Hayashi and R. Tsujino, Anal. Lett., 5 (1972) 419.
18 Y. Yamamoto, T. Kumamaru, Y. Hayashi and T. Kamada, Bunseki Kagaku, 22 (1973) 876.
19 F. J. Schmidt and J. L. Royer, Anal. Lett., 6 (1973) 17.
20 Kwok-Tai Kan, Anal. Lett., 6 (1973) 603.
21 Y. Yamamoto, T. Kumamaru, Y. Hayashi and T. Kamada, Bull. Chem. Soc. Jpn., 46 (1973) 2604.
22 E. N. Pollock and S. J. West, At. Absorpt. Newsl., 12 (1973) 6.
23 P. D. Goulden and P. Brooksbank, Anal. Chem., 46 (1974) 1431.
24 K. C. Thompson and D. R. Thomerson, Analyst, 99 (1974) 595.
25 A. E. Smith, Analyst, 100 (1975) 300.
26 K. C. Thompson, Analyst, 100 (1975) 307.
27 T. Maruta and G. Sudoh, Anal. Chim. Acta, 77 (1975) 37.
28 J. A. Fiorino, J. W. Jones and S. G. Capar, Anal. Chem., 48 (1976) 120.
29 K. Tsujii and K. Kuga, Anal. Chim. Acta, 72 (1974) 85.
30 K. Tsujii, K. Kuga and I. Sugaya, Chem. Lett., (1975) 695.
31 R. M. Dagnall, K. C. Thompson and T. S. West, Talanta, 15 (1968) 677.
32 D. Kolihova and V. Sychra, Anal. Chim. Acta, 59 (1972) 477.

Analytica Chimica Acta, 97 (1978) 59—68

MOLEKÜLABSORPTIONSSPEKTROMETRIE BEI ELEKTROTHERMISCHER VERDAMPFUNG IN EINER GRAPHITROHRKÜVETTE I. GRUNDLAGEN DER METHODE UND UNTERSUCHUNGEN ÜBER DIE MOLEKÜLABSORPTION VON Ga- UND In-HALOGENIDEN

K. DITTRICH

Sektion Chemie der Karl-Marx-Universität Leipzig, Analytisches Zentrum, 701 Leipzig (D.D.R.)

(Eingegangen am 19. Juli 1977)

ZUSAMMENFASSUNG

Es wird ein neues Analysenprinzip — die Molekülabsorptionsspektrometrie (MAS) durch elektrothermische Verdampfung einfacher Moleküle in einem Graphitrohratomisator — vorgeschlagen. Die Absorptionsspektren der GaX- und InX-Moleküle wurden gemessen. Starke Absorptionsbanden wurden für folgende Moleküle gefunden: GaO, GaF, GaCl, InO, InF, InCl, InBr. Das GaBr-Molekül zeigt nur ein schwaches Kontinuum. Keine Absorptionsbanden wurden für die GaJ- und InJ-Moleküle gefunden, weil diese Moleküle im Plasma des Graphitrohres nicht existieren. Die Resultate werden mit Werten aus der Literatur verglichen. Schlußfolgerungen für die Nutzung der MAS zur analytischen Bestimmung von Halogenspuren werden gezogen.

SUMMARY

Molecular absorption spectrometry by electrothermal volatilization in a graphite furnace. Part 1. Basis of the method and studies of the molecular absorption of gallium and indium halides

A new principle of analysis — molecular absorption spectrometry (m.a.s.) by electrothermal volatilization of simple molecules in a graphite furnace — is proposed. The absorption spectra of GaX and InX molecules were measured (X = halogen). Strong absorption bands were found for GaO, GaF, GaCl, InO, InF, InCl and InBr. The GaBr molecule showed only a weak continuum. Absorption bands were not found for the GaI and InI species, which do not exist in the plasma of the graphite tube. The results are compared with literature data. The use of m.a.s. for determinations of traces of halogens is outlined.

Seit der Einführung der Graphitrohrküvette für die Atomabsorptionsspektrometrie (AAS) durch L'vov [1] und die Entwicklung des Prinzips zur Routinemethode durch Massmann [2] hat sich diese Technik wegen ihres ausgezeichneten Nachweisvermögens zur führenden Einzelelementbestimmungsmethode für Spuren entwickelt.

In den vergangenen Jahren wurde begonnen, die Verdampfungs- und Atombildungsprozesse in der Graphitrohrküvette eingehend zu untersuchen.

Dabei richtet sich das Interesse in jüngster Zeit auch auf die spektrale Abhängigkeit der die AAS störenden, unspezifischen Molekülabsorption (MA). So wiesen Massmann und Gücer [3, 4] auf Probleme der Nichtkompensierbarkeit von Molekülabsorptionen hin, wenn schon eine starke Aufspaltung der Bande in einzelne Rotationslinien vorliegt. Über Störungen durch die Molekülabsorption von Alkalihalogeniden bei der flammenlosen AAS und deren spektrale Abhängigkeit berichten Culver und Surles [5].

Zur Optimierung analytischer Verfahren für die Spurenanalyse durch AAS in $A^{III}B^{V}$-Halbleitermaterialien führten wir Untersuchungen über die Verdampfung und Atombildung sowohl der Spuren als auch der Matrices (GaAs, GaP, InAs) in der Graphitrohrküvette durch [6, 7]. Die dabei festgestellten Resultate über die spektrale Abhängigkeit der Molekülabsorptionen und vor allem deren hohe Absorptionswerte führten uns zu dem Schluß, daß eine analytische Nutzung der Molekülabsorptionsspektrometrie für die Spurenbestimmung anionischer Komponenten bei Verwendung von Graphitrohrküvetten möglich ist. Es wird vorgeschlagen, in Analogie zur AAS für diese neue Methode die Abkürzung MAS mit elektrothermischer Verdampfung zu verwenden.

Einige Untersuchungen über die MA von Indiumhalogeniden in Flammen wurden bereits durchgeführt. Haraguchi und Fuwa [8] berichten über das InCl-Absorptionsspektrum in Flammen im Zusammenhang mit der Depression der In-Atomabsorption (In-AA) durch HCl. Über Rekombinationsprozesse zwischen In und Cl in Flammen ist eine Miteilung von Haraguchi et al. [9] erschienen. Weitere Untersuchungen wurden von den gleichen Autoren über chemische Interferenzen bei der In-AA und Cu-AA durch Cl- und Br-Atome durchgeführt [10]. Auch Nakahara und Musha [11] berichten über die InCl-MA. Erklärungen für die Ursachen der InO-MA werden von Haraguchi et al. [12] gegeben. Analytische Anwendungen für die Bestimmung von Halogenen fanden diese Methoden bisher nicht. Lediglich die Molekülemission von Indiumhalogeniden wird für die Bestimmung von Halogenen ausgenutzt [13].

In dieser ersten Mitteilung soll über die Molekülabsorptionsspektren der Gallium- und Indiumhalogenide, die bei Verdampfung entsprechender Lösungsrückstände in der Graphitrohrküvette erhalten werden, berichtet werden. Die folgenden Mitteilungen sind den analytischen Anwendungen gewidmet.

EXPERIMENTELLES

Apparatur. Zweikanal-Zweistrahl-AA-Spektrometer Typ 811 (Jarrell-Ash, USA), H_2-Hohlkathodenlampe (H_2-HKL) 30 mA. Spektrale Bandbreite: 420—210 nm, 0,2 nm; 210—195 nm, 0,4 nm; 195—190 nm, 1,0 nm. Die verschiedenen spektralen Bandbreiten waren wegen der unterschiedlichen Lichintensität der H_2-HKL erforderlich. Graphitrohrküvette Typ 1268 (Beckman); Thermische Bedingungen: Siehe Abbildungen.

Reagenzien. Die Ga^{3+}- und In^{3+}-Stammlösungen (100 mg Metall ml^{-1}) wurden durch Auflösen hochreiner Metalle (99,9999%) in konz. HNO_3 (suprapur, Merck), Abdampfen der Säure und Aufnehmen in 1 M HNO_3 hergestellt. Außerdem wurden verwendet: 2 M NaOH- und 0,1 M NaF-, NaCl-, NaBr- und NaJ-Lösungen. Durch Mischen und Verdünnen wurden die Untersuchslösungen hergestellt. Zur Vermeidung von Halogenidverlusten bei der Eindampfung der Lösungen in der Graphitrohrküvette wurde vorher mit NaOH neutralisiert. Das Ionenverhältnis der Lösungen (M:X) war jeweils 1:1 ($M = Ga^{3+}, In^{3+}$; $X = F^-, Cl^-, Br^-, J^-$).

Verfahrensweise. Volumina von 10 µl wurden mit einer Eppendorf-Pipette in die Graphitrohrküvette gegeben, getrocknet und verdampft. Die Aufnahme der Spektren erfolgte durch Einzelmessungen bei verschiedenen Wellenlängen. Die Wellenlängendifferenzen für die einzelnen Messungen wurden entsprechend der Spektrenstruktur gewählt: 5—10 nm für wenig strukturierte Gebiete, 0,1—0,2 nm für stark strukturierte Gebiete. Diese Verfahrensweise ermöglichte eine Spektrenaufnahme in vertretbarer Zeit, birgt jedoch die Gefahr in sich, daß schmale Banden der Spektren nicht festgestellt werden.

RESULTATE UND DISKUSSION

In der Abb. 1 sind die Spektren für Ga-haltige und in der Abb. 2 für In-haltige Lösungen dargestellt. In der Tab. 1 wurden die möglichen Übergänge der Moleküle nach [14] charakterisiert und die spektroskopischen Ergebnisse mit den Dissoziationsenergien (E_D) der Moleküle verglichen.

Spektren halogenidfreier Lösungen des Galliums und Indiums

In den Abb. 1 A und 2 A sind die Spektren für halogenidfreie Lösungen des Galliums und Indiums dargestellt. Für Ga-haltige Lösungen ist eine Bande zwischen 220 und 270 nm (Max. 240 nm) und ein starker Anstieg unterhalb von 205 nm und für In-haltige Lösungen sind 2 Banden zwischen 250 und 300 nm (Max. 270 nm) und zwischen 200 und 230 nm (Max. 206 nm) zu erkennen. Die Spektren 1 (in Abwesenheit von Na^+, 1 M HNO_3 Medium) und Spektren 2 (in Gegenwart von $NaNO_3$, neutrales Medium) zeigen nur unwesentliche Unterschiede, so daß davon ausgegangen werden kann, daß lediglich Ga- und In-haltige Moleküle für die Absorption verantwortlich sind. Die Identifizierung der Banden durch Vergleich mit Literaturwerten (s. Tab. 1) war nicht möglich. In älteren Veröffentlichungen [15] wurden Banden zwischen 220 und 270 nm (Ga) und 250—300 nm (In) der GaCl-MA bzw. InCl-MA zugeschrieben. In Übereinstimmung mit [8] kann diese Angabe widerlegt werden. Somit kommen folgende Moleküle als Ursache für die Absorption in Frage: GaO, InO, GaOH, InOH, GaN, InN. Davon können die N-haltigen Moleküle ausgeschlossen werden, denn auch in Abwesenheit von Nitrat treten die Banden auf [6]. Über GaOH- und InOH-Moleküle und deren Stabilität sind keine Angaben bekannt. Am wahrschein-

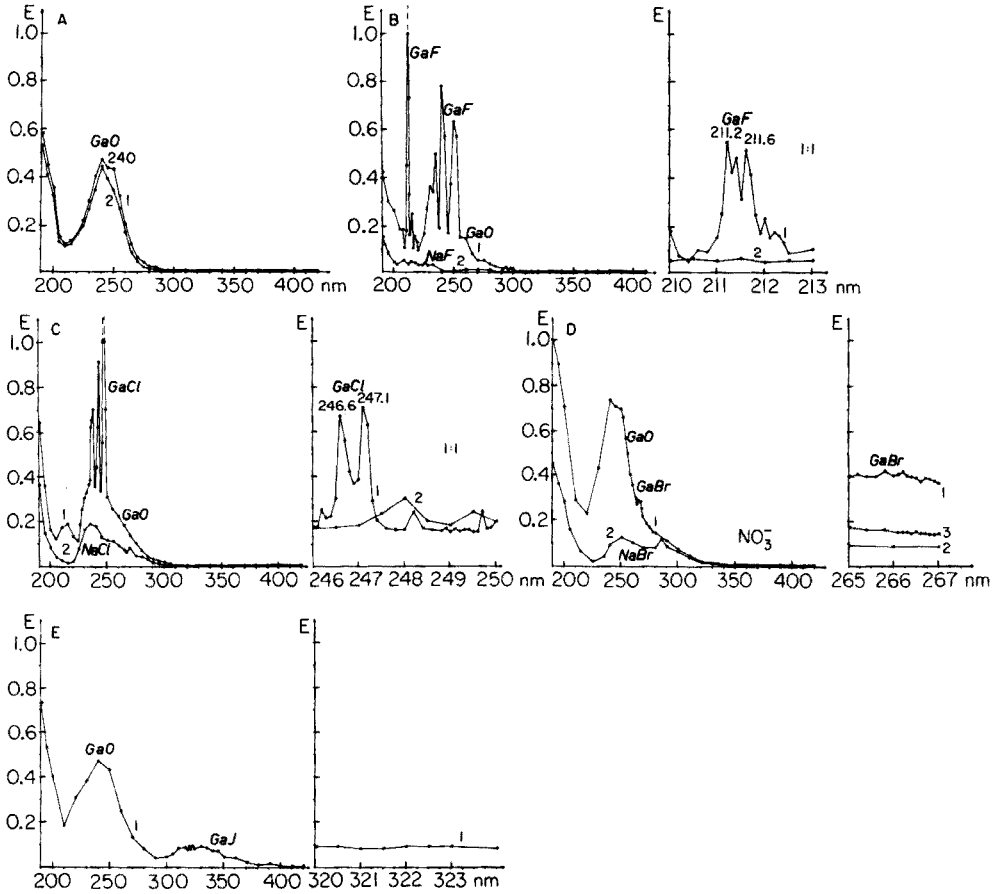

Abb. 1. Molekülabsorptionsspektren Ga-haltiger Moleküle bei Verdampfung der Substanzen in einer Graphitrohrküvette.

(A) Kurve 1: 2 µg Ga^{3+}/10 µl. Kurve 2: 2 µg Ga^{3+}/2 µg Na^{+}/10 µl.

(B) Kurve 1. 2 µg Ga^{3+}/2,5 µg Na^{+}/0,53 µg F^{-}/10 µl. Kurve 2: 2.5 µg Na^{+}/0,53 µg F^{-}/10 µl.

(C) Kurve 1: 2 µg Ga^{3+}/2,5 µg Na^{+}/1 µg Cl^{-}/10 µl. Kurve 2: 2.5 µg Na^{+}/1 µg Cl^{-}/10 µl.

(D) Kurve 1: 2 µg Ga^{3+}/2,5 µg Na^{+}/2,2 µg Br^{-}/10 µl. Kurve 2: 2,5 µg Na^{+}/2,2 µg Br^{-}/10 µl. Kurve 3: 2 µg Ga^{3+}/2,5 µg Na^{+}/10 µl.

(E) Kurve 1: 2 µg Ga^{3+}/2,5 µg Na^{+}/3,6 µg J^{-}/10 µl.

Die Lösungen für aufgelöste Spektren (rechte Seite) waren jeweils 1:1 mit H_2O verdünnt.

(A) Kurve 1: Medium: 1 M HNO_3. (A) Kurve2 u. B—E: Medium: Neutral (NO_3^{-}).

Thermische Bedingungen der Graphitrohrküvette: (A—D): Trockn.: 30 s/140°C, Verasch.: 15 s/1200°C, Molekülbildung/Verdampfung: 10 s/3150°C. (E): Trockn.: 30 s/140°C, Verasch.: 15 s/380°C, Molekülbildung/Verdampfung: 10 s/2800°C.

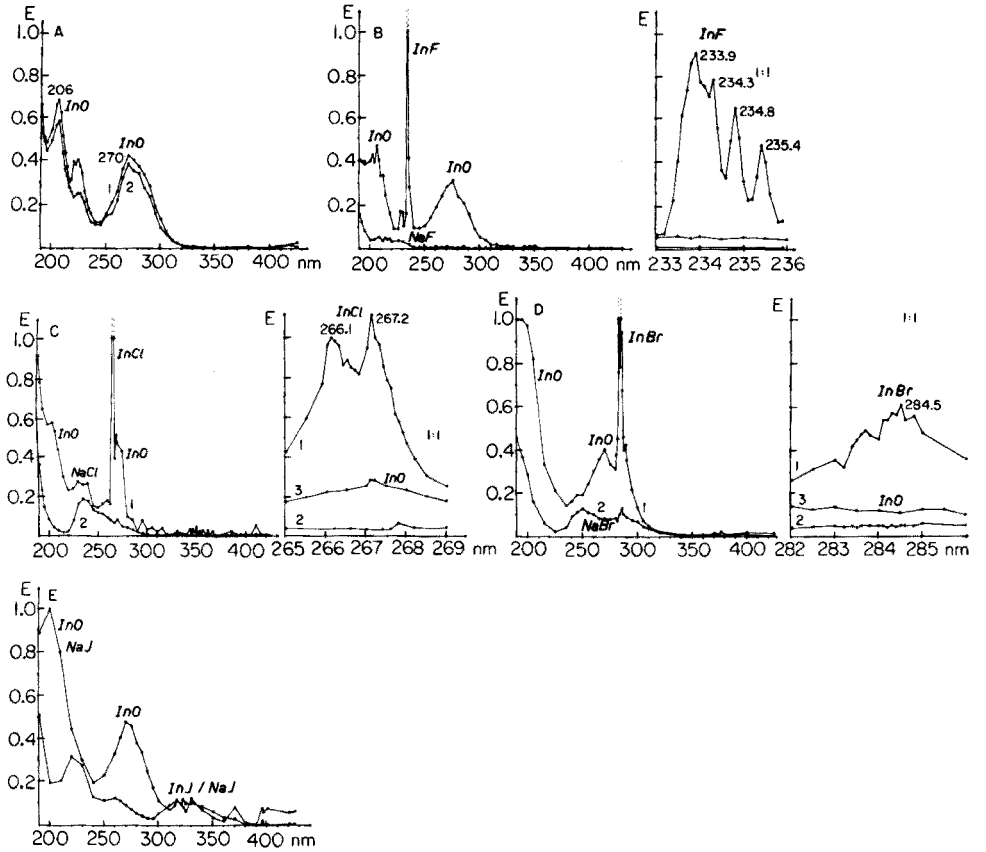

Abb. 2. Molekülabsorptionsspektren In-haltiger Moleküle bei Verdampfung der Substanzen in einer Graphitrohrküvette.
(A) Kurve 1: 3,3 μg In^{3+}/10 μl. Kurve 2: 3,3 μg In^{3+}/3 μg Na^+/10 μl
(B) Kurve 1: 3,3 μg In^{3+}/3,5 μg Na^+/0,53 μg F^-/10 μl. Kurve 2: 3,5 μg Na^+/0,53 μg F^-/10 μl.
(C) Kurve 1: 3,3 μg In^{3+}/3,5 μg Na^+/1 μg Cl^-/10 μl. Kurve 2: 3,5 μg Na^+/1 μg Cl^-/10 μl. Kurve 3: 1,6 μg In^{3+}/1,5 μg Na^+/10 μl.
(D) Kurve 1: 3,3 μg In^{3+}/3,5 μg Na^+/2,2 μg Br^-/10 μl. Kurve 2: 3,5 μg Na^+/2,2 μg Br^-/10 μl. Kurve 3: 1,6 μg In^{3+}/1,5 μg Na^+/10 μl.
(E) Kurve 1: 3,3 μg In^{3+}/3,5 μg Na^+/3,6 μg J^-/10 μl. Kurve 2: 3,5 μg Na^+/3,6 μg J^-/10 μl.
(A) Kurve 1: Medium: 1 M HNO_3. (A) Kurve 2: B—E: Medium: Neutral (NO_3^-).
Thermische Bedingungen der Graphitrohrküvette: (A—C) Trockn.: 30 s/140°C, Verasch.: 15 s/1200°C, Molekülbildung/Verdampfung: 10 s/3150°C. (D—E) Trockn.: 30 s/140°C, Verasch.: 15 s/380°C, Molekülbildung/Verdampfung: 10 s/2300°C.

lichsten ist es, daß es sich um Banden des GaO- bzw. InO-Moleküls handelt, die durch die reduzierende Wirkung des Kohlenstoffs bei höheren Temperaturen in der Graphitrohrküvette entstehen. Ausgehend von der Analogie der Spektren der Abb. 1 A und 2 A und der Verschiebung aller Banden der

TABELLE 1

Zustände, Übergänge und Dissoziationsenergien zweiatomiger Moleküle des Galliums und Indiums [14] im Vergleich mit den Wellenlängen der gefundenen Extinktionsmaxima

Molekül-Dissoziationsenergie (eV)	Grundzustand	angeregter Zustand	Wellenlängengebeit (nm)	gefundene Ergebnisse	
				Wellenlänge der maximalen Extinktion (nm)	aufgenommener Energiebetrag (eV)
GaF	$X^1\Sigma_0^+$	$A^3\Pi_0^+$	302,0—295,0		
5,98		$B^3\Pi_1$	304,5—292,0		
		$C^1\Pi$	220,0—209,4	211,2	5,87
GaCl	$X^2\Sigma_0^+$	$A^3\Pi_0^+$	347,0—325,4		
4,92		$B^3\Pi_1$	343,0—322,1		
		$C^1\Pi$	270,0—242,0	246,6; 247,1	5,02
		C'	241,7		
GaBr	$X^1\Sigma_0^+$	$A^3\Pi_0^+$	361,7—345,3		
4,31		$B^3\Pi_1$	356,8—344,0		
		$C^1\Pi$	304,4—268,0	265 ?	4,7
GaJ	$X^1\Sigma_0^+$	$A^3\Pi_0^+$	414,0—381,0		
3,47		$B^3\Pi_1$	414,0—381,0		
		$C^1\Pi$	306,5	—	—
GaO	$X^2\Sigma$	—	490,0—430,0		
3,91		$^2\Sigma$	413,0—350,0	240,0	5,16
InF	$X^1\Sigma_0^+$	$A^3\Pi_0^+$	320,0—304,0		
5,25—5,42		$B^3\Pi_1$	335,5—312,5		
		$C^1\Pi$	253,0—227,5	233,9	5,30
		?	213,0—210,0		
		?	223,0—218,5		
InCl	$X^1\Sigma_0^+$	$A^3\Pi_0^+$	364,1—338,0		
4,43—4,5		$B^3\Pi_1$	364,1—338,0		
		$C^1\Pi$	296,3—265,0	266,1; 267,2	4,66; 4,64
		C'	265,0—260,0		
		D	210,0		
InBr	$X^1\Sigma_0^+$	$A^3\Pi_0^+$	385,2—364,2		
3,93—4,2		$B^3\Pi_1$	372,7—356,8		
		$C^1\Pi$	308,3—285,2	284,5	4,36
InJ	$X^1\Sigma_0^+$	$A^3\Pi_0^+$	429,3—394,8		
3,42		$B^3\Pi_1$	429,3—394,8		
		$C^1\Pi$	318,0	—	—
InO	?	?	476,3—384,7	206,0; 270,0	6,01; 4,59
3,32					

GaX-Moleküle (X = Halogen) gegenüber denen der InX-Moleküle nach kürzeren Wellenlängen (Ursache ist der kleinere Atom- und Ionenradius des Ga), kann man annehmen, daß der starke Anstieg der Extinktion unterhalb 205 nm (Abb. 1 A) auf eine zweite GaO-Bande zurückzuführen ist.

Vergleicht man die Dissoziationsenergien für GaO und InO mit den an der Stelle der maximalen Absorption aufgenommenen Energiewerten (Tab. 1), so liegen diese aufgenommenen Energiewerte beträchtlich über den der

Literatur entnommenen Dissoziationsenergien. Diese angeregten Zustände sind demzufolge instabil. Dies würde auch erklären, daß diese Übergänge in Emission bisher nicht beobachtet wurden. Allerdings muß bemerkt werden, daß über GaO-und InO-Banden nur sehr wenig Angaben vorliegen. Einige Erklärungen für die Ursachen der InO-Bande bei 270 nm wurden jedoch bereits gegeben [12].

Spektren des GaF und InF

Die Abb. 1 B und 2 B enthalten die Spektren für Lösungen des Na^+, F^- und NO_3^- in Gegenwart und Abwesenheit von Gallium und Indium. Es sind starke Absorptionsbanden zu erkennen, die auf GaF- und InF-Moleküle zurückzuführen sind. Beide Moleküle entstehen durch die reduzierende Wirkung des Kohlenstoffs der Graphitrohrküvette bei den angewandten hohen Temperaturen. In Gegenwart von GaF-Molekülen werden zwei Banden beobachtet: 210—220 nm und 220—245 nm. Die erste Bande ist als C-Bandensystem in der Literatur beschrieben (vgl. Tab. 1). Die zweite Bande mit Maxima bei 235, 240 und 250 nm ist bisher nicht beschrieben und vorläufig nicht eindeutig zu charakterisieren. Es kann sich hierbei u.U. auch um die Absorption eines dreiatomigen Moleküls handeln. Eine Verunreinigung durch Cl ist auszuschließen, da kein direktes Zusammenfallen mit den Maxima der GaCl-MA (Abb. 1 C) vorliegt. Diese 2. Bande überlappt mit der GaO-Bande.

Für InF-Moleküle wird lediglich die dem C-Bandesystem entsprechende Bande zwischen 225 und 240 nm beobachtet.

Die beiden intensivsten Banden (GaF Max.: 211,2 nm und InF Max.: 233,9 nm) liegen genau in Minimum zwischen den beiden GaO- bzw. InO-Banden. Beide Banden zeigen eine Feinstruktur, die wegen des zu geringen Auflösungsvermögens des Spektrometers nicht besser dargestellt werden konnte (siehe rechte Seite der Abb. 1 B und 2 B).

Ein Vergleich der Anregungsenergien an der Stelle der maximalen Extinktion mit den beschriebenen Dissoziationsenergien für GaF und InF (s. Tab. 1) zeigt, daß in beiden Fällen die aufgenommenen Energiewerte nicht ausreichen, das GaF- bzw. InF-Molekül zu zerstören.

Die trotz des eingesetzten Atomverhältnisses (M: F = 1:1) auftretenden GaO- und InO-Banden geben an, daß nicht das gesamte Ga bzw. In als GaF- bzw. InF-Molekül vorliegt.

Eine analytische Ausnutzung der Ergebnisse für Spurenbestimmungen von Fluoridionen ist möglich [16], denn die Störungen durch die geringe NaF-Absorption zwischen 210 und 240 nm, deren Ursache bisher nicht bekannt ist (vgl. auch [5]), sind zu vernachlässigen bzw. zu kompensieren.

Spektren des GaCl und InCl

Die Abb. 1 C und 2 C enthalten die Spektren für Lösungen des Na^+, Cl^- und NO_3^- in Gegenwart und Abwesenheit von Gallium und Indium. Beide Abbildungen zeigen starke Absorptionsbanden, die auf die C-Bandensysteme

des GaCl-Moleküls (235—250 nm) bzw. des InCl-Moleküls (260—280 nm) zurückzufuhren sind. Auch diese einwertigen Moleküle des Galliums und Indiums entstehen durch die reduzierende Wirkung des Kohlenstoffs der Graphitrohrküvette; Beide Banden überlappen mit den entsprechenden GaO- bzw. InO-Banden. Es treten jeweils zwei nahezu gleichwertige Maxima in den Spektren auf: GaCl-MA: 246,6 und 247,1 nm; InCl-MA: 266,1 und 267,2 nm (vgl. rechte Seite der Abb. 1 C und 2 C). Vergleicht man die Dissoziationsenergien der GaCl- bzw. InCl-Moleküle mit den Energiewerten, die an der Stelle der maximalen Extinktion aufgenommen werden, so stellt man fest, daß beide aufgenommenen Energiewerte größer als die beschriebenen Dissoziationsenergien sind (s. Tab. 1). Demzufolge entstehen, wie im Fall des GaO und InO, durch die Absorption instabile Teilchen. Auch in diesen Fällen kann durch Spektrenvergleich (Abb. 1 A mit 1 C und Abb. 2 A mit 2 C) geschlußfolgert werden, daß trotz des vorgegebenen Ionenverhältnisses von 1:1 nicht alle Ga-bzw. In-Atome in Plasma als GaCl-bzw. InCl-Moleküle sondern auch als GaO- und InO-Moleküle vorliegen. Über das Ausmaß dieser Verteilungen bzw. die Lage der Gleichgewichte können bis jetzt keine Aussagen gemacht werden.

Eine analytische Ausnutzung der Ergebnisse für die Spurenbestimmung von Chloridionen ist nach unserer Auffassung trotz der Bandenüberlappung möglich. Entsprechende Untersuchungen sind vorgesehen. Auch die im Gebiet zwischen 220 und 260 nm auftretende NaCl-Absorption (vgl. auch [5]) dürfte keine entscheidenden Störungen bewirken.

Spektren des GaBr und InBr

Die Abb. 1 D und 2 D enthalten die Spektren für Lösungen des Na^+, Br^- und NO_3^- in Gegenwart und Abwesenheit von Gallium und Indium.

Wie aus der Tab. 1 zu entnehmen ist, sind Absorptionsbanden zwischen 268 und 304 nm für GaBr und zwischen 285 und 308 nm für InBr zu erwarten. Die Abb. 1 D zeigt, daß keine scharfe und intensive GaBr-Bande beobachtet wird. Im Gebiet zwischen 265 und 267 nm bewirkt die Gegenwart von Br^- eine stärkere Absorption, die u.E. vom GaBr-Molekül verursacht wird. Außerdem tritt im Gebiet zwischen 220 und 280 nm gegenüber Br^--freien Lösungen eine Verstärkung der als GaO-MA gekennzeichneten Absorption auf. Ein Vergleich der bei 265 nm aufgenommenen Energie mit der Dissoziationsenergie des GaBr-Moleküls (s. Tab. 1) zeigt, daß die Dissoziationsenergie erheblich kleiner ist.

In Gegenwart von In^{3+} tritt eine intensive InBr-Bande mit einem Maximum bei 284,5 nm auf (vgl. Abb. 2 D). Ähnlich wie die InCl-Bande überlappt auch diese Bande mit der InO-Bande. Aus der Tab. 1 geht hervor, daß die bei 284,5 nm aufgenommene Energie zwar auch größer als die in der Literatur beschriebene Dissoziationsenergie für das InBr-Molekül ist. Die Differenz zwischen beiden Energiewerten ist jedoch kleiner als beim GaBr-Molekül. Es ist auch zu berücksichtigen, daß in diesem Fall bei einer niedrigeren Verdampfungstemperatur gearbeitet werden konnte, da Indium einen

niedrigeren Siedepunkt als Gallium hat. Damit wird auch die thermische Dissoziation der InBr-Moleküle im Plasma eingeschränkt. In beiden Fällen ist außerdem im Spektralgebiet zwischen 240 und 300 nm eine Absorption durch das NaBr-Molekül zu beobachten. Da die NaBr-Absorption jedoch nicht intensiv ist, sind keine Störungen zu erwarten.

Es ist zu vermuten, daß eine analytische Nutzung der Ergebnisse zur Bestimmung von Br^- nur im Fall der InBr-MA möglich ist.

Spektren des GaJ und InJ

Die Abb. 1 E und 2 E enthalten die Spektren für Lösungen des Na^+, J^- und NO_3^- in Gegenwart und Abwesenheit von Gallium und Indium. Entsprechend der Tab. 1 sind Kontinua in Absorption mit Maxima bei 306,5 nm für das GaJ-Molekül und bei 318 nm für das InJ-Molekül zu erwarten. In beiden Fällen werden von uns keine Absorptionsbanden beobachtet. Die Bande zwischen 300 und 350 nm, die auch in Abwesenheit von Gallium auftritt (vgl. auch Abb. 2 E) wird hauptsächlich durch NaJ- weniger durch GaJ-Moleküle verursacht. Aus der Abb. 2 E geht hervor, daß im vermuteten Bandengebiet eine strukturierte Absorption geringen Ausmaßes auftritt, die auf eine Beteiligung des InJ-Moleküls schließen läßt. Es ist zu schlußfolgern, daß sowohl das GaJ- als auch das InJ-Molekül (trotz der milderen thermischen Bedingungen) im Plasma dissoziieren. Vergleicht man außerdem die Dissoziationsenergie der Moleküle mit den bei den erwarteteten Maxima aufzunehmenden Energiebeträgen (s. Tab. 1), so stellt man fest, daß die Dissoziationsenergie erheblich niedriger liegt. Möglichkeiten für die analytische Bestimmung von J^- ergeben sich somit nicht.

Allgemeine Schlußfolgerungen

1. Intensive Absorptionsbanden wurden für GaF-, GaCl-, InF-, InCl- und InBr-Moleküle gefunden. Die Ergebnisse zeigen, daß die in der AAS gebräuchliche Graphitrohrküvette für die Messung von Molekülabsorptionsspektren eingesetzt werden kann.

2. Alle gefundenen intensiven Molekülabsorptionsbanden gehören zum C-Bandensystem der GaX-bzw. InX-Moleküle. Für die A- und B-Bandensysteme (vgl. Tab. 1, Abb. 1 u. 2) wird in keinem Fall eine intensive Absorption beobachtet, obwohl gerade diese Banden für die analytische Bestimmung der Halogene auf der Basis der Emission angewendet wurden. Die Ursachen für diese Intensitätsunterschiede können noch nicht angegeben werden.

3. Die unter 1. genannten Molekülabsorptionen lassen eine analytische Nutzung zu. Damit ist in Erweiterung des Prinzips der AAS mit elektrothermischer Verdampfung eine direkte Bestimmung der Halogene F, Cl und Br möglich. Es ist jedoch damit zu rechnen, daß eine erhebliche Beeinflussung der Molekülbildung und damit der MA-Signalintensität durch die Matrix und die Plasmatemperatur erfolgt. Über die Ergebnisse entsprechender Untersuchungen wird in Kürze berichtet.

LITERATUR

1 B. V. L'vov, Spectrochim. Acta, 17 (1961) 761.
2 H. Massmann, Spectrochim. Acta Part B, 23 (1968) 215.
3 H. Massmann und S. Gücer, Spectrochim. Acta Part B, 29 (1974) 283.
4 S. Gücer, H. Massmann und Z. El Gohary, Chim. Acta Turc., 4 (1976) 1.
5 B. R. Culver und T. Surles, Anal. Chem., 47 (1975) 920.
6 K. Dittrich, Talanta, im Druck.
7 K. Dittrich, Talanta, im Druck.
8 H. Haraguchi und K. Fuwa, Chem. Lett., (1972) 913.
9 H. Haraguchi, M. Siraishi und K. Fuwa, Chem. Lett., (1973) 251.
10 H. Haraguchi und K. Fuwa, Bull. Chem. Soc. Jpn., 48 (1975) 3056.
11 T. Nakahara und S. Musha, Anal. Chim. Acta, 80 (1975) 47.
12 H. Haraguchi, N. Furuta, E. Yoshimura und K. Fuwa, Anal. Chem., 48 (1976) 2066.
13 B. Gutsche und R. Herrmann, Z. Anal. Chem., 249 (1970) 168; B. Gutsche, K. Rüdiger und R. Herrmann, Z. Anal. Chem., 285 (1977) 103; G. Henrion und D. Marquardt, Z. Chem., 17 (1977) 28.
14 B. Rosen, Spectroscopic Data relative to Diatomic Molecules, Bd. 17 aus International Tables of selected constants, Pergamon Press, Oxford, 1970, S. 148—153 und S. 225—231.
15 E. Miescher und H. Wehrli, Helv. Physic. Acta, 6 (1933) 256; 7 (1934) 298.
16 K. Dittrich, Anal. Chim. Acta, 97 (1978) 69.

Analytica Chimica Acta, 97 (1978) 69—80

MOLEKÜLABSORPTIONSSPEKTROMETRIE BEI ELEKTROTHERMISCHER VERDAMPFUNG IN EINER GRAPHITROHRKÜVETTE II. BESTIMMUNG VON FLUORIDSPUREN IN MIKROVOLUMINA DURCH DIE MOLEKÜLABSORPTION VON GaF-MOLEKÜLEN

K. DITTRICH

Sektion Chemie der Karl-Marx-Universität Leipzig, Analytisches Zentrum, 701 Leipzig (D.D.R.)

(Eingegangen am 19. Juli 1977)

ZUSAMMENFASSUNG

Eine direkte Bestimmungsmethode von Fluoridspuren durch Messung der GaF-MA in einem Graphitrohratomisator wird beschrieben. Die apparativen Bedingungen (Kompensation der unspezifischen Absorption, Temperaturen der Veraschungsphase und der Phase der Verdampfung/Molekülbildung) wurden optimiert. Der Einfluß der Ga^{3+}- und Na^{+}-Konzentration und der Konzentration verschiedener Säuren auf die Bestimmung wurde untersucht und diskutiert. Höhere Konzentrationen an Ga^{3+}-Ionen bewirken eine höhere Konzentration der GaF-Moleküle im Plasma des Graphitrohres. Höhere Na^{+}-Konzentrationen bewirken einen geringeren Verlust an HF während der Trocknungsphase. Die Nachweisgrenze (3 s) ist 1,6 ng F^{-}/10 µl; die reziproke Empfindlichkeit ist 0,8 ng F^{-}/10 µl bezogen auf 0,01 E. Der Einfluß von Cl^{-}, Br^{-}, J^{-}, SO_4^{2-}, BO_3^{3-}, SiO_3^{2-}, Li^{+}, K^{+}, Be^{2+}, Mg^{2+}, Ca^{2+}, Al^{3+}, In^{3+}, Zn^{2+}, Cd^{2+} und Fe^{3+}-Ionen auf die Bestimmung wurde untersucht.

SUMMARY

Molecular absorption spectrometry by electrothermal volatilization in a graphite furnace. Part 2. The determination of traces of fluoride by GaF molecular absorption

A direct determination of traces of fluoride by measurement of the GaF molecular absorption in a graphite furnace is described. The optimal conditions, for compensation of the non-specific absorption and for temperatures of ashing and volatilization, are discussed. The effects of the Ga^{3+} and Na^{+} concentrations and of several acids on the determination are reported. Increasing concentrations of Ga^{3+} ions increase the concentration of GaF molecules in the graphite furnace plasma. Higher Na^{+}-concentrations decrease the loss of HF in the drying time. The detection limit (3 s) is 1.6 ng F^{-}/10 µl; the sensitivity is 0.8 ng F^{-}/10 µl for 0.01 absorbance units. The influence of Cl^{-}, Br^{-}, I^{-}, SO_4^{2-}, BO_3^{3-}, SiO_3^{2-}, Li^{+}, K^{+}, Be^{2+}, Mg^{2+}, Ca^{2+}, Al^{3+}, In^{3+}, Zn^{2+}, Cd^{2+} and Fe^{3+} ions on the determination are described.

Für die Bestimmung von Fluorid auf spektroskopischem Weg wurde bisher hauptsächlich die Emission stabiler Radikale, wie CaF (im Gleichstrombogen [1]), SrF (in einer C_2H_2/O_2-Flamme [2]) und InF (in einer kühlen H_2/N_2-Diffusionsflamme [3]) ausgenutzt. Bestimmungen von Fluorid durch

Atomabsorptionsspektrometrie (AAS) sind nur auf indirektem Wege durchgeführt worden. Es wurden bei Zr und Ti die Erhöhung [4, 5] und bei Mg die Depression [5, 6] der Atomabsorption durch Fluorid bei Anwendung von Flammen genutzt. Die erzielten Nachweisgrenzen liegen zwischen 0,2 und 5 $\mu g\ F^-\ ml^{-1}$ (vgl. auch [7]).

Auch die Abtrennung des Fluorids als SiF_4 durch Hinzufügen von Silikat und Schwefelsäure zur Probe mit nachfolgender Bestimmung des Siliziums durch AAS wurde für die Fluoridbestimmung benutzt [8]. Das SiF_4 kann in einer Flamme (Nachweisgrenze 30 $\mu g\ F^-$) oder einer Graphitrohrküvette (Nachweisgrenze 0,17 $\mu g\ F^-$) atomisiert werden. Zum Nachweis von Fluor in organischen Verbindungen wurde nach gaschromatographischer Trennung der Substanzen die Hochtemperaturreaktion mit Natrium, die zum NaF führte, ausgenutzt. Bei kontinuierlichem Transport des Natriumdampfes durch eine beheizte Küvette führt die Bildung von NaF zu einer Depression des Na-Absorptionssignals. Es wird eine Nachweisgrenze von 0,8 ng F erreicht [9]. Zur weiteren Charakterisierung der Möglichkeiten der Fluoridspurenanalyse sei die Anwendung ionenselektiver Elektroden erwähnt. Durch Anwendung spezieller Elektroden gelingt es, in 1 $\mu l\ 10^{-11}$ g F^- nachzuweisen [10]. Über Störungen wird in den meisten Fällen nur wenig berichtet.

Ausgehend von unserer 1. Mitteilung [11] über die Messung von Molekülabsorptionen (MA) von Gallium- und Indiummolekülen nach ihrer Erzeugung durch elektrothermische Verdampfung in einer Graphitrohrküvette, soll in dieser Mitteilung über die Möglichkeiten der analytischen Nutzung des Prinzips für die direkte Fluoridspurenbestimmung durch GaF-MA berichtet werden.

EXPERIMENTELLES

Apparatur: Zweikanal-Zweistrahl-AA-Gerät Typ 811 (Jarrell-Ash, USA); Hohlkathodenlampe (H_2-HKL), 30 mA, Spektrale Bandbreite: 0,4 nm. Wellenlängen: 211,4 nm für Gesamtabsorption (Kanal A), und 215,5 nm für Untergrundkompensation (Kanal B) (vgl. Abschnitt 1 s.u.). Graphitrohrküvette Typ 1268 (Beckman). Thermische Bedingungen: Vgl. Abschn. 2.

Reagenzien: Die $Ga(NO_3)_3$-Stammlösungen (100 mg $Ga^{3+}\ ml^{-1}$) wurden durch Auflösen von 99,9999% igem Gallium in konz. Salpetersäure, Abdampfen der Säure und Aufnahme in 1 M HNO_3 hergestellt. Außerdem wurden folgende Lösungen eingesetzt: 0,1 M NaF, 2 M NaOH, $LiNO_3$, $NaNO_3$, KNO_3, $Be(NO_3)_2$, $Mg(NO_3)_3$, $Ca(NO_3)_2$, $Al(NO_3)_3$, $In(NO_3)_3$, $Zn(NO_3)_2$, $Cd(NO_3)_2$, $Fe(NO_3)_3$ (10—100 mg Me ml^{-1}), $ZnCl_2$, $ZnBr_2$, ZnJ_2, $ZnSO_4$, Na_2SiO_3 und H_3BO_3 (10—100 mg des Anions ml^{-1}) Lösungen.

Verfahrensweise: Volumina von 10 μl entsprechend zusammengesetzter Lösungen (vgl. Text) wurden mit einer Eppendorf-Pipette in die Graphitrohrküvette gegeben, getrocknet und verdampft.

OPTIMIERUNG DER EXPERIMENTELLEN BEDINGUNGEN FÜR DIE GaF-MA

Auswahl des Spektralgebietes

In der Abb. 1 ist die Abhängigkeit der GaF-MA für ausgewählte thermische Bedingungen von der Wellenlänge dargestellt. Aus der Abbildung geht hervor, daß die intensivste GaF-MA bei 211,4 nm auftritt. Es zeigte sich, daß bei dieser Wellenlänge infolge der gegenüber der 1. Mitteilung veränderten thermischen Bedingungen die größte Extinktion bei größter Reproduzierbarkeit gemessen wurde.

Weiterhin ist zu entnehmen, daß die F^--freien Ga^{3+}-Lösungen und die Ga^{3+}-freien NaF-Lösungen ebenfalls eine geringe Absorption zeigen. Für die Messung der spezifischen GaF-MA ist deshalb eine Untergrundkompensation erforderlich. Da uns ein echtes Zweikanal-Spektrometer zur Verfügung stand, konnte die Untergrundkompensation nach der Zweilinienmethode durchgeführt werden. AAS-Geräte mit nur einem Kanal und Deuterium-Untergrundkompensation sind für diese Methode nicht einsetzbar. Es ist prinzipiell möglich, die Kompensation auf beiden Seiten der GaF-Bande durchzuführen. Aus der Abb. 1 geht hervor, daß bei 209,5 und 215,5 nm jeweils ein Absorptionsminimum der GaF-MA bei gleichbleibender Untergrundabsorption gemessen wird. Es wurde die Wellenlänge von 215,5 nm trotz des größeren Abstandes gewählt, weil das Minimum bei 209,5 nm schmaler ist und danach sofort der Anstieg der 2. GaO-Bande [11] beginnt. Außerdem nimmt die Intensität der H_2-HKL von 210 nm stark ab. Die geringfügige GaF-MA, die bei 215,5 nm noch auftritt, beeinträchtigt die Empfindlichkeit nur ganz unwesentlich.

Abhängigkeit der GaF-MA von den thermischen Bedingungen

Zur Erzielung einer maximalen GaF-MA ist eine hohe GaF-Konzentration im Plasma und eine geringe Untergrundabsorption erforderlich. Die GaF-Konzentration kann durch die Plasmatemperatur beeinflußt werden. Zu niedrige, Temperatur führt zur langsamen Reduktion und Verdampfung der Ga-Spezies und somit zur Senkung der GaF-Konzentration im Plasma. Zu hohe Temperatur führt zur zunehmenden Dissoziation der GaF-Moleküle bzw. deren verminderter Bildung. Auch die Untergrundabsorption kann

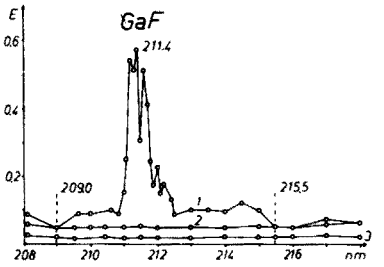

Abb. 1. Abhängigkeit der GaF-MA von der Wellenlänge. Bedingungen: 1 µg Ga^{3+}/1,2 µg Na^+/0,26 µg F^-/NO_3^-/10 µl. Thermische Bedingungen: Vgl. Abb. 2.

durch die Plasmatemperatur beeinflußt werden. In Abhängigkeit von der Zusammensetzung der Probe sollte (wie bei der AAS) eine möglichst vollständige Trennung der Matrices und der Spuren durch fraktionierte Verdampfung angestrebt werden. Mit Hilfe der programmierbaren Veraschungs- und Atomisierungs-Phase (die bei der MAS besser Molekülbildungs- oder Verdampfungsphase genannt werden sollte) wurden die optimalen Bedingungen ermittelt (Abb. 2).

Aus der Abb. 2 (Kurve 1) geht hervor, daß bei der maximal erreichbaren Temperatur des Gerätes (3300°C) die höchste GaF-MA gemessen wird. Daraus ist zu schlußfolgern, daß im gegebenen Temperaturintervall die thermische GaF-Dissoziation den anderen Effekten untergeordnet ist. Die Temperatur der Veraschungsphase (Kurve 2) beeinflußt bis zu einer Temperatur von 520°C die Ergebnisse nur unwesentlich. Oberhalb dieser Temperatur vermindert sich die Intensität der GaF-MA, weil bereits in der Veraschungsphase Verluste an Fluorid durch hydrolytische Abspaltung von HF aus dem hydratisierten GaF_3 auftreten [12] (Tab. 1).

Als optimale thermische Bedingungen ergeben sich: Trocknung 30 s, 140°C; Veraschung 15 s, 520°C; Verdampfung/Molekülbildung 3300°C, 10 s. Es ist zu berücksichtigen, daß diese Temperaturen nicht gemessen wurden, sondern den Geräteunterlagen entnommen wurden. Es handelt sich jeweils um die Endtemperatur der Küvette, die erst nach einer bestimmten Zeit erreicht wird.

Einfluß der Ga^{3+}-Konzentration auf die GaF-MA

Da bei einem vorgegebenen Atomverhältnis Ga: F von 1:1 auch GaO-MA beobachtet wird [11] und der ebenfalls gefundenen Temperaturabhängigkeit der GaF-MA konnte gefolgert werden, daß sich im Plasma ein Gleichgewicht zwischen Ga- und F-Atomen sowie dem GaF-Molekül einstellt

$$Ga + F \rightleftharpoons GaF \qquad (1)$$

welches stark auf die linke Seite verschoben ist. Eine Zunahme der Ga-Konzentration im Plasma müßte demzufolge eine Erhöhung der GaF-Konzentration bewirken. Aus der Abb. 3 geht hervor, daß neben der erwarteten

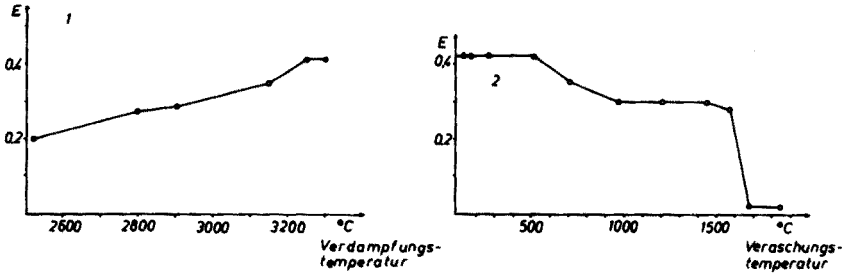

Abb. 2. Abhängigkeit der Intensität der GaF-MA von der Temperatur. Bedingungen: 2 µg Ga^{3+}/1,4 µg Na^+/0,19 µg F^-/NO_3^-/10 µl. (1) Veraschungsphase: 15 s, 520°C, (2) Verdampfungs-/Molekülbildungsphase: 10 s, 3300°C.

TABELLE 1

Stabilität von Fluoriden und F-haltiger Moleküle bzw. Radikale [13, 14]

Salz	Siedepunkt (°C)	Hydrolytische Zersetzung der hydratis. Salze beim Erhitzen	Radikal/Molekül	Dissoziationsenergie (eV)
LiF	1676	—	LiF	5,89
NaF	1704	—	NaF	4,94
KF	1505	—	KF	5,32—5,16
BeF_2	800 subl.	teilweise	BeF	5,76
MgF_2	2239	—	MgF	4,75
CaF_2	2500	—	CaF	5,48
AlF_3	1291 subl.	teilweise	AlF	5,89
GaF_3	800 subl.	teilweise	GaF	6,24
InF_3	1200	teilweise	InF	5,45—5,25
ZbF_2	$1500_{wfr.}$[a]	vollständig	ZnF	?
CdF_2	$1758_{wfr.}$	?	CdF	3,16
FeF_3	$1000_{wfr.}$	vollständig	FeF	?

[a] wfr.: wasserfreie Salze.

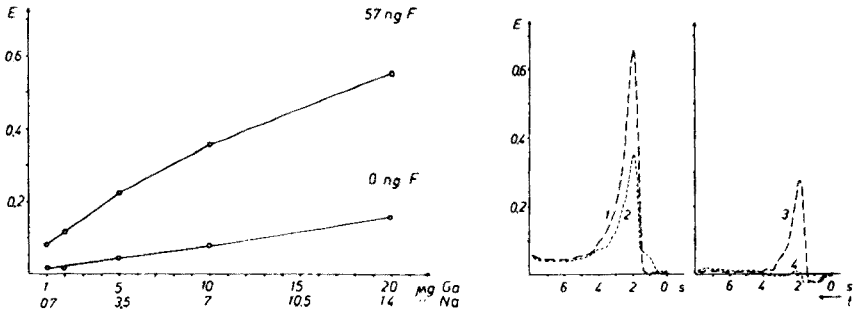

Abb. 3. Abhängigkeit der Intensität der GaF-MA von der Ga^{3+}-Konzentration. Thermische Bedingungen: Vgl. Abb. 2. Mengenangaben bezogen auf 10 µl Probevolumen, neutrales Medium durch Hinzufügen von NaOH.

Abb. 4. Extinktions—Zeit-Kurven für die GaF-MA in der Verdampfungsphase. Bedingungen: 10 µg Ga^{3+}/7 µg Na^+/0,038 µg F^-/NO_3^-/10 µl für Kurven 1—3, Kurve 4: Ohne F^--Zusatz. Thermische Bedingungen: Vgl. Abb. 2. (1) Extinktion bei 211,4 nm. (2) Extinktion bei 215,5 nm. (3) und (4) Differenz $E_{211,4} - E_{215,5}$.

Erhöhung der GaF-MA mit zunehmender Ga-Konzentration auch eine Erhöhung des nicht mehr kompensierbaren Blindwertes auftritt. Unter Berücksichtigung beider Gesichtspunkte wird für analytische Bestimmungen eine Konzentration von 10 µg Ga^{3+}/10 µl vorgeschlagen.

In der Abb. 4 sind die Extinktions—Zeit-Kurven zur Untersuchung der Zeitabhängigkeit der Verdampfung dargestellt. Es ist zu sehen, daß bei den gewählten thermischen Bedingungen kaum fraktionierte Verdampfungen vorliegen. In der Anfangsphase ist die auf Kanal B gemessene Extinktion etwas größer als die auf Kanal A. Die Differenzbildung (A — B) führt in dieser Phase zu einem kleinen negativen Wert, der sich jedoch auf das Ergebnis nicht auswirkt. Der in F^--freien Lösungen auftretende, nicht kompensierbare Blindwert liegt direkt unter der spezifischen GaF-MA und ist deshalb bei den Eichkurven zu berücksichtigen.

Einfluß der Azidität und der Na^+-Konzentration auf die GaF-MA

Die Abb. 5 stellt die Abhängigkeit der GaF-MA von der Konzentration verschiedener Säuren dar. Trotz der Tatsache, daß die Fluorwasserstoffsäure nur eine mittelstarke und außerdem leichtflüchtige Säure ist, wird in Gegenwart von Salz- und Salpetersäure erst unterhalb des pH-Wertes 2 eine Depression der GaF-MA festgestellt, die auf Verflüchtigung der HF während der Trocknungsphase zurückzuführen ist. Die stärkere depressive Wirkung der Salzsäure deutet auf einen zusätzlichen Effekt hin. Eine höhere Salzsäurekonzentration in der Lösung führt auch zu einem größeren Chlorid-Gehalt des in der Trocknungsphase entstehenden Rückstandes. Während der Verdampfungs- und Molekülbildungsphase bilden die freigesetzten Cl-Atome mit den Ga-Atomen thermisch stabile GaCl-Moleküle, wodurch die Konzentration freier Ga-Atome und damit auch die der GaF-Moleküle vermindert wird (Ionenverhältnis bei pH 1 durch HCl, F^-: Cl^- gleich 1 : 500). Die Gegenwart von Schwefelsäure bewirkt ab pH 4 eine geringe Depression, ab pH 3 (0,48 μg SO_4^{2-}/10 μl) entsteht außerdem ein starkes nicht kompensierbares, unspezifisches Signal, so daß die Messung der GaF-MA unmöglich ist.

Vergleichsuntersuchungen zwischen Lösungen gleicher Azidität, die einmal durch Mischen von sauren Ga^{3+}-Lösungen mit NaF-Lösungen und zum anderen durch Zusatz von Säuren zu vorher mit NaOH neutralisierten $Ga^{3+}/Na^+/F^-/NO_3^-$-Lösungen hergestellt wurden, zeigten, daß der Zusatz von Na^+-Ionen eine starke Erhöhung der GaF-MA bewirkte. Dieser unerwartete Effekt, der sich auch in Gegenwart einiger anderer Kationen (vgl. Abb. 5) ergab, ist nicht mit der Flüchtigkeit der HF in der Trocknungsphase zu erklären.

Der Einfluß der Na^+-Konzentration auf die GaF-MA wurde untersucht (Abb. 6). Es ist zu sehen daß die GaF-MA ab einer Natriummenge von 1 μg/10 μl stark zunimmt.

Wir erklären diesen Effekt wie folgt: NaF, welches sich in Gegenwart von Na^+-Ionen während der Trocknungsphase neben GaF_3 u.a. bildet, ist eine thermisch stabile Substanz (Siedepunkt 1704°C), die bewirkt, daß während der Veraschungsphase bei Temperaturen von 500°C keine F^--Verluste auftreten. In Abwesenheit von Na^+-Ionen besteht der Rückstand nur aus gemischten Salzen (z.T. basisch) des weniger basischen Galliums. Dieser Rückstand gibt während der Veraschungsphase wegen der geringen thermischen Stabilität von $GaFX_2 \cdot nH_2O$ (X = andere Anionen), bereits Fluor

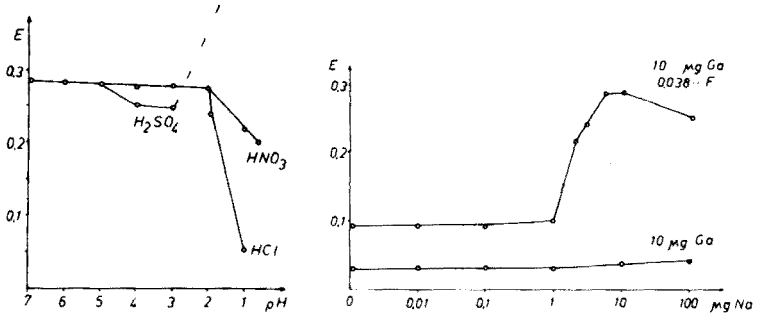

Abb. 5. Abhängigkeit der Intensität der GaF-MA von der Azidität der Lösungen. Bedingungen: 10 µg Ga^{3+}/7 µg Na^+/0,038 µg F^-/NO_3^-/10 µl. Thermische Bedingungen: Vgl. Abb. 2.

Abb. 6. Abhängigkeit der Intensität der GaF-MA von der Na^+-Konzentration. Bedingungen: 10 µg Ga^{3+}/0,038 µg F^-/NO_3^-/10 µl. Na-Menge bezogen auf 10 µl, Thermische Bedingungen: Vgl. Abb. 2.

in Form von HF ab, so daß in der Verdampfungs-/Molekülbildungsphase nur eine geringe F-Atomkonzentration vorhanden ist. Aus diesem Grund wird für die Bestimmungen von Fluorid folgende Lösungszusammensetzung empfohlen: 10 µg Ga^{3+}/10 µl, 7 µg Na^+/10 µl; Medium neutral — pH 2.

Einfluß anderer Kationen auf die GaF-MA

Ausgehend von den im Abb. 4 dargestellten Ergebnissen, wurde der Einfluß anderer Kationen (in Abwesenheit von Na^+) auf die GaF-MA untersucht (Abb. 7). Die auf den Abszissen der Bilder der Abb. 7 angegebenen

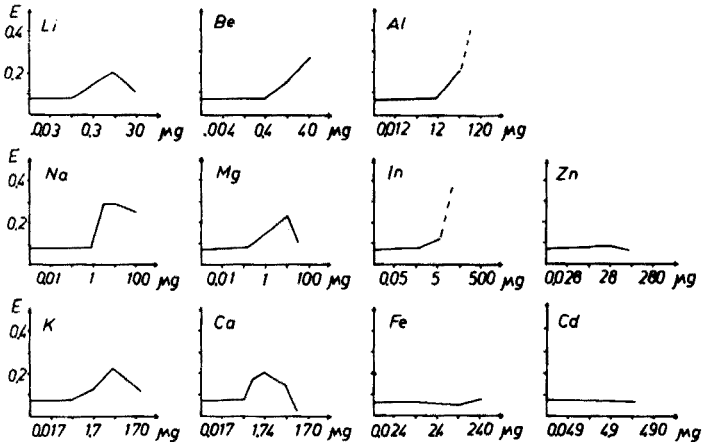

Abb. 7. Abhängigkeit der Intensität der GaF-MA vom Zusatz anderer Kationen. Bedingungen: 10 µg Ga^{3+}/0,038 µg F^-/NO_3^-/10 µl. Mengenangaben: Kationen 10 µl, Zusatz als Nitrat. Durch unterschiedliche erfolgte Einstellung gleicher Atom- bzw. Ionenkonzentrationen.

Kationenmengen ergeben gleiche Atomkonzentrationen und entsprechen den in der Abb. 6 angegebenen Natriummengen. Im Ergebnis der Untersuchungen kann man verschiedene Einflüsse erkennen, die mit den in der Tab. 1 angegebenen Daten erklärt werden können.

Die Kationen K^+, Li^+, Be^{2+}, Mg^{2+}, Ca^{2+}, Al^{3+} und In^{3+} bewirken eine Steigerung der GaF-MA ähnlich der der Na^+-Ionen. Aus der Tab. 1 ist zu entnehmen, daß die Salze LiF, KF, NaF, MgF_2 und CaF_2 beim Erhitzen keine hydrolytische Zersetzung erleiden. Die hydratisierten-Salze $BeF_2 \cdot nH_2O$, $AlF_3 \cdot nH_2O$ und $InF_3 \cdot nH_2O$ geben beim Erhitzen einen Teil des Fluorids als HF ab. Aus diesem Grund wird die intensitätssteigernde Wirkung dieser Kationen erst bei höheren Konzentrationen festgestellt. Damit wird die gegebene Erklärung bestätigt. In diesen Fällen verdampft das stabil gebundene Fluorid gleichzeitig mit dem Gallium in der Verdampfungs-/Molekülbildungsphase. Die GaF-Moleküle bilden sich danach im Plasma.

In Gegenwart sehr großer Mengen Li^+, K^+, Mg^{2+} und Ca^{2+} ist eine Depression der GaF-MA zu erkennen. Das ist auf die teilweise Bindung von F-Atomen in Form thermisch stabiler Radikale bzw. Moleküle (Dissoziationsenergien vgl. Tab. 1) zurückzuführen. In Gegenwart großer Mengen Al^{3+}- und In^{3+}-Ionen tritt eine starke, nicht kompensierbare Blindabsorption auf, die im Fall des Indiums auf die im gewählten Spektralgebiet auftretende InO-Bande [11] zurückzuführen ist.

Die Kationen Fe^{3+}, Zn^{2+} und Cd^{2+} haben keine intensitätssteigernde Wirkung für die GaF-MA. Laut Tab. 1 werden die hydratisierten Salze des $ZnF_2 \cdot nH_2O$ und $FeF_3 \cdot nH_2O$ beim Erhitzen vollständig zersetzt. Es ist anzunehmen, daß dies auch beim CdF_2 in Gegenwart von Wasser der Fall ist, obwohl dieses Salz ohne Kristallwasser kristallisiert. Damit sind diese Kationen nicht in der Lage Fluorid während der Trocknungs- und Veraschungsphase zu binden. Auch dieses Ergebnis bestätigt die gegebenen Erklärungen.

Verfahrensweise für die Durchführung von Fluoridbestimmungen

Neutrale bis schwach saure (pH 3) Probelösungen werden mit neutralen $Ga(NO_3)_3/NaNO_3$-Lösungen (10 mg Ga^{3+}/7 mg Na^+/ml) im Verhältnis 9 zu 1 gemischt (z.B. 90 µl Probelösung + 10 µl Additionslösung). Jeweils 10 µl der erhaltenen Lösung werden in die Graphitrohrküvette gegeben und bei den oben angegebenen thermischen Bedingungen verdampft. Die Messung der spezifischen GaF-MA erfolgte unter Anwendung der Untergrundkompensation ($E_{GaF,211,4} = E_{Gesamt,211,4} - E_{unspezifisch,215,5}$). Die Auswertung kann nach dem Eichkurvenverfahren erfolgen. Es ist jedoch zu empfehlen — vor allem bei unbekannten Proben — die Richtigkeit der Werte durch die Additionsmethode zu überprüfen.

RESULTATE UND DISKUSSION

Ergebnisse der Fluorid-Bestimmung in reinen Lösungen

Auf der Basis der vorgeschlagenen Verfahrenweise wurde eine Eichkurve für die Fluoridspurenbestimmung in Mikroproben aufgestellt (Abb. 8). Die

gefundene Eichkurve ist leicht gekrümmt, so daß keine Regressionsrechnung durchgeführt wurde. Die Berechnung der reziproken Empfindlichkeit bezogen auf 0,01 Extinktionseinheiten ergibt einen Wert von 0,8 ng Fluorid. Die Standardabweichung der Blindwerte liegt bei 0,007 Extinktionseinheiten (15 Freiheitsgrade, Messung an verschiedenen Tagen mit verschiedenen Graphitrohren). Nach dem 3 s-Kriterium ergibt sich eine Nachweisgrenze von 1,6 ng Fluorid/10 µl. Das bedeutet, daß Fluoridbestimmungen in Mikrovolumina bis zu einer Fluoridkonzentration von $4—8 \cdot 10^{-6}$ Mol l^{-1} möglich sind.

Einfluß verschiedener Anionen auf die Fluoridbestimmung durch GaF-MA

Es wurde der Einfluß folgender Anionen untersucht: Cl^-, Br^-, J^-, BO_3^{3-}, SO_4^{2-}, SiO_3^{2-}. Da Zn^{2+}-Ionen nur einen geringen Einfluß auf die GaF-MA ausübten, wurden für die Untersuchungen die Salze $ZnCl_2$, $ZnBr_2$, ZnJ_2 und

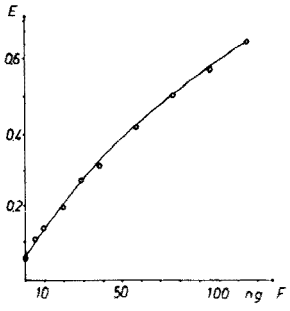

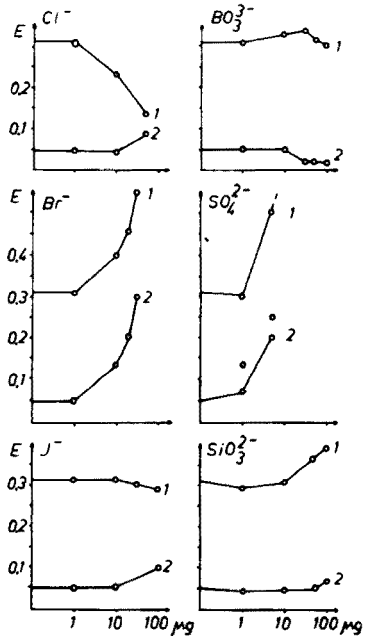

Abb. 8. Eichkurve für die Fluorid-Bestimmung durch GaF-MA. Bedingungen: 10 µg Ga^{3+}/7 µg Na^+/NO_3^-/10 µl. Thermische Bedingungen: Trocknung: 20 s, 150°C, Veraschung: 15 s, 520°C, Verdampfung: 10 s, 3300°C. Untergrundkompensation: $E_{211,4} - E_{215,5}$.

Abb. 9. Einfluß anderer Anionen auf die Fluorid-Bestimmung durch GaF-MA. Bedingungen: (1) 10 µg Ga^{3+}/7 µg Na^+/0,038 µg F^-/NO_3^-/10 µl; (2) Ohne F^--Zusatz. Thermische Bedingungen: Vgl. Abb. 2. Mengenangaben bezogen auf 10 µl Probevolumen. Salze: $ZnCl_2$, $ZnBr_2$, ZnJ_2, $ZnSO_4$, H_2BO_3, Na_2SiO_3.

$ZnSO_4$ eingesetzt. Außerdem wurden H_3BO_3 (schwache Säure) und Na_2SiO_3 verwendet. Die Resultate sind in der Abb. 9 dargestellt. Es ist zu entnehmen, daß sehr unterschiedliche Einflüsse wirken. Die Gegenwart von Cl^--Ionen bewirkt nur ein geringes Ansteigen des nicht kompensierbaren Blindwertes und eine starke Depression der GaF-MA ab 10 μg Cl^-/10 μl. Das ist auf die Bildung des ebenfalls stabilen GaCl-Moleküls (E_D = 4,92 eV) im Plasma und die damit verbundene Reduzierung der GaF-Konzentration zurückzuführen. In Gegenwart von Br^--Ionen tritt nur eine geringe Depression der GaF-MA auf. Allerdings steigt der nichtkompensierbare Blindwert stark an. J^--Ionen verursachen nur eine geringe Depression und einen geringen Anstieg des Blindwertes. Die Gegenwart größerer Sulfatmengen macht die Messung der GaF-MA wegen des starken nichtkompensierbaren Blindwertes unmöglich.

H_3BO_3 bewirkt ebenfalls keine Blindwerterhöhung und auch keine Depression. Infolge der schlechten Verdampfbarkeit der Borsäure (Bildung von Borcarbid) tritt dieser Einfluss nicht auf. Auch die Gegenwart von Na_3SiO_3 verursacht nur geringe Effekte.

Als allgemeine Schlußfolgerung kann festgestellt werden, daß die GaF-MA für die Bestimmung von Fluorid-Spuren in Proben unbekannter Zusammensetzung eingesetzt werden kann, wenn mit der Additionsmethode gearbeitet wird. Proben bekannter Zusammensetzung können auch unter Anwendung des Eichkurven-Verfahrens analysiert werden.

Unter Berücksichtigung der in Abb. 9 dargestellten Resultate — vor allem der nichtkompensierbaren Blindwerte — und der gefundenen Nachweisgrenze sind Bestimmungen für folgende Masseverhältnisse möglich: Cl:F = 5000; Br:F = 15000; J:F = 60000; BO_3:F = 60000; SO_4:F = 2500; SiO_3:F = 60000.

Einfluß verschiedener Kationen auf die Fluoridbestimmung durch GaF-MA

Es wurde der Einfluß folgender Kationen auf die Bestimmung des F^- untersucht: Li^+, Na^+, K^+, Be^{2+}, Mg^{2+}, Ca^{2+}, Al^{3+}, In^{3+}, Zn^{2+}, Cd^{2+} und Fe^{3+}. Sie wurden den Lösungen, die bereits 10 μg Ga^{3+}, 7 μg Na^+ und 38 ng F^-/10 μl enthielten, in Form der Nitrate zugefügt. Das Ergebnisse ist in der Abb. 10 dargestellt worden. Beim Vergleich der Abb. 10 mit der 7 stellt man fest, daß die vorgegebene Na^+-Konzentration (7 μg/10 μl) einen entscheidenden Einfluß auf die Beeinflussung der GaF-MA durch andere Kationen hat. In Gegenwart dieser Na^+-Konzentrationen haben Li^+-, weitere Na^+-, K^+-, Be^{2+}-, Mg^{2+}-, Ca^{2+}- und Al^{3+}-Ionen keinen signalerhöhenden und erst bei hohen Konzentrationen einen geringen depressiven Einfluß. Dieser ist besonders bei Gegenwart von Li^+, Mg^{2+}- und Ca^{2+}-Ionen mit der zunehmenden Bildung stabiler Moleküle und Radikale, wie LiF, MgF und CaF, im Plasma zu erklären. Der geringere Einfluß von Be^{2+}- und Al^{3+}-Ionen, die gleichfalls stabile Radikale BeF und AlF bilden, ist auf eine fraktionierte Verdampfung zurückzuführen. Beide Substanzen verdampfen erst nach den fluoridhaltigen Rückständen des Ga^{3+} und Na^+. In Gegenwart von In^{3+}-Ionen sind wegen der intensiven Absorption durch InO-Moleküle nur Messungen bis zu einer Konzentration von 1,0 μg In/10 μl möglich.

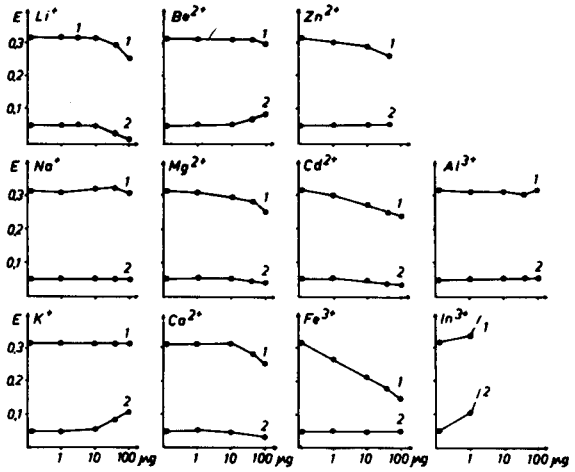

Abb. 10. Einfluß von Kationen auf die Fluorid-Bestimmung durch GaF-MA. Bedingungen: (1) 10 µg Ga^{3+}/7 µg Na^+/0,038 µg F^-/NO_3^-/10 µl; (2) Ohne F^--Zusatz. Thermische Bedingungen: Vgl. Abb. 2. Mengenangaben bezogen auf 10 µl Probevolumen.

Im Gegensatz zu den in Abb. 7 gezeigten Resultaten bewirken Zn^{2+}-, Cd^{2+}- und Fe^{3+}-Ionen in Gegenwart der Na^+-Ionen einen zunehmend depressiven Einfluß. Beim Trocknungsprozeß entstehen besonders bei hoher Konzentration dieser Kationen anteilig auch die Fluoride dieser Kationen. Beim weiteren Erhitzen erleiden diese Substanzen eine hydrolytische Spaltung. Damit wird die in der Verdampfungs-/Molekülbildungsphase vorhandene F-Konzentration reduziert. Besonders stark ist dieser depressive Effekt in Gegenwart der Fe^{3+}-Ionen, denn diese bilden in wäßriger Lösung Komplexe mit den F^--Ionen und binden somit das Fluorid stärker als die anderen Kationen. Unter Berücksichtigung der in Abb. 10 dargestellten Ergebnisse und der gefundenen Nachweisgrenze sind Bestimmungen für folgende Masseverhältnisse möglich: Li, Na, K, Be, Mg, Ca, Al, Zn, Cd): F wie 10^5:1; Fe:F wie 10^4:1; In:F wie 10^3:1.

Mit diesen Ergebnissen konnte gezeigt werden, daß die MAS bei Verdampfung anorganischer Substanzen in einer Graphitrohrküvette eine Methode ist, die für die Lösung realer analytischer Probleme nach Optimierung der Bedingungen und Parameter eingesetzt werden kann. In anbetracht der Verschiedenartigkeit der Matrixeffekte, die zur systematischen Einordnung noch weiterer intensiver Untersuchungen bedürfen, ist bis jetzt als analytisches Auswerteverfahren die Additionstechnik dem Eichkurvenverfahren vorzuziehen.

LITERATUR

1 I. Schoenfeld, Appl. Spectrosc., 24 (1970) 359.
2 B. Gutsche und R. Herrmann, Z. Anal. Chem., 269 (1974) 260.
3 G. Henrion und D. Marquardt, Z. Chem., 17 (1977) 28.

4 A. M. Bond und T. A. O'Donnell, Anal. Chem., 40 (1968) 560.
5 M. Pinta, Method. Phys. Anal., 6 (1970) 268.
6 C. C. Fong und C. O. Huber, Spectrochim. Acta Part B, 31 (1976) 113.
7 M. M. Goldschtein, I. G. Judelewitsch, Zh. Anal. Khim., 31 (1976) 810.
8 B. Gutsche, K. Rüdiger und R. Herrmann, Spectrochim. Acta Part B, 30 (1975) 192.
9 B. Gutsche, H. Kleinoeder und R. Herrmann, Analyst, 100 (1975) 192.
10 A. S. Hallsworth, J. A. Weatherell und D. Deutsch, Anal. Chem., 48 (1976) 1660.
11 K. Dittrich, Anal. Chim. Acta, 97 (1978) 59. (Teil 1).
12 S. A. Polishchuk, Chem. Abstr., 71 (1969) 45179.
13 B. Rosen, Spectroscopic Data relative to Diatomic Molecules, Bd. 17 aus International Tables of Selected Constants, Pergamon Press, Oxford, 1970.
4 J. C. Bailar, H. J. Emeleus, R. Nyholm und A. F. Trotman-Dickinson, Comprehensive Inorganic Chemistry, Pergamon Press, Oxford, 1973.

Analytica Chimica Acta, 97 (1978) 81—86

STORAGE AND PROCESSING OF ESTUARINE WATER SAMPLES FOR TRACE METAL ANALYSIS BY ATOMIC ABSORPTION SPECTROMETRY

R. E. PELLENBARG and T. M. CHURCH*

College of Marine Studies, University of Delaware, Newark, Delaware 19711 (U.S.A.)

(Received 22nd August 1977)

SUMMARY

Saline water samples from the Delaware Bay estuary were sampled, processed, and stored in a variety of ways to allow different methods of maintaining their integrity to be compared. Samples were processed onboard ship, immediately after collection, by extraction with ammonium pyrollidinedithiocarbamate in methyl isobutyl ketone. Duplicate samples were processed onshore after a variety of storage procedures. All samples were analyzed for copper and iron by atomic absorption spectrometry. Only samples filtered (<1 μm), acidified, and stored frozen gave extractable copper and iron results comparable with those for samples extracted immediately after collection. Cold storage with sample acidification in polyethylene containers appeared less satisfactory. Organic extracts from samples processed onboard are best retained in all-Teflon containers pending complete digestion and analysis onshore. Unless clean (ultra-filtered air) conditions can be ensured onboard, the estuarine water samples are best returned in a filtered, acidified, and frozen condition for onshore processing.

Data from the analysis of natural waters are no better than the techniques by which such samples are gathered, prepared, and stored pending analysis. There have been numerous recent developments of techniques for the collection, processing, and storage of water samples that minimize contamination and maximize the integrity of the initial dissolved metal loading [1—4]. The loss of a metal analyte from water samples is lessened through storage of acidified samples (pH 1.5) in polyethylene containers, as opposed to storage of unacidified samples in glass vessels [3]. The storage of sea-water samples in polyethylene bottles with subsequent processing in Teflon ware has become widespread in recent years.

The present work was initiated to re-examine problems associated with the storage of saline estuarine water samples to maintain dissolved metal burdens. The experiments evaluated the utility and precision associated with rapid "onboard" chelation-solvent extraction for dissolved iron and copper as opposed to cleaner "onshore" processing with attendant longer sample storage.

EXPERIMENTAL

Apparatus

Water samples were taken in a PVC hydrographic bottle closing below the surface. A Varian 1200 atomic absorption spectrometer equipped with a Model 63 carbon rod atomizer was used for the trace metal analyses. The carbon rod atomizer was flushed with nitrogen gas and used for copper analyses. Iron was determined by air—acetylene flame atomization.

Procedures

Saline water samples were gathered during two cruises on Delaware Bay, U.S.A. Cruise I sampled a location near mid-bay (salinity 27.1°/₀₀), while Cruise II sampled waters near the Delaware Bay terminus of the Chesapeake and Delaware Canal (salinity 5.0°/₀₀).

During Cruise I, water samples were filtered through Gelman A/E glass fiber filters (approximately 0.3 μm pore size) within 30 min after collection. The trace metals were extracted twice from ca. 1 kg of filtered water at pH 3.1, after chelation with 2-ml aliquots of a 4% ammonium pyrollidinedithiocarbamate (APDC) solution into 15-ml aliquots of methyl isobutyl ketone (MIBK), in a slight modification of the method of Brewer et al. [5]. All liquid reagents were distilled and condensed in silica ware prior to use. The APDC was synthesized as described by Slavin [6]. The effectiveness of similar APDC/MIBK procedures has been demonstrated [7].

Trace metal processing

Half the samples were extracted "onboard" within 3 h of collection. The organic extracts were placed in acid-washed 50-ml wide-mouth polyethylene bottles, combined with 10 ml of silica-condensed hydrochloric acid, and stored at 10°C. Within three weeks of collection, all stored whole water samples had been processed. The whole water samples had been acidified and were stored cold (10°C) after collection. Organic extracts from samples processed onboard during Cruise II were retained in all-Teflon containers, however, and stored at 10°C. All duplicate 1-l water samples were filtered, acidified,with 2 ml of HNO_3, and frozen.

Half of the water samples gathered during both cruises were returned refrigerated to the laboratory for processing onshore. After being brought to room temperature (23°C), they were extracted as onboard.

Laboratory processing of organic extracts

Organic extracts from onboard Cruise I were transferred to 125-ml Teflon beakers and evaporated to dryness. The polyethylene storage containers were rinsed with 4-ml aliquots of concentrated nitric acid which were added to the corresponding beakers to digest the MIBK residues.

Vessels containing organic extracts from Cruise II were transferred to a hot plate and evaporated to dryness, and 4 ml of concentrated nitric acid was

added to each container to wet-ash the residues. Thus, the same container served as a storage and reaction vessel.

The organic extracts obtained onshore were evaporated to dryness, then wet-ashed with 4.0-ml portions of concentrated nitric acid in the Teflon beakers closed with Teflon watch glasses. The nitric acid was evaporated, and the moist residue made up to 5.0 ml with 0.1 M nitric acid.

RESULTS AND DISCUSSION

Data from saline samples gathered during two cruises are presented in Tables 1 and 2. Duplicate whole water samples were retained for onshore processing, to accentuate storage problems. Also, samples were gathered and are tabulated as a function of depth to examine whether proximity to the surface microlayer or detrital loading would affect processing and storage during or after filtration. There appears to be no significant effect attributable to film or detritus, and results are reproducible regardless of sample depth.

Processing conditions

Rapid onboard processing minimized sample deterioration caused by contact with a container surface as shown by higher values for samples stored over a shorter period of time. However, samples returned to shore for full processing on Cruise II yielded much more consistent iron results than did samples from Cruise II processed onboard. Standard deviations for onshore samples from Cruise II were only 11% of extractable iron concentrations, whereas onboard samples showed standard deviations of 20% of the extractable iron.

General laboratory conditions onboard probably exposed samples to more contamination than did laboratory conditions onshore where a laminar flow clean bench was available to eliminate aeolian particulate contamination. Contamination in the processing area may have led to the large scatter in the data from onboard extraction compared with data from duplicates processed onshore.

Storage of organic extracts

Final results were influenced by the way organic extracts from water samples were stored. Organic extracts generated onboard during Cruise I were stored in polyethylene containers. Since APDC metal chelates are labile and can decompose significantly within 1 h after formation [7] the storage containers were rinsed with cold, concentrated nitric acid after final processing onshore. The nitric acid rinse appeared inconsistent in removing metals which may have settled onto the container walls. Again, the scatter in the data, as shown by the lack of agreement between Cruise I duplicates, may have been influenced by an inability to recover metals quantitatively from the containers storing organic extracts. However, standard deviations of onboard samples from Cruise II averaged only 21% of corresponding metal concentrations for extracts which had been stored and digested with hot nitric

TABLE 1

APDC—MIBK extractable trace metal concentrations for filtered estuarine water samples (27°/$_{oo}$ salinity) from Delaware Bay, Cruise I

Sample[a]	Treatment/storage period	Cu, ppb	Fe, ppb
Surface A	extr. onboard, short	1.36	2.65
Surface B	extr. onboard, short	0.99	2.27
		Av. 1.17	2.46
Surface C	extr. onboard	0.84	2.90
Surface D	extr. onboard	0.83	4.83
		Av. 0.83	3.86
Surface E	acid, cold	0.81	4.06
Surface F	acid, cold	0.88	3.46
		Av. 0.84	3.76
Surface G	acid, frozen	1.06	4.41
Surface H	acid, frozen	1.13	1.96
		Av. 1.09	3.18
11 meters A	onboard, short	0.95	2.17
11 meters B	onboard, short	0.95	3.32
		Av. 0.95	2.75
11 meters C	onboard	0.54	0.35
11 meters D	onboard	0.64	0.70
		Av. 0.59	0.52
11 meters E	acid, cold	0.57	1.41
11 meters F	acid, cold	0.65	2.23
		Av. 0.61	1.82
11 meters G	acid, frozen	0.91	3.01
11 meters H	acid, frozen	0.99	3.51
		Av. 0.95	3.26
16 meters A	onboard, short	0.92	2.49
16 meters B	onboard, short	0.71	0.72
		Av. 0.81	1.60
16 meters C	onboard	0.79	1.84
16 meters D	onboard	1.04	2.41
		Av. 0.91	2.12
16 meters E	acid, cold	1.01	3.33
16 meters F	acid, cold	0.45	1.54
		Av. 0.73	2.44
16 meters G	acid, frozen	0.86	6.64
16 meters H	acid, frozen	0.71	3.80
		Av. 0.78	5.22

[a]All samples and extracts processed and stored in polyethylene containers.

TABLE 2

APDC—MIBK extractable metal concentrations for filtered estuarine water samples (5°/$_{oo}$ salinity) from Delaware Bay, Cruise II

Sample[a]	Treatment/storage period		Cu, ppb	Fe, ppb
Surface A	onboard		1.54	19.9
Surface B	onboard		2.85	21.4
Surface C	onboard		2.17	18.6
		Av.	2.19	20.0
		S.d.	0.66	1.40
Surface D	acid, frozen		2.22	28.2
Surface E	acid, frozen		1.65	34.1
Surface F	acid, frozen		2.26	40.1
Surface G	acid, frozen		2.31	35.2
Surface H	acid, frozen		2.44	37.9
		Av.	2.18	35.1
		S.d.	0.31	4.51
7 meters A	onboard		1.84	32.5
7 meters B	onboard		2.24	39.4
7 meters C	onboard		2.11	19.3
		Av.	2.04	30.4
		S.d.	0.28	10.21
7 meters	acid, frozen		1.91	32.4
7 meters	acid, frozen		2.43	35.1
7 meters	acid, frozen		2.29	36.7
7 meters	acid, frozen		2.06	31.6
7 meters	acid, frozen		1.92	28.9
		Av.	2.16	32.9
		S.d.	0.23	30.5

[a]Onboard extracts stored in Teflon containers.

acid in all-Teflon vessels, suggesting the stable nature of the metal chelate adsorption onto Teflon.

Storage of estuarine waters

The loss of dissolved trace metals from water samples stored as a liquid agrees with work by several authors [2, 3]. Plastic containers are capable of sorbing a variety of metal ions from solution, especially over a long period of time. It has been recommended that aqueous samples for metal content analysis be acidified prior to storage [3]. Data from Cruise I show that acidification with cold storage appears to lessen, but not eliminate Fe and Cu loss to storage-container surfaces for unfrozen estuarine samples. Results from this study indicate that samples returned to a shore laboratory are best preserved filtered, acidified, and frozen. Data from Cruise I also indicate that onboard extracts stored for a short period of time give extractable metal burdens which are matched most closely by those shore-processed samples which have been

stored frozen. For example, in the case of copper, filtered and acidified water samples (Cruise I) stored cold exhibited metal loadings which were, on average, 24% less than those obtained from onboard extracts. Frozen water samples (Cruise I), however, showed only 5% less copper. Results were similar for extractable iron. Average iron contents were 31% less in the cold storage samples than in the corresponding frozen samples. Thus, sample preservation by freezing appears to be effective in maintaining sample integrity. This observation was confirmed by data generated during Cruise II. Again, copper concentrations in frozen samples were, on average, only 2% less than those determined for samples extracted onboard.

Conclusions

(1) If water samples are to be processed by chelation—solvent extraction techniques, the samples should be processed soon after collection and filtration. The organic extracts are stored most effectively in all-Teflon vessels, with subsequent processing in the same Teflon container. (2) If unprocessed water samples are to be stored, they should be filtered, acidified, and stored frozen, pending complete processing.

This study was supported under the National Science Foundation, NSF Grants GI-41896 and DES-74-12512. Time aboard the R/V *Ridgely Warfield* was made available by the Chesapeake Bay Institute, The Johns Hopkins University.

REFERENCES

1 G. G. Eichnolz, A. E. Nagel, and R. B. Hughes, Anal. Chem., 37 (1965) 863.
2 F. K. West, P. W. West, and F. A. Iddings, Anal. Chim. Acta, 37 (1967) 112.
3 D. E. Robertson, Anal. Chim. Acta, 42 (1968) 533.
4 A. W. Struempler, Anal. Chim. Acta, 45 (1973) 2251.
5 P. G. Brewer, D. W. Spencer, and C. L. Smith, Atomic Absorption Spectrometry, American Society for Testing and Materials, STP 443 (1969) p. 70.
6 W. Slavin, At. Absorpt. Newsl., 3 (1964) 141.
7 S. R. Koirtyohann and J. W. Wen, Anal. Chem., 45 (1973) 1986.
8 R. J. Stolzberg, Analytical Methods in Oceanography, T. R. P. Gibbs, Jr., (Ed.), American Chemical Society, Washington, D. C. (1975).

Analytica Chimica Acta, 97 (1978) 87—91

IMPROVED SEPARATION OF CADMIUM-109 FROM SILVER CYCLOTRON TARGETS BY ANION-EXCHANGE CHROMATOGRAPHY IN NITRIC ACID—HYDROBROMIC ACID MIXTURES

F. W. E. STRELOW

National Chemical Research Laboratory, Pretoria (South Africa)

(Received 5th September 1977)

SUMMARY

A method is presented for improved separation of ^{109}Cd from silver cyclotron targets. After dissolution of the target material in nitric acid and removal of silver by precipitation with copper metal, at pH 5, the cadmium is separated from zinc, copper and other elements by anion exchange chromatography. The solution in 0.5 M nitric acid plus 0.1 M hydrobromic acid is percolated through a column containing 4 ml of AG1-X8 anion-exchange resin (100—200 mesh), equilibrated with the same acid mixture. Zinc, copper(II) and other elements are eluted with 50 ml of this mixture. Cadmium is retained and finally eluted with 50 ml of 3 M nitric acid. The cadmium is retained much more strongly from the hydrobromic acid mixture than from the 0.02 M hydrochloric acid used for such separations previously; the presence of the strongly absorbed nitrate anion in fairly high concentration completely eliminates the tailing of zinc observed in 0.02 M hydrochloric acid. A typical elution curve and results of quantitative separations are presented.

Carrier-free ^{109}Cd, produced from silver targets by the ^{109}Ag (d, 2n)^{109}Cd reaction, is an important source material for x-ray fluorescence spectrometry, and is becoming especially important as the source in portable x-ray fluorescence instruments used for the direct determination of gold in South African mines. The requirements are for the cyclotron product to be as carrier-free as possible, to contain a minimum of foreign solid material and no other activities.

One of the first methods for the separation of ^{109}Cd from silver targets was based on a system of solvent extractions [1], while Grachev et al. [2] precipitated silver and copper(I) as iodides followed by an anion-exchange separation of cadmium from the filtrate with dilute hydrochloric acid as eluant for impurities. Both methods give products of insufficient purity; in the iodide precipitation, substantial amounts of cadmium activity are lost through adsorption on and inclusion in the precipitate. To avoid the precipitation step, anion exchange in concentrated hydrochloric acid can be used for the separation of cadmium from silver according to known distribution coefficients [3]. Zinc, copper(II), and most other elements are eluted with 0.02 M hydrochloric acid, while cadmium is still retained [3, 4]. Because silver has a limited solubility in hydrochloric acid and is somewhat more

soluble in hydrobromic acid of high concentration, the latter has been used [5] but the volumes of solution become inconveniently large when several grams of silver are present. Neirinckx [6] therefore removed silver by electrochemical precipitation with copper metal and showed that adsorption losses were negligible. The problem therefore reduces to a separation of cadmium from large amounts of copper(II), residual traces of silver and some impurities e.g. ^{65}Zn originating from the ^{65}Cu(d, 2n)^{65}Zn reaction from traces of copper present in the silver target. In the procedure developed by Neirinckx, copper(II) and zinc are eluted with 0.02 M hydrochloric acid from a column containing 25 ml of Dowex 1-X8 anion-exchange resin; the cadmium is retained and finally eluted with 3 M nitric acid [6]. Unfortunately, zinc shows fairly pronounced tailing on elution with 0.02 M hydrochloric acid, and in routine separations the ^{109}Cd is often contaminated with radiometrically measurable amounts of ^{65}Zn. This decreases the value of the product and often forces one or two repetitions of the ion-exchange separation step to be made.

Andersen and Knudsen [7] showed that cadmium is adsorbed by anion-exchange resins from bromide solutions of low concentration considerably more strongly than from corresponding chloride solutions, but did not present information on the elution behaviour of cadmium with zinc or copper. Zinc is less strongly adsorbed from bromide than from chloride solutions; the separation factor between cadmium and zinc and also between cadmium and copper(II) is therefore much larger in bromide than in chloride solutions. A separation in hydrobromic acid should therefore require a much smaller column, but work in this laboratory indicated that, on elution with dilute hydrobromic acid, zinc also shows considerable tailing [5]. A systematic investigation of anion exchange distribution coefficients in nitric—hydrobromic acid mixtures has shown [8] that very large separation factors between cadmium and zinc can be obtained when the nitric acid concentration is fairly high and the hydrobromic acid concentration is low. Furthermore, the presence of a reasonable concentration of nitrate anion reduces the tailing of zinc so much that it practically disappears. From this a procedure for the separation of ^{109}Cd from silver targets has been developed; a column containing only 4 ml of AG1-X8 anion exchange resin and small elution volumes gives a product of considerably better purity than that obtained previously.

EXPERIMENTAL

Reagents and apparatus

Analytical reagent-grade chemicals were used throughout. Water was distilled and then passed through an Elgastat deionizer. The resin used was the AG1-X8 quaternary amine anion exchanger (polystyrene base; Bio-Rad Laboratories, Richmond, California). Borosilicate glass tubes (11.5 or 9 mm i.d., ca. 250 mm long) fitted with a No. 2 porosity glass sinter and a burette tap at the bottom and a B14 joint at the top, were used as columns. Atomic absorption measurements were carried out with a Techtron AA-5 instrument.

Elution curve

A column containing 5 ml of AG1-X8 resin (200—400 mesh) was prepared and equilibrated with 100 ml of 0.5 M nitric acid containing 0.1 M hydrobromic acid. The resin column was ca. 50 mm in length and 11.5 mm in diameter. A solution (25 ml) containing 1.5 g of copper(II), 2 mg of zinc and 1.5 mg of cadmium (as the nitrates in 0.5 M nitric acid which was also 0.1 M in hydrobromic acid) was passed through the column. The ions were washed onto the resin with a few portions of 0.5 M nitric acid containing 0.1 M hydrobromic acid; the elution was continued with the same reagent at a flow rate of 1.5 ± 0.5 ml min^{-1}. Fractions (5 ml) were taken with an automatic fractionator; the amounts of cadmium, zinc and copper in the fractions were determined by a.a.s. with an air—acetylene flame and the 228.8 nm and 213.9 nm and 324.8 nm lines, respectively. The experimental elution curve is shown in Fig. 1.

Quantitative separations

Ion-exchange columns containing 4 ml of AG1-X8 resin (200—400 mesh) particle size were prepared and equilibrated with ca. 100 ml of 0.5 M nitric acid containing 0.1 M hydrobromic acid. The resin columns were ca. 60 mm in length and 9.5 mm in diameter. A solution (30 ml) containing ca. 1 g of either copper(II) or zinc (as the nitrates in 0.5 M nitric acid containing 0.1 M HBr) and cadmium in the amounts shown in Table 1 was percolated through the column. The ions were washed onto the resin with a few portions of mixed acid of the same concentration and then eluted with a total of ca. 60 ml of the eluting agent and a flow rate of 1.5 ± 0.5 ml min^{-1}. The copper(II) and zinc fractions were taken from the beginning of the adsorption step, evaporated to dryness on the water bath and made up to 25 ml with 0.1 M hydrochloric acid for the determination of cadmium by a.a.s. The cadmium remaining on the column was eluted with 50 ml of 3 M nitric acid, at the same flow rate. The cadmium fractions were also evaporated to dryness and

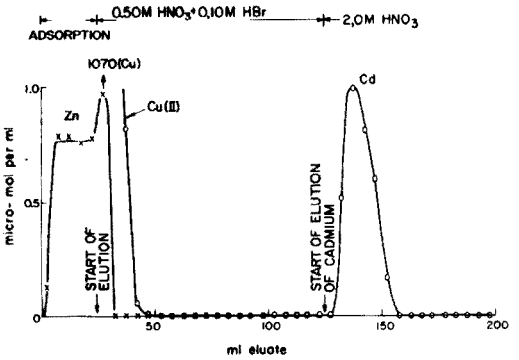

Fig. 1. Elution curve for Cd—Zn—Cu(II) with 0.5 M HNO_3 + 0.1 M HBr. Column 5 ml (50 × 11.5 mm) AG1-X8 resin, 200—400 mesh, equilibrated with 0.5 M HNO_3 + 0.1 M HBr. Flow rate 1.5 ± 0.5 ml min^{-1}.

TABLE 1

Results of quantitative separations

Taken		Cd found in Cd fraction[a, b] (μg)	Cu or Zn found in Cd fraction[a] (μg)
Other element (g)	Cadmium (μg)		
1.05 g Cu	11.71	11.73 ± 0.05	0.4—0.8 μg Cu
1.05 g Cu	117.1	117.2 ± 0.1	0.3—0.8 μg Cu
1.05 g Cu	586	586 ± 1	0.2—0.9 μg Cu
1.12 g Zn	11.71	11.72 ± 0.08	1.4—2.7 μg Zn
1.12 g Zn	117.1	117.1 ± 0.2	1.9—2.8 μg Zn
1.12 g Zn	586	587 ± 1	1.7—2.6 μg Zn

[a]Averages of 3 separations. [b]The amount of Cd found in the other fraction was <0.1.

made up to 10 ml in 0.1 M hydrochloric acid. Copper and zinc were determined in these fractions and, after suitable dilution, cadmium was determined by a.a.s. with an air—acetylene flame and the 324.8 nm (Cu), 213.9 nm (Zn) and 228.8 nm (Cd) lines, respectively. Blank runs were carried out on the copper and zinc; the results obtained for cadmium were corrected accordingly. The results are presented in Table 1.

Recommended procedure for the separation of cadmium-109

After the target material has been dissolved in nitric acid and silver has been deposited with copper metal as described by Neirinckx [6], ^{109}Cd is separated from zinc, copper(II) and other elements as described under Quantitative separations, but with 100—200 mesh resin and a flow rate of 3.0 ± 0.5 ml min^{-1}. The cadmium fraction is evaporated to dryness, and after the addition of ca. 1 ml of 12M hydrochloric acid, the evaporation is repeated. The dry chlorides are then made up with the desired solvent.

DISCUSSION

The results (Table 1) show that the proposed method completely separates microgram-amounts of cadmium from gram-amounts of copper and zinc; less than 1 μg of copper and 1—3 μg of zinc are found in the cadmium fraction when ca. 1 g of these elements is present. As only micrograms of zinc are present in an actual target processing solution and the ^{65}Zn activity is considerably lower than the ^{109}Cd activity, detectable amounts of ^{65}Zn or inactive zinc do not remain with the cadmium product. Cadmium recoveries are quantitative for amounts ranging from a few to a few hundred micrograms, the amounts remaining in the zinc and copper fractions being less than 0.1 μg, the detection limit. This covers the actual situation; the silver target material used at the cyclotron contains ca. 40 μg of cadmium per gram of silver according to specification. About 3—10 g of target material are removed and

processed in a normal run. Activity measurements indicated that the separation of cadmium is also quantitative at submicrogram levels. The products obtained are of higher purity with respect to solid material than those obtained previously [6]. The solid material content, on evaporation, was ca. 2—3 μg per mCi of ^{109}Cd. Most of this is inactive cadmium salt originating from the silver target, or reactions in the target.

Because the distribution coefficient of cadmium in 0.5 M nitric acid containing 0.1 M hydrobromic acid is ca. 10 times larger than that in 0.02 M hydrochloric acid, while the coefficients for copper(II) and zinc are smaller than 1, a column of only 4 ml bed volume can be used in this procedure compared with the 25-ml column used by Neirinckx [6]. In addition, the 200—400 mesh resin could be replaced by 100—200 mesh resin; a fairly fast flow rate could therefore be used, and this, together with the small elution volume, also reduced considerably the time required for the separation.

The proposed eluant (0.5 M nitric acid and 0.1 M hydrobromic acid) for zinc completely eliminates the tailing of zinc given by 0.02 M hydrochloric acid; after 25 ml, (Fig. 1) the zinc in the eluate was below the detection limit of the a.a.s. method. The volume of 60 ml was used to ensure quantitative elution of copper; because of its very high initial concentration, copper persists longer in the eluate through concentration diffusion processes. It was also an additional safety measure to ensure complete separation under routine conditions. The elution volume for cadmium (50 ml of 3 M HNO_3) also has a large safety margin; 30 ml gives more than 95% recovery.

Other elements (e.g. iron(III), gallium, indium, cobalt(II) and manganese) which have a lesser tendency to bromide complex formation than zinc have not been investigated in detail but should also be separated from cadmium by the described procedure. The same applies to elements with negligible tendencies to bromide complex formation, e.g. aluminium, titanium(II), zirconium, the alkali metals, the alkaline earths, and the rare earth elements.

REFERENCES

1 R. D. Maxwell, H. R. Haymond, W. M. Garrison and J. G. Hamilton, J. Chem. Phys., 17 (1949) 1006.
2 S. A. Grachev, V. N. Melkinov, in A. Ryukhin and M. A. Toropova, Radiokhimiya, 3 (1961) 116.
3 K. A. Kraus and F. Nelson, Proc. Int. Conf., Peaceful Uses At. Energy, Geneva, 1955 (1956) 113.
4 S. Kallmann, H. Oberthin and R. Liu, Anal. Chem., 32 (1960) 58.
5 F. W. E. Strelow, W. J. Louw and C. H. S. W. Weinert, Anal. Chem., 40 (1968) 2021.
6 R. D. Neirinckx, Anal. Chim. Acta, 58 (1972) 127.
7 T. Andersen and A. B. Knudsen, Acta Chem. Scand., 16 (1962) 849.
8 F. W. E. Strelow, to be published.

Analytica Chimica Acta, 97 (1978) 93—110

NUCLEAR MAGNETIC RELAXATION TITRATION OF Cu^{2+}, Ni^{2+}, Mn^{2+}, Zn^{2+}, AND Fe^{3+} WITH 1,10-PHENANTHROLINE HYDROCHLORIDE IN THE PRESENCE OF THIOCYANATE

A. SCHLÜTER and ALARICH WEISS*

Institut für Physikalische Chemie, Physikalische Chemie III, Technische Hochschule Darmstadt, Petersenstrasse 20, D-6100 Darmstadt (West Germany)

(Received 17th August 1977)

SUMMARY

Nuclear magnetic relaxation titration is used to determine Cu^{2+}, Ni^{2+}, Mn^{2+}, Zn^{2+}, and Fe^{3+} with 1,10-phenanthroline hydrochloride in the presence of thiocyanate; separation of the precipitated complex $Me(1,10\text{-phen})_x(SCN)_y$ from the remaining solution is unnecessary. The stoichiometry of the complexes can be determined. The concentration of diamagnetic ions in solution is measurable if a paramagnetic transition metal is used as a magnetic indicator.

Two possibilities are available when magnetic measurements are applied to analytical problems: (a) the magnetic susceptibility of a sample can be determined and, as it is proportional to the number of paramagnetic atoms, ions, and molecules, it is a measure of the concentration of these species; and (b) the magnetic moments of nuclei, particularly of protons, can be used for chemical analysis in nuclear magnetic resonance (n.m.r.) measurements. The main difficulty in a "magnetic analysis" is the fact that particles are either paramagnetic or diamagnetic; susceptibility measurements are overall measurements. Considering n.m.r. experiments, this difficulty is somewhat lessened as the resonance frequency and the relaxation behavior are specific properties of a certain nucleus.

In applying n.m.r. methods to analytical problems, two main directions may be distinguished. (a) Nuclear magnetic relaxation, a property of the interaction between the nuclear spins or between the spins and its surroundings, is most easily used in performing a nuclear magnetic relaxation titration (n.m.r.t.) in aqueous solutions. The spin—lattice relaxation time T_1 of the ^1H nuclei is measured as a function of the concentration C of paramagnetic species in solution; the quantitative relation between T_1 and C is simply $1/T_1 \sim C$. Equally useful is the determination of the spin—spin relaxation time T_2, for which, to a first approximation, $1/T_2 \approx C$. N.m.r.t. was introduced into quantitative chemical analysis by Nothnagel and Weiss [1] and applied [1, 2] in several ways, including redox reactions. Also, the paramagnetic ion may act solely as a magnetic indicator, as shown by

Schlüter and Weiss [2] in titrating Ce^{4+} with thiosulfate in the presence of Fe^{3+} as the indicating magnetic ion. Another useful application is the precipitation of the paramagnetic ions and the determination of T_1 (or T_2) in the remaining solution as a function of the added amount of precipitation reagent [1, 2]. Furthermore, the formation of complex ions, often accompanied by a change of the effective magnetic moment μ_{eff}, can be used in n.m.r.t. for the determination of Ni^{2+} [1] or Cu^{2+} [2] with potassium cyanide. (b) The second way of using the magnetic properties of nuclei, particularly ^1H (or ^{13}C), is the observation of the chemical shift of the ^1H-n.m.r. signal as a function of paramagnetic ions in solutions. Such a study is the determination of Ni^{2+} by complex formation with cyanide [3].

The applicability of classical susceptibility measurements to chemical analysis was shown by Heit and Ryan [4], who titrated Ni^{2+} in aqueous solution with cyanide solution. The whole system is suspended on the magnetic balance and the concentration of Ni^{2+} determined by the change of weight of the system during the reaction

$$Ni^{2+}(\text{paramagnetic}) + 4CN^-(\text{diamagnetic}) \rightarrow [Ni(CN)_4]^{2-}(\text{diamagnetic})$$

Two aspects of n.m.r.t., which seems to be the most simple and versatile of the possible magneto–analytical methods, will be discussed: (a) small concentrations of ions can be determined by applying corrections (available from experiment) for the diamagnetic part of the relaxation time, and (b) paramagnetic ions can be determined by precipitation without removing the precipitated solid from the solution. This method can be extended to the coprecipitation of diamagnetic ions together with paramagnetic indicator ions. In the experiments reported here, 1,10-phenanthroline hydrochloride in the presence of thiocyanate is used as the precipitating reagent.

THEORY

This treatment is restricted to aqueous solutions containing paramagnetic species and to the hydrogen nucleus ^1H (nuclear spin $I = 1/2$) as the probe nucleus. Subject to an external magnetic field H_0, the nuclear spins populate two energy levels and their population at a given equilibrium temperature T_s is governed by the Boltzmann distribution

$$N_{-1/2}/N_{+1/2} = \exp\{-\gamma\hbar H_0/kT_s\} \tag{1}$$

where γ is the gyromagnetic ratio of the proton, $\hbar = h/2\pi$ = Dirac's constant, and k is the Boltzmann constant. The resulting total nuclear spin magnetization M_0 is given by

$$M_0 = \chi_0 H_0, \tag{2}$$

where χ_0 is the nuclear magnetic susceptibility.

Under the influence of an oscillating magnetic field H_1 of frequency $\nu_0 = \gamma H_0/2\pi$, the Boltzmann distribution is disturbed and this is equivalent

to a new spin temperature T_a. Turning off H_1, the spin system relaxes back to T_s, the lattice temperature. The dominant time constant for this process is T_1, the spin–lattice relaxation time, which depends on the coupling between the spin system and the surrounding lattice.

In the basic theory for spin–lattice relaxation in liquids [5], the relaxation rate in diamagnetic liquids, $(1/T_1)_d$, is the sum of the rates due to the translational and rotational motions

$$(1/T_1)_d = (1/T_1)_t + (1/T_1)_r \tag{3}$$

Both terms were treated in detail by Bloembergen [5] and by Abragam [6]. The relaxation rate depends on the number of protons per unit volume, the viscosity of the solution, the temperature, the intramolecular hydrogen distance, the fourth power of the gyromagnetic ratio of the proton, and other factors. In diamagnetic liquids (liquid solutions) the frequencies of the thermal molecular motions (rotational and translational motions) are of the order of 10^{11} Hz. The n.m.r. frequency of protons in a field $H_0 \approx 0.5$ T is about 2×10^7 Hz. Therefore, T_1 (^{1}H) in diamagnetic liquids is rather long (order of seconds at $T = 300$ K).

In paramagnetic aqueous solutions the interaction of the magnetic moment of the protons and the magnetic moment of the paramagnetic ion (electron magnetic moment) has to be considered. This interaction is much more effective in the relaxation mechanism than the proton-proton interaction because $\mu_B/\mu_{proton} \approx 1000$. In such paramagnetic solutions the nuclear magnetic relaxation rate of protons is given by

$$(1/T_1)_{tot} = (1/T_1)_p + (1/T_1)_d \tag{4}$$

where "tot", "p", and "d" stand for "total", "paramagnetic", and "diamagnetic".

The spin–lattice relaxation time T_1 of protons in aqueous solutions depends strongly on the concentration of paramagnetic ions in the solution and on their effective magnetic moment, μ_{eff}. The theory of Bloembergen [5] describes the contribution of the interaction between the nuclear magnetic moments and the magnetic moment of the unpaired electrons of the paramagnetic ions by the relation

$$(1/T_1)_p = (12/5)\,\pi^2\gamma^2\mu_{eff}^2\,N'\eta/kT \tag{5a}$$

where N' is the number of paramagnetic ions per unit volume, η is the viscosity of the solution, and μ_{eff} is the magnetic moment of the paramagnetic ion. A slightly different treatment [6] of the relaxation theory leads to a numerical modification of eqn. (5a)

$$(1/T_1)_p = (16/15)\,\pi^2\gamma^2\mu_{eff}^2 N'\eta/kT \tag{5b}$$

The equations given above are valid only for a dipole–dipole interaction between the electron spin and the nuclear spin. If this relaxation mechanism alone determines the relaxation time, the relation $T_1 = T_2$ should be valid, as

shown by Bloembergen et al. [7]. Solomon [8] has confirmed this relation for the nuclear magnetic relaxation of the protons in aqueous Fe^{3+} solutions; T_2, analogously applicable as a measurable quantity in n.m.r.t., will not be considered further here.

In addition to the dipole–dipole interaction, the nuclear magnetic relaxation time can be influenced by other relaxation mechanisms, e.g. scalar coupling, quadrupole relaxation, etc. This is not critical in n.m.r.t. because all terms which determine the relaxation rate in paramagnetic solutions are proportional to the concentration C of the paramagnetic ions in the solution. Therefore, eqn. (5) can be written in the form (at constant temperature)

$$(1/T_1)_p = a \cdot C \tag{6}$$

The factor a depends on μ_{eff} and γ, and also on the number of protons within the coordination sphere of the paramagnetic ion, on the internal motions within the solution, and on the rate of exchange of hydrogen atoms, protons or hydrogen-containing molecules within the coordination sphere of the paramagnetic ion with the "free" solution [1, 2]. During the n.m.r.t. experiment, either the factor $a = f(\mu_{eff}, \gamma, N, \ldots)$, or the concentration C, or both, are changed. The factor a is affected in redox reactions and by the formation of complexes. During precipitation the concentration C of the paramagnetic ions diminishes and $(1/T_1)_{tot}$ and $(1/T_1)_p$ approach zero.

N.m.r.t. is not restricted to one species of paramagnetic ions. In aqueous solutions of k species of paramagnetic ions, the relaxation rate is given by

$$(1/T_1)_p = \sum_{i=1}^{k} a_i C_i \tag{7}$$

The factor a_i may be different for each kind of ions or molecules. For diamagnetic particles, $a_i = 0$.

The relation between the paramagnetic relaxation rate $(1/T_1)_p$ and the added volume V_B of the titration reagent is discussed below. An initial volume V_0 of the solution which contains $(n_{A_i})_0$ moles of the ion species A_i is assumed. The paramagnetic part of the relaxation rate of this solution is:

$$(1/T_1)_p = \sum_{i=1}^{k} a_i C_i = \sum_{i=1}^{k} a_i (n_{A_i})_0 / V_0 = (1/T_1)_{p,0} \tag{8}$$

Now volume V_B of the reagent, which contains the reactant of concentration $[B]_0$ is added. Solution B may be paramagnetic or diamagnetic. It is assumed that one of the species A_i (here A_1) reacts with B according to

$$\alpha A_1 + \beta B \rightarrow \gamma_j P_j \tag{9}$$

No special assumptions are made about the products P_j which may be either paramagnetic or diamagnetic. Until the equivalence point is reached, the balance condition is

$$n_{A_1} = (n_{A_1})_0 - (\alpha/\beta)\, n_B = (n_{A_1})_0 - (\alpha/\beta)\, [B]_0\, V_B \tag{10a}$$

$$n_{p_j} = (\gamma_j/\beta)\, n_B = (\gamma_j/\beta)\, [B]_0\, V_B \tag{10b}$$

$$n'_B = 0 \tag{10c}$$

The species B is not present in the solution ($n'_B = 0$) before the equivalence point is reached. Combining these relations with eqn. (7), the relaxation rate is given by

$$(1/T_1)_p = 1/V_{tot} \left\{ a_1[(n_{A_1})_0 - (\alpha/\beta)\, n_B] + \sum_{i=2}^{k} a_i (n_{A_i})_0 + \sum_{j=k+1}^{m} a_j (\gamma_j/\beta)\, n_B \right\} \tag{11a}$$

or

$$(V_{tot}/T_1)_p = \left\{ \sum_{j=k+1}^{m} a_j (\gamma_j/\beta) - a_1 (\alpha/\beta) \right\} n_B + \sum_{i=1}^{k} a_i (n_{A_i})_0 \tag{11b}$$

respectively

$$(V_{tot}/T_1)_p = \left\{ \sum_{j=k+1}^{m} a_j (\gamma_j/\beta) - a_1 (\alpha/\beta) \right\} [B]_0\, V_B + (V_0/T_1)_{p,0} \tag{11c}$$

A further simplification of eqn. (11c) is possible by normalizing the total volume V_{tot} with respect to the initial volume V_0 to obtain

$$(V_{tot}/V_0)\, (1/T_1)_p = \left\{ \sum_{j=k+1}^{m} a_j (\gamma_j/\beta) - a_1 (\alpha/\beta) \right\} ([B]_0/V_0)\, V_B + (1/T_1)_{p,0} \tag{12}$$

Equation (12) relates $V_{tot}/(V_0 \cdot T_1)_p$ linearly with V_B until the equivalence point is reached. The slope of the straight line is determined by the differing magnetic properties of the different species summarized in the coefficients a_i. Interception with the ordinate is given by the relaxation rate of the initial solution (eqn. 8). By multiplication of the paramagnetic relaxation rate $(1/T_1)_p$ by the factor V_{tot}/V_0, the dilution effect caused by the addition of volume V_B of the titration reagent is compensated. This is readily seen if the dilution of a solution of one paramagnetic species is being considered. Then

$$(1/T_1)_p = a \cdot C = a \cdot n/V_{tot}, \text{ with } n = C_0\, V_0 \tag{13}$$

From this results

$$(1/T_1)_p = a \cdot C_0\, V_0/V_{tot}; \quad (V_{tot}/V_0)\, (1/T_1)_p = a \cdot C_0 = (1/T_1)_{p,0} \tag{14}$$

At the equivalence point in the n.m.r.t., this gives

$$n_B = (\beta/\alpha)\, (n_{A_1})_0 = [B]_0\, V_{eq} \tag{15}$$

Hence eqn. (12) changes to:

$$(V_{tot}/V_0)\, (1/T_1)_p = \left\{ \sum_{j=k+1}^{m} a_j (\gamma_j/\alpha) - a_1 \right\} (n_{A_1})_0/V_0 + (1/T_1)_{p,0} \tag{16}$$

Beyond the equivalence point the component B is present in the solution. When B is paramagnetic, it will add to $(1/T_1)_p$. The following relations are valid

$$n_{A_1} = 0; \quad n'_B = n_B - (\beta/\alpha)\,(n_{A_1})_0; \quad n_{p_j} = (\gamma_j/\alpha)\,(n_{A_1})_0 \tag{17}$$

The relaxation rate $(1/T_1)_p$ is

$$(1/T_1)_p = (1/V_{tot})\left\{ a_B\, n'_B + \sum_{j=k+1}^{m} (\gamma_j a_j/\alpha)\,(n_{A_1})_0 + \sum_{i=2}^{k} a_i (n_{A_i})_0 \right\} \tag{18a}$$

or

$$(1/T_1)_p = (1/V_{tot})\left\{ a_B [n_B - (\beta/\alpha)\,(n_{A_1})_0] + \sum_{j=k+1}^{m} (\gamma_j\, a_j/\alpha)\,(n_{A_1})_0 + \sum_{i=2}^{k} a_i (n_{A_i})_0 \right\} \tag{18b}$$

Combining eqns. (18b) and (15),

$$(1/T_1)_p = (1/V_{tot})\left\{ a_B\,[B]_0\,(V_B - V_{eq}) + \sum_{j=k+1}^{m} (\gamma_j a_j/\alpha)\,(n_{A_1})_0 + \sum_{i=2}^{k} a_i (n_{A_i})_0 \right\} \tag{19}$$

Multiplication of eqn. (19) by V_{tot}/V_0 gives

$$(V_{tot}/V_0)\,(1/T_1)_p = a_B\,[B]_0\,V_B/V_0 - a_B\,[B]_0\,V_{eq}/V_0 + 1/V_0 \left\{ \sum_{j=k+1}^{m} \gamma_j a_j/\alpha\,(n_{A_1})_0 + \sum_{i=2}^{k} a_i (n_{A_i})_0 \right\} \tag{20}$$

Equation (20) represents a straight line which describes the behavior of $V_{tot}/(V_0 \cdot T_1)_p$ beyond the equivalence point. Therefore, V_{eq} is found at the interception of the straight lines given by eqn. (12) (reaction line) and eqn. (20) (excess line). The accuracy in determining V_{eq} depends on the slopes of the reaction line and the excess line and increases with increasing difference in the slopes.

Thus far, only the paramagnetic part of the relaxation rate has been considered. This is incorrect if, for example, the final solution is diamagnetic, as when precipitating a paramagnetic species with a diamagnetic reagent. Here, $(1/T_1)_{tot}$ reaches a value of about 0.3 s^{-1}, comparable with $1/T_1$ for pure water. To determine the paramagnetic part of $(1/T_1)_{tot}$ the experimentally measured relaxation rate must be corrected according to

$$(1/T_1)_p = (1/T_1)_{exp} - (1/T_1)_d = (1/T_1)_{tot} - (1/T_1)_d \tag{21}$$

Multiplying $(1/T_1)_p$ in eqn. (21) by V_{tot}/V_0, the true paramagnetic relaxation rate is found.

Figure 1 shows theoretical curves. The concave ones show the uncorrected relaxation rate $(1/T_1)_{tot}$ as a function of the normalized added volume V_B/V_{eq} (V_{eq} is the total added volume of B at the equivalence point $V_{tot} = 2V_0$). Three different values of the paramagnetic part $(1/T_1)_{p,0}$ were chosen, e.g. 2.5 s^{-1}, 5 s^{-1}, and 10 s^{-1}. The diamagnetic part $(1/T_1)_d$ is constant and equal to 0.5s $^{-1}$. The straight lines in Fig. 1 are obtained by applying the corrections discussed above. At the equivalence point, $V_B/V_{eq} = 1$, the solution is diamagnetic.

A further possibility of normalization is the division of $V_{tot}/(V_0 \cdot T_1)_p$ by $(1/T_1)_{p,0}$ (initial relaxation rate). Thereby the concentration dependence of the relaxation is corrected. All the curves start at $(V_{tot}/V_0)\,(T_{1,0}/T_1)_p = 1$. During the titration this ratio will increase or decrease.

EXPERIMENTAL

To determine T_1, the spin echo method [9] is normally used. To measure the spin lattice relaxation time, T_1, a commercial spectrometer (Bruker-Minispec P 20) was used.

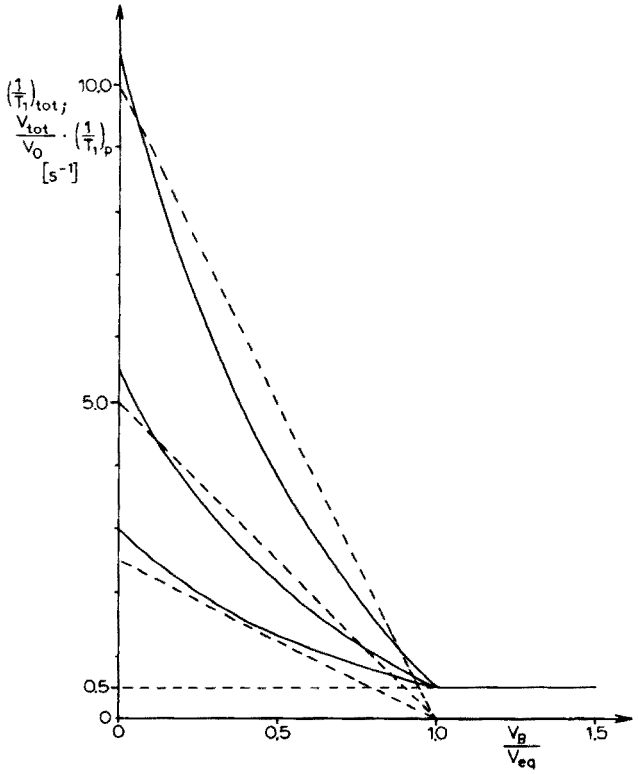

Fig. 1. Theoretical ^1H nuclear magnetic relaxation rate, $(1/T_1)_{tot}$ (full lines), and corrected values, $(V_{tot}/V_0)\,(1/T_1)_p$ (dashed lines), as a function of the volume ratio V_B/V_{eq} of the precipitating reagent ($V_{eq} = V_B$ at the equivalence point) for three different initial rates: $(1/T_1)_p$ = 10 s^{-1}, 5 s^{-1}, and 2.5 s^{-1}; $(1/T_1)_d$ = 0.5 s^{-1}.

The sample under investigation was kept at constant temperature within the homogeneous field H_0 of a magnet and was irradiated with the resonance frequency $\omega_0 = \gamma H_0$ at certain time intervals for short periods. An irradiation of duration $t = \pi/(2\gamma H_1)$ (H_1 is the magnetic field strength of the irradiating field) is called a $\pi/2$-pulse or 90° pulse. Here Hahn's 180° — τ — 90° pulse sequence [9] was used (τ = time interval between the two high-frequency pulses). The 180° pulse (π-pulse) inverts the ^{1}H magnetization $\vec{M}_z$ of the sample from the direction $+z \| \vec{H}_0$ to $-z$. Spin lattice relaxation (longitudinal relaxation) occurs, and the magnetization returns to its original direction. The relaxation is described by the Bloch equation [10]

$$dM_z/dt = -(M_z - M_0)/T_1 \tag{22}$$

whereby $M_0 = M_z$ ($\tau = 0$). By integration

$$M_z = M_0 (1 - 2 \exp(-\tau/T_1)). \tag{23}$$

The value of M_z at time τ is measured by applying a 90° pulse ($\pi/2$-pulse) τ seconds after the application of the 180° pulse. This pulse rotates the magnetization M_z by 90°, i.e. into the plane (xy). A free induction decay (f.i.d.) signal is thus induced in the receiver coil of the spectrometer. The amplitude A of the f.i.d. is proportional to the magnetization M_z at time τ. Equation (23) and the relationship $A(\tau) \sim M_z$ give

$$\ln(A_0 - A(\tau)) = \ln(2 \cdot A_0) - \tau/T_1 \tag{24}$$

where $A(\tau)$ is the maximum amplitude of the f.i.d. of the 90° pulse at time τ, and A_0 is the amplitude for $\tau \to \infty$ (in practice for $\tau \gg T_1$). Figure 2 shows the function $A(\tau)/A_0 = f(\tau)$. The plot of $\ln(A_0 - A(\tau))$ versus τ gives a straight line of slope $-1/T_1$.

A second method of measuring T_1 in n.m.r.t. is the determination of τ_{min} for which $A(\tau) = 0$, when $\tau_{min} = T_1 \ln 2$. Here the absolute accuracy is somewhat lower, but this is of minor importance in determining $1/T_1 = f(C)$.

In this work, the application of eqn. (24) was preferred; rearrangement of eqn. (24) gives

$$-(1/\tau) \ln (1 - A(\tau)/A_0)/2 = (1/T_1)_{tot} \tag{25}$$

Since T_1 is independent of τ, $A(\tau)/A_0$ is determined at different times and τ is adjusted so that $A(\tau)/A_0 \sim 0.6$; $A(\tau)/A_0 = 0.6$ is the optimum value, as an estimate of the possible errors shows. In the n.m.r.t. experiment both amplitudes $A(\tau)$ and A_0 are measured for only one τ value, and $1/T_1$ is calculated according to eqn. (25).

In experiments where $\tau \leqslant 1$ s, the process of the ^{1}H-T_1 measurement is not the time-determining step in n.m.r.t. of paramagnetic solutions.

All chemicals used were of analytical grade (Merck AG, Darmstadt). Stock solutions of the paramagnetic salts were prepared and checked by complexometric titrations.

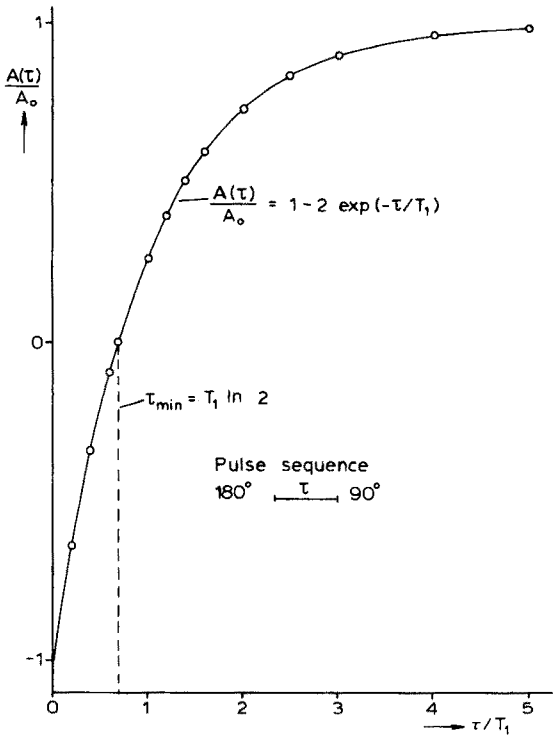

Fig. 2. Determination of T_1 by the $180° - \tau - 90°$ pulse sequence with phase-sensitive detection. The ratio $A(\tau)/A_0$ is plotted as a function of the time interval τ between the two pulses.

The solutions investigated, contained in simple test tubes, were placed in the probe coil of the oscillator. After $1/T_1$ had been determined (respectively $A(\tau)/A_0$), a definite volume of the reagent solution was added (e.g. a standard 1,10-phenanthroline hydrochloride solution) and the sample tube was shaken or the solution stirred. Then the next value of $1/T_1$ was determined, and so on.

N.M.R.T. BY PRECIPITATION

Since $(1/T_1)_p$ (or $(1/T_2)_p$) are proportional to the concentration of the paramagnetic species, strong changes in the relaxation rates can be expected during precipitation. A necessary condition for the application of n.m.r.t. to such reactions is a complete and stoichiometric reaction, and the following questions arise. (a) Is filtration necessary? (b) Must the precipitate be of definite stoichiometry? (c) If filtering is unnecessary, what influence has the particle size and the formation of colloids on the relaxation rate and thus on the n.m.r.t. results?

The applicability of n.m.r.t. to precipitation reactions was shown [1, 2] for the determination of Ni^{2+} with diacetyldioxime ($C_4H_8N_2O_2$), and of Cu^{2+} with benzoinoxime ($C_{14}H_{11}NO_2$). In both cases the precipitate was separated from the solution by filtration — only the weighing process was therefore saved compared with classical gravimetry.

The questions raised above were answered by investigating the precipitation of Cu^{2+}, Ni^{2+}, Mn^{2+}, Zn^{2+}, and Fe^{3+} with 1,10-phenanthroline hydrochloride in the presence of thiocyanate; complexes with very slight solubilities in water are formed, of the type $Me(1,10\text{-phen})_2(SCN)_2$ for Cu^{2+}, Ni^{2+}, Mn^{2+}, and Zn^{2+}, and of the type $Me(1,10\text{-phen})_2(SCN)_3$ for Fe^{3+}. Well-developed crystals which precipitate instantaneously in ammoniacal solution are formed, whereas in acidified solution the formation is often markedly hindered. The reactions are similar to those investigated [11, 12] with pyridine as the complexing ligand.

In precipitations with 1,10-phenanthroline hydrochloride (1,10-phen · HCl) plus thiocyanate, different experimental paths are possible in n.m.r.t. One way involves adding an excess of KSCN to the solution of paramagnetic ions and then titration with a solution of 1,10-phen · HCl. The reverse order, i.e. titration of a solution of 1,10-phen · HCl plus an excess of KSCN with a solution of paramagnetic ions is also possible. Alternatively, an excess of 1,10-phen · HCl can be added to the paramagnetic solution and this solution can be used to titrate a standardized thiocyanate solution. The latter method, however, has some disadvantages. The paramagnetic ions form complexes with 1,10-phenanthroline, whereby μ_{eff} and consequently $(1/T_1)_p$ are appreciably lowered, as shown in Fig. 3. For Ni^{2+}, Cu^{2+}, and Fe^{3+}, $(1/T_1)_p$ is diminished by a factor of 4—10; Ni^{2+} and Cu^{2+} were titrated in ammoniacal solution, whereas the Fe^{3+} solution was slightly acidified. A rather weak effect on the relaxation rate in solution was found for the complexes formed by Mn^{2+} with 1,10-phen · HCl. The complex formation also depends on the pH of the solution.

The addition of thiocyanate to the paramagnetic solution has only small effects on the relaxation rate; the complex formation $Me(SCN)_x^{2-x}$ has little effect on μ_{eff} and on the exchange of H_2O. A somewhat stronger influence of thiocyanate on T_1 is apparent for Fe^{3+} ions. Nevertheless, the n.m.r.t. results are not affected.

An adequate procedure for n.m.r.t. of Ni^{2+}, Cu^{2+}, Mn^{2+}, Zn^{2+}, and Fe^{3+} in the presence of thiocyanate involves: (a) addition of an excess of KSCN to the aqueous solution of $Me^{+\nu}$, and (b) n.m.r.t. precipitation with a solution of 1,10-phen · HCl. The solid complexes were not separated from the solution. No interference by the suspended solid occurred during the n.m.r.t. The addition of a small amount of benzene to the solution is helpful; it makes the precipitate rise to the surface of the liquid so that the titration is not disturbed by the motions of small crystals within the solution.

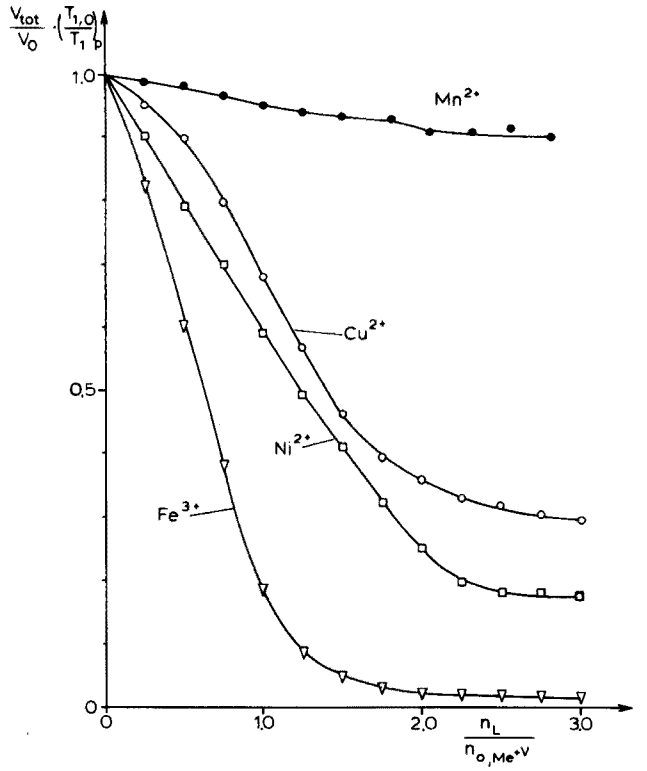

Fig. 3. Corrected relaxation rate, $(V_{tot}/V_0)\,(1/T_1)_p$, as a function of the ratio in the solution: mol number n_L of organic ligand 1,10-phen · HCl/mol number of transition metal $n_{o,Me^{+\nu}}$.

RESULTS

Titration of Cu^{2+} with 1,10-phenanthroline hydrochloride in the presence of thiocyanate

The reaction is: $Cu^{2+} + 2(1,10\text{-phen}) + 2SCN^- \rightarrow Cu(1,10\text{-phen})_2(SCN)_2$. The complex is a green flocculent precipitate on the bottom of the vessel, and has no influence on T_1. Figure 4 shows $(1/T_1)_{tot}$ (uncorrected) and $(V_{tot}/V_0)\,(1/T_1)_p$ plotted as a function of V_B.

At low ammonia concentrations, Cu(1,10-phen) $(SCN)_2$ is formed (Fig. 5); $(1/T_1)_{p,0}$ is slightly influenced by the concentration of ammonia because of the different equilibria between the copper ammine complexes.

Titration of Ni^{2+} with 1,10-phenanthroline hydrochloride in the presence of thiocyanate

The reaction in dilute ammonia is: $Ni^{2+} + 2(1,10\text{-phen}) + 2SCN^- \rightarrow Ni(1,10\text{-phen})_2(SCN)_2$. The results are shown in Fig. 6. Independent of the

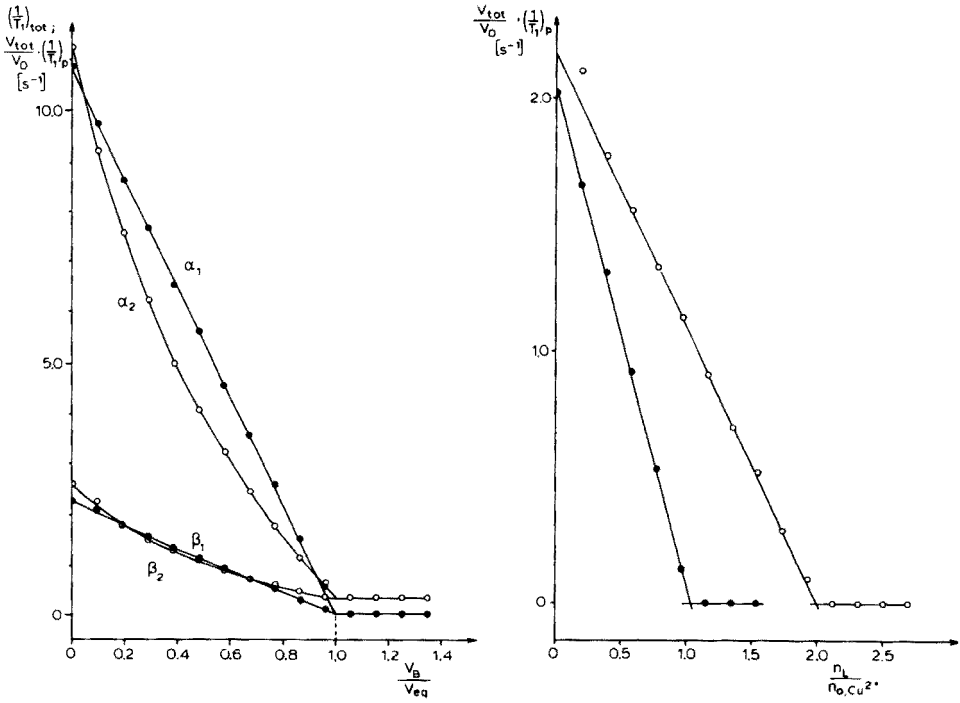

Fig. 4. Relaxation rate, $(1/T_1)_{tot}$ (α_2, β_2) and corrected relaxation rate, $(V_{tot}/V_0)\,(1/T_1)_p$ (α_1, β_1), as a function of normalized added volume of titrant. (α) 0.0208 M Cu^{2+} solution (V_0 = 5.0 ml); titration with 0.040 M 1,10-phen solution. (β) 0.00416 M Cu^{2+} solution (V_0 = 5.0 ml); titration with 0.008 M 1,10-phen · HCl solution.

Fig. 5. N.m.r.t. of Cu^{2+} with 1,10-phen · HCl plus thiocyanate. The paramagnetic relaxation rate corrected for dilution effects is plotted versus molar ratio of 1,10-phen/Cu^{2+}. ○: ammoniacal 0.00416 M Cu^{2+} solution. ●: neutral 0.00416 M Cu^{2+} solution.

initial Ni^{2+} concentrations the straight lines have the same slope, in agreement with eqn. (12). Stoichiometry of the complexes $Ni(1,10\text{-phen})_2(SCN)_2$ can be checked; the relation $[Ni^{2+}]_0 = a\,V_{B,eq}$ is strictly linear, with a slope of 0.00516 M ml^{-1} (Theory: 0.00518 M ml^{-1}). N.m.r.t. of neutral or acidic solutions was unsuccessful. In neutral solution the complex $Ni(1,10\text{-phen})(SCN)_2$ may be formed; in acidic solution, precipitation is very slow. This kinetic hindrance is probably due to the strong protonation of the organic ligand. In Fig. 7, the n.m.r.t. of 10.0 ml of 0.004 M Ni^{2+} solutions is shown. Correct results were found in ammoniacal solution, but in neutral solution the apparent concentration of Ni^{2+} was too low.

N.m.r.t. of Fe^{3+} with 1,10-phenanthroline hydrochloride in the presence of thiocyanate

A complex $Fe(1,10\text{-phen})_2(SCN)_3$ is precipitated. Contrary to the behavior of Ni^{2+} and Cu^{2+}, the Fe^{3+} complex is formed immediately in acidic solutions

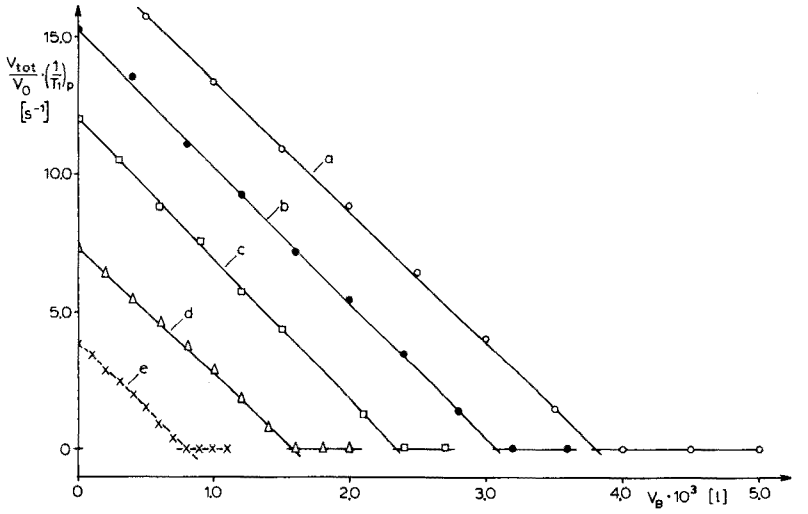

Fig. 6. N.m.r.t. of Ni^{2+} with 1,10-phen · HCl in the presence of thiocyanate. Corrected paramagnetic relaxation rate, $(V_{tot}/V_0)\,(1/T_1)_p$, is plotted against added volume V_B of titrant (0.1036 M 1,10-phen · HCl solution). $[Ni^{2+}]_0$ = 0.02 (a), 0.016 (b), 0.012 (c), 0.008 (d), and 0.004 (e) mol l^{-1}. V_0 = 10 ml in all cases.

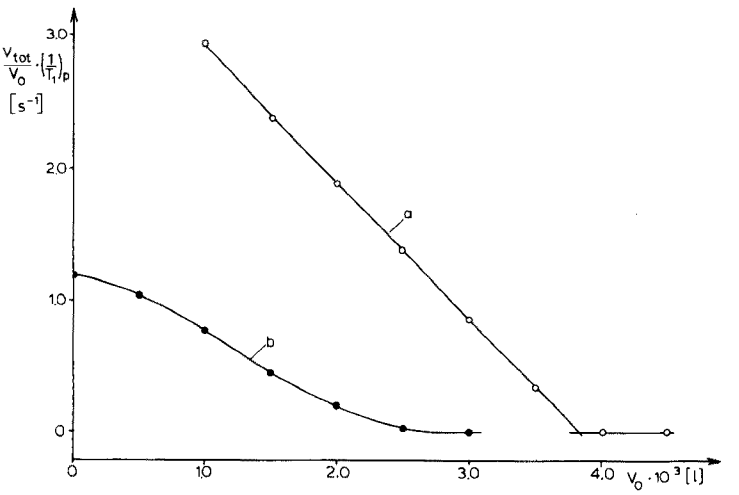

Fig. 7. Corrected paramagnetic relaxation rate $(V_{tot}/V_0)\,(1/T_1)_p$ for n.m.r.t. of Ni^{2+} as a function of added 1,10-phen · HCl solution (0.0207 M) at different acidities. (a) 0.004 M Ni^{2+} (V_0 = 10.0 ml, ammoniacal solution), (b) 0.004 M Ni^{2+} (V_0 = 10.0 ml, neutral solution).

and the use of ammoniacal solutions is impracticable. Because of the large value of μ_{eff} for Fe^{3+}, the procedure can be applied to small concentrations of Fe^{3+} (ca. 10^{-3} mol l^{-1}). The titrations of solutions with different Fe^{3+} concentrations are given in Fig. 8, and the data are listed in Table 1.

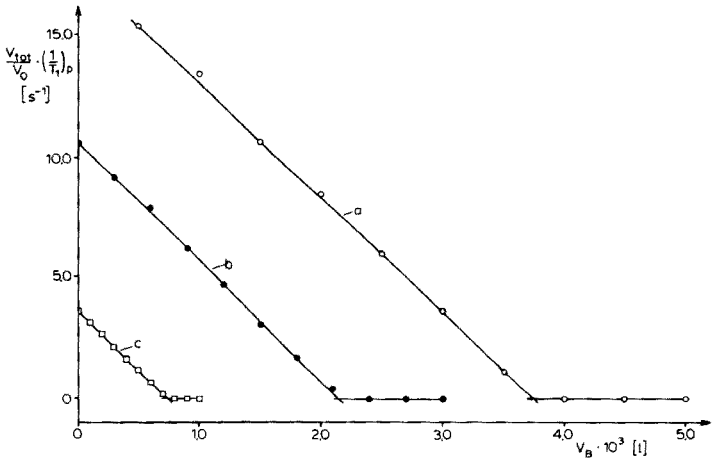

Fig. 8. N.m.r.t. of Fe^{3+} with 1,10-phen · HCl in the presence of KSCN. Corrected paramagnetic relaxation rate, $(V_{tot}/V_0)\,(1/T_1)_p$, is plotted against added volume V_B of titrant (0.02072 M 1,10-phen · HCl solution). $[Fe^{3+}]_0$ = 0.00386 (a), 0.002316 (b), 0.000772 (c) mol l^{-1}. V_0 = 10.0 ml in all cases.

TABLE 1

N.m.r.t. of transition metal ions with 1,10-phenanthroline hydrochloride in the presence of KSCN

Ion	$[Me^{+\nu}]_0$ (mol l^{-1})	$V_0\,10^3$ (l)	[1,10-phen · HCl] (mol l^{-1})	$V_{eq,calc}$ (ml)	$V_{eq,exp}$ (ml)	Error (%)
Cu^{2+} (ammoniacal solution)						
	0.0208	5	0.040	5.20	5.24	+0.8
	0.00416	5	0.008	5.20	5.16	−0.8
Ni^{2+} (ammoniacal solution)						
	0.020	10	0.1036	3.86	3.81	−1.2
	0.016	10	0.1036	3.09	3.07	−0.7
	0.012	10	0.1036	2.32	2.34	+0.9
	0.008	10	0.1036	1.54	1.58	+2.5
	0.004	10	0.1036	0.77	0.78	+1.2
Fe^{3+} (acidic solution)						
	0.003860	10	0.02072	3.73	3.76	+0.8
	0.002316	10	0.02072	2.24	2.18	−2.5
	0.000772	10	0.02072	0.75	0.75	0
Mn^{2+} (buffered solution)						
	0.003970	10	0.02072	3.83	4.08	+6.5
	0.002383	10	0.02072	2.30	2.44	+6.1
	0.000794	10	0.02072	0.77	0.81	+5.2
Zn^{2+} (buffered solution)						
	0.01165	10	0.100	2.33	2.30	−1.2
	0.005825	10	0.100	1.16	1.14	−1.7

N.m.r.t. of Mn^{2+} with 1,10-phenanthroline hydrochloride in the presence of thiocyanate

The scarcely soluble complex $Mn(1,10\text{-phen})_2(SCN)_2$ is formed. In ammoniacal solutions, $Mn(OH)_2$ precipitates; in acidic solutions, the precipitation of the complex is hindered. Therefore, the reaction was conducted in buffered solution. The titration curves are shown in Fig. 9, and the results are given in Table 1. As the experimental values are constantly ca. 5% above theoretical, a correction is possible. As for Fe^{3+}, Mn^{2+} may be determined by n.m.r.t. easily (large factor a, see eqn. (6)). The weak dependence of $(1/T_1)_p$ for the Mn^{2+} solution shown in Fig. 3 suggests that only weak complexes $Mn(1,10\text{-phen})_x^{2+}$ are formed.

N.m.r.t. of diamagnetic ions (molecules) with 1,10-phenanthroline hydrochloride in the presence of thiocyanate with a magnetic indicator

Diamagnetic ions or molecules have very little effect on the nuclear magnetic relaxation rate of ^1H in solution. Direct n.m.r.t. is therefore not feasible. There are two possible ways of applying n.m.r.t. to such problems: (a) precipitation of the diamagnetic ions (molecules) with an excess of the precipitant and back-titration of the excess with a paramagnetic ion of high μ_{eff}, e.g. Fe^{3+} or Mn^{2+} (magnetic indicator); or (b) co-precipitation of the diamagnetic ions (molecules) and the paramagnetic indicator (e.g. Mn^{2+}) with the precipitant, e.g. 1,10-phen · HCl.

Proposal (a) was applied to the determination of Zn^{2+} with 1,10-phen · HCl and using 0.0199 M $MnSO_4$ as magnetic indicator. A defined amount of 1,10-phen · HCl, plus an excess of thiocyanate was added to the solution of Zn^{2+} and the excess of 1,10-phen · HCl was back-titrated with the $MnSO_4$

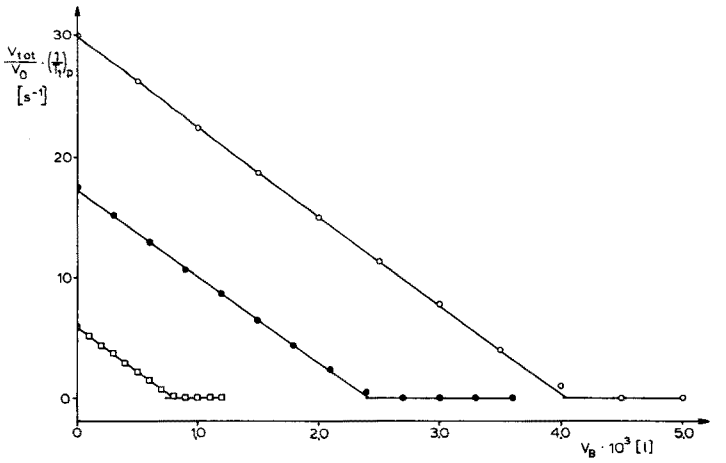

Fig. 9. N.m.r.t. of Mn^{2+} with 1,10-phen · HCl in the presence of KSCN. Corrected relaxation rate, $(V_{tot}/V_0)\,(1/T_1)_p$, is plotted as a function of added volume V_B of titrant (0.02072 M 1,10-phen · HCl solution). $[Mn^{2+}]_0$ = 0.00397 (○), 0.002383 (●), 0.000794 (□) mol l^{-1}. V_0 = 10.0 ml in all cases.

solution; results are shown in Fig. 10. The solution is diamagnetic as long as 1,10-phen · HCl exists in it, but after the equivalence point the solution becomes paramagnetic and the relaxation rate increases. Curve c in Fig. 10 shows the n.m.r.t. for a solution of 1,10-phen · HCl without Zn^{2+} ions; the analytical data are listed in Table 1.

In another experiment (proposal b), the co-precipitation of Zn^{2+} and Mn^{2+} with 1,10-phen · HCl in the presence of thiocyanate was followed by n.m.r.t. The interaction between the paramagnetic Mn^{2+} ions and the protons determines the relaxation rate $(1/T_1)_p$; the Mn^{2+} ions act as a paramagnetic indicator. The resulting titration curves are given in Fig. 11. Initially, the ratio of the amount of the two precipitated ions, Zn^{2+} and Mn^{2+}, does not equal their molar ratio in solution. This effect is probably caused by the different formation rates of the two complexes. Similar results were found for the co-precipitation of Zn^{2+} with Fe^{3+} as the paramagnetic indicator.

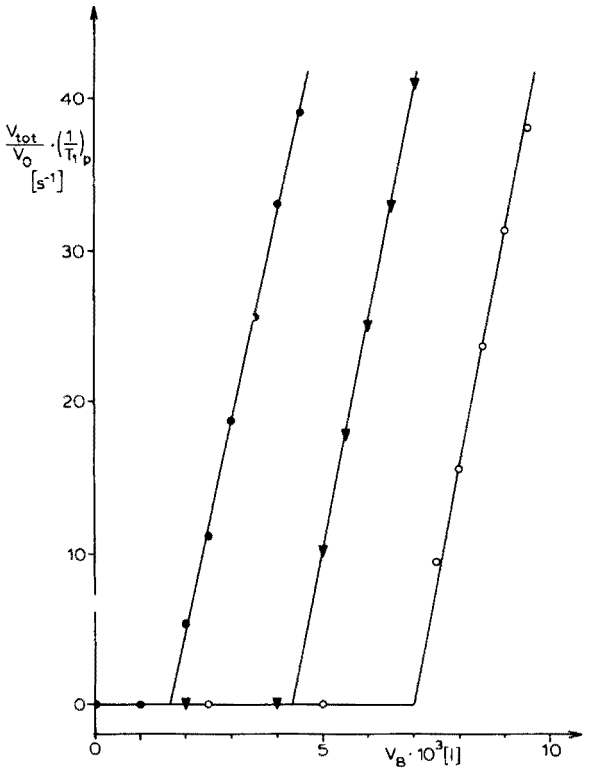

Fig. 10. N.m.r.t. of Zn^{2+} with 1,10-phen · HCl in the presence of KSCN with Mn^{2+} (0.0199 M $MnSO_4$ solution) as paramagnetic indicator. To 3.0 ml of 1,10-phen · HCl solution (0.1 M) were added 10.0 ml of a 0.01165 M (•) or 0.005825 M (▾) solution of $ZnSO_4$. Excess of 1,10-phen · HCl was back-titrated with $MnSO_4$ solution. (○) Titration of 1,10-phen · HCl plus KSCN without Zn^{2+}.

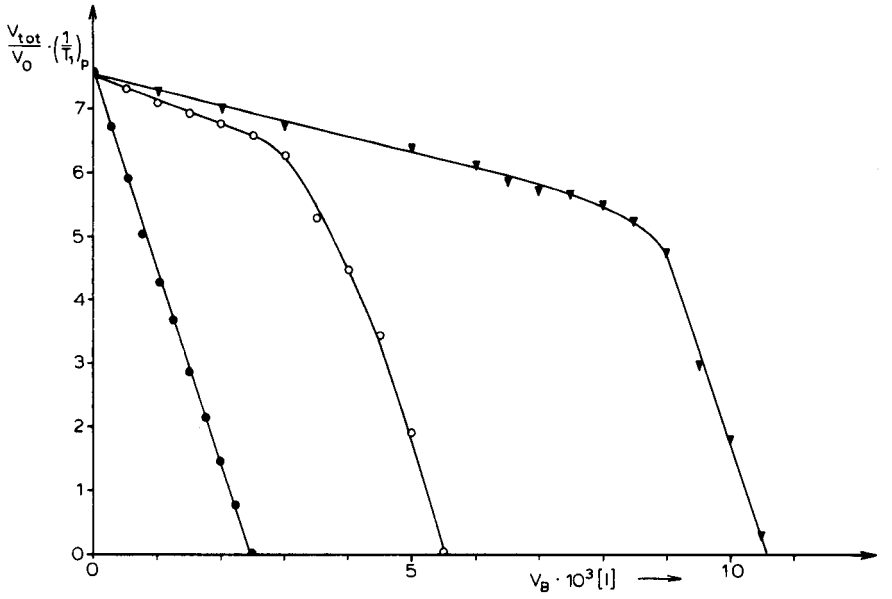

Fig. 11. Co-precipitation of Mn^{2+} and Zn^{2+} by titration with 1,10-phen · HCl in the presence of KSCN. Corrected paramagnetic relaxation rate, $(V_{tot}/V_0)\,(1/T_1)_p$ is plotted against added 1,10-phen · HCl solution (0.0083 M). Mn^{2+} concentration is the same for all three titration curves (0.001 mol l^{-1}). $[Zn^{2+}]_0$ = 0 (•), 0.001165 (○), 0.003495 (▾) mol l^{-1}. V_0 = 10.0 ml in each case.

DISCUSSION

The results show that n.m.r.t. can be used to follow precipitation reactions. Determination of the concentration of paramagnetic ions in solution is possible without separation of the precipitate. A linear relation between the initial concentration of Ni^{2+} and the equivalence point showed that it is not influenced by the amount or form of the precipitate. In n.m.r.t. of Fe^{3+} and Mn^{2+}, the slope of the reaction line is independent of the initial concentration of the paramagnetic ions (see Figs. 8 and 9) and the equivalence point is proportional to the initial concentration. The total relaxation rate $(1/T_1)_{tot}$ beyond the equivalence point is ca. 0.4 s^{-1} in all the titrations of paramagnetic ions reported. A comparison of this value with $1/T_1$ = 0.34 s^{-1} for pure water at 25°C shows that the relaxation rate of ^1H is not affected by the precipitate, and therefore filtration is unnecessary.

During these experiments, the formation of colloids was not observed. If colloid formation occurs, a non-linear reaction line should appear; this behavior was observed in n.m.r.t. of Fe^{3+} with NaOH. As the precipitate does not require separation, relatively fast determinations of the concentration of paramagnetic ions by precipitation can be made. The relaxation time in paramagnetic solutions for each concentration point is measured

within about 30 s and a precipitation titration with n.m.r.t. requires ca. 10 to 15 min. This is very fast in comparison with classical gravimetry.

The method is not limited to the determination of paramagnetic ions; diamagnetic ions or molecules can also be treated, e.g. 1,10-phenanthroline hydrochloride can be titrated with a standard solution of a paramagnetic ion in the presence of thiocyanate, so that the solution is diamagnetic until the equivalence point is reached (T_1 is practically constant in this region). N.m.r.t. may be helpful in the determination of organic molecules in solution. Diamagnetic ions, e.g. Zn^{2+}, can also be determined by back-titration of the excess of 1,10-phenanthroline hydrochloride with a standard solution of paramagnetic ions.

The selectivity of the titration of paramagnetic ions with 1,10-phenanthroline hydrochloride in the presence of thiocyanate is not very pronounced; for specific determination of ions, specific precipitants [1] must be chosen.

The accuracy of the method is satisfactory. In most titrations the accuracy is ca. 1% (Table 1).

We are grateful to the Deutsche Forschungsgemeinschaft for support.

REFERENCES

1 K. H. Nothnagel and A. Weiss, Ber. Bunsenges. Phys. Chem., 74 (1970) 659.
2 A. Schlüter and A. Weiss, Z. Anal. Chem., 166 (1973) 177.
3 D. F. Evans, J. Chem. Soc., (1973) 2587.
4 M. L. Heit and D. E. Ryan, Anal. Chim. Acta, 29 (1963) 524.
5 N. Bloembergen, Nuclear Magnetic Relaxation, New York, Benjamin, 1961.
6 A. Abragam, The Principles of Nuclear Magnetism, Clarendon Press, Oxford, 1961.
7 N. Bloembergen, E. M. Purcell and R. V. Pound, Phys. Rev., 73 (1948) 679.
8 I. Solomon, Phys. Rev., 99 (1955) 559.
9 E. L. Hahn, Phys. Rev., 77 (1950) 297.
10 F. Bloch, Phys. Rev., 70 (1946) 460.
11 G. Spacu, Bul. Soc. Stiint. Cluj., 1 (1923) 284, 361.
12 G. Spacu and J. Dick, Z. Anal. Chem., 71 (1927) 185, 442.

Analytica Chimica Acta, 97 (1978) 111—120

KINETIC MICRODETERMINATION OF MANGANESE IN NATURAL WATERS AND OF OSMIUM AND ETHYLENEDIAMINETETRAACETIC ACID

D. P. NIKOLELIS and T. P. HADJIIOANNOU*

Laboratory of Analytical Chemistry, University of Athens, Athens (Greece)

(Received 2nd September 1977)

SUMMARY

Automatic spectrophotometric kinetic methods are described for the microdetermination of manganese and osmium, based on their catalytic effect on the periodate—acetylacetone reaction, and for the determination of EDTA, on the basis of its inhibitory effect on the manganese-catalyzed periodate—acetylacetone reaction; the time required for the formation of a small fixed amount of colored product is measured automatically and related directly to the catalyst or inhibitor concentration. Manganese at the 10^{-8}—10^{-7} M level, and osmium and EDTA at the 10^{-7}—10^{-6} M level, can be determined with an average error of ca. 2%. The method has been applied to the determination of manganese in natural waters, but is capable of more general applications.

Trace determinations of manganese by catalytic methods have been reported by several authors [1—3]. In the case of metal ion catalysis, complexing agents forming highly stable metal complexes with such catalysts can be determined by their inhibitory effect on the catalyzed reactions [4].

The periodate—acetylacetone reaction, catalyzed by trace amounts of manganese(II) [5], is also accelerated by amounts of osmium(IV) ions in the ppb range. The present paper describes a kinetic spectrophotometric method for the ultramicrodetermination of manganese and osmium, based on their catalytic effect on the periodate—acetylacetone reaction. The method has also been used for the determination of trace amounts of EDTA on the basis of its inhibitory effect on the manganese-catalyzed periodate—acetylacetone reaction. The time required for the periodate—acetylacetone reaction to proceed to a small fixed extent, and thus for the absorbance to increase by a preselected amount, is measured automatically with a solid-state "double-switching" network [6, 7] and related directly to the catalyst (Mn or Os) or inhibitor (EDTA) concentration.

The automatic procedure is rapid, accurate, precise, and simple. The sample is pipetted into the reaction cell containing the reagents, acetylacetone is injected to start the reaction, and the data are read off a dial shortly after the start. Ultramicro amounts of manganese in the range 6—60 ng (2.7×10^{-8}—2.7×10^{-7} M) and osmium in the range 0.2—2 μg

(2.6×10^{-7}—2.6×10^{-6} M) were determined with an average error and relative standard deviation (r.s.d.) of ca. 2% and measurement times of 40—180 s. The method has been applied to the determination of manganese in natural waters. Also, nanogram amounts of EDTA were determined with an average error and r.s.d. of ca. 2%.

EXPERIMENTAL

Apparatus

The apparatus was as previously described [6, 7]. The "double-switching" network was adjusted to measure the time required for the recorder pen to cross preselected positions on the chart corresponding to 0.03 and 0.08 absorbance units for manganese and EDTA, and 0.11 and 0.13 absorbance units for osmium.

Reagents

Water, purified by doubly distilling deionized water through an all borosilicate glass still, passed the dithizone test [8] and was used throughout this work.

Sodium metaperiodate stock solution, 0.100 M. As previously described [7]; prepare more dilute solutions daily by dilution.

Acetylacetone stock solution. Dissolve 24.0 g of recently distilled acetylacetone in 400 ml of water, add 1.00 ml of 0.50 M H_3PO_4, and dilute with water to 500 ml (in the presence of H_3PO_4 the solution is more stable). Store the solution in an amber bottle; when refrigerated, this solution is stable for at least one week.

Phosphate buffer 0.50 M, pH 6.10, as previously described [7].

Manganese standards. (a) For the stock solution (2000 ppm Mn), dissolve 2.002 g of reagent-grade manganese (>99.9%) in 40 ml of dilute hydrochloric acid (1 + 1) and dilute to 1 l with water. (b) For working solutions prepare solutions containing 2.3 ppm, 750 ppb, and 100 ppb of manganese from the stock solution by dilution. Prepare standards containing 1.5, 7, and 15 ppb of manganese from the 100-ppb solution by dilution.

Osmium standard (100 ppm). Dissolve 0.2308 g $(NH_4)_2\ OsCl_6$ in 1 l of water.

Ethylenediaminetetraacetic acid stock solution (0.01000 M). Dissolve 3.722 g of EDTA in water, neutralize with 5 M NaOH to pH 6.10 and dilute to 1 l. Prepare working standards of 1.00×10^{-7}, 2.5×10^{-7}, 5.00×10^{-7} and 7.50×10^{-7} M from the stock solution by dilution. Keep the stock solution in polyethylene bottles. Prepare the very dilute EDTA solutions ($<10^{-6}$ M) just before measurements.

All working standards, reagent solutions and samples are kept in a water bath at 17 ± 0.1°C, except for the osmium determination, when they are kept at 28 ± 0.1°C.

Procedure

Prepare the equipment as described previously [7], but set the wavelength at 385 nm.

Prepare the water samples as described previously [2]. Prepare osmium standards and samples as described previously for iridium [9]. Prepare four standards, 50, 100, 250, and 500 ppb of Os (by dilution from 1 ppm Os solution which has been boiled for 30 min) for construction of the calibration curve.

Determination of manganese. Into the thermostated (17°C) reaction cell, pipet 1.00 ml of buffer and 4.00 ml of sample or standard manganese solution and inject 0.100 ml of 0.100 M sodium periodate solution with a 0.1-ml Hamilton syringe. Start the reaction by injecting 0.250 ml of 0.48 M acetylacetone solution (0.25-ml hypodermic syringe). Close the compartment and immediately press the start button on the U.D.I. The measurement is completed automatically. Record the number on the U.D.I., press the Reset button and empty the cell with suction. Repeat the procedure for each analysis.

Determination of blank. Standard solutions containing 1.5, 7, and 15 ppb of manganese are analyzed by the procedure, and reciprocal times are plotted linearly against the concentrations of the standards. The straight line intercepting the abscissa gives the blank.

Determination of EDTA. Into the thermostated (17°C) reaction cell, pipet 1.00 ml of buffer and 4.00 ml of sample or standard EDTA solution and inject 0.100 ml of 750-ppb manganese solution with a 0.1-ml Hamilton syringe. Continue as in the determination of manganese from the sodium periodate addition stage.

Determination of osmium. Into the thermostated (28°C) reaction cell pipet 1.00 ml of buffer and 4.00 ml of sample or standard osmium solution; inject 0.100 ml of 0.030 M sodium periodate solution with a 0.1-ml Hamilton syringe and continue as in the determination of manganese from the acetylacetone addition stage.

Calculations

Construct calibration curves, obtained by plotting the reciprocal of the readout vs. manganese or EDTA concentration or $[Os]^{2/3}$, to give molar concentration for EDTA or ppb for manganese and osmium. For the determination of manganese in water by the standard addition method, sample A (the water sample without added manganese) is plotted as 0 ppb of manganese and its actual concentration is obtained from the intercept of the calibration curve with the abscissa. The blank should be subtracted from this value.

RESULTS AND DISCUSSION

Basic considerations concerning reducing and oxidizing agents, contamination, control of experimental conditions, and preparation of calibration curves are similar to those previously reported [2].

Both the manganese-catalyzed and the osmium-catalyzed periodate—acetylacetone reactions are critically pH-dependent; the pH should be kept constant to better than ±0.1 pH unit in the range pH 6.1—6.2. Of the various buffers (acetate, phthalate, phosphate), the phosphate buffer did not affect the formation of the yellow product.

In both catalyzed reactions, variation in acetylacetone concentration showed that the reaction rate and the blank increase with increasing concentration of this reagent, while the sensitivity remains practically constant. Variation in periodate concentration showed that, in the manganese-catalyzed reaction, the sensitivity increases and the blank remains practically constant; in the osmium-catalyzed reaction, the blank increases and the sensitivity decreases with increasing concentration of reagent. The concentrations chosen are a compromise to ensure small blanks and measurement times in the range 40—180 s.

The reaction can be started by adding either the periodate or acetylacetone; the latter alternative was chosen because of better precision and accuracy.

The rate of the manganese-catalyzed reaction, and the sensitivity, decrease with an increase in ionic strength of the solution. Manganese can be determined even in solutions of high ionic strength, provided that the composition of the standard manganese solutions is similar to that of the samples. Otherwise, the standard addition method should be used [2].

Linear calibration curves are obtained for manganese in the temperature range 17—26°C. The blank increases sharply with increasing temperature, whereas the sensitivity increases only to a small extent. A temperature of 17°C was chosen to secure a small blank. Similarly, linear calibration curves are obtained for osmium in the temperature range 18—28°C. Within this range, the sensitivity increases with increasing temperature, while the blank remains practically constant; a temperature of 28°C was chosen because of the better sensitivity.

The catalytic activity of the chloro-osmate solutions increases to a maximum constant value after several months. U.v. radiation, heating in a water-bath, and boiling were tried to speed up the increase in catalytic activity of the osmium solutions. The last approach proved successful; the maximum catalytic activity is reached after boiling the solutions for 30 min. Similar results were obtained for ammonium chloroiridite [9] and chlororhodite solutions, which also catalyze the periodate—acetylacetone reaction. This increase in catalytic activity upon aging or boiling probably arises through hydrolysis of the chloro-osmate solutions [10].

To investigate the effect of various ions that might interfere with the determination of manganese and osmium, the measurement step was modified as follows. After the addition of a manganese or osmium standard, 7 or 250 ppb respectively, 0.250 ml of water or of the solution being examined was injected into the reaction cell. Strongly alkaline solutions were neutralized with sulfuric acid, and acidic solutions with sodium hydroxide,

before their effect on the reaction rate was studied. The following ions did not affect the rate of the manganese-catalyzed reaction, even when their concentrations were several thousand times that of the manganese : potassium, sodium, calcium, magnesium, zinc, nickel, copper, and lead. Tables 1 and 2 show the effect of interfering ions on manganese and osmium determinations, respectively.

With the initial-rate method, the oxidation of acetylacetone by periodate in the presence of manganese obeys the equation

$$d[P]/dt = k_0[IO_4^-]^{1.5}[acac] + k_c[IO_4^-][acac][Mn(II)]$$

where k_0 and k_c are the observed rate constants for the uncatalyzed and the catalyzed reaction respectively, and P represents the colored product.

For the uncatalyzed reaction in the temperature range 23—31.5°C, from Arrhenius plots of the logarithm of the initial rate $(dA/dt)_0$ vs. reciprocal temperature, the activation energy was 17.9 kcal mol^{-1}.

Figure 1 shows the dependence of the initial reaction rate on pH, at constant ionic strength (EDTA is added to mask interfering ions).

TABLE 1

Effect of various ions on manganese determination at a concentration of 1.27×10^{-7} M (7 ppb)

Ion	Source	Ion : Mn ratio	Ion	Source	Ion : Mn ratio
A[a]			B[b]		
Fe(II)	$FeSO_4 \cdot 7H_2O$	80	Cd(II)	$3CdSO_4 \cdot 8H_2O$	200
Cr(III)	$Cr(NO_3)_3 \cdot 9H_2O$	120	Al(III)	$NH_4Al(SO_4)_2 \cdot 12H_2O$	200
Fe(III)	$Fe(NO_3)_3 \cdot 9H_2O$	120	Co(II)	$Co(NO_3)_2 \cdot 6H_2O$	300
			Th(IV)	$Th(NO_3)_4 \cdot 3H_2O$	500

[a]These ions in the stated ratio caused a positive relative error of less than 5%.
[b]These ions in the stated ratio caused a negative relative error of less than 5%.

TABLE 2

Effect of various ions on osmium determination at a concentration of 1.31×10^{-6} M (250 ppb)

Ion	Source	Ion : Os ratio	Ion	Source	Ion : Os ratio
A[a]			B[a]		
Ru(III)	$(NH_4)_2RuCl_5 \cdot H_2O$	0.5	Pt(IV)	$(NH_4)_2PtCl_6$	2
Hg(II)	$HgCl_2$	1.3	Ag(I)	$AgNO_3$	5.5
Au(III)	NH_4AuCl_4	1.5	EDTA	Na_2-EDTA	85
Ir(III)	$(NH_4)_3IrCl_6 \cdot H_2O$	12			
Rh(III)	$(NH_4)_3RhCl_6 \cdot \frac{1}{2}H_2O$	25			

[a]See footnotes to Table 1.

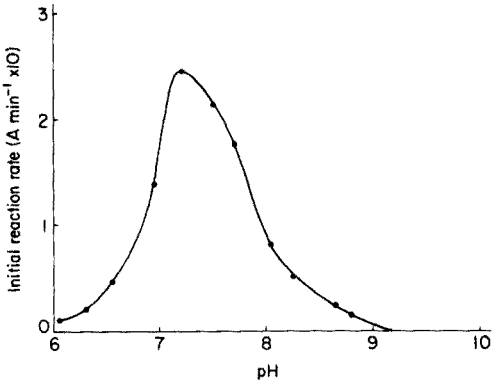

Fig. 1. Dependence of the initial reaction rate on the pH of the reaction mixture. Initial concentrations: $NaIO_4$, 0.00182 M; acetylacetone, 0.0364 M; EDTA, 0.00091 M; total phosphate, 0.40 M.

Aqueous manganese solutions of known concentrations gave the results shown in Table 3; ultramicro amounts of manganese in the range 6—60 ng (4-ml samples of solutions containing 1.5—15 ppb of Mn) can be determined with an average error of ca. 1%. The reaction is pseudo first-order with respect to manganese in the range 1.5—15 ppb of manganese. At higher manganese concentrations the slope of the calibration curve decreases and therefore the manganese concentration of such samples should be adjusted by dilution. The relative standard deviation (r.s.d.) was 2.0% for 7 ppb of manganese (n = 6).

Boiled aqueous osmium solutions gave the results shown in Table 4; micro amounts of Os(IV) in the range 0.2—2 μg can be determined with an average error of about 2% (r.s.d. = 3.4% for 250 ppb of osmium, n = 6). Similar results were obtained with old (20 d) osmium solutions which had not been boiled, but the measurement times were ca. 15% greater.

TABLE 3

Results for aqueous manganese solutions

Reciprocal time ($s^{-1} \times 10^3$)	Manganese in 4-ml sample (ng)		Relative error (%)	
	Taken	Found[a]		
5.38	6.00	6.00	0.0	
6.66	9.20	9.60	+4.3	
9.66	18.4	18.0	−2.2	
13.4	28.0	28.2	+0.7	
19.6	44.0	44.0	0.0	
25.0	60.0	60.0	0.0	Av. 1.2

[a]From straight-line calibration curve, average of two values.

TABLE 4

Results for boiled aqueous osmium solutions

Reciprocal time ($s^{-1} \times 10^3$)	Osmium in 4-ml sample (μg)		Relative error (%)	
	Taken	Found[a]		
5.45	0.200	0.210	+5.0	
6.64	0.300	0.300	0.0	
8.30	0.400	0.400	0.0	
13.5	0.800	0.800	0.0	
16.0	1.00	1.02	+2.0	
21.5	1.60	1.60	0.0	
24.2	2.00	1.91	−4.5	Av. 1.6

[a]From straight-line calibration curve, average of two values.

To check the precision of the complete procedure, five aliquots of a standard sample (1-ppm Os) were boiled, diluted to the 250-ppb Os level, and measured; the r.s.d. was 3.5%.

Complexing agents are expected to reduce the catalytic effect of manganese; with EDTA, there is a linear relationship between reaction rate and concentration, making possible the determination of EDTA in very dilute solutions (10^{-7}—10^{-6} M) on the basis of its inhibitory effect.

Analysis of aqueous EDTA solutions of known concentrations gave the results shown in Table 5. Micro amounts of EDTA in the range 150—1100 ng (1.0×10^{-7}—7.5×10^{-7} M) can be determined with an average error of ca. 2%; for 5.0×10^{-7} M EDTA solution, r.s.d. was 2.1% ($n = 6$).

EDTA analogs which can be expected to interfere on the basis of their stability constants, and sodium oxalate and tartaric acid, were tested; the results are summarized in Table 6.

Table 7 shows the results read from the readout dial of the automatic system for a typical series of determinations run in duplicate to illustrate

TABLE 5

Results for aqueous EDTA solutions

EDTA in 4-ml sample (ng)		Relative error (%)	
Taken	Found[a]		
149	149	0.0	
372	372	0.0	
558	528	−5.4	
744	760	+2.2	
930	989	+6.3	
1117	1117	0.0	Av. 2.3

[a]From straight-line calibration curve, average of two values.

TABLE 6

Effect of foreign species on the determination of 4.25×10^{-7} M EDTA by the Mn(II)-catalyzed periodate—acetylacetone reaction

Foreign species	Molarity giving 5% positive error
Nitrilotriacetic acid (NTA)	6.2×10^{-4}
1,2-Diaminocyclohexanetetraacetic acid (DCTA)	1.9×10^{-6}
Triethylenetetraaminehexaacetic acid (TTHA)	3.2×10^{-7}
Diethylenetriaminepentaacetic acid (DTPA)	6.2×10^{-7}
Ethyleneglycol-bis(2-aminoethylether)-NNN'N' tetraacetic acid (EGTA)	6.2×10^{-6}
Sodium oxalate	1.2×10^{-6}
Tartaric acid	6.2×10^{-5}

TABLE 7

Automatic results for manganese in potable waters

Sample	Direct time readout (s)	$[Mn] \cdot t$
1.5 ppb Mn	184.85, 186.89	
7.0 ppb Mn	74.72, 74.99	669—683
15.0 ppb Mn	39.86, 39.98	
A[a]	112.80, 113.74	
A +2.3 ppb Mn	87.38, 87.75	842—867
A +4.6 ppb Mn	69.01, 69.07	
B[a]	160.18, 158.09	
B +2.3 ppb Mn	107.75, 109.64	767—795
B +4.6 ppb Mn	79.89, 79.81	
C[a]	150.40, 152.31	
C +2.3 ppb Mn	113.46, 113.50	905—942
C +4.6 ppb Mn	85.45, 85.34	

[a]Origin of samples given in Table 8.

the reproducibility. The values for manganese obtained by the standard addition method and those obtained from a calibration curve are shown in Table 8.

The reciprocals of the average readout values from Table 7 are plotted against concentration in Fig. 2. If the reaction rate in all samples was constant for a fixed manganese concentration, the calibration curves would have the same slope and the product of the manganese concentration in ppb (including the blank, equivalent in this series to 2.1 ppb) multiplied by the measurement times in seconds, $[Mn] \cdot t$, would be the same for all samples. This is not the case because interfering substances affect the reaction rate. Any substance that oxidizes acetylacetone or reduces

TABLE 8

Comparison of standard addition method and calibration curve results for the determination of manganese in potable waters

Sample	Origin	Manganese (ppb)	
		Standard addition method	Calibration curve
A	Loutraki	5.5	5.0
B	Athens	2.9	2.2
C	Andros	3.9	2.4

periodate, under the conditions of the procedure, constitutes a potential interference. In addition, large amounts of salts decrease the reaction rate. To compensate for the effect of interfering substances, the composition of the standard manganese solutions should be similar to that of the samples but as interfering substances may be present in different amounts in different samples, it is not feasible to prepare such standard solutions. Calibration curves obtained with pure solutions of manganese in distilled water can therefore lead to erroneous results (Table 8). By applying the standard addition method, the concentration of all substances (except manganese) is the same in all the solutions used in each analysis.

Standard reference samples were not available, but the accuracy of the method was checked by recovery experiments; the recovery of manganese ranged from 99 to 107% (average 101.4%). Although this application deals with the determination of manganese in water, the scope of the method can be more general. A basic procedure and general considerations have been given so that the method can be adapted to determine manganese in tissue, bone, blood, etc.

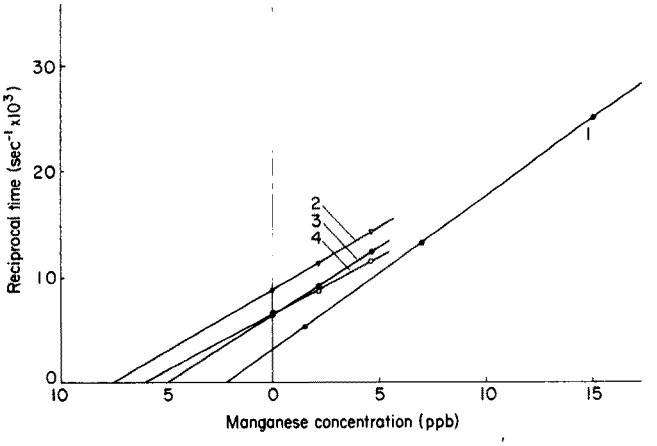

Fig. 2. Plot of reciprocal time vs. manganese concentration. 1, blank; 2, 3, 4, potable water samples.

REFERENCES

1 T. J. Janjiic, G. A. Milovanovic and M. B. Celap, Anal. Chem., 42 (1970) 27.
2 T. P. Hadjiioannou and T. A. Kephalas, Mikrochim. Acta (Wien), (1969) 1215.
3 H. A. Mottola and C. R. Harrison, Talanta, 18 (1971) 683.
4 H. A. Mottola and H. Freiser, Anal. Chem., 39 (1967) 1294.
5 C. Efstathiou and T. P. Hadjiioannou, Talanta, 24 (1977) 270.
6 C. Efstathiou and T. P. Hadjiioannou, Anal. Chim. Acta, 89 (1977) 55.
7 D. P. Nikolelis and T. P. Hadjiioannou, Mikrochim. Acta (Wien), (1977) 125.
8 E. B. Sandell, Colorimetric Determination of Traces of Metals, 3rd edn., Interscience, New York, 1965, pp. 17—18.
9 T. P. Hadjiioannou and P. A. Siskos, Chim. Chron., New Series, 2 (1973) 107.
10 G. H. Faye, Anal. Chem., 37 (1965) 296.

Analytica Chimica Acta, 97 (1978) 121—128

SIMULTANEOUS DETERMINATIONS OF METAL 5-SULFO-8-QUINOLINOLATES BY DIFFERENCES IN THEIR FLUORESCENCE LIFETIMES

KEIZŌ HIRAKI, KIYOTOSHI MORISHIGE and YASUHARU NISHIKAWA*

Department of Chemistry, Faculty of Science and Technology, Kinki University, 3-4-1, Kowakae, Higashi-Osaka-shi, Osaka (Japan)

(Received 27th September 1977)

SUMMARY

Fluorescence lifetimes of aluminium, gallium, indium, magnesium, zinc, and cadmium 5-sulfo-8-quinolinolates are reported. A method for the simultaneous determination of two components based on the difference in their fluorescence lifetimes is given. The method is applied to determinations of aluminium in magnesium alloy and of magnesium in aluminium alloy. The procedure is simple and rapid, and gives accurate results.

Fluorimetric analysis is based on the formation of a fluorescent compound, and on the measurement of its fluorescence spectrum, quantum yield, polarization, or fluorescence lifetime. Measurement of fluorescence lifetimes has become feasible by the development of suitable apparatus [1]. The fluorescences of many metal chelates show lifetimes ranging from a few to several tens of nanoseconds [2]. The fluorescence lifetimes of group II and III metal 5-sulfo-8-quinolinolates were measured [3] with a time-resolved spectrofluorimeter, and the following values were obtained at 20°C: 11.3 ± 0.7 ns for aluminium at pH 4.5; 6.5 ± 0.3 ns for gallium at pH 2.5; 4.0 ± 0.3 ns for indium at pH 6.5; 10.8 ± 0.7 ns for magnesium at pH 10; 4.0 ± 0.3 ns for zinc at pH 7.0; and 5.0 ± 0.3 ns for cadmium at pH 7.5. It was suggested that when the difference between the fluorescence lifetimes of metal chelates exceeded about 4 ns, each component in the mixed system could be determined simultaneously by analyzing the fluorescence decay curve [3].

The analysis of the decay curve can be applied to the simultaneous determination of the aluminium—gallium and magnesium—cadmium systems, for which the differences in lifetime are ca. 7 ns at pH 4.5, and ca. 5 ns at pH 10, respectively. A simple, rapid method is also reported for the determination of aluminium in magnesium alloy and for magnesium in aluminium alloy, by taking advantage of the difference in the optimum pH value for aluminium (pH 4.5) and for magnesium (pH 10).

EXPERIMENTAL

Apparatus

Fluorescence decay curves were measured with a Hitachi MPF—2A spectrofluorimeter, fitted with a time-resolving device (Fig. 1.) The sample was irradiated by a light pulse from lamp D_2, and the monochromatic fluorescence emitted from the sample was detected by a photomultiplier (R106 UH). Time-resolved measurement was performed by controlling the time interval between the light pulse and detection signal. The characteristics of the apparatus were as follows; time resolution, 4, 6, 10, or 20 ns; scanning time, 100, 200, or 500 ns; sampling frequency, 2 kHz; halfwidth of the exciting pulse, less than 12 ns. The spectrofluorimetric measurements were made with a Hitachi spectrofluorimeter, Model 204.

Materials

5-Sulfo-8-quinolinol solution, 0.045% (w/v). Dissolve 0.2252 g of 5-sulfo-8-quinolinol in distilled water and dilute to 500 ml.

Standard solutions of metal ions. Prepare stock solutions of aluminium, magnesium, cadmium and zinc by dissolving the pure sulfates in 0.5 M sulfuric acid. Prepare stock solutions of gallium and indium by dissolving the oxides (99.99% pure) in 6 M hydrochloric acid. Dilute the stock solutions suitably to give standard solutions.

Uranin solution. Dissolve 0.1 g of uranin (fluorescein sodium A. R.) in water and dilute to 100 ml with water. The stock solution, diluted with water to give a solution containing 0.125 μg of uranin per ml, is used as reference standard to adjust the sensitivity of the instrument.

All other chemicals were special grade. Hydrochloric acid and ammonia were distilled until the fluorescence disappeared. Redistilled water was used throughout.

General procedure

To 15—20 ml of a sample solution containing appropriate amounts of metal ions, e.g. aluminium, gallium, indium, magnesium, zinc, or cadmium, add 1 ml

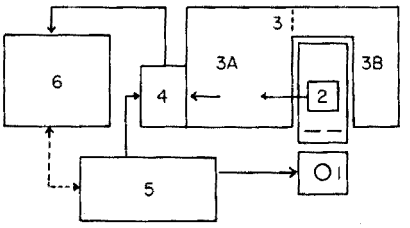

Fig. 1. Schematic diagram of time-resolved fluorimeter (sampling method). 1, D_2 flash lamp. 2, Cell. 3, Spectrofluorimeter (3A, fluorescence monochromator, 3B, excitation monochromator). 4, Detector (R-106 UH). 5, Control unit. 6, Recorder.

of 0.045% 5-sulfo-8-quinolinol solution and 2 ml of 20% ammonium acetate solution or 20% ammonium chloride solution. Adjust the pH of the solution to the desired value with dilute hydrochloric acid, ammonia, or sodium hydroxide solution, and dilute to 25 ml with water. Measure the fluorescence decay curve with the time-resolved spectrofluorimeter.

Measurement of fluorescence lifetime

The fluorescence intensity of the chelates decays exponentially with time t, and obeys the following equation

$$F = F_0 e^{-t/\tau} = F_0 e^{-k_f t}$$

where F and F_0 are the fluorescence intensities at time t and at zero time, respectively; τ and k_f are the lifetime and the rate constant for the process of fluorescence emission. The fluorescence lifetime is obtained from the decay curve by measuring the time interval required for the fluorescence intensity to fall to 1/e of a particular value.

RESULTS AND DISCUSSION

Lifetime of metal 5-sulfo-8-quinolinolates

The excitation and fluorescence spectra of the metal 5-sulfo-8-quinolinolates studied, the optimum conditions for the formation of the fluorescent chelates, and the composition of the chelates were reported previously [3]. Fluorescence properties of the chelates and the optimum conditions for the determination of the metals are summarized in Table 1, and the pH-dependencies of the fluorescence intensity and the lifetime are shown in Fig. 2. Aluminium and magnesium chelates, which emit relatively intense fluorescence, give longer lifetimes, 11.3 ±0.7 ns and 10.8 ± 0.7 ns, respectively, than others.

TABLE 1

Optimal fluorescence conditions and properties of chelates

	Al	Ga	In	Mg	Zn	Cd
$\lambda_{ex.}$ uncorrected (nm)	360	365	365	360	365	365
$\lambda_{em.}$ uncorrected (nm)	490	505	510	495	515	510
$\lambda_{em.}$ corrected (nm)	503	530	546	515	540	539
Optimum pH	4.5	2.5(7)	6.5(7)	10—10.7	7	7.5
Metal to ligand ratio	1:1	1:1(1:3)	1:1(1:2)	1:1	1:1	1:1
0.045% reagent solution (ml)	1	0.7—1	1	1	1	1
Fluorescence intensity ratio	12.8	1.3	1	9.7	2.3	1.8
Quantum yield[a]	0.011	0.005	0.003	0.010	0.011	0.015
Sensitivity index[a]	1.1×10^{-4}	6.5×10^{-5}	4.8×10^{-5}	3.4×10^{-4}	3.0×10^{-4}	2.4×10^{-4}
Formation constants[b] log K_{ML_1}	9.76	13.56	11.44	4.79	8.65	7.70
K_{ML_2}	9.01	11.21	8.06	3.4	7.5	6.5
Fluorescence lifetime (ns)	11.3 ± 0.7	6.5 ± 0.3	4.0 ± 0.3	10.8 ± 0.7	4.0 ± 0.3	5.0 ± 0.3

[a] $Al(Ox \cdot SO_3Na)_3$, $Ga(Ox \cdot SO_3Na)_3$, $In(Ox \cdot SO_3Na)_3$, $Mg(Ox \cdot SO_3Na)_2$, $Zn(Ox \cdot SO_3Na)_2$ and $Cd(Ox \cdot SO_3Na)_2$ were prepared by the Vaisman method [4] and 1×10^{-4} M solutions of these chelates (ionic strength: 0.1) were used. Ox: C_9H_6ON.

[b] Reference [5, 6].

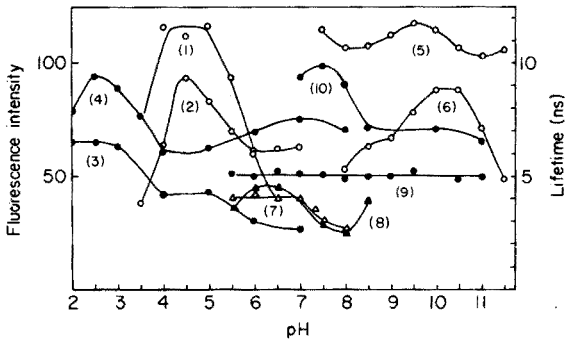

Fig. 2. The relation between fluorescence intensity, lifetime of the metal chelates and pH of the solution. (1) Al-τ; (2) Al-F.I.; (3) Ga-τ; (4) Ga-F.I.; (5) Mg-τ; (6) Mg-F.I.; (7) Zn-τ; (8) Zn-F.I.; (9) Cd-τ; (10) Cd-F.I. τ: Lifetime of the chelate; F.I.: fluorescence intensity of the chelate.

A significant difference (ca. 7 ns) in the fluorescence lifetime is observed between the aluminium and gallium chelates at pH 4.5, and of ca. 6 ns between the magnesium and cadmium chelates at pH 10. The difference in the decay rate can therefore be used to analyze those two-component systems.

Aluminium does not emit fluorescence at pH 10, the optimum pH for magnesium, and magnesium does not emit at pH 4.5, the optimum for aluminium. Fluorescence lifetimes of zinc, indium, and cadmium chelates are short compared with those of aluminium and magnesium chelates. Accordingly, aluminium in the presence of large amounts of magnesium can be determined at pH 4.5, and magnesium in the presence of aluminium can be determined at pH 10.

Simultaneous determination of aluminium and gallium

The fluorescence decays of solutions, which contained 2—5 μg of aluminium and 5—20 μg of gallium and were adjusted to pH 4.5 as in the General procedure, were measured. Typical decay curves are shown in Fig. 3 as fluorescence intensity vs. time plots, and in Fig. 4 as logarithm of fluorescence intensity vs. time plots. The logarithmic decay curve of the composite sample is concave (curve 3 in Fig. 4), because the short-lived component becomes less significant as time passes. After 15 ns, the long-lived component predominates, and the decay curve gives a straight line, the slope of which is the same as that of the aluminium chelate (τ = 10.8 ns, curve 1). By extrapolating the straight line to zero time (curve 4) and by subtracting it from the composite decay curve, the linear decay curve of the short-lived component is obtained (curve 5). The slope of the latter straight line is in fair agreement with that of the gallium chelate (τ = 4.3 ns, curve 2). Aluminium and gallium can be determined when the fluorescence intensities are compared between curves 4 and 1, and curves 5 and 2, respectively. Analytical results for some samples are presented in Table 2. Aluminium and gallium can be determined accurately

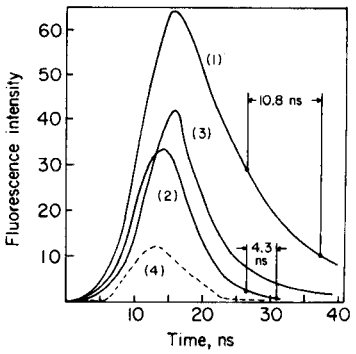

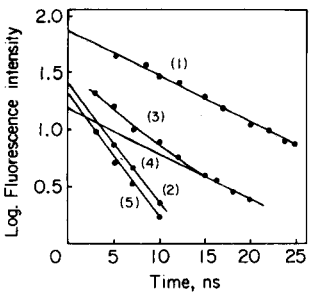

Fig. 3. Decay curves of aluminium and gallium 5-sulfo-8-quinolinolates. (1) 10 μg Al/25 ml standard, pH 4.5; (2) 20 μg Ga/25 ml standard, pH 4.5; (3) composite curve (2 μg Al + 20 μg Ga/25 ml), pH 4.5; (4) reagent blank (1 ml of 0.045% $HOx \cdot SO_3H$ solution), pH 4.5. Slit width, 40 nm.

Fig. 4. The logarithmic plot of fluorescence decay curves of standard aluminium and gallium chelates, and their composite chelates. Curves (1)—(3) as in Fig. 3; (4) Al component; (5) Ga component.

TABLE 2

Simultaneous determination of groups III and II metals
(1 ml of 0.045% 5-sulfo-8-quinolinol, pH 4.5, Slit: 40 nm, R.R.: 0.5 V for Al/Ga and 1 V for Mg/Cd. Wavelength, open; T.R.: 4 ns; sens, 2)

Composite sample	Al found (μg)	Ga found (μg)	Composite sample	Mg found (μg)	Cd found (μg)
Al 2 μg, Ga 20 μg	2.1	18.2	Mg 5 μg, Cd 15 μg	5.1	14.4
Al 5 μg, Ga 5 μg	5.3	5.6	Mg 5 μg, Cd 20 μg	5.3	20.0
Al 4 μg, Ga 10 μg	3.7	10.0	Mg 10 μg, Cd 10 μg	9.0	11.4
			Mg 10 μg, Cd 15 μg	9.8	14.6

in the ranges 2—5 μg of aluminium and 5—20 μg of gallium and at [Ga]/[Al] ratios of 1—10.

Simultaneous determination of magnesium and cadmium

Typical decay curves of the magnesium and cadmium chelates, and of the mixture obtained at pH 10 are shown in Figs. 5 and 6. As seen in Table 2, magnesium and cadmium in the mixtures can be determined simultaneously in the concentration range 5—10 μg of magnesium and in [Cd]/[Mg] ratios of 1.5—4, when the composite decay curves are resolved in the way described above.

Determination of aluminium and magnesium in light alloys

Although the fluorescence lifetimes of the aluminium and magnesium chelates resemble each other, the optimum pH value for formation of their

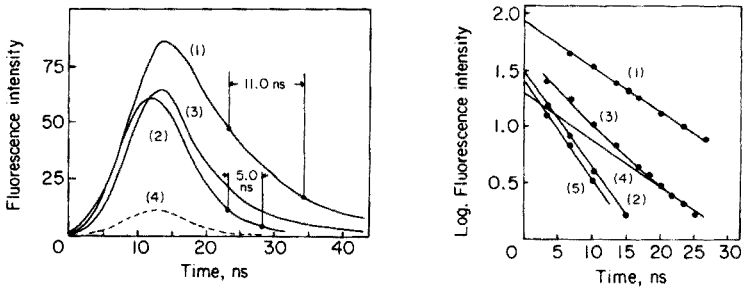

Fig. 5. Decay curves of magnesium and cadmium 5-sulfo-8-quinolinolates. (1) 20 μg Mg/25 ml standard, pH 10; (2) 15 μg Cd/25 ml standard, pH 10; (3) composite curve (5 μg Mg + 15 μg Cd/25 ml), pH 10; (4) reagent blank (1 ml of 0.045% HOx · SO_3H solution), pH 10.

Fig. 6. The logarithmic plot of the fluorescence decay curves of standard magnesium and cadmium chelates, and their composite chelates. Curves (1)—(3) as in Fig. 5; (4) Mg component; (5) Cd component.

chelates is quite different; pH control can therefore be applied not only for the determination of aluminium in large amounts of magnesium and for magnesium in large amounts of aluminium, but for the determination of aluminium and magnesium in light alloys. The procedure used is as follows. Sample (20 mg) is dissolved in 10 ml of concentrated hydrochloric acid and diluted to 100 ml with distilled water; an appropriate aliquot of the solution is treated by the general procedure, and the fluorescence decay curves are observed at pH 4.5 for aluminium and at pH 10 for magnesium. Decay curves for aluminium in a magnesium alloy (Furukawa Mg Co. Ltd., 25T, J-8-1) and for magnesium in an aluminium alloy (Nikei Co. Ltd., 74S) are shown in Figs. 7 and 8 respectively. The analytical results are presented in Table 3.

As shown in Fig. 7, the decay curve of the magnesium alloy is consistent with that of an aluminium chelate, i.e. the fluorescence emitted from the alloy

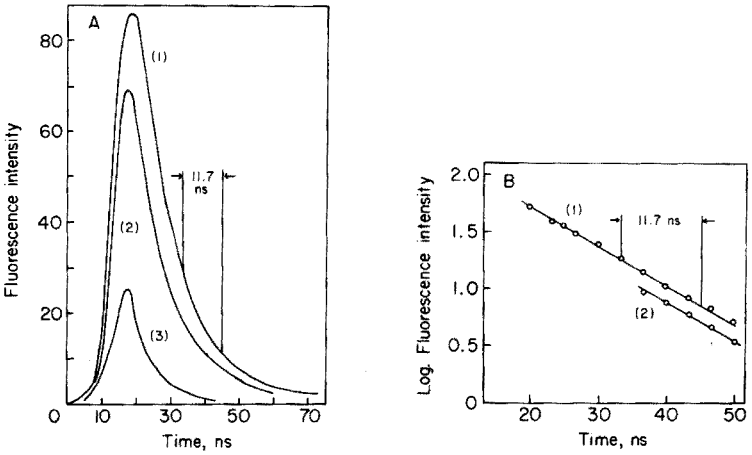

Fig. 7. Decay curves of Al and Mg alloy sample (A) and the logarithmic plot of the decay curves (B). (1) 5 μg Al/25 ml standard; (2) Mg alloy (0.3 ml of 20 mg/100 ml solution in 1.2 M HCl with 1.0 ml of 0.045% 5-sulfo-8-quinolinol; pH 4.5); (3) reagent blank.

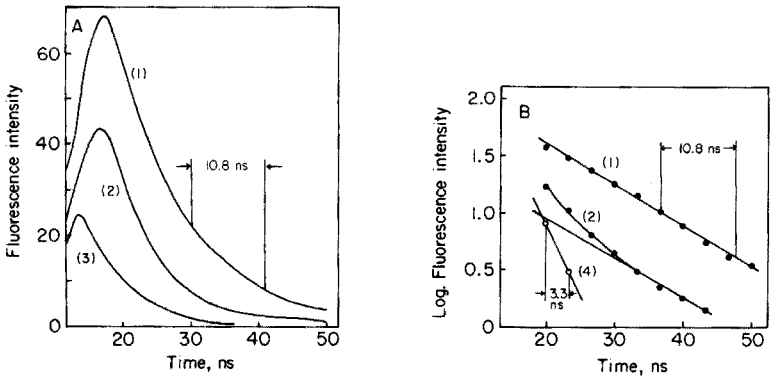

Fig. 8. Decay curves of Mg and Al alloy sample (A) and the logarithmic plot of the decay curves (B). (1) 5 μg Mg/25 ml standard (1 ml of 0.045% 5-sulfo-8-quinolinol; pH 10); (2) Al alloy (0.3 ml of 20 mg/100 ml solution in 1.2 M HCl); (3) reagent blank; (4) zinc component.

TABLE 3

Determination of aluminium and magnesium in alloys

Sample	Aliquot taken (ml)	Found (μg)	Found (%)
Aluminium alloy-74S[a]	0.3	Mg 1.1_5	1.92
	0.3	Mg 1.0_8	1.80
	0.5	Mg 2.0_5	2.05
	0.5	Mg 1.9_9	1.99
	0.5	Mg 1.9_5	1.90
			Mean: 1.93 ± 0.10
Magnesium alloy-25T (J-8-1)[b]	0.3	Al 3.5_7	5.95
	0.3	Al 3.6_0	5.99
	0.3	Al 3.7_8	6.29
			Mean: 6.08 ± 0.15

[a]Mg 1.93; Si 0.15; Cu 0.06; Cr 0.13; Zr 0.14; Fe 0.20; Zn 4.28; Mn 0.58; Ti 0.09%.
[b]Al 6.15; Mn 0.39; Zn 2.79; Si 0.011; Cu 0.0005; Fe 0.0005%; Ni trace.

sample at pH 4.5 is attributable to aluminium. The decay curve of the aluminium alloy consists of two components, at least (curve 2 in Fig. 8B). The lifetimes of the two components obtained by analyzing the decay curve indicate that the long-lived component is the magnesium chelate (τ = 10.8 ns); the short-lived component appears to be the zinc chelate (τ = 3.3 ns). The sample contained 4.28% of zinc which might give a positive error, if magnesium were determined normally by fluorimetry. The error is eliminated by resolving the fluorescence decay curves, without any separation procedure.

The authors express their sincere thanks to Professor Tsunenobu Shigematsu (Kyoto University) and Professor Masayuki Tabushi (College of Medical Technology, Hirosaki University), for their advice and suggestions. Financial support from the Ministry of Education, Japanese Government, is gratefully acknowledged.

REFERENCES

1 T. Nogami, Y. Onishi, K. Fukuda and H. Okagaki, 8th Applied Spectrometry Symposium, 1972, p. 7.
2 H. Kokubun, Kagaku No Ryoiki, 24 (1970) 51.
3 Y. Nishikawa, K. Hiraki, K. Morishige and T. Katagi, Bunseki Kagaku, 26 (1977) 365.
4 G. A. Vaisman, Ukr. Gos. Inst. Eksptl. Farm. Kons. Materialy, (1940) 143.
5 F. J. Langmyhr and A. R. Storm, Acta Chem. Scand., 15 (1961) 1461.
6 J. A. Bishop, Anal. Chim. Acta, 63 (1973) 305.

Analytica Chimica Acta, 97 (1978) 129—133

SEPARATION AND DETERMINATION OF RHENIUM WITH 5,6-DIPHENYL-2,3-DIHYDRO(ASYM)TRIAZINE-3-THIONE

A. K. MAJUMDAR* and B. DATTA

Department of Chemistry, Jadavpur University, Calcutta 700032 (India)

(Received 21st September 1977)

SUMMARY

5,6-Diphenyl-2,3-dihydro(asym)triazine-3-thione can be used as a gravimetric reagent for the determination of rhenium (4—50 mg) in the presence of 0.7—1.7 M hydrochloric acid and tin(II) chloride. The composition of the dried complex, which can be weighed directly, is $[ReO(C_{15}H_{10}N_3S)_2]_2$. The method is simple and rhenium can be determined in the presence of a number of foreign ions.

All the gravimetric methods [1—11] described so far for the determination of rhenium, except the sulphide one, involve either salt formation or ion-association with perrhenate, hexachlororhenate or hexabromorhenate. Consequently, most of the methods have the disadvantage of coprecipitation of several anions and the precipitates have to be washed with a saturated solution of the precipitated compound itself to compensate for solubility losses. The determination of rhenium as sulphide also suffers from considerable errors, because of the precipitation of free sulphur, which is difficult to remove completely.

Not a single reagent capable of forming an insoluble but washable chelate of definite composition suitable for the gravimetric determination of rhenium has so far been proposed. 5,6-Diphenyl-2,3-dihydro(asym)triazine-3-thione is such a reagent. Rhenium(IV) can be precipitated from acidic solution, so that the defects of coprecipitation are overcome, and rhenium can be determined in the presence of many foreign ions.

The method involves the reduction of rhenium(VII) to rhenium(IV) with tin(II) chloride in hydrochloric acid medium in the presence of the reagent [12—14], with which rhenium(IV) combines in a 1:2 ratio to form a green chelate. The presence of tetravalent rhenium in the compound was confirmed by comparing the absorption spectrum of a chloroform extract of the isolated compound with that of a compound prepared from K_2ReCl_6 as described in the general procedure but without the addition of tin(II) chloride. The nature of the absorption curves, and the compositions of the complexes established by elemental analysis, showed that the compounds are the same with an absorption peak at 680 nm.

Thermogravimetry showed that the complex is stable up to 126°C. Molecular weight determinations (vapour pressure osmometry, suggested that the isolated complex is dimeric (m.w. 1233; 14.8 mg/10 ml of benzene solution). Magnetic susceptibility measurements showed that the complex has a low paramagnetic value (1.0 B.M.); the ligand field around each rhenium(IV) appears to be octahedral. Thin-layer chromatography of the compound in acetone—chloroform (3:22) furnished a single spot (R_F = 0.71), indicating that a pure complex is formed.

IR spectroscopy showed that the groups participating in complex formation are —NH and =CS, so that reagent behaves as a bidentate ligand. The

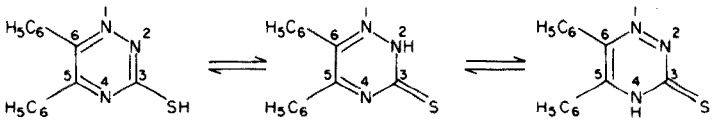

A B C

ligand may exist in tautomeric forms A, B (-2,3-dihydro) and C (-3,4-dihydro). The absence of a band around 2600 cm^{-1} indicated that there is no SH group (form A), whereas a broad band at 2860 cm^{-1} suggested the presence of an NH group; the band was probably broadened by intermolecular hydrogen bonding. A band at 1190 cm^{-1}, characteristic of the =CS group, clearly indicated that the ligand exists in form B or C. In the complex, the absence of a band near 3000 cm^{-1} shows the loss of a proton. Shifting of the C=S stretching frequency to 1125 cm^{-1} shows the participation of this group in the complex formation. Further coordination of rhenium is satisfied by a nitrogen atom, for the bands at 1580, 1560 and 1535 cm^{-1} are shifted to a lower region, but which nitrogen atom is involved could not be ascertained definitely. Of structures B and C, the N_2-atom is more likely to be involved in bonding than the N_4-atom, because of steric hindrance. No Re=O stretching vibration appeared. The Re—O vibration could not be identified up to 250 cm^{-1}, possibly because it was obscured by ligand vibrations. Although a Re—O band could not be definitely proved, all the other factors can be reconciled by the following structure, where rhenium is hexacoordinated:

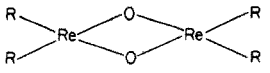

R= $C_{15}H_{10}N_3S$

EXPERIMENTAL

Apparatus

A Chevenard thermobalance type 3 (Adamel, Paris) was used to record thermogravimetric curves. A Perkin-Elmer 457 i.r. spectrophotometer was used with KBr discs. An electrodynamically controlled Curie-type balance with a photoelectric detector ($CuSO_4 \cdot 5H_2O$ standard) was used for the magnetic susceptibility values. The vapour-pressure osmometer was the Knauer (Berlin) model.

Reagents and standard solutions

The reagent was prepared by the method of Polonvski and Pesson [15]. A 0.20% (w/v) solution of the reagent in acetone was used for precipitations.

Tin(II) chloride (G.R., Merck) was used as a 1.0 M solution in 6 M hydrochloric acid solution.

A standard rhenium solution was prepared by dissolving an accurately weighed quantity of potassium perrhenate (Johnson Matthey) in double-distilled water, and determining the rhenium in an aliquot by internal electrolysis [16]. Solutions of other cations were prepared from their chlorides or sulphates and those of anions from their sodium, potassium or ammonium salts; they were standardized by conventional methods. All other chemicals were of highest available purity.

General procedure

Take the neutral perrhenate solution containing 4—50 mg of rhenium. Add enough reagent solution to give about 1.25 times the stoichiometric amount. Add 4 ml of the tin(II) solution and enough 6 M hydrochloric acid to make the final solution (50—60 ml) 0.7—1.7 M. The green precipitate appears and precipitation is complete in 10—15 min. Dilute the mixture to about 175 ml with 1.5 M hydrochloric acid and heat on a boiling water bath for 1.5—2 h to remove acetone. Cool, filter through a sintered glass crucible, wash with 10—30 ml of concentrated hydrochloric acid, and finally with water, dry at 110°C and weigh. The conversion factor for rhenium is 0.2548.

RESULTS AND DISCUSSION

The effects of varying the acidity and tin(II) chloride concentration were examined for 10.12 mg of rhenium. Precipitation was quantitative in the range 0.7—1.7 M HCl and with the addition of 3—5 ml of 1 M tin(II) chloride solution. A 25% excess of reagent over the stoichiometric amount is sufficient to complete the precipitation. Addition of more reagent, up to 20—30 mg in excess, has no adverse effect.

For repeated (10) determinations of 10.12 mg of rhenium, the standard deviation was 0.041 and the relative standard deviation 0.41%.

Composition of the rhenium complex

The rhenium complex was precipitated, filtered, washed and dried as described above. The dried complex was fused with sodium peroxide and anhydrous sodium carbonate, the fused mass was taken up in water and filtered, and an aliquot of the filtrate was subjected to internal electrolysis [16] for rhenium determination. Carbon, hydrogen and nitrogen were determined by the usual combustion methods, and sulphur as $BaSO_4$. The composition found agreed with the formula $[ReO(C_{15}H_{10}N_3S)_2]_2$. (Found; 49.75% C, 3.3% H, 11.5% N, 8.9% S, 25.7% Re. Calculated; 49.2% C, 2.8% H, 11.5% N, 8.8% S, 25.5% Re.) Spectrophotometric studies [17] have shown that the same 1:2 complex is formed in solution.

TABLE 1

Direct determination and separation of rhenium (10.12 mg) from other ions

Ion added	Amount added (mg)	Wt. of complex (mg)	Re found (mg)
UO_2^{2+}	50	39.70	10.12
V^{5+}	100	40.10	10.22
Mn^{2+}	200	39.90	10.17
Fe^{3+}	150	40.10	10.22
Al^{3+}, Zn^{2+}, Be^{2+}, Cd^{2+}	150 (each)	40.00	10.20
Co^{2+}, Ni^{2+}	150 (each)	39.80	10.14
Pb^{2+}	100	40.00	10.20
Mo^{6+}	20	39.40	10.04
Hg^{2+}	50	40.00	10.20
As^{3+}	100	40.00	10.20
Sb^{3+}	200	40.10	10.22
Nb^{5+}, Ta^{5+}	100 (each)	39.80	10.14
Zr^{4+}	50	40.10	10.22
Ti^{4+}	200	39.40	10.04
Cr^{3+}	150	39.90	10.17
Oxalic acid	700	39.40	10.04
Citric acid	1000	39.80	10.14
Tartaric acid	1000	39.50	10.07
EDTA	750	39.60	10.09
ClO_4^-	100	39.90	10.17
MnO_4^-	100	39.60	10.09
F^-	100	39.40	10.04
PO_4^{3-}	100	40.00	10.20
CH_3COO^-	100	39.80	10.14
SO_4^{2-}	100	40.10	10.22
NO_3^-	50	39.70	10.12

Separation from foreign ions

Solutions containing known amounts of different foreign ions plus known amounts of rhenium were mixed and the procedure for rhenium determination was followed. The results are shown in Table 1. The interfering effect of mercury(II) (50 mg) was eliminated by the addition of tartaric acid, that of chromium(III) (150 mg) by EDTA and that of nitrate (50 mg) by adding more reagent (ca. 2 times the stoichiometric amount). However, copper(II), osmium(VIII), palladium(II), platinum(IV), silver(I), ruthenium(III) and tungsten(VI) interfered with the determination.

REFERENCES

1 W. Geilmann and A. Voigt, Z. Anorg. Allg. Chem., 193 (1930) 311.
2 W. Geilmann and F. Weibke, Z. Anorg. Allg. Chem., 195 (1931) 289; 199 (1931) 347.
3 H. H. Willard and G. M. Smith, Ind. Eng. Chem. Anal. Ed., 11 (1939) 305.
4 V. K. Akimov, A. I. Busev and B. E. Zaitser, Zh. Anal. Khim., 25 (1970) 518.

5 M. H. B. Morton and W. I. Stephen, Anal. Chim. Acta, 44 (1969) 147.
6 W. Geilmann and L. C. Hurd, Z. Anorg. Allg. Chem., 213 (1933) 336.
7 V. K. Akimov, A. I. Busev and I. A. Emel'yanova, Zh. Anal. Khim., 25 (1970) 1752.
8 F. Krauss and H. Steinfeld, Z. Anorg. Allg. Chem., 197 (1931) 52.
9 H. V. A. Briscoe, P. L. Robinson and E. M. Stoddart, J. Chem. Soc., 134 (1931) 1439.
10 I. K. Taimni and G. B. S. Salaria, Anal. Chim. Acta, 12 (1955) 519.
11 J. H. Muller and W. A. La Lande, J. Am. Chem. Soc., 55 (1933) 2378.
12 J. E. Fergusson and J. H. Gainsford, Inorg. Chem., 3 (1964) 290.
13 L. V. Borisova, E. I. Plastinina and A. N. Ermakov, Zh. Anal. Khim., 29 (1974) 1362.
14 N. Iordanov and M. Pavlova, Zh. Anal. Khim., 24 (1969) 865.
15 M. Polonvski and M. Pesson, Compt. Rend., 232 (1951) 1260.
16 A. K. Majumdar and G. Bhowal, Anal. Chim. Acta, 48 (1969) 192.
17 A. K. Majumdar, S. Bhowal and B. Datta, Anal. Chim. Acta, 93 (1977) 249.

Analytica Chimica Acta, 97 (1978) 135—147

ETUDE STATISTIQUE DES TITRAGES ACIDO—BASIQUES EN SOLUTIONS AQUEUSES DILUEES
2e. Partie. Cas de l'acide polyméthacrylique

CLAUDE ROSSI et SERGE COMBET*

Laboratoire de Physicochimie Ionique et Macromoléculaire, Université de Provence, 13331 Marseille-Cedex 3 (France)

(Reçu le 18 juillet 1977)

RÉSUMÉ

Le titrage de l'acide polyméthacrylique en solution aqueuse de force ionique voisine de 0,5 mol l^{-1} est étudié dans un domaine de coefficient de dissociation α compris entre 0,01 et 0,98. L'équation de Henderson—Hasselbalch modifiée convient moins bien à l'analyse de ce titrage hors de la zone de transition que l'équation thermodynamique à terme d'excès linéarisé en α. Le pK intrinsèque de la forme moléculaire étendue est trouvé supérieur à celui de la forme compacte et une valeur de 80 calories est proposée pour l'enthalpie libre de transition par motif monomère.

SUMMARY

The titration of polymethacrylic acid in aqueous solution of ionic strength close to 0.5 mol l^{-1} is studied over a dissociation coefficient range of 0.01—0.98. The Henderson—Hasselbalch equation is less convenient for the description of this titration outside the transition range than the thermodynamic equation with an excess term linearized in α. The intrinsic pK of the extended molecular form is greater than that of the compact form and a value of 80 calories is proposed for the transition free enthalpy for one monomeric unit.

Dans la première partie de ce mémoire [1], a été décrite une méthode d'étalonnage d'une pile protométrique qui est appliquée ci-après au titrage de l'acide polyméthacrylique. Les études expérimentales de la dissociation acido—basique de polyélectrolytes synthétiques en solution aqueuse ont souvent servi de modèle pour la compréhension du comportement de macromolécules naturelles. En particulier, l'analyse des courbes de titrage sert à mettre en évidence le passage d'une conformation moléculaire compacte, parfois hélicoïdale, stable en milieu acide à une conformation en pelote plus étendue et désordonnée en milieu basique. Des exemples de polyélectrolytes modèles souvent étudiés sont: l'acide polyglutamique [2—6] pour une chaîne polypeptidique simple et les acides polyméthacrylique [7—13] et polyacrylique [14—19] présentant une chaîne vinylique encore plus simple.

Pratiquement, on peut dire qu'il n'existe pas d'équation simple applicable à l'étendue complète du titrage d'un polyélectrolyte subissant une transition

de conformation en cours de neutralisation. La thermodynamique statistique a permis la formulation d'une théorie [20] de cette transition de conformation pour des macromolécules chargées et des solutions numériques de plus en plus rigoureuses [21—23] incluant le cas des copolymères, mais d'application fastidieuse. Cependant, si l'on considère les zones de la courbe de titrage encadrant la zone de transition, il est raisonnable de tenter d'appliquer à chacune d'elle la théorie convenable pour le type de conformation considéré. Ces théories ont été nombreuses [14]. Certaines s'appuient sur divers modèles à charge répartie et interactions du type Debye—Hückel, comme celle de Hill [24] pour le modèle cylindrique ou sphérique rigide avec laquelle Wada [2] obtient de bons résultats dans l'application au cas de l'acide polyglutamique. Les autres théories [25, 26] utilisent des modèles à interactions entre charge localisées, fondamentalement plus satisfaisants, mais d'application généralement malaisée.

L'équation générale de titrage pH = f(degré de dissociation α) qui a la forme suivante [6]

$$\mathrm{pH} = \mathrm{p}K_0 + \log\left[\alpha/(1-\alpha)\right] + \left[0{,}43/\mathrm{RT}\right]\left[\partial\,\Delta_E G/\partial\,\nu\right] \qquad (1)$$

comporte donc un terme de variation de l'enthalpie libre molaire d'excès avec le nombre ν de groupements dissociés dont l'expression est délicate parce qu'on ignore un grand nombre de paramètres descriptifs du modèle macromoléculaire. Le choix de conditions expérimentales favorables peut néanmoins permettre de s'affranchir de l'influence de certains de ces paramètres par exemple [14] en rendant négligeable les interactions à longue distance dans un milieu de force ionique assez élevé.

Toutefois, des renseignements importants peuvent être obtenus simplement par extrapolation des courbes de titrage tracées dans les zones extérieures à la zone de transition. Cette extrapolation peut être tentée en dehors de tout emploi de modèle, par exemple au moyen d'un polynôme [17] mais dans le plus grand nombre de cas, elle est faite au moyen de l'équation de Henderson—Hasselbalch modifiée [7, 8].

$$\mathrm{pH} = \mathrm{p}K_a + n\log\left[\alpha/(1-\alpha)\right] \qquad (2)$$

$\mathrm{p}K_a$ étant la valeur pour $\alpha = 0{,}5$. Si cette équation est réputée rendre assez correctement compte des courbes de titrage de certains polyélectrolytes ne présentant pas de transition de conformation, elle est néanmoins empirique dans sa forme et dans la valeur du paramètre ajustable n. Une interprétation thermodynamique de la forme de cette équation au voisinage de la demi-neutralisation, a été donnée par Grégor et Frederick [27], et Katchalsky et Spitnik [7] ont proposé une explication statistique. Il parait néanmoins risqué de faire reposer le processus d'extrapolation uniquement sur cette équation empirique sans en essayer d'autres.

Dans ce travail, l'acide polyméthacrylique est étudié par titrage potentiométrique qui est la méthode la plus utilisée d'étude du changement de conformation. On montre comment la maîtrise des données expérimentales

et leur traitement rigoureux peut permettre une discrimination objective entre deux méthodes analytiques basées sur des équations différentes. Le choix d'un milieu aqueux de force ionique voisine de 0,5 mol l^{-1} permet d'utiliser une linéarisation [14] du terme d'enthalpie libre molaire partielle d'excès de l'équation thermodynamique (éqn. 1). D'autre part assez peu de résultats détaillés ont été publiés pour un tel milieu, la modification de la courbe de titrage induite par le changement de conformation s'atténuant beaucoup aux forces ioniques élevées. La méthode expérimentale utilisée permet d'étendre le domaine de dissociation connu vers ses limites inférieures et supérieures. Cette extension vers le degré de dissociation nul est tout particulièrement intéressante en relation avec de nombreux travaux [2—4, 6, 8, 19] dans cette région où l'importance des erreurs expérimentales est généralement susceptible de modifier considérablement les résultats. Enfin, une nouvelle valeur de l'enthalpie libre de transition par motif monomère est proposée.

PARTIE EXPERIMENTALE

Produits réactifs et appareillage

L'acide polyméthacrylique a été obtenu [28] à partir de l'acide méthacrylique stabilisé par l'hydroquinone et purifié par distillation sous pression réduite d'azote. La polymérisation a été réalisée en milieu aqueux selon la technique de l'amorçage radicalaire [29] en présence d'eau oxygénée comme initiateur. Les solutions diluées obtenues en fin de traitement sont lyophilisées.

L'étude des spectres infra-rouge [28] montre que le polymère possède une structure à prédominance syndiotactique. L'appareillage et la technique expérimentale ont été présentés dans le mémoire précédent [1]. L'acide fort introduit dans les titrages de polymère pour en limiter l'autodissociation provient d'une solution concentrée d'acide nitrique (Prolabo RP, d = 1,38). Les divers sels de fond sont des produits très purs (Merck) et la température est 25 ± 0,01°C.

La méthode d'étalonnage

La méthode d'étalonnage a été simplifiée en introduisant l'ajustement de deux paramètres D'_1 et D'_2 en lieu et place des paramètres D_1 et D_2 selon les équations

$$D_1 = D'_1 - \mathrm{pH_E}\,(1 - (1/\alpha^*)) \qquad (3)$$

$$D_2 = D'_2 - \mathrm{pH_E}\,(1 - (1/\alpha^*)) \qquad (4)$$

avec $D'_1 = -\log m\gamma_{H^+}$ et $D'_2 = \log m\gamma_{H^+} + \mathrm{p}K_W$.

Aucune différence significative n'est à relever entre les résultats provenant des deux modes d'exploitation comme l'indique le Tableau 1. Enfin, une éventuelle erreur sur $\mathrm{pH_E}$ ne peut introduire qu'un décalage des mesures dans l'échelle de pH sans perturber l'ajustement.

TABLEAU 1

Etalonnage de la pile de mesure par titrage d'un acide fort. Comparaison des deux méthodes d'exploitation appliquées à l'étalonnage utilisé pour la courbe a Fig. 2
(V = volume initial de solution à doser; m = titre molaire de la solution de soude; t = paramètre de Student pour $P = 0{,}05$; $\alpha^* = \alpha'^*_a + \alpha'^*_b (pH_{lu} - pK_W/2)$ si $(pH_{lu} > pK_W/2)$, $\alpha^* = \alpha'^*_a$ si $(pH_{lu} < pK_W/2)$; $pH_E = 1{,}098$. $V = 40$ ml; force ionique $I = 0{,}64$ mol l^{-1} $NaNO_3$; [acide] = $3 \cdot 210^{-2}$ mol l^{-1}; nombre de points $N = 57$)

Domaine de pH_{lu} exploité	α'^*_a β	α'^*_b β	D_1 β	D_2 β	D'_1 β	D'_2 β	v_e β	$\sigma_{ext.}$	pK_W β	Méthode
1,572—12,144	1,022 ±0,004	—0,0014 ±0,0005	0,186 ±0,010	13,50 ±0,04	—	—	2,0057 ±0,0010	$1{,}77 \cdot 10^{-3}$	13,73 ±0,05	[1]
									13,73	
	1,022 ±0,003	—0,0015 ±0,0005	—	—	0,210 ±0,004	13,52 ±0,03	2,0057 ±0,0010	$1{,}76 \cdot 10^{-3}$	±0,04	Présent mémoire

$\beta = \pm t\sigma$.

TABLEAU 2

Etalonnage de la pile de mesure par titrage d'un acide fort. Paramètres d'étalonnage retenus pour les autres titrages de la Fig. 2 ($V = 50$ ml)

[Acide] mol l^{-1}	I mol l^{-1}	m mol l^{-1}	Domaine de pH_{lu} exploité	α'^*_a β	α'^*_b β	D'_1 β	D'_2 β	v_e β	$\sigma_{ext.}$	N	pK_W β	Fig. 2 Courbe
$2 \cdot 10^{-2}$	0,52 (KNO_3)	0,52	(1,785—11,428)	1,014 ±0,008	0,007 ±0,002	0,36 ±0,01	13,06 ±0,11	1,9266 ±0,0022	$3{,}49 \cdot 10^{-3}$	47	13,42 ±0,12	b
$3{,}16 \cdot 10^{-2}$	0,55 ($NaNO_3$)	0,55	(1,476—11,892)	1,029 ±0,004	—0,0048 ±0,0005	0,210 ±0,004	13,33 ±0,03	2,8779 ±0,0014	$2{,}37 \cdot 10^{-3}$	60	13,54 ±0,04	c
$3{,}37 \cdot 10^{-2}$	0,55 ($NaNO_3$)	0,55	(1,465—11,875)	1,022 ±0,004	—0,0034 ±0,0006	0,228 ±0,004	13,35 ±0,04	3,067 ±0,014	$2{,}50 \cdot 10^{-3}$	53	13,58 ±0,04	d

$\beta = \pm t\sigma$.

METHODE D'EXPLOITATION

Cas d'un monoacide faible

L'expression donnant le nombre de groupements réellement dissociés h_i par unité de masse de l'acide faible est donnée [1] en fonction des volumes de base forte (titre molaire m) et de la masse G de l'acide titré par l'expression suivante

$$h_i = [(v_{i\,II} - v'_{i\,II})\ (m\ 10^{-3}/G)] - [(v_{e\,II} - v_{e\,I})\ (m\ 10^{-3}/G)] \qquad (5)$$

soit encore l'expression plus condensée

$$h_i = h_{i\,exp} - h^0 \qquad (6)$$

$h_{i\,exp}$ est le seul terme directement accessible expérimentalement, h^0 provenant de la non-identité des quantités d'acide fort mises en jeu dans les titrages I et II [1] respectivement (Fig. 1). Un changement de variable permet d'éliminer le terme constant mais inconnu h^0 en prenant comme origine une valeur arbitraire h^*_{exp} du tableau de données.

On définit la nouvelle variable X_i soit

$$X_i = h^*_{exp} - h_{i\,exp} = h^* - h_i \qquad (7)$$

Dans le cas simple d'un monoacide faible de constante apparente de dissociation K_a, l'équation de la dissociation s'écrit alors

$$pH_i = pK_a + \log\,[(B - X_i)/(E + X_i)] \qquad (8)$$

avec $B - X_i = h_i$, $E + X_i = (1/M) - h_i$, et $Mh_i = (B - X_i)/(B + E) = \alpha_i$. M est la masse molaire du motif monomère du polyacide. Les paramètres B et E tous deux positifs correspondant aux deux positions asymptotiques sont ajustables statistiquement par la méthode des moindres carrés pondérés [30]. En fait l'expression de $h_{i\,exp}$ contient le facteur multiplicatif non ajustable directement $(m \cdot 10^{-3}/G)$ auquel on ne sait attribuer initialement qu'une valeur expérimentale qui n'est pas forcément la valeur vraie. Si bien que les grandeurs expérimentales de X_i, B et E sont elles-mêmes dépendantes de

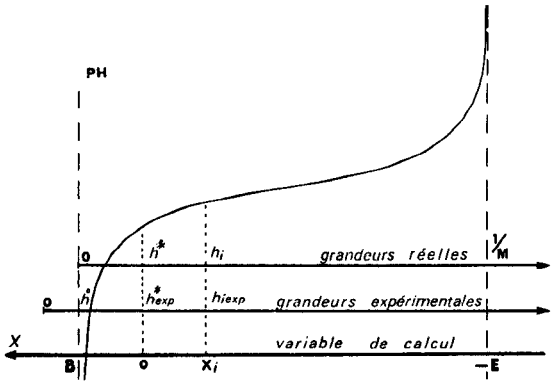

Fig. 1. Courbe théorique de titrage d'un polyacide faible et changements de variables.

l'évaluation de ce facteur. Aussi $(B + E)$ n'est égal à la valeur stoechiométrique $(1/M)$ que dans le cas où la valeur choisie pour ce facteur est juste. Dans tous les autres cas, la grandeur déduite de l'ajustement est

$$B + E = (1/M)\,(m\ 10^{-3}/G)_{\text{exp}}\,(G/m\ 10^{-3})_{\text{juste}} \qquad (9)$$

Mais la valeur attribuée dans le calcul à ce facteur n'altère en rien la validité de l'éqn. (8). L'introduction des paramètres d'étalonnage [1] dans l'éqn. (8) donne l'expression

$$\text{pH}_{\text{lu}} = \alpha^* \text{p}K_a + \alpha^* \log\,[(B - X_i)/(E + X_i)] - \text{pH}_E\,(\alpha^* - 1) \qquad (10)$$

où α^* est le terme d'étalonnage indiqué dans les Tableaux 1 et 2.

Cas des polyacides

L'équation d'Henderson—Hasselbalch modifiée (H—H) s'exprime en fonction (éqn. 2) du degré de dissociation α, d'un facteur empirique n [7, 8] et de $\text{p}K_a$ ($\alpha = 0{,}5$) qui est la valeur particulière de la constante apparente de dissociation à demi-neutralisation. En tout point i du titrage, le pK apparent est donné par

$$\text{p}K_i = \text{pH}_i - \log\,[\alpha_i/(1 - \alpha_i)] = \text{p}K_a\,(\alpha = 0{,}5) + (n - 1) \log\,[\alpha_i/(1 - \alpha_i)] \qquad (11)$$

En introduisant nos variables et paramètres d'étalonnage, l'équation H—H s'écrit

$$\text{pH}_{\text{lu}} = \alpha^* A + \alpha^* n \log\,[(B - X_i)/(E + X_i)] - \text{pH}_E\,(\alpha^* - 1) \qquad (12)$$

avec $A = \text{p}K_a\,(\alpha = 0{,}5)$ et $(B - X_i) = h_i = \alpha_i/M$. Les paramètres ajustables de cette équation sont A, B, E et n, le terme α^* étant une fonction des paramètres d'étalonnage indiquée aux Tableaux 1 et 2. L'équation du pK apparent devient alors

$$\text{p}K_i = A + (n - 1) \log\,[(B - X_i)/(E + X_i)] \qquad (13)$$

L'équation thermodynamique générale (éqn. 1) fait intervenir un terme d'enthalpie libre d'excès molaire partielle des groupes chargés qui sont ici les ν_i groupes bases conjuguées par molécule de polyacide contenant N motifs monomères ($\nu_i = N\alpha_i$). On a vu dans l'introduction de ce travail, que ce terme qui représente l'énergie extrinsèque de dissociation, distincte de l'énergie du processus intrinsèque de dissociation liée à $\text{p}K_0$, pouvait être approximativement représentée par une fonction linéaire de α_i dans des conditions expérimentales de force ionique élevée.

$$\text{pH}_i = \text{p}K_0 + \log\,[\alpha_i/1 - \alpha_i)] + \alpha \cdot \text{Constante} \qquad (14)$$

Cette formulation est assez largement controversée. Par exemple, tandis que Hermans [3] et Wada [2] montrent qu'une telle équation semble applicable à l'acide polyglutamique (force ionique supérieure à 0,1 mol l^{-1}) dans les zones situées de part et d'autre du maximum de déformation de la courbe $\text{pH}_i = f(\alpha_i)$, Olander et Holtzer [4] contestent l'opportunité d'une telle équation pour représenter la forme étendue de la macromolécule.

Etant donné cependant qu'aucun auteur ne tient compte formellement de la fonction de réponse de la pile de mesure, on testera l'hypothèse simple représentée par l'éqn. (14), ce qui conduit à l'expression

$$pH_{1u} = \alpha^* A + \alpha^* \log [(B - X_i)/(E + X_i)] - pH_E (\alpha^* - 1) - (DR)\alpha^* X_i \quad (15)$$

où pH_E, α^*, B et E sont les grandeurs définies précédemment, avec $A = pK_0 + B(DR)$, et $DR = M \cdot$ Constante.

Dans ces conditions le pK apparent s'exprime linéairement en fonction de X_i, tel que

$$pK_i = A - (DR)X_i \quad (16)$$

L'exploitation statistique des titrages de l'acide polyméthacrylique est envisagée dans cette étude à partir de l'éqn. (12) et de l'éqn. (15).

RESULTATS

Dépouillement des données expérimentales

A partir des données brutes (pH_{1u}, v_{iII}) des titrages II (mélange d'un acide fort et du polyacide faible), les courbes de titrage (pH_{1u}, X_i) sont en premier lieu calculées au moyen du changement de variable exposé précédemment (éqns. 5—7). Des exemples sont fournis dans la Fig. 2. Sur chaque courbe

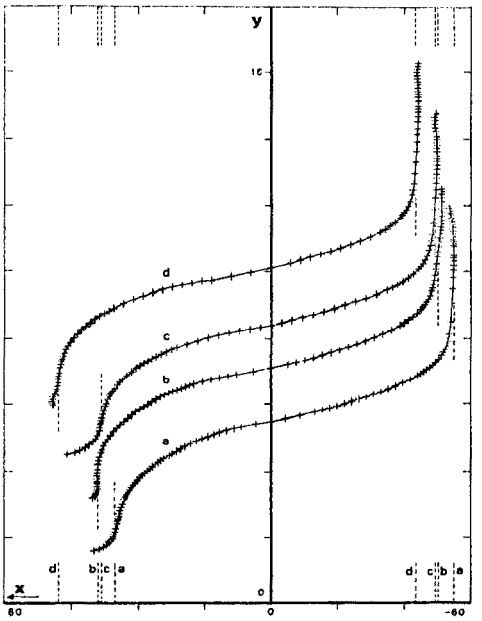

Fig. 2. Courbes expérimentales (voir Tableau 2 pour les paramètres d'étalonnage retenus). $Y = pH_{1u}$; les courbes b, c et d sont décalées vers le haut par rapport à la courbe a respectivement de 1,5; et 4,5 unités. La masse G d'acide polyméthacrylique introduite dans chaque essai est: (a) 0,0805 g; (b) 0,1002 g; (c) 0,0868 g; (d) 0,0922 g.

les deux droites limites tracées au trait pointillé donnent une estimation expérimentale de $(B + E)$. Pour chaque cas les anomalies observées aux extrémités acide et basique sont dues à une faible erreur rendue systématique par le calcul en retour des volumes v'_{ii} et amplifiée par la fonction d'erreur dans ces zones. Réciproquement un même titrage d'acide polyméthacrylique exploité à partir de différents étalonnages (titrage I [1]) peut présenter l'allure de l'une quelconque des courbes de la Fig. 2, seule la portion de courbe comprise entre les traits pointillés restant inchangée quel que soit l'étalonnage. Ceci souligne l'absence de corrélation entre l'origine de ces anomalies et le comportement du polyacide. De ce fait, ne sera considérée pour la suite de l'exploitation des exemples présentés (Fig. 2) que la partie continue de chaque courbe délimitée par les traits pointillés.

L'ajustement des paramètres de l'éqn. (12) ou de l'éqn. (15) est fait par la méthode des moindres carrés pondérés [30] respectivement dans le domaine de faible dissociation ($\alpha < 0{,}2$) et dans celui de forte dissociation ($\alpha > 0{,}57$) de la façon suivante. Dans le premier domaine, on ajuste tous les paramètres sauf E auquel on donne une valeur provisoire estimée à partir de la Fig. 2. Ensuite, on procède de façon similaire dans le second domaine, le paramètre B étant cette fois celui qui est maintenu constant avec la valeur trouvée dans le premier ajustement. On a ainsi un processus itératif jusqu'à convergence sur un ensemble unique de valeur (B, E) qui donne la meilleure estimation ajustée de la somme $(B + E)$ (éqn. 9).

Ajustement selon l'éqn. (12) et interprétation

Pour s'en tenir aux résultats de l'un des titrages représentatifs de l'ensemble des expériences (Fig. 2, courbe c), les valeurs des paramètres de l'ajustement sont indiquées dans le Tableau 3. La Figure 3 représente l'ensemble des résultats

TABLEAU 3

Résultats de l'ajustement paramétrique à partir des éqns. (12) et (15)
(Les données sont celles relatives au titrage c, Fig. 2; $\sigma_{pH_{iu}} = 0{,}001$; $\sigma_{X_i} = 0{,}278 \cdot 10^{-4}$; $pH_E = 1{,}098$; force ionique $I = 0{,}55$ mol l^{-1} $NaNO_3$)

Domaine de pH_{iu} exploité	A β	$B \cdot 10^4$ β	$E \cdot 10^4$ β	n β	$10^4 \sigma_{ext.}$	Nombre de points
Ajustement à partir de l'éqn. (12)						
2,377—4.532	5,48	52,67	49,95	1,67	0,175	27
	±0,02	±0,16	(fixe)	±0,03		
5,538—8,480	5,24	52,67	49,95	1,40	0,402	25
	±0,01	(fixe)	±0,34	±0,03		
Ajustement à partir de l'éqn. (15)						
2,377—4,532	5,90	51,51	48,90	0,024	0,127	27
	±0,10	±0,24	(fixe)	±0,003		
5,538—8,480	5,22	51,51	48,90	0,00863	0,076	25
	±0,01	(fixe)	±0,22	±0,0006		

$\beta = \pm t\sigma$.

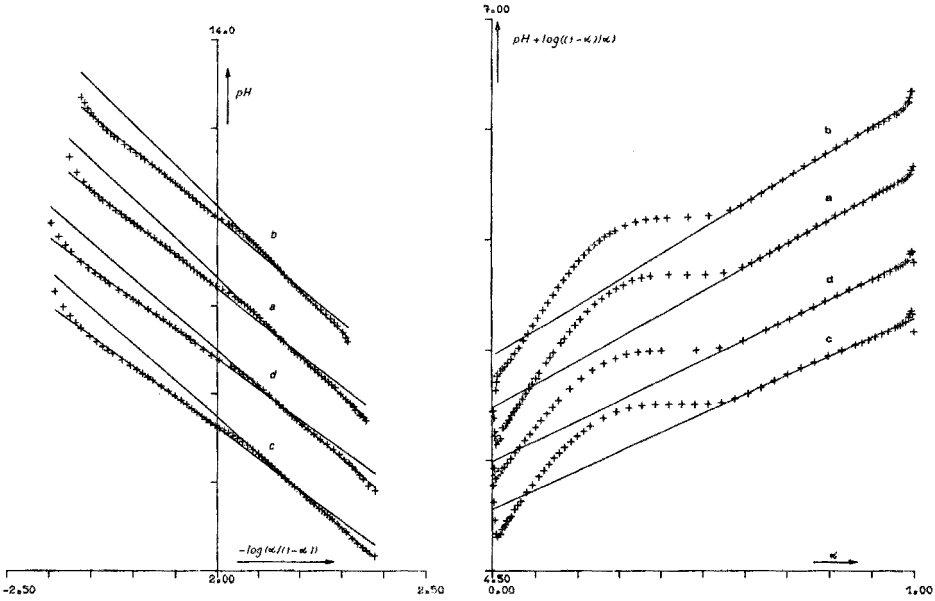

Fig. 3. Courbes expérimentales et recalculées. Les courbes en trait continu sont calculées d'après l'éqn. (12) où $pH = pH_{1u}/\alpha^* + pH_E\ (\alpha^* - 1)/\alpha^*$, les croix représentent les points expérimentaux. Les courbes d, a et b sont décalées vers le haut par rapport à la courbe c respectivement de 1,5; 3; 4,5 unités.

Fig. 4. Courbes expérimentales et recalculées. Les courbes en trait continu sont calculées d'après l'éqn. (15) où $pH = pH_{1u}/\alpha^* + pH_E\ (\alpha^* - 1)/\alpha^*$, les croix représentent les points expérimentaux. Les courbes d, a et b sont décalées vers le haut par rapport à la courbe c respectivement de 0,2; 0,4; 0,6 unités.

obtenus avec les titrages présentés par application de l'équation H—H, α (=Mh) étant calculé à partir des définitions de l'éqn. (8). La répartition des écarts entre valeurs expérimentales et ajustées présente, dans chacun des deux domaines précédemment définis, une distribution assez systématique particulièrement dans le deuxième domaine (partie gauche de la Fig. 3) où les écarts sont très significatifs compte tenu de la petite échelle de la Fig. 3. L'équation H—H paraît donc peu adaptée pour analyser nos courbes de titrage, surtout dans le domaine de coefficient de dissociation élevé comme le montre la valeur très élevée de σ_{ext} obtenue.

Ajustement selon l'éqn. (15) et interprétation

Les résultats de l'ajustement paramétrique pour le même titrage que ci-dessus sont consignés dans le Tableau 3. Si l'accord des données expérimentales avec l'éqn. (15) dans le domaine des faibles valeurs de α paraît à peine meilleur que celui obtenu avec l'éqn. H—H, la variance externe n'étant améliorée que dans un facteur de 1,9, par contre, il y a un accord excellent avec cette éqn. (15) dans le domaine des valeurs de α élevées. Si l'on considère

le graphe de la variation du pK apparent en fonction de α pour les quatre titrages étudiés (Fig. 4), la répartition des points expérimentaux par rapport à la fonction recalculée représentée en trait plein ne fait pas apparaître d'erreur systématique pour $\alpha > 0{,}57$. L'écart observable parfois pour $0{,}85 < \alpha < 0{,}95$ ne paraît pas significatif. D'autre part, les "anomalies" observées aux deux extrémités du domaine de dissociation, soit $\alpha < 0{,}01$ et $\alpha > 0{,}98$, sont dues à une erreur rendue systématique par le calcul en retour des valeurs de α à partir des paramètres ajustés. Précisions que la variable α représente le coefficient de dissociation correct, excluant toute erreur du type de celle mentionnée par Muresan et Zador [19]. L'étendue du domaine de dissociation exploité est donc seulement limitée par ces deux "anomalies" aux extrémités.

L'examen des résultats pour le titrage c dans le Tableau 3 fait apparaître un désaccord significatif entre les valeurs de la somme $(B + E)$ obtenues, respectivement, à partir de l'équation H—H et de l'éqn. (15) (Tableau 3). Ceci s'explique en partie par le mauvais accord de l'équation H—H avec l'expérience conduisant à surévaluer la position des asymptotes. Cependant, une évaluation thermogravimétrique du taux d'humidité d'échantillons semblables a donné des résultats compatibles avec les deux types d'exploitation: 10 ± 3% d'eau.

Enfin l'ensemble des résultats obtenus par l'éqn. (15) avec les titrages présentés est consigné dans le Tableau 4.

TABLEAU 4

Résultats découlant de l'ajustement des paramètres de l'éqn. (15) pour les titrages représentés (Fig. 2)

Titrage	Domaine de pH_{iu} exploité	pK_A^0 β	pK_B^0 β	$(B + E)10^4$ β	$10^4\sigma_{ext.}$	$10^4\sigma_X$	$DR \cdot 10^{-4}$ β	Nombre de points
a	2,42—4,532	4,67 ±0,07	—	100,8	0,066	0,388	0,029 ±0,005	29
	5,802—8,494	—	4,84 ±0,06	±0,7	0,050	0,388	0,0105 ±0,0005	28
b	2,715—4,566	4,73 ±0,06	—	102,8 ±0,5	0,043	0,225	0,029 ±0,003	20
	5,774—8,388	—	4,87 ±0,03		0,084	0,225	0,0112 ±0,0005	28
c	2,377—4,532	4,65 ±0,05	—	100,4	0,127	0,278	0,024 ∓0,003	27
	5,538—8,480	—	4,78 ±0,04	±0,5	0,076	0,278	0,0086 ±0,0006	25
d	2,342—4,543	4,71 ±0,05	—	107,4	0,070	0,262	±0,022 ∓0,003	22
	5,763—8,475	—	4,79 ±0.05	±0,5	0,064	0,262	0,0086 ±0,0007	23

$\beta = \pm t\sigma$.

CARACTERISATION DU CHANGEMENT DE CONFORMATION

Selon l'interprétation classique, la courbe de titrage comprend deux domaines de dissociation de deux formes moléculaires différentes, A et B, séparées par une zone de transition. La Figure 4 montre que les pK apparents extrapolés à $\alpha = 0$ sont différents pour la forme existant dans le premier domaine ($\alpha < 0{,}2$) et pour celle existant dans le deuxième domaine ($\alpha > 0{,}57$). Ces deux valeurs, désignées respectivement par pK_{A^0} et pK_{B^0}, sont relevées dans le Tableau 4. Elles donnent les constantes d'acidité intrinsèques, c'est-à-dire à charge nulle, en l'absence de toute interaction électrostatique intramoléculaire, des groupes carboxyles du polyacide sous la forme A et sous la forme B.

Si la valeur de pK_{A^0} s'impose par une très courte extrapolation des données expérimentales sur la Fig. 4, la valeur attribuée à pK_{B^0} dépend indiscutablement de la méthode d'extrapolation choisie à partir des données expérimentales à α élevé. Cette question a été très discutée, en particulier dans le cas d'autres polyacides comme l'acide polyglutamique. La controverse peut se résumer par l'opposition entre les partisans d'une extrapolation linéaire à force ionique généralement élevée [2, 3] et ceux d'une extrapolation curviligne [4, 6] encore que dans certains cas [31] un doute puisse exister sur le parti pris par les auteurs. En fait, l'extrapolation curviligne paraît souvent motivée surtout par la nécessité alléguée d'avoir le même pK intrinsèque pour les formes A et B, ce qui peut provenir d'une conception erronée de l'état de référence dans l'analyse thermodynamique [32]. Quoi qu'il en soit, on peut remarquer sur la Fig. 3 que l'exploitation par l'équation H—H, très largement utilisée dans le cas de l'acide polyméthacrylique, indiquerait aussi un croisement très net des deux courbes caractérisant, dans cette représentation, les formes A et B et, par suite, un comportement plus acide à $\alpha = 0$ de la forme A que de la forme B. L'inégalité $pK_{B^0} > pK_{A^0}$ paraît donc bien, dans notre cas, indépendante de la méthode d'exploitation graphique et elle est compatible avec certains résultats sur l'acide polyglutamique [3] à température supérieure à 25°C.

Enfin le sens même de cette inégalité est compatible avec l'hypothèse communément admise d'une forme moléculaire A compacte et d'une forme B plus étendue, et l'on peut aborder l'évaluation de l'énergie associée à la transition conformationnelle à charge nulle $A^0 \rightarrow B^0$. On peut montrer [6, 8] que l'enthalpie libre de transition standard par motif monomère est donnée par $\Delta_T G^0/N = 2{,}303\, RT\, A$, où A est la différence des aires comprises, respectivement sous la courbe expérimentale et sous la courbe théorique relative à la forme B dans la Fig. 4. Le calcul numérique des aires, obtenu par intégration du polynôme d'interpolation de Lagrange (pivots non équidistants) calculé sur sept points au plus, conduit aux résultats de la 3° colonne du Tableau 5.

Il est évident que les valeurs proposées sont inférieures aux valeurs déjà publiées. Cependant si l'on procédait comme à l'habitude à une extrapolation

TABLEAU 5

Valeurs en calories de l'enthalpie libre de transition standard $A^0 \rightarrow B^0$ par motif monomère à 25°C

Titrages	I	Valeurs proposées avec $pK_{B^0} > pK_{A^0}$	Hypothèse de l'extrapolation curviligne jusqu'à pK_{A^0}
a	0,64 (KNO_3)	85	165
b	0,52 (KNO_3)	85	146
c	0,55 ($NaNO_3$)	65	149
d	0,55 ($NaNO_3$)	84	131

curviligne du domaine de la forme B jusqu'à pK_{A^0}, on obtiendrait les valeurs de la 4° colonne du Tableau 5 qui sont en bon accord avec la valeur moyenne de 136 ± 27 calories par motif dégagée par Crescenzi et al. [12]. Ce ne sont donc pas les titrages présentés ici qui sont très différents de ceux déjà publiés, c'est leur méthode d'exploitation qui diffère nettement.

Nous exprimons nos remerciements à Monsieur R. Romanetti, responsable du Centre de Calcul de l'Université de Provence, à Madame L. Perichaud qui ont bien voulu élaborer pour nous le programme d'intégration du polynôme d'interpolation de Lagrange, et à Mademoiselle M. Bernard et Monsieur J. Lleras membres de notre laboratoire qui ont synthétisé le polymère et réalisé son étude spectrophotométrique et thermogravimétrique.

BIBLIOGRAPHIE

1 C. Rossi et S. Combet, Anal. Chim. Acta, 89 (1977) 189.
2 A. Wada, J. Mol. Phys., 3 (1960) 409.
3 J. Hermans, Jr., J. Phys. Chem., 70 (1966) 510.
4 D. S. Olander et A. Holtzer, J. Am. Chem. Soc., 90 (1968) 4549.
5 M. Morcellet et C. Loucheux, Polymer, 16 (1975) 785.
6 M. Nagasawa et A. Holtzer, J. Am. Chem. Soc., 86 (1964) 538.
7 A. Katchalsky et P. Spitnik, J. Polym. Sci., 2 (1947) 432.
8 J. C. Leyte et M. Mandel, J. Polym. Sci. Part A, 2 (1964) 1879.
9 E. V. Anufrieva, T. M. Birshtein, T. N. Nekrasova, O. B. Ptitsyn et T. V. Sheveleva, J. Polym. Sci. Part C, (1968) 3519.
10 C. Braud, G. Muller, J. C. Fenyo et E. Selegny, J. Polym. Sci., 12 (1974) 2767.
11 H. Okamoto et Y. Wada, J. Polym. Sci., 12 (1974) 2413.
12 V. Crescenzi, F. Quadrifoglio et F. Delben, J. Polym. Sci. Part A-2, 10 (1972) 357.
13 M. Mandel, J. C. Leyte et M. G. Stadhouder, J. Phys. Chem., 71 (1967) 603.
14 S. Combet, Thèse Doctorat Sciences Physiques, Montpellier, 1962.
15 B. N. Ghosh, Indian J. Chem., Sect. A, 14 (1976) 219.
16 I. Muresan et L. Zador, Stud. Univ. Babes-Bolyai, Ser. Chem., 21 (1976) 20.
17 M. Mandel, Eur. Polym. J., 6 (1970) 807; J. Polym. Sci., 8 (1970) 1841.
18 A. R. Mathieson et J. V. McLaren, J. Polym. Sci. Part A, 3 (1965) 2555.
19 I. Muresan et L. Zador, Rev. Roum. Chim., 20 (1975) 1119.
20 B. H. Zimm et S. A. Rice, Mol. Phys., 3 (1960) 391.
21 S. Lifson, Biopolymers, 1 (1963) 25.
22 G. Allegra, J. Polym. Sci. Part C, 16 (1967) 2815.

23 G. W. Lehman et J. P. McTague, J. Chem. Phys., 49 (1968) 3170.
24 T. L. Hill, Arch. Biochem. Biophys., 57 (1955) 229.
25 R. A. Marcus, J. Phys. Chem., 58 (1954) 621.
26 S. Lifson, J. Polym. Sci., 23 (1957) 431; J. Chem. Phys., 26 (1957) 727.
27 H. P. Gregor et M. Frederick, J. Polym. Sci., 23 (1957) 477.
28 M. Bernard, Thèse de Spécialité, Marseille, 1976.
29 P. Meares, Polymer Structures and Bulk Properties, Van Nostrand, London, 1965.
30 W. E. Wenthworth, J. Chem. Educ., 42 (1965) 96.
31 F. R. Maxfield, J. E. Alter, G. T. Taylor, et H. A. Scheraga, Macromolécules, 8 (1975) 479.
32 S. Combet et C. Rossi, C.R. Acad. Sci. Paris, à paraître.

Analytica Chimica Acta, 97 (1978) 149—154

VOLTAMMETRIC DETERMINATION OF MORPHINE ON STATIONARY PLATINUM AND GRAPHITE ELECTRODES

B. PROKSA

Institute of Experimental Pharmacology, Slovak Academy of Sciences, Bratislava (Czechoslovakia)

L. MOLNÁR*

Pharmaceutical Works Slovakofarma, Hlohovec (Czechoslovakia)

(Received 17th June 1977)

SUMMARY

A voltammetric method for the determination of morphine in poppy seeds, crude morphine and pharmaceutical preparations is described. The method is based on electrochemical oxidation of morphine at a stationary graphite or platinum electrode in basic electrolyte. The mechanism of the electrochemical oxidation of morphine and its derivatives are discussed. The proposed method shows good reproducibility, and sample preparation is simple. The working ranges are 6×10^{-5}—10^{-3} M with the graphite electrode and 10^{-5}—10^{-3} M with the platinum electrode. There is no interference from various morphine derivatives or minor alkaloids at the 10^{-3} M level.

The polarographic inactivity of morphine [1] and its derivatives has led to the adoption of an indirect polarographic method developed by Baggesgaard-Rasmussen et al. [2], which is based on the action of nitrous acid on morphine during nitration [3]. The product of the reaction is polarographically reducible. Even though the nitration process is quantitative, the 2-nitromorphine obtained is not the final product of the chemical reaction; its concentration decreases with time, and this phenomenon can be utilized for a kinetic polarographic determination of morphine [4].

The development of a fast, precise electrochemical method for the determination of morphine is, however, possible because morphine is easily oxidized in basic media. The electrochemical oxidation of morphine at solid electrodes (Au, Te, Ta, Pd, Pt, C) has been studied [5]; only the rotating platinum electrode [6] satisfies the requirements needed in the study of morphine oxidation reactions. The platinum electrode has also been used in the electrochemical preparative oxidation of morphine [7].

In the work described here, the voltammetric determination and oxidation of morphine, its derivatives and some minor alkaloids were examined at a graphite—silicone rubber electrode (Fig. 1). Derivative voltammetry [8] at a platinum electrode of large surface area was also examined (Fig. 2). To examine the mechanism of the electrochemical reaction, the effects of

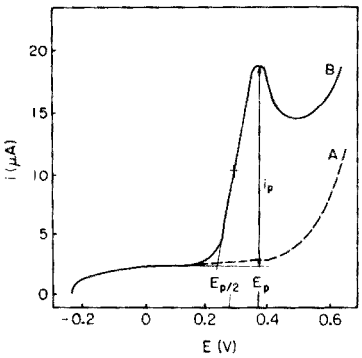

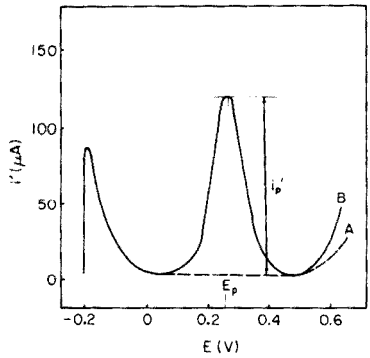

Fig. 1. Voltammogram of the oxidation of morphine at a graphite electrode in 0.2 M KOH. A. Supporting electrolyte. B. Wave after addition of morphine.

Fig. 2. Derivative voltammogram ($i' = -di/dt$) for the oxidation of morphine at a platinum electrode of large surface area in 0.2 M KOH. A. Supporting electrolyte. B. Wave after addition of morphine.

temperature, pH value, morphine concentration and rate of voltage scan were investigated. The $E_{p/2}$ values have no thermodynamic significance, but are often more useful in practice than the E_p values [9].

EXPERIMENTAL

Chemicals and equipment

The following chemicals were used: morphine (basic), morphine hydrochloride, codeine phosphate, narceine hydrochloride, narceinimide oxalate, thebaine, ethylmorphine, pseudomorphine [10], morphine-*N*-oxide [11], 2-nitromorphine [12], diacetylmorphine, and papaverine hydrochloride, Britton-Robinson (BR) and phosphate buffer solutions were examined. All chemicals were of analytical grade.

A Radelkis OH 105 polarograph was used with a graphite electrode (OP-C 7112 D) and a platinum electrode (OH-935) from Radelkis, Budapest. The pH meter was a Radiometer PHM 26 model.

Regeneration of electrodes. After each recording, the graphite electrode was wiped with tissue. At the end of a series of measurements, the graphite electrode was cleaned with 0.1 M HCl, rinsed with distilled water and finally air-dried. At the start of each series, at least 3 voltammograms of the supporting electrolyte and 3 voltammograms of morphine solutions were measured; subsequent measurements were used for evaluation. The regeneration process for the platinum electrode was the same as that for the graphite electrode except that the electrode was stored in 10% chromic acid between series of measurements.

Voltammetric oxidation of morphine

The dependence of the $E_{p/2}$-value of morphine and its derivatives at a graphite electrode on the pH value is shown in Fig. 3.

The oxidation of morphine, and consequently the voltammetric curve, are sensitive to the temperature of reaction, so that constant temperature is necessary. The dependence is shown in Fig. 4.

The effect of the voltage scan rate (v) on the i_p, E_p, $E_{p/2}$ and $i_p \cdot v^{-1/2}$ values was investigated. Of these measured values, only the most significant are reported; Fig. 5 shows the values $i_p\, v^{-1/2}$ and E_p measured at the graphite electrode, as functions of the logarithmic scan rate. To examine the mechanism of the electrochemical reactions and their reversibility, both

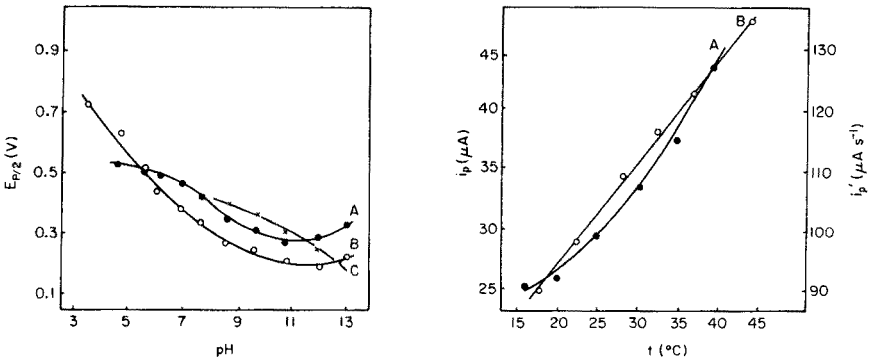

Fig. 3. Dependence of the half-wave potential ($E_{p/2}$) on pH at a graphite electrode. [Compound] = 10^{-3} M; v = 400 mV min^{-1}. A. Morphine. B. Morphine-*N*-oxide. C. Pseudomorphine.

Fig. 4. Dependence of the diffusion current on the temperature (°C) during the oxidation of morphine. A. At a graphite electrode in BR-buffer solution, pH 11.80; [morphine] = 10^{-3} M; v = 1 V min^{-1}. B. At a Pt electrode in 0.2 M KOH; [morphine] = 2.4 × 10^{-4} M; v = 1 V min^{-1}.

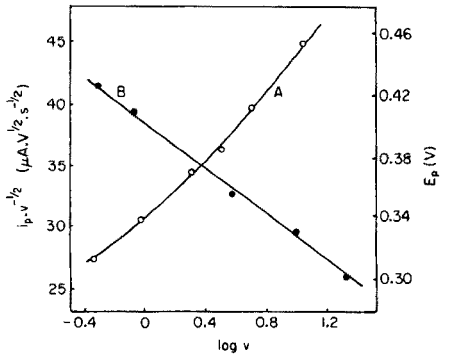

Fig. 5. Curve A. Dependence of the oxidation diffusion current of morphine ($i_p\, v^{-\frac{1}{2}}$) on the logarithm of the voltage scan rate. Curve B. Dependence of the half-wave potential (E_p) on the logarithm of the voltage scan rate in a BR-buffer solution, pH 11.80. [Morphine] 10^{-3} M, v = 200 mV min^{-1} at a graphite electrode.

cyclic and derivative cyclic voltammetry were used, with the results shown in Fig. 6.

For analytical purposes, curves were constructed showing the dependence of the diffusion current, i_p, on the concentration of morphine in BR buffer solution of pH 11.5, as well as curves for $E_{p/2} = +0.23$ V at the graphite electrode. With the platinum electrode, a derivative voltammogram of i' in 0.2 M KOH was obtained, and then the derivative curve was measured at $E_{p/2} = +0.33$ V.

The reproducibility of the determination was calculated on the basis of measuring six waves for each of four samples of freshly prepared 10^{-3} M morphine solutions in BR buffer solution of pH 11.5 with a graphite electrode, with respect to 2.4×10^{-4}M morphine solutions in 0.2 M KOH with a platinum electrode. With the graphite electrode the mean current was 30.78 μA, range 1.92 μA and standard deviation 1.48; with the platinum electrode the mean current was 93.29 μA, range 0.63 μA and standard deviation 1.06.

Voltammetric oxidation of minor alkaloids

Within the pH range 3—12 and in 0.2 M KOH, voltammetric waves were not obtained at the graphite or platinum electrode, from 10^{-3} M concentrations of the minor alkaloids and morphine derivatives: papaverine, codeine, thebaine, narceine, narcotine, ethylmorphine, diacetylmorphine and narceinimide.

Determination of morphine in crude morphine

Because only morphine gives an anodic wave, it is possible to determine morphine even in the presence of minor alkaloids. Crude morphine (0.07—0.1 g) was dissolved in 15 ml of 0.1 M HCl, diluted to 50 ml with distilled water, and

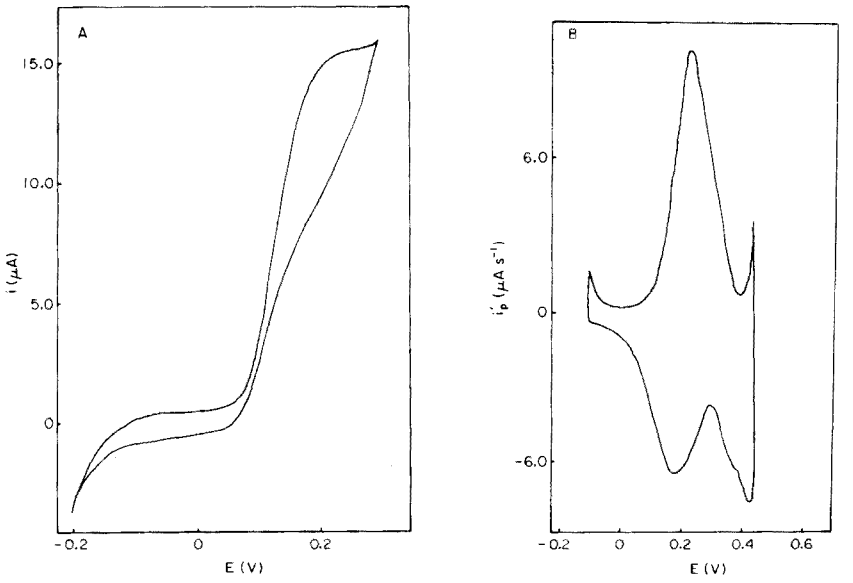

Fig. 6. Voltammograms for morphine (10^{-3} M) in 0.2 M KOH at a graphite electrode. $v = 1$ V min^{-1}. A. cyclic voltammogram. B. Derivative cyclic voltammogram.

1 ml of this solution was diluted with BR buffer pH 11.5 to 10 ml for determination at the graphite electrode, or with 0.2 M KOH to 10 ml for determination at the platinum electrode. The voltammetric wave was recorded at a scan rate of 400mV min^{-1} for the graphite electrode, and at a scan rate of 1 V min^{-1} for the platinum electrode. The values i_p or i' obtained were evaluated from calibration graphs with relative standard deviation 4.81% at the graphite electrode, 1.36% at the platinum electrode and 3.32% by determination after nitration following the Baggesgaard-Rassmussen method [2]. The sensitivity of the platinum electrode was approximately three times that of the graphite electrode.

Determination of morphine in injections

Morphine hydrochloride injection solution (0.1 ml of 1% solution) was diluted with 0.2 M KOH to 10 ml, and the voltammetric curve was recorded at the platinum electrode at a scan rate of 1 V min^{-1}. The concentrations were read from a calibration graph. The stabilizers present ($NaHSO_3$, chlorocresol) did not interfere with the determination. After each determination, it was necessary to regenerate the electrode and deaerate the next solution briefly by passing nitrogen.

Determination of morphine in poppy seed extracts

Morphine was isolated from poppy seeds by the methods of Pinxteren and Verloop [13] or of Zsadon [14]. Poppy seeds (20 g) were extracted with 0.1 M HCl in 80% ethanol. The evaporated extract was purified with benzene—butanol mixture. After evaporation, the residue was dissolved in 0.2 M KOH, and morphine was determined at the platinum electrode.

DISCUSSION

The morphine gives an anodic wave at both the graphite and platinum electrodes; the i_p and E_p values depend on the pH value. At the graphite electrode, the oxidation proceeds best at pH 11.5, giving an easily measurable wave. With the platinum electrode, it is better to use a 0.2 M KOH supporting electrolyte and derivative voltammetry. The peak current is also significantly affected by the temperature. The temperature coefficient valid for the oxidation of morphine at the graphite electrode is 3.27%/°C, and at the platinum electrode 1.77%/°C within the temperature interval 20—40°C. With the graphite electrode the working concentration range is 6×10^{-5}—10^{-3} M and the voltage scan rate is 200—400 mV min^{-1}. With the platinum electrode and derivative voltammetry, the optimal concentration range is 9×10^{-6}—10^{-3} M at a scan rate of 1 V min^{-1}.

The dependence $i\,v^{-1/2}$ as a function of the logarithmic scan rate shows a positive slope, whereas a plot of E_p vs. logarithmic scan rate shows a negative slope. Both these relationships indicate a first-order reaction, in this case, dimerization.

The derivative cyclic voltammetric results indicate that the electrochemical oxidation of morphine (Fig. 6), pseudomorphine and morphine-*N*-oxide is partially reversible. The results obtained show that the mechanisms of the

medium followed by reaction at the electrode surface probably produces an intermediate, pseudomorphine, according to the scheme:

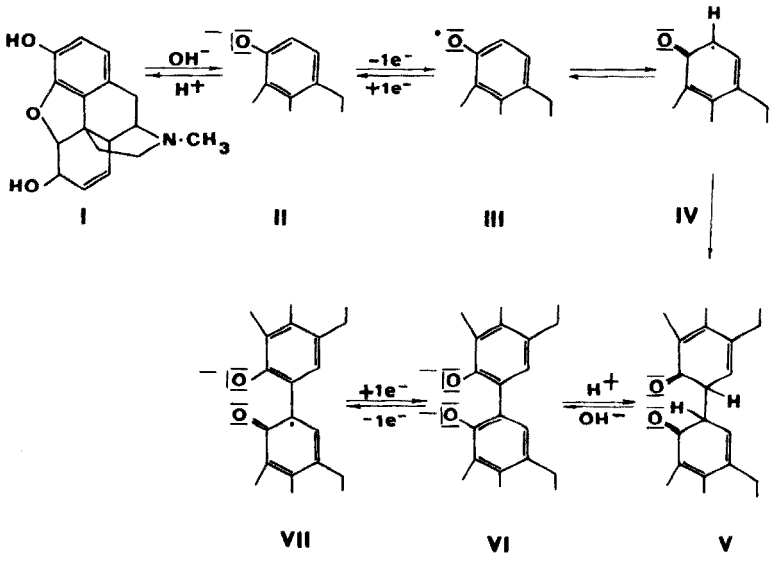

reaction in acidic and alkaline electrolytes are quite different and that the reactions are quasi-reversible. The electrochemical oxidation in a basic A free phenolic group is necessary for the electrochemical oxidation. The mechanism of the subsequent reaction, i.e. the oxidation of pseudomorphine, at the free hydroxyl group, requires further investigation.

The advantage of the method for analytical purposes lies in the rapid determination of the morphine content in crude morphine, and in plant material even if minor alkaloids are present. Preparation of the samples is easy, and the reproducibility is good. The necessity of checking the calibration curve before each series of measurements may be considered as a disadvantage of the method.

REFERENCES

1 H. F. W. Kirpatrick, Q. J. Pharm., Pharmacol., 20 (1947) 87.
2 H. Baggesgaard-Rasmussen, C. Hahn and K. Ilver, Dan. Tidsskr. Farm., 19 (1945) 41.
3 H. Lund, Acta Chem. Scand., 12 (1958) 1444.
4 B. Zsadon and T. Paál, Herba Hung., 8 (1969) 157.
5 H. P. Deys, Pharm. Weekblad, 99 (1964) 737.
6 Isaka Hiroshi, Yakugaku Zasshi, 91 (1971) 1027 (C.A. 76, 9789r).
7 A. Rashid and R. Kalvoda, Česk. Farm., 20 (1971) 143.
8 S. P. Perone and J. R. Birk, Anal. Chem., 37 (1965) 2.
9 R. S. Nicholson and I. Shain, Anal. Chem., 36 (1964) 706.
10 K. W. Bentley and S. F. Dyke, J. Chem. Soc., (1959) 2574.
11 B. Kelentey, E. Stenszky, F. Czollner, L. Szlávik and Z. Mészáros, Arzneim. Forsch., 7 (1957) 594.
12 R. Bognár and G. D. Gaál, Magy. Kém. Foly., 69 (1963) 17.
13 J. A. C. van Pinxteren and M. E. Verloop, Pharm. Acta Helv., 38 (1963) 437.
14 B. Zsadon and Paál, Acta Chim. Acad. Sci. Hung., 57 (1968) 323.

Analytica Chimica Acta, 97 (1978) 155—164

CONDUCTOMETRY OF NITROBENZENE SOLUTIONS OF TRIALKYLAMMONIUM SALTS

MICHEL GÉRIN and JAMES FRESCO*

Department of Chemistry, McGill University, Montreal H3A 2K6 (Canada)

(Received 30th August 1977)

SUMMARY

The conductance of water-saturated nitrobenzene solutions of unbranched trialkylammonium salts has been measured. Dissociation constants of the salts decrease in the order; perchlorate, iodide, bromide, and chloride. Dissociation does not appear to increase with increasing alkyl chain length.

Conductivity measurements of water-saturated nitrobenzene solutions of tertiary alkylammonium salts were undertaken to determine the nature of the solute and the equilibria prevalent among the different solute species. In nitrobenzene, ionophores usually experience a partial dissociation [1] depending on the sizes of anion and cation.

Conductometry of solutions of quaternary ammonium salts in nitrobenzene has led to the estimation of their dissociation constants; dissociation increased with increasing size of anion and cation, in agreement with an electrostatic model for their association [1]. Tertiary ammonium salts generally experience a much smaller dissociation than quaternary ammonium salts in dipolar aprotic solvents because of the formation of an internal hydrogen bond between cation and anion in the ion-pair.

Only fragmentary data exist on the dissociation of tertiary alkylammonium salts in nitrobenzene [2—5]. In this study, the chain length of the alkylammonium cation was increased and anions of differing hydrogen bonding affinities were introduced to reveal the influence of the structure of tertiary amine salts on their solution properties.

EXPERIMENTAL

Conductivity measurements were performed on water-saturated nitrobenzene solutions of tripropylammonium, tributylammonium, tripentylammonium, trihexylammonium, trioctylammonium and tridodecylammonium chlorides, bromides, iodides, and perchlorates.

Chemicals

Nitrobenzene (Fisher, certified A.C.S.) was distilled (spinning band column, 86°C and 10 mm). The distillate was transferred to a separatory funnel and extracted 3 times with equal volumes of 1 M NaOH. After 1 extraction with distilled water, 3 extractions with 0.5 M H_2SO_4 and 4 extractions with deionized distilled water followed. The pH of the last washing was checked for neutrality [5]. The specific conductance of the water-saturated nitrobenzene was $(2.9 \pm 0.2) \times 10^{-8}\ \Omega^{-1}\ cm^{-1}$ at 25°C. The purified water-saturated nitrobenzene was stored in stoppered brown bottles.

The preparations of tripropylammonium chloride (TPrAHCl), bromide (TPrAHBr), iodide (TPrAHI), and perchlorate ($TPrAHClO_4$); tributylammonium chloride (TBAHCl), bromide (TBAHBr), iodide (TBAHI), and perchlorate ($TBAHClO_4$); tripentylammonium chloride (TPTAHCl), bromide (TPTAHBr), and iodide (TPTAHI); trihexylammonium chloride (THAHCl), bromide (THAHBr), and iodide (THAHI); trioctylammonium chloride (TOAHCl), bromide (TOAHBr), and iodide (TOAHI) and tridodecylammonium chloride (TLAHCl), bromide (TLAHBr), iodide (TLAHI) and perchlorate ($TLAHClO_4$) have been described [6].

Concentrated acids HI (65%, BDH AnalaR), $HClO_4$ (70%, Anachemia, reagent grade) and HBr (47.9%, Baker, reagent grade) were used without further purification.

Amines which were converted subsequently to salts in situ were distilled under reduced pressure over KOH by use of a spinning band column. These were tripentylamine (Eastman; 72°C and 1 mm), trihexylamine (Eastman; 128°C and 3 mm) and trioctylamine (Aldrich; 110°C and less than 1 mm).

Preparation and standardization of 0.1 M trialkylammonium salt solutions

Salts obtained as pure solids were dissolved in water-saturated nitrobenzene and diluted to ca. 0.1 M solutions. Nitrobenzene solutions of the other salts which were not isolated as pure crystalline compounds were prepared by neutralization of the appropriate amine solution in nitrobenzene with an aqueous solution of the corresponding acid. A solution (ca. 0.1 M) of amine in nitrobenzene was prepared and shaken with an equal volume of aqueous 0.2 M acid. The separated organic phase was therefore 0.1 M in ammonium salt. To ensure that the organic phase was water-saturated at the temperature of the conductometric measurements, the salt solutions prepared in either way were further equilibrated at 25°C with a solution of the corresponding aqueous 0.1 M acid; 1 M acid solution was used for the more soluble TBAHCl, TPrAHBr, TPrAHI. The TPrAHCl solution was not further equilibrated with water. The acid was introduced to prevent hydrolysis of the trialkylammonium ions.

The trialkylammonium salt solutions were standardized by potentiometric titration with standard potassium hydroxide in ethanol. The end-point was detected with a calomel—glass electrode pair.

The standardized 0.1 M solution was used to prepare a series of 8 dilutions ranging from 10^{-2} to 10^{-4} M.

Conductance measurements

The conductivity cell was a cylindrical glass-stoppered flask (40 ml) with two planar square parallel platinum electrodes situated near the bottom of the flask. The electrodes, covered with platinum black, were in electrical contact with pools of mercury contained in sealed glass tubes. Platinum wires immersed in the mercury pools were connected to the conductivity bridge. Temperature control was achieved by immersing the cell in water in a double-walled beaker maintained at 25.00 ± .02°C by a circulating bath (Hetotherm, type 623) calibrated with a 2801 A H.P. Quartz thermometer. The Teflon-encased magnetic bar used to stir the water in the beaker actuated a 1-cm stirring bar in the conductivity cell. Solution volumes (25 ml) were transferred to the cell. The resistance of the solution increased with decreasing volume of solution for volumes below 20 ml. This was probably caused by a gradual cut-off of current lines as the level of the solution approached the electrodes.

The conductance was measured with a Beckman RC-16 B2 bridge. The accuracy of the resistance scale of the bridge was verified at the two available frequencies (50 Hz and 1 kHz) by means of a calibrated resistance decade box. In the range 200000 to 500 Ω, the bridge showed no deviation higher than 0.3%. This corresponds to the sensitivity claimed by the manufacturer.

In this study, solutions with resistances between 1000 and 100000 Ω gave readings at 50 and 1000 Hz which did not differ by more than 0.5% and were 0.5% only at these limits. Consequently, only solutions falling within this resistance range were used. The frequency dependence increases rapidly outside these limits with a change of 2% for a solution of 200 Ω resistance and 1% for a solution of 150000 Ω.

The resistance of a 1.000×10^{-3} M solution of KCl was measured at 50 Hz and 1 kHz; the value of k, the cell constant, was 0.239 ± 0.001 cm^{-1}.

Density, viscosity and dielectric constant measurements on water-saturated nitrobenzene

The density of purified and water-saturated nitrobenzene determined at 25°C was 1.197 (lit. 1.1986 for anhydrous nitrobenzene) [2]. The viscosity determined at 25°C with calibrated U-tube capillary viscosimeters (Cannon-Fenske) was 1.82 ± 0.01 cp for the density value previously determined (lit: 1.811 cp for anhydrous nitrobenzene) [2]. The dielectric constant at 25°C of the water-saturated nitrobenzene was determined with a Dipolmeter type DM 01 WTW with distilled, deionized water and anhydrous nitrobenzene (distilled and stored over 4A molecular sieves) used as reference points. The dielectric constant was 34.87 compared with 34.82 for anhydrous nitrobenzene [2].

General procedure

Before measurements, the cell was rinsed with acetone and dried with a stream of air. A volume of the test solution was used to rinse the cell. A second volume was transferred from its flask maintained at 25°C to the conductivity cell. The resistance was measured at 50 Hz and 1 kHz after stirring for 5 min. For all cases 2 series of measurements were undertaken on each system, with dilutions starting from the same 0.1 M solutions. A characteristic set of concentrations was: 10^{-2}, 6.0×10^{-3}, 4.0×10^{-3} 2.0×10^{-3}, 10^{-3}, 4.0×10^{-4}, 2.0×10^{-4} and 1.0×10^{-4} M.

Method of calculation

An estimate of the limiting equivalent conductance and the dissociation constant, K_d, of each salt was obtainable from measured solution resistances. The molar conductance, Λ, is calculated from $\Lambda = (k/R - K_s)\, 10^3/c$ where R is the solution resistance and K_s is the specific conductance of the solvent. A phoreogram is prepared by plotting Λ vs. $c^{1/2}$, where c is the solute concentration. The data were treated by the method of Shedlovsky [7] for poorly dissociated solutes. By extrapolation of the linear part of the phoreogram on the low concentration side, an initial value of Λ_0 is obtained. The Shedlovsky parameter $S(z)$ and $\gamma_\pm$ [7] were related to Λ_0, K_d, Λ and c according to

$$1/\Lambda S(z) = (1/\Lambda_0) + (\Lambda c \gamma_\pm^2 S(z)/K_d \Lambda_0^2) \quad (1)$$

A plot of $1/\Lambda S(z)$ vs. $\Lambda c \gamma_\pm^2 S(z)$ yields values for Λ_0 and K_d from the intercept I and slope S. A least-squares method was used to fit the data to a straight line. The new value Λ_0' for the limiting molar conductance was used to iterate the calculation, yielding final values of Λ_0 and K_d. In the least-squares method, equal weight was given to all points and standard deviations were calculated for the slope, σ_s, and intercept, σ_I. Standard deviations for $\Lambda_0 (\sigma_\Lambda)$ and $K_d (\sigma_{K_d})$ were evaluated by

$$\sigma_{\Lambda_0}/\Lambda_0 = \sigma_I/I \quad \text{and} \quad \sigma_{K_d}/K_d = [(4\sigma_I^2/I^2) + (\sigma_s^2/s^2)]^{1/2}$$

RESULTS

The perchlorate and iodide systems

For these systems 2 series of measurements at 8 different concentrations ranging from 10^{-2} to 10^{-4} M were obtained. Phoreograms for a typical set of salts appear in Fig. 1. Extrapolations in the low concentration range of the perchlorate and iodide phoreograms yielded preliminary values of Λ_0. These values were used for first calculations of Shedlovsky plots. Visual inspection of the Shedlovsky plots indicated the critical concentration above which calculated data points deviate from a straight line. In general, points at 10^{-2} M and some at 6×10^{-3} M deviated in a systematic fashion and the data were recalculated with 4×10^{-3} M taken as the limiting

concentration. Data for the trioctylammonium salts, which are representative, are presented in Fig. 2. New values of Λ_0 thus obtained were used to determine final Λ_0 and K_d values reported in Table 1.

The bromide and chloride systems

For these systems, measurements at low concentrations were limited by solution high resistance (the lower limit was at 6×10^{-4} M for chlorides and 3×10^{-4} M for bromides). For this reason extrapolations to infinite dilution could not be used to obtain initial Λ_0 values. The following procedure was adopted. Literature values [5] for the ionic limiting conductance of perchlorate, 20.9, and iodide, 20.4, in nitrobenzene and the experimentally determined limiting conductances of the trialkylammonium perchlorates and iodides were combined to estimate average values for the limiting conductance of the tertiary ammonium cations (Table 2). These values and literature values [5] of the limiting conductance of chloride, 22.2, and bromide, 21.6, yielded estimates of Λ_0 for the different trialkylammonium chlorides and bromides. The estimated Λ_0 values were used to calculate the points of the Shedlovsky plots.

In the bromide plots, points at 10^{-2} M and 6×10^{-3} M were rejected. In all cases but one, recalculated Λ_0 values fell within 10% of the initial ones and were associated with standard deviations of 5—10%. This fact and the sensitivity of the calculated Λ_0 value to experimental errors in the case of solutes with very low dissociation constants [8—10] render the direct use

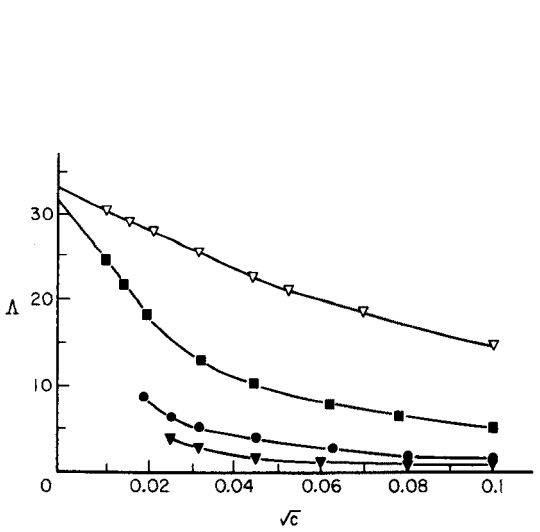

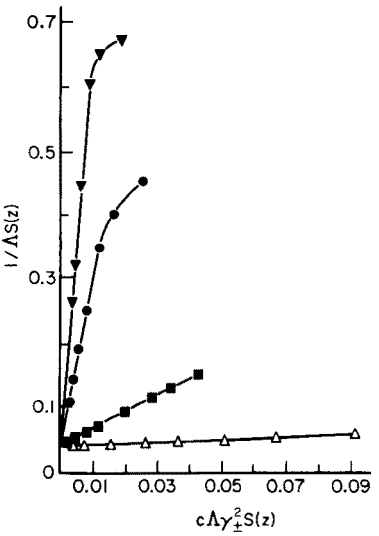

Fig. 1. Phoreograms of trioctylammonium salts. Λ in Ω^{-1} cm^2 mol^{-1}; c in molarity. ▾ chloride, • bromide, ▪ iodide, ▿ perchlorate.

Fig. 2. Shedlovsky plots of trioctylammonium salts. ▾ chloride, • bromide, ▪ iodide, ▿ perchlorate.

TABLE 1

Limiting equivalent conductances and dissociation constants of trialkylammonium salts in nitrobenzene

Amine	R_3NHClO_4		R_3NHI		R_3NHBr	R_3NHCl
	Λ_0	$-\log K_d$	Λ_0	$-\log K_d$	$-\log K_d$	$-\log K_d$
Tripropyl TPrA	36.5 ± 0.1	2.38 ± 0.01	34.8 ± 0.4	3.40 ± 0.01	4.5 ± 0.1	5.0 ± 0.1
Tributyl TBA	35.1 ± 0.2	2.41 ± 0.01	33.4 ± 0.5	3.41 ± 0.01	4.5 ± 0.1	5.0 ± 0.1
Tripentyl TPTA	33.9 ± 0.1	2.45 ± 0.01	31.9 ± 0.4	3.41 ± 0.01	4.5 ± 0.1	5.0 ± 0.1
Trihexyl THA	33.3 ± 0.1	2.46 ± 0.01	31.0 ± 0.3	3.43 ± 0.01	4.5 ± 0.1	5.0 ± 0.1
Trioctyl TOA	32.2 ± 0.2	2.46 ± 0.01	30.6 ± 0.3	3.48 ± 0.01	4.5 ± 0.1	5.0 ± 0.1
Tridodecyl TLA	30.9 ± 0.2	2.47 ± 0.01	29.5 ± 0.2	3.50 ± 0.01	4.5 ± 0.1	5.0 ± 0.1

of the Shedlovsky method uncertain. In this case Λ_0 values were assumed to be as estimated initially from the perchlorate and iodide experiments and K_d values were calculated for each point from eqn. (1) and averaged for each system. These values are recorded in Table 1. The standard deviations of K_d values thus obtained are roughly 3%; however the confidence limit is close to 20% since it is ca. 10% for Λ_0.

In the chloride system, points at 4×10^{-3}, 6×10^{-3} and 10^{-2} M were rejected. Calculated values of Λ_0 from the Shedlovsky plot were not used for the calculation of K_d for the reason advanced for the bromides. The estimated Λ_0 values yield values of K_d for each salt with relative standard deviations and limits of confidence similar to the bromide values (Table 1).

Reproducibility

Reproducibility of conductance data between two independent sets of measurements was ca. 1% and was usually poorer on the low concentration side than on the high concentration side. A limitation to the method arises from terms in the Fuoss—Onsager general equation which have to be abandoned in the Shedlovsky equation. However, a complete analysis by the Fuoss—Onsager equation necessitates a reproducibility of the order of 0.1% [11]. The error introduced by the use of a simpler equation should be reflected in the K_d value [11]. This has been estimated to be ca. 10% in nitrobenzene for a salt with a pK_d of 1.7 [12]. The error should be minimal for the more strongly associated salts in this study ($pK_d > 2$) [11].

DISCUSSION

The limiting equivalent conductance of trialkylammonium salts

Values of the limiting equivalent conductance of trialkylammonium salts in nitrobenzene, as in other solvents, are as sparse as data on their dissociation constants [5, 13, 14]. The value for TBAHI (33.33) can be compared with 33.4 ± 0.5 obtained in this work. An estimate of the single ion conductance of the trialkylammonium cations (Table 2) can be obtained from published values for the anions [5]. As expected, these values appear to decrease when the chain length is increased. Similar values and trends are observed with tetraalkylammonium salts [5, 13].

Ion pairing and internal hydrogen bonding

In dipolar aprotic solvents, salts of tertiary amines experience a degree of internal hydrogen bonding [15]. Spectroscopic studies of solid and dissolved salts [16—18] by n.m.r. and i.r. techniques have shown that the hydrogen atom bound to the central nitrogen atom interacts strongly with a small or basic anion. This has the effect of increasing the association of the ion-pair in dipolar aprotic solvents over the purely electrostatic association. Dissociation constants from conductometry in various solvents are orders of magnitude lower than for the corresponding quaternary ammonium ions [5, 13, 15, 19, 20]. This comparison appears in Table 3.

Dissociation and anion basicity

The dissociation constants of trialkylammonium salts found are strongly dependent on the anion species. Although no significant dissociation of trilaurylammonium chloride was observed. Diamond and co-workers [3, 4] reported that the bromide, iodide and perchlorate salts were increasingly dissociated, but dissociation constants were not reported. The average K_d from each series in this study are ca. 3.6×10^{-3} for R_3NHClO_4, 3.7×10^{-4} for R_3NHI, 3.1×10^{-5} for R_3NHBr and 1.0×10^{-5} for R_3NHCl. For tetrabutylammonium salts in nitrobenzene (Table 3 and [22]) the decrease in K_d going from I^- to Br^- and Cl^- is of a much smaller amplitude. Again this difference may be explained by the influence of hydrogen bonding on the ion-pairing of partially substituted ammonium salts.

TABLE 2

Limiting equivalent conductance of tertiary and quaternary ammonium salts

Alkylammonium ion	λ_0^+	Alkylammonium ion	λ_0^+
Tripropyl	15.0 ± 1	Tridodecyl	9.5 ± 1
Tributyl	13.6 ± 1	Tetraethyl	16.4
Tripentyl	12.3 ± 1	Tetrapropyl	13.5
Trihexyl	11.5 ± 1	Tetrabutyl	11.9
Trioctyl	10.8 ± 1	Tetraphenyl	10.8

TABLE 3

Comparison of K_d values for butylammonium salts

Anion	Tributylammonium	Tetrabutylammonium
Bromide	3.1×10^{-5} [a]	1.79×10^{-2} [5]
Iodide	3.9×10^{-4} [a]	3.7×10^{-2} [21]
	9.5×10^{-5} [5]	
Picrate	1.9×10^{-4} [19]	3.3×10^{-1} [13]
		1.4×10^{-1} [21]

[a]This work.

Hydrogen bonding of the type $NH^+...X^-$ should be stronger, the smaller and more basic the anion [23]. By i.r. spectroscopic measurements of long-chain partially substituted ammonium salts, Kertes et al. [16] related hydrogen bonding strength to ionic radius and proton affinity of the anions, the strength decreasing in the order $Cl^- > Br^- > I^- > ClO_4^-$. Keder and Burger [17] studied CCl_4 solutions of trioctylammonium salts by n.m.r. and observed a similar order. Chenon and Sandorfy [24] reported similar observations on shorter-chain trialkylammonium halides.

Dissociation and alkyl chain length

The data in Table 1 on experimental dissociation constants show that dissociation of tertiary ammonium salts does not increase with increasing chain length. Indeed a slight increase in association is observed going from tripropyl- to tridodecyl-ammonium salts. The trends in the chloride and bromide systems are not considered significant as these data have been associated with a large confidence limit.

The relative 20% decrease in dissociation constant observed on proceeding from tripropyl to tridodecylammonium iodides or perchlorates has to be compared with the situation for quaternary ammonium salts. For quaternary ammonium salts of short to medium chain length in most solvents, an increase in chain length is reflected in an increase in the dissociation constant [1, 25]. This is in agreement with the electrostatic theory of ion-pairing, where the contact distance of the ions increases with increasing chain length.

For the tertiary ammonium cation, an increase in alkyl chain length should not provide additional steric hindrance to the approach of the anion, since the positively charged attracting site is situated close to the apex of a pyramid. Thus the purely electrostatic part of the association of tertiary ammonium salts should not be directly influenced by alkyl chain length.

It has been reported that, at least up to a certain chain length, hydrogen bonding increases with chain length [16, 26] in tertiary ammonium salts. However, this effect tapers off after a chain of three or four is reached and does not explain the observed dissociation trends. Solvation of the cation could also pay a role. The alkylammonium cation in the dissociated salt

should experience a stronger stabilization by ion—dipole interaction with nitrobenzene molecules the smaller its size, thus favoring dissociation. This could partly explain the observed trends.

Triple ions and higher aggregates

Tertiary ammonium salts dissolved in organic solvents can exist as species more complex than ions and ion-pairs [27]. The limited information available on high-molecular-weight halides and perchlorates [3, 4, 28] indicates that aggregation beyond the ion-pair seems not to occur in nitrobenzene up to concentrations of ca. 0.1 M. In conductivity studies, minima in phoreograms and deviations from a straight-line relationship in the Shedlovsky plots have been attributed to triple ion formation [29].

In this study, the absence of a minimum in the phoreograms up to concentrations of 10^{-1} M indicates no significant triple ion formation [29]. However, for the bromide and chloride salts, data points on the high concentration side deviate below the Shedlovsky straight line. Thus the possibility exists of limited triple ion formation for these systems.

Influence of hydration on dissociation

In this study the dissociation constant of TBAHI appears different (4×10^{-4}) from that found by Witschonke and Kraus [5] in anhydrous nitrobenzene (10^{-4}). This may be attributed to the effect of water.

Tertiary alkylammonium salts in organic solvents are usually hydrated [23, 30]. The extent of hydration depends on the anion species and on the solvent. In aromatic solvents, trialkylammonium chlorides exist as monohydrates [27]. Tridodecylammonium chloride is entirely monohydrated in nitrobenzene [31]. In general, the extent of hydration decreases in the sequence $Cl^- > Br^- > I^-, ClO_4^-$, which corresponds to the decreasing order of basicity of the anions [4, 32, 33]. Water, generally believed to be associated with the anion, has also been described as associated with the cation [34]. On this basis, it can be assumed that the tertiary alkylammonium salts reported here are at least partially hydrated in nitrobenzene.

Interaction of the anion of the dissociated ion-pair with water molecules by ion—dipole and hydrogen bonding should be stronger than the interaction of water with the neutral non-dissociated ion-pair. Dissociation should thus be more important in water-saturated nitrobenzene than in anhydrous solutions.

Support by the National Research Council of Canada is gratefully acknowledged.

REFERENCES

1 R. Fernandez-Prini, in A. K. Covington and T. Dickinson (Eds.), Physical Chemistry of Organic Solvent Systems, Plenum, New York, Chap. 5 and App. 5.1 (1973).
2 G. J. Janz and R. P. T. Tomkins, Nonaqueous Electrolytes Handbook, Academic, New York, 1972.
3 J. J. Bucher and R. M. Diamond, J. Phys. Chem., 69 (1965) 1565.
4 W. Müller and R. M. Diamond, J. Phys. Chem., 70 (1966) 3469.
5 C. R. Witschonke and C. A. Kraus, J. Am. Chem. Soc., 69 (1947) 2472.
6 M. Gérin and J. Fresco, Anal. Chim. Acta, 97 (1978) 165.
7 T. Shedlovsky, in A. Weissberger (Ed.), Physical Methods of Organic Chemistry, Vol. I, Part IV, Chap. 45, Interscience, New York, (1960).
8 D. Belcher, J. Am. Chem. Soc., 60 (1938) 2744.
9 T. Shedlovsky and R. L. Kay, J. Phys. Chem., 60 (1956) 151.
10 F. J. C. Rossotti and H. Rossotti, The Determination of Stability Constants, Chap. 15, McGraw-Hill, New York, 1961.
11 R. Fuoss and F. Accascina, Electrolytic Conductance, Chap. 17, Interscience, New York, 1959.
12 H. Sadek, E. Hirsch and R. M. Fuoss, in B. Pesce (Ed.), Electrolytes, Pergamon, London, 1962, p. 132.
13 E. G. Taylor and C. A. Kraus, J. Am. Chem. Soc., 69 (1947) 1731.
14 H. Gutmann and A. S. Kertes, Israel J. Chem., 8 (1970) 947.
15 A. J. Parker, Q. Rev. Chem. Soc., 16 (1962) 163.
16 A. S. Kertes, H. Gutmann, O. Levy and G. Markovits, Israel J. Chem., 6 (1968) 463.
17 W. E. Keder and L. L. Burger, J. Phys. Chem., 69 (1965) 3075.
18 V. S. Shmidt and E. A. Mezhov, Russ. Chem. Rev., 34 (1965) 584.
19 C. A. Kraus, J. Phys. Chem., 60 (1956) 129.
20 E. Price, in J. J. Lagowski (Ed.), The Chemistry of Non-Aqueous Solvents, Academic Press, 1966, p. 67.
21 E. Hirsch and R. M. Fuoss, J. Am. Chem. Soc., 82 (1960) 1018.
22 R. L. Buckson and S. G. Smith, J. Phys. Chem., 68 (1964) 1875.
23 R. M. Diamond, in D. Dyrssen, J. O. Liljenzin and J. Rydberg (Eds.), Solvent Extraction Chemistry, North-Holland, Amsterdam, 1967, p. 349.
24 B. Chenon and C. Sandorfy, Can. J. Chem., 36 (1958) 1181.
25 B. Kratochvil and H. L. Yeager, Nonaqueous Chemistry, Topics in Current Chemistry, No. 27, Springer-Verlag, Berlin, 1972, p. 1.
26 C. D. Strehlov, A. S. Kertes and J. W. Irvine, Lab. Nucl. Sci. Progr. Rep. Mass. Inst. Techn., May 1964.
27 Y. Marcus and A. S. Kertes, Ion Exchange and Solvent Extraction of Metal Complexes, Chap. 10, Wiley, New York, 1969.
28 A. D. Nelson, J. L. Fasching and R. L. McDonald, J. Inorg. Nucl. Chem., 27 (1965) 439.
29 R. Fuoss and F. Accascina, Electrolytic Conductance, Chap 18, Interscience, New York, 1959.
30 W. E. Keder and A. S. Wilson, Nucl. Sci. Eng., 17 (1963) 287.
31 W. Muller and G. Duyckaerts, Euratom Report EUR-2246e (1965).
32 Yu. G. Frolov, V. V. Sergievskii and G. I. Sergievskaya, Russ. J. Inorg. Chem., 13 (1968) 994.
33 J. F. Desreux, Anal. Chim. Acta, 52 (1970) 207.
34 G. Duyckaerts, J. Fuger and W. Muller, Euratom Report EUR-426f (1963).

Analytica Chimica Acta, 97 (1978) 165—176

SOLVENT EXTRACTION OF TRIALKYLAMMONIUM SALTS

MICHEL GÉRIN and JAMES FRESCO*

Department of Chemistry, McGill University, Montreal H3A 2K6 (Canada)

(Received 30th August 1977)

SUMMARY

Partition constants have been determined for a series of trialkylammonium chlorides, bromides, iodides and perchlorates between water and nitrobenzene. Extraction of these salts into nitrobenzene increases in the order $Cl^- < Br^- < I^- < ClO_4^-$. The extraction constant for salts with the same anion increases with increasing chain length of the ammonium ion from tripropyl to trihexyl. An electrostatic model of the Born-charging type was not sufficient to predict transfer equilibrium constants of the dissociated ions.

Amines and ammonium salts have been widely applied to achieve chemical separations in the metallurgical and nuclear industries [1—3]. Applications in inorganic analysis involve solvent extraction of metal ions down to trace levels [4, 5]. Among amine extractants, long chain tertiary aliphatic amines and their salts dissolved in non-aqueous solvents appear to be most widely utilized [1, 4, 6].

The amine may be used to extract aqueous solutions of Lewis acids while the amine salt may extract an aqueous anionic species through trans-phase exchange. Detailed extraction studies of nitrobenzene solutions of tertiary amine salts have not been presented previously. The present study surveys factors which influence the extraction of trialkylammonium salts.

EXPERIMENTAL

Trialkylammonium salts unavailable commercially were prepared by treating a solution of the purified amine in water or an organic solvent with an excess (ca. 10%) of concentrated acid. All salts were recrystallized, dried, and stored in vacuo. Purity was checked by potentiometric titration with standard ethanolic KOH. Analytical results appear in Table 1.

Chemicals

Tripropylamine (98%, Aldrich), tributylamine (Eastman), tripentylamine (Eastman), trihexylamine (Eastman), and trioctylamine (97%, Aldrich) were distilled under reduced pressure (spinning band column). Tridodecylamine (Eastman) was used without purification. The acids used were concentrated

TABLE 1

Analysis of trialkylammonium salts

Ammonium compound	M.p.		Titrimetric purity (%)	Elemental analysis					
	Meas.	Lit.		Halide, %		C, %		H, %	
				Obs.	Calc.	Obs.	Calc.	Obs.	Calc.
Tripropyl									
-chloride	140—141	137 [7]	99.8						
-bromide	185—186	180 [8]	99.7						
-iodide	233—5	166 [9]	99.7						
-perchlorate	265—7		99.5			42.3	44.3	9.2	9.1
Tributyl									
-chloride	72—73	182 [10]	100.0	16.0	16.0				
-bromide	74	74—75 [11]	99.7						
-iodide	101—102	101—102 [11]	99.7						
-perchlorate	85		99.7			50.1	50.4	9.8	9.9
Tripentyl									
-chloride	33		99.7	13.5	13.4	67.5	68.3	13.4	13.0
-bromide	65—67		99.7	25.9	25.9	58.1	58.4	10.8	11.1
-iodide	50—51		100.0	35.8	35.7	50.9	50.7	9.8	9.6
Trihexyl									
-chloride	50		100.0	11.7	11.6	70.7	70.7	13.0	13.2
-bromide	56		99.8	22.7	22.8	63.3	61.7	11.6	11.5
-iodide	40		99.7	31.9	31.9	54.4	54.4	9.8	10.1
Trioctyl									
-chloride	72	72—74 [8]	100.0						
-bromide	72—73	72—73 [12]	99.9						
-iodide	60		99.8	26.3	26.4	58.2	59.9	11.0	10.9
-perchlorate	49		99.9			64.4	63.5	11.6	11.5
Tridodecyl									
-chloride	84—85	84—85 [13]	99.7						
-bromide	86	86—87 [13]	99.8						
-iodide	67—68	52 [12]	99.6			67.0	66.5	11.7	11.8
-perchlorate	59	58—59 [13]	99.7						

aqueous solutions: HCl (37.9%, Baker, reagent grade), HBr (47.9%, Baker, reagent grade), HI (64%, BDH, AnalaR), $HClO_4$ (70%, Anachemia, reagent grade). The solvents used for recrystallizations were acetone (Fisher, reagent grade), ethyl acetate (Fisher, reagent grade), diethyl ether (Mallinckrodt, USP) and petroleum ether (37—51°C, Fisher certified).

Microanalyses were performed by Microanalysis Laboratories Ltd., Toronto, Ontario, and Daessle Microanalyses, Montreal, Quebec.

Preparations

Tripropylammonium chloride (TPrAHCl). Concentrated HCl (20 g) was added to 28 g of tripropylamine dissolved in 100 ml of water. After the

volume was reduced to 50% by heating, the salt precipitated on cooling. The solid was redissolved in 250 ml of hot acetone and recrystallized in an ice bath. After two further recrystallizations from acetone, the product was oven-dried at 110°C.

Tripropylammonium bromide (TPrAHBr). Concentrated HBr (36 g) was added to 30 g of tripropylamine dissolved in 400 ml of acetone. The salt separated upon cooling the solution in a dry ice—acetone bath. The filtered product was redissolved in hot ethyl acetate and crystals precipitated from the cooled solution. The compound was recrystallized twice from ethyl acetate and oven-dried at 110°C.

Tripropylammonium iodide (TPrAHI). The procedure used was as described for TPrAHBr, with 28 g of tripropylamine and 42 g of concentrated HI.

Tripropylammonium perchlorate (TPrAHClO$_4$). Concentrated $HClO_4$ (16 g) was added to 15 g of tripropylamine dissolved in 200 ml of acetone. The acetone was evaporated under vacuum and the crystalline residue was redissolved in a minimum volume of acetone. Ethyl acetate was added gradually until the compound precipitated. Precipitation was completed by cooling the mixture in an ice bath. The salt was filtered and washed with ether. Recrystallization twice by the same procedure followed, dissolving first in the minimum amount of acetone, then adding ethyl acetate.

Tributylammonium chloride (TBAHCl). Concentrated HCl (12 g) was added to 20 g of tributylamine dissolved in 100 ml of water. The volume was reduced in a warm rotavapor still under vacuum. The product was dissolved in a small volume of ethyl acetate and crystallized in an ice—acetone bath, washed with cold ether, and recrystallized twice from ethyl acetate in the same manner.

Tributylammonium bromide (TBAHBr). Concentrated HBr (18 g) was added to 18 g of tributylamine dissolved in 125 ml of ethyl acetate. After the salt precipitated in a dry ice—acetone bath, it was filtered on a pre-cooled Buchner fritted glass filter, washed with cold ether, and recrystallized twice from 100 ml of ethyl acetate, cooled in an acetone—ice bath, and washed with ether.

Tributylammonium iodide (TBAHI). The procedure used was the same as for TBAHBr, with 18 g of tributylamine, 22 g of concentrated HI and an ice bath for recrystallizations.

Tributylammonium perchlorate (TBAHClO$_4$). The procedure was as described for TBAHBr with 18 g of tributylamine, 16 g of concentrated $HClO_4$, 75 ml of ethyl acetate and a dry ice—acetone bath for recrystallizations.

Tripentylammonium chloride (TPTAHCl). Concentrated HCl (7 g) was added to 15 g of tripentylamine dissolved in 150 ml of ethyl acetate. The precipitate formed in an acetone—dry ice bath was filtered, washed with cold solvent and cold ether, recrystallized twice from ethyl acetate in an acetone—ice bath, washed on the filter with cold solvent, and dried under suction.

Tripentylammonium bromide (TPTAHBr). The procedure described for the chloride salt was used with 15 g of tripentylamine and 12 g of concentrated HBr.

Tripentylammonium iodide (TPTAHI). The procedure was as described for the chloride, with 15 g of tripentylamine and 14 g of concentrated HI and dry ice—acetone baths for recrystallizations.

Trihexylammonium chloride (THAHCl). Concentrated HCl (5.6 g) was added to 15 g of trihexylamine dissolved in 100 ml of ethyl acetate. The solid was precipitated in a dry ice—acetone bath and filtered on a precooled fritted-glass Buchner, washed with cold ether and dried under suction. The salt was recrystallized twice under the same conditions.

Trihexylammonium bromide (THAHBr). The procedure was as described for the chloride, with 15 g of trihexylamine and 10 g of concentrated HBr.

Trihexylammonium iodide (THAHI). The procedure was as described for the chloride, with 15 g of trihexylamine and 12 g of concentrated HI.

Trioctylammonium chloride (TOAHCl). Concentrated HCl (5.4 g) was added to 18 g of trioctylamine dissolved in 200 ml of ethyl acetate. The precipitate formed in a dry ice—acetone bath was filtered, washed with cold solvent and cold ether. The salt was recrystallized twice from ethyl acetate in an acetone—ice bath and washed with cold solvent and ether.

Trioctylammonium bromide (TOAHBr). Concentrated HBr (5.3 g) was added to 10 g of trioctylamine dissolved in 200 ml of ether and the solution shaken. Crystals which separated after placing the solution in a dry ice—acetone bath were dried on the filter under vacuum. The salt was recrystallized twice under the same conditions.

Trioctylammonium iodide (TOAHI). Concentrated HI (6.1 g) was added to 10 g of trioctylamine dissolved in 200 ml of diethyl ether. The precipitated product was collected from the solution cooled at dry ice—acetone bath temperature. The precipitate was recrystallized 3 times from ether at the same temperature.

Trioctylammonium perchlorate ($TOAHClO_4$). Concentrated $HClO_4$ (4.5 g) was added to 10 g of trioctylamine dissolved in 250 ml of ether. The salt precipitated at acetone—dry ice temperature and was recrystallized twice under these conditions.

Tridodecylammonium chloride (TLAHCl). Concentrated HCl (4 g) was added to 20 g of tridodecylamine dissolved in 200 ml of diethyl ether. A precipitate formed when the solution was cooled in an ice bath. The salt was recrystallized 4 times from petroleum ether in an ice bath.

Tridodecylammonium bromide (TLAHBr). Concentrated HBr (7 g) was added to 20 g of tridodecylamine dissolved in 100 ml of petroleum ether. The precipitate formed at ice bath temperature was collected and recrystallized 3 times under the same conditions.

Tridodecylammonium iodide (TLAHI). Concentrated HI (8.3 g) was added to 20 g of tridodecylamine dissolved in 200 ml of acetone. The salt separated in an acetone—ice bath and was recrystallized 4 times from petroleum ether in an ice bath.

Tridodecylammonium perchlorate ($TLAHClO_4$). Concentrated $HClO_4$ (6 g) was added to 20 g of tridodecylamine dissolved in 200 ml of acetone. A precipitate separated in a dry ice—acetone bath. The salt was recrystallized 3 times from acetone in an ice—acetone bath then twice from petroleum ether in an ice bath.

Solutions

Aqueous solutions of the salts TPrAHCl, TBAHCl, TPTAHCl, TPrAHBr, TBAHBr, TPrAHI and $TPrAHClO_4$ were prepared by dissolution of the solid salt in nitrobenzene-saturated and deionized water. Solutions of TPTAHCl, THAHCl, TOAHCl, TBAHBr, TPTAHBr, TPrAHI, TBAHI, TPTAHI, THAHI and $TBAHClO_4$ were prepared by dissolving the salt in water-saturated, purified nitrobenzene. Solutions of $THAHClO_4$, $TPrAHClO_4$ and $TPTAHClO_4$ were prepared by contacting nitrobenzene solutions of the parent amine with aqueous solutions of the corresponding acid.

All nitrobenzene solutions were standardized by acid—base titration with standard alcoholic KOH.

Extraction procedure

In a typical determination, volumes of nitrobenzene solution (or water-saturated nitrobenzene) and aqueous solution (or nitrobenzene-saturated water) were transferred to a jacketed beaker. The beaker was maintained at 25°C by circulation of water from a constant temperature bath. The beaker was covered with a plastic lid and the solution was blanketed with N_2. The two phases were equilibrated by slowly rotating a Teflon-enclosed magnetic bar. After 30 min the pH of the aqueous phase was measured with a glass—calomel electrode pair. An aliquot of the organic phase was removed and titrated with alcoholic KOH.

The phases were mixed for 30 min even though equilibration was probably achieved in 5—10 min as suggested by constant pH readings. To verify attainment of equilibrium test solutions were stirred for 2 h; differences were not observed in final concentrations. Only for THAHI, $THAHClO_4$ and TOAHCl solutions was more than 30 min required to reach equilibrium; these phases were contacted for 1 h and compared with duplicates run for 2 h.

In a typical determination, a nitrobenzene solution of the ammonium salt was contacted with water. Three initial organic phase concentrations, 10^{-1} M, 3.3×10^{-2} M and 10^{-2} M were used. The ratio of organic/aqueous phase volumes was made small enough that the change in organic phase concentration was at least 10%.

The transfer of solute did not appear to alter the phase volumes significantly. Since the concentration changes in the organic phase did not exceed 2×10^{-2} M, volume changes of not more than 0.6% would be expected on the basis of a 300-cm^3 molar volume for the salt.

For salts that would undergo excessive transfer into the aqueous phase because of high partition constants, the organic phase was equilibrated with an aqueous solution having a concentration near equilibrium. In those few cases where the partition constant was very high, the salt was initially present only in the aqueous solution. Duplicates were run for all determinations to produce 6 measurements for each salt.

Method of calculation

The organic and/or aqueous R_3NHX concentrations before and after equilibration and the pH of the aqueous phase may be used to calculate an apparent partition constant. If C^0_{or} and C^0_{aq} are the initial salt concentrations in the organic and aqueous phases of volumes V_0 and V_{aq} respectively, the mass balance equation for the anion, X^-, is

$$[\overline{R_3NHX}]_T\, V_0 + [X^-]\, V_{aq} = C^0_{or} V_0 + C^0_{aq} V_{aq} \qquad (1)$$

Acid—base titration of an aliquot of the organic phase gives the total, $[\overline{R_3NH^+}] + [\overline{R_3NHX}]$, or C_{or}. Thus $[X^-]$ can be calculated from eqn. (1). The value $[R_3NH^+]$ can be determined from the charge balance equation for the aqueous phase: $[R_3NH^+] + [H^+] = [X^-] + [OH^-]$. The hydrogen ion concentration was obtained from the pH, after an activity coefficient correction [5]. The apparent partition constant Q_1 is obtained from

$$Q_1 = [R_3NH^+]\,[X^-]/[\overline{R_3NHX}]_T. \qquad (2)$$

The thermodynamic partition constant, K_p, is obtained from Q_1 by correcting the total organic phase concentration for dissociation and estimating the activity of the aqueous salt. The mean activity coefficient $\gamma_\pm$ of the aqueous salt is calculated from a Debye—Hückel equation of the form: $-\log \gamma_\pm^2 = 1.02\,[X^-]^{1/2}/(1 + 3.92a\,[X^-]^{1/2})$.

The dissociation constant of the salt in nitrobenzene, K_d, was previously determined from conductivity measurements [14]. By denoting $[\overline{R_3NH^+}]$ as x, the expression of K_d is

$$\log K_d = \log (x^2/(C_{or} - x)) - 3.44x^{1/2}/(1 + 0.49ax^{1/2}) \qquad (3)$$

Values of the parameter a were estimated by taking the average of values for a for anion and cation as published [15] or as estimated from van der Waals diameters [16]. The values used were Cl^-, Br^- and I^-, 3; ClO_4^-, 3.5; tripropylamine, 7; tributylamine, 7.6; tripentylamine, 8.2; and trihexylamine, 8.6. The calculation of x in eqn. (3) was performed in two steps. A preliminary low value was calculated by disregarding the exponential term; this was then increased by 0.5% steps until right and left sides of eqn. (3) became equal.

RESULTS

The values of Q_1 and K_p, are listed in Table 2. Since corrections for salt dissociation in nitrobenzene and aqueous activity coefficients were made,

TABLE 2

Partition constants and coefficients of trialkylammonium salts between nitrobenzene and water: log K_p and Q_1

		Cl	Br	I	ClO_4
TPrAH	log Q_1	1.90 ± 0.01	0.731 ± 0.002	−0.53 ± 0.08	−1.781 ± 0.16
	log K_p	[b]1.60 ± 0.01	[a]0.586 ± 0.002	−0.672 ± 0.026	−1.595 ± 0.014
TBAH	log Q_1	0.228 ± 0.018	−0.763 ± 0.04	−2.253 ± 0.06	−3.274 ± 0.14
	log K_p	[a]0.055 ± 0.011	−0.924 ± 0.02	−2.269 ± 0.01	−3.088 ± 0.02
TPTAH	log Q_1	−1.547 ± 0.01	−2.619 ± 0.01	−3.96 ± 0.06	−4.99 ± 0.08
	log K_p	−1.666 ± 0.01	−2.676 ± 0.023	−3.928 ± 0.026	−4.793 ± 0.013
THAH	log Q_1	−3.31 ± 0.01	−4.445 ± 0.03	−5.714 ± 0.01	−6.249 ± 0.013
	log K_p	−3.362 ± 0.02	−4.458 ± 0.012	−5.688 ± 0.01	[a]−6.133 ± 0.015
TOAH	log Q_1	−6.12 ± 0.13			
	log K_p	[a]−6.15 ± 0.13			

[a]Based on one concentration level in the aqueous or organic phase, because of very high or low values of the extraction constants.
[b]Based on aqueous 0.5 M solution.

the relative standard deviation is less for K_p than Q_1 for the constants determined over a range of organic phase concentrations. Thus aggregation was probably negligible in the more concentrated solutions.

Differences between Q_1 and K_p arising from dissociation in the organic phase are best observed among the perchlorates.

The influence on K_p of altered solution conditions was tested. An error in K_d of 10% will change the final K_p value by 3% for perchlorate salts, by 1% for iodides, and by 0.2% and 0.1% for bromides and chlorides. Results would differ by 13% for perchlorate salts, by 3% for iodides, and by 0.4% and 0.2% for bromides and chlorides if activity coefficient corrections for the dissociated salt in nitrobenzene were not applied.

The partition constant determinations for TOAHCl, THAHI and $THAHClO_4$ represent limiting cases. A partition constant below 10^{-5} required an impractically large aqueous-to-organic phase volume ratio to observe a significant transfer to the aqueous phase. For this reason extraction data could not be obtained for the other trioctylamine and tridodecylamine salts.

In Table 2, the values for the partition constants of TOAHCl and $THAHClO_4$ were obtained at only one concentration level and have been reported to test trends in the data.

In the case of salts with high partition constants, it was necessary to use aqueous solutions of high salt concentration to obtain a measurable equilibrium concentration in the organic phase. The K_p value obtained for TPrAHCl from aqueous 0.5 M solution is an estimate, since the calculated activity coefficients were approximate.

DISCUSSION

Only a few studies have dealt with the partition constants of alkylammonium salts [17—20]. Smulek and Siekerski [17] reported approximate distribution coefficients for some tertiary amines between several immiscible solvents (including nitrobenzene) and 8 M HCl. From these data, obtained under conditions different from those in this work, the ratio of partition constants for TBAHCl and THAHCl in nitrobenzene is about 1000, compared with 2700 found in this work.

James et al. [18] studied the partition of various tetrahexylammonium salts between water and various aliphatic alcohols. With organic anions, extraction increased as the number of carbon atoms in the anion increased; a systematic study [19] dealt with the partition of various tetraalkylammonium salts of inorganic anions between water and methylene chloride. The same trends were observed as in the present study, i.e. a regular increase in the extraction constant in the order $Cl^- < Br^- < I^- < ClO_4^-$. Similarly the extraction constant for the same anion increases drastically with increasing chain length of the alkyl chain of the ammonium ion from tetrapropyl to tetrahexyl.

To provide a more fundamental basis for the trends observed, the free energy of transfer of the dissociated ions was computed and an electrostatic model of the Born-charging type was tested.

Transfer equilibrium constant of dissociated ions

The equilibrium constant K_t for the transfer of the dissociated ions is defined as

$$K_t = [R_3NH^+]\ [X^-]/\overline{[R_3NH^+]}\ \overline{[X^-]}$$

For the reaction

$$\overline{R_3NH^+} + \overline{X^-} \rightleftarrows R_3NH^+ + X^-$$

K_t is related to K_p and K_d through $K_t = K_p/K_d$. The relationship between the three equilibria can be represented in the following cycle

$$\overline{R_3NH^+} + \overline{X^-} \underset{K_d^{-1}}{\overset{-\Delta G_d^0}{\longleftrightarrow}} \overline{R_3NHX} \underset{K_p}{\overset{\Delta G_p^0}{\longleftrightarrow}} R_3NH^+ + X^- \underset{K_t^{-1}}{\overset{-\Delta G_t^0}{\longleftrightarrow}} \overline{R_3NH^+} + \overline{X^-}$$

where ΔG^0 is the standard free energy for each reaction.

The calculated values for K_t and ΔG_t^0 from the experimental K_p and K_d are summarized in Table 3. The transfer equilibrium constant of the dissociated ion-pair between nitrobenzene and water is highest for the chloride salts in the order $Cl^- > Br^- > I^- > ClO_4^-$ and highest for the lowest-molecular-weight alkylammonium salts in the order tripropyl > tributyl > tripentyl > trihexyl. This order is to be expected on the basis of a simple electrostatic model of the transfer of ions between two phases.

TABLE 3

Equilibrium constants for the transfer of the dissociated ions and related quantities

	$\log K_t$	ΔG_t^0 (kcal)	
		Experimental	Born[a]
TPrAHCl	6.6 ± 0.1	−9.00 ± 0.14	−2.21
TBAHCl	5.06 ± 0.1	−6.90 ± 0.14	−2.15
TPTAHCl	3.33 ± 0.1	−4.54 ± 0.14	−2.11
THAHCl	1.64 ± 0.1	−2.24 ± 0.14	−2.07
TPrAHBr	5.09 ± 0.1	−6.94 ± 0.14	−2.10
TBAHBr	3.58 ± 0.1	−4.88 ± 0.14	−2.04
TPTAHBr	1.82 ± 0.1	−2.48 ± 0.14	−2.00
THAHBr	0.04 ± 0.1	−0.05 ± 0.14	−1.96
TPrAHI	2.73 ± 0.04	−3.72 ± 0.06	−1.96
TBAHI	1.14 ± 0.02	−1.55 ± 0.03	−1.90
TPTAHI	−0.52 ± 0.04	0.71 ± 0.06	−1.86
THAHI	−2.26 ± 0.02	3.07 ± 0.03	−1.82
$TPrAHClO_4$	0.78 ± 0.02	−1.06 ± 0.03	−1.83
$TBAHClO_4$	−0.68 ± 0.03	0.92 ± 0.04	−1.77
$TPTAHClO_4$	−2.34 ± 0.02	3.18 ± 0.03	−1.73

[a]Values of anionic radii used [22]: Cl^-, 1.81; Br^-, 1.96; I^-, 2.19; ClO_4^-, 2.45.

Electrostatic model

The Born charging expression, applied to the transfer of 2 separated ions of radii r_+ and r_- from a medium of dielectric constant ϵ_2 to a medium of dielectric constant ϵ_1, gives an expression for the standard free energy of transfer [20] on a molar scale [21]

$$\Delta G_t^0 = \frac{Ne^2}{2}\left(\frac{1}{r_+} + \frac{1}{r_-}\right)\left(\frac{1}{\epsilon_1} - \frac{1}{\epsilon_2}\right)$$

For the transfer from nitrobenzene to water

$$\Delta G_t^0 = -2.64\left(\frac{1}{r_+} + \frac{1}{r_-}\right) \text{ kcal} \quad \text{or} \quad \log K_t = 1.94\left(\frac{1}{r_+} + \frac{1}{r_-}\right)$$

(with r in Å). Values for ΔG_t^0 (or $\log K_t$) can be calculated from these equations from known values of ionic radii. Van der Waals radii were calculated for the cations [16] and crystal radii used for the anions [22]. The theoretical ΔG_t^0 values thus obtained are listed in the last column of Table 3.

The trends predicted by the above $\log K_t$ relation correspond to the experimentally observed K_t values. The transfer equilibrium constant K_t increases with decreasing size of the anion and decreasing size of the cation. However, these values differ very significantly from the experimental values by magnitude and sometimes by sign. This confirms the well-established fact

that the simple electrostatic model is often insufficient to describe details of the ionic solute transfer process properly.

Anionic and cationic contributions to ΔG_t^0

The experimentally determined free energy of transfer of a pair of ions can be decomposed into its cationic and anionic parts.

$$\Delta G^0_{tR_3NH^+,X^-} = \Delta G^0_{tR_3NH^+} + \Delta G^0_{tX^-}$$

From the values in Table 3, it is possible to calculate differences in free energy of transfer of single ions by subtracting the values of two salts having another ion in common. These values, listed in Table 4, are at least an order of magnitude larger than the predicted values from a Born charging model. For the halides they are, however, comparable with values obtained in transfers between water and other dipolar aprotic solvents of polarity similar to that of nitrobenzene, e.g. in acetonitrile $\Delta G^0_{tCl^-} - \Delta G^0_{tBr^-} = -3.4$ kcal, $\Delta G^0_{tBr^-} - \Delta G^0_{tI^-} = -3.3$ kcal; in nitromethane $\Delta G^0_{tCl^-} - \Delta G^0_{tI^-} = -4.5$ kcal [23].

The simple Born charging model considers each solvent as a continuum and does not take into account specific interactions between the ions and the solvent molecules [24].

The larger the ion introduced in the aqueous phase the more hydrogen bonds linking water molecules will be broken in order to fit the ion into the water structure [25].The anions considered here are solvated in water mostly through hydrogen bonding with water molecules and ion—dipole interactions. However the smaller, more basic, Cl^- is more stabilized by hydration than the larger ClO_4^-. Hydration energy decreases in the order $Cl^- > Br^- > I^- > ClO_4^-$ which is also the order of hydrogen bonding affinity of the anions and the reverse order of their size. Thus the transfer into water of the anions can be explained through the combined effects of water structure breaking and ion solvent interactions [25, 26].

In the dipolar aprotic solvent nitrobenzene, anions are solvated through ion—dipole interactions and interactions due to the mutual polarizability of the ion and the solvent molecule [27]. The solvation energy in anhydrous nitrobenzene should decrease in the order $ClO_4^- > I^- > Br^- > Cl^-$. However, tertiary alkylammonium salts are partially hydrated in nitrobenzene and the anion is usually considered to carry water of hydration [14]. Thus solvation of the anions in the organic phase is a complex process.

TABLE 4

Differences of free energies of transfer of single ions

$\Delta G^0_{t_1} - \Delta G^0_{t_2}$	kcal	$\Delta G^0_{t_1} - \Delta G^0_{t_2}$	kcal
$Cl^- - Br^-$	−2.08 ± 0.07	$TPrAH^+ - TBAH^+$	−2.08 ± 0.08
$Br^- - I^-$	−3.22 ± 0.09	$TBAH^+ - TPTAH^+$	−2.32 ± 0.07
$I^- - ClO_4^-$	−2.53 ± 0.09	$TPTAH^+ - THAH^+$	−2.36 ± 0.07

Plots of ΔG_t^0 vs. the reciprocal of the ionic radius for the anions appeared to be linear. This dependence on the ionic size has been observed in many systems [28—30]. The Born charging approach is not supported, however, since the slopes of the plots differ widely from the theoretical Born slope; furthermore, the linearity is only approximate and depends on the value chosen for the radius of ClO_4^-.

Alfenaar and DeLigny [22] suggested that, for very large ions, ΔG_t^0 could be decomposed into the sum of two terms, one being the Born charging term, and the other being the free energy of transfer of a neutral molecule of the same size as the ion: $\Delta G_t^0 = \Delta G^0_{t\text{neutral}} + \Delta G^0_{t\text{Born}}$. It was reasoned that a very large ion, having a weak electrical field, would interact with solvents in a fashion similar to a neutral species of the same size.

For the anions considered here, the free energy of transfer could not be decomposed in such a way because of their small size and specific solvation effects. For the larger trialkylammonium ions, a similar decomposition is probably also unrealistic because of the existence of a high charge density centre near the N—H bond. However, the importance of a non-electrostatic term could be indicated by the apparent existence of a methylene effect. Values of ΔG_t^0 appear to increase regularly in each series of salts as the alkyl chain length increases by the addition of methylene groups. An increase in chain length must have the effect of disturbing the hydrogen bonded structure of water. Additive methylene effects have been observed in many systems. These are reflected either in values of the enthalpy of transfer of ions or neutral molecules between organic solvents and water [31] or their distribution ratios [24].

An empirical rule governing the partition ratio of free amines and of ammonium salts (K_p) between organic solvents and water has been pointed out [32, 33]: the logarithm of the equilibrium constant is a linear function of the number, n, of methylene groups, the slope being 0.6. In this work a similar result can be found. The log K_p values (Table 2) decrease on average by 0.51 per methylene group between tripropyl and tributylammonium salts by 0.57 between tributyl and tripentylammonium salts and by 0.58 between tripentyl and trihexylammonium salts.

Additive methylene effects may be attributed to hydrophobic effects in the aqueous phase. The free energy of solvation of a $-CH_2$ group in water is positive and made up of two contributions [34, 35]. The coulombic or "normal" hydration involves the breaking down of hydrogen bonds linking water molecules to create a cavity for the group (positive enthalpy change). The structural contribution concerns the rearrangement of water molecules as an "iceberg" around the hydrocarbon group. Similar effects are observed around non-polar gases in solution. The structural contribution contains a negative enthalpy term. Considering entropy, the overall entropy of solvation should be negative because of the rearrangement of the water structure into the more ordered ice-like structure. The relative importance of the different terms forming the free energy of solvation is controversial, but the total effect of all contributions should be a strong positive free energy of hydration

of—CH_2 groups coming mostly from the positive enthalpy of the coulombic part of the hydration [29].

Financial support by the National Research Council of Canada is gratefully acknowledged.

REFERENCES

1 V. S. Shmidt, Amine Extraction, Israel Program for Scientific Translations, Jerusalem, 1971.
2 C. F. Coleman, Nucl. Sci. Eng., 17 (1963) 274.
3 R. Kunin and A. G. Winger, Angew. Chem. Int. Ed. Eng., 1 (1962) 149.
4 H. Green, Talanta, 20 (1973) 139.
5 F. L. Moore, Anal. Chem., 33 (1961) 748.
6 E. Högfeldt, in J. A. Marinsky (Ed.), Ion Exchange, Vol. 1, Dekker, New York, 1966, p. 139.
7 R. E. Varrall and B. E. Conway, J. Phys. Chem., 70 (1966) 3961.
8 L. S. Spialter and J. A. Pappalardo, The Acyclic Aliphatic Tertiary Amines, Macmillan, 1965.
9 W. R. G. Atkins and E. A. Werner, J. Chem. Soc., 101 (1912) 1990.
10 J. A. Geddes and C. A. Kraus, Trans. Faraday Soc., 32 (1936) 585.
11 E. K. Ralph and W. R. Gilkerson, J. Am. Chem. Soc., 86 (1964) 4783.
12 Y. Marcus and A. S. Kertes, Ion Exchange and Solvent Extraction of Metal Complexes Wiley-Interscience, New York, 1969, p. 746.
13 I. Mayer, G. Markovits and A. S. Kertes, J. Inorg. Nucl. Chem., 29 (1967) 1377.
14 M. Gérin and J. Fresco, Anal. Chim. Acta, 97 (1978) 155.
15 J. Kielland, J. Am. Chem. Soc., 59 (1937) 1675.
16 J. T. Edward, in J. C. Giddings and R. A. Keller (Eds.), Advances in Chromatography, Dekker, 1966, Chap. 2.
17 W. Smulek and S. Siekerski, J. Inorg. Nucl. Chem., 24 (1962) 1651.
18 H. J. James, G. P. Carmack and H. Freiser, Anal. Chem., 44 (1972) 853.
19 K. Gustavii and G. Schill, Acta Pharm. Suecica, 3 (1966) 241; 3, (1966) 259.
20 J. T. Denison and J. B. Ramsey, J. Am. Chem. Soc., 77 (1955) 2615.
21 H. L. Friedman and C. V. Krishnan, in F. Franks (Ed.), Water, Volume 3, Chap. 1, Plenum, 1973.
22 M. Alfenaar and C. L. DeLigny, Rec. Trav. Chim. Pays-Bas, 86 (1967) 929.
23 C. M. Criss and M. Salomon, in A. K. Covington and T. Dickinson (Eds.), Physical Chemistry of Organic Solvent Systems, Appendix 2-11-12, Plenum, 1973.
24 R. M. Diamond and D. G. Tuck, Progr. Inorg. Chem., 2 (1960) 109.
25 B. Chu, D. C. Whitney and R. M. Diamond, J. Inorg. Nucl. Chem., 24 (1962) 1405.
26 J. T. Edward, in S. C. Skoryna and D. Waldron-Edward (Eds.), Intestinal Absorption of Metal Ions, Trace Elements and Radionuclides, Pergamon, 1970, p. 3.
27 A. J. Parker, Q. Rev. Chem. Soc., 16 (1962) 163.
28 B. E. Conway, Annual Review of Physical Chemistry, 17 (1966) 481.
29 D. Feakins, in F. Franks (Ed.), Physico-Chemical Processes in Mixed Aqueous Solvents, Elsevier, 1967, p. 71.
30 C. M. Criss and M. Salomon, in A. K. Covington and T. Dickinson (Eds.), Solvent Systems, Plenum, 1973, Chap. II, part 4.
31 C. V. Krishnan and H. L. Friedman, J. Phys. Chem., 73 (1969) 1572; 73 (1969) 3934; J. Soln. Chem., 2 (1973) 37.
32 E. Högfeldt, P. R. Danesi and F. Fredlund, Acta Chem. Scand., 25 (1971) 1338.
33 D. Dyrssen, Sven. Kem. Tidskr., 77 (1965) 387.
34 G. Nemethy and H. Scheraga, J. Chem. Phys., 36 (1962) 3401.
35 J. E. Desnoyers and C. Jolicoeur, in J. O'M. Bockris and B. E. Conway (Eds.), Modern Aspects of Electrochemistry, N5, Plenum, 1969, p. 1.

Analytica Chimica Acta, 97 (1978) 177—179

Short Communication

SELECTIVE SPECTROPHOTOMETRIC DETERMINATION OF THALLIUM THROUGH LIGAND EXCHANGE AT A SOLID SURFACE

M. K. GADIA and M. C. MEHRA*

Environmental Contaminants Research Group, Chemistry Department, Université de Moncton, Moncton, N.B. E1A 3E9 (Canada)

(Received 11th May 1977)

The toxicity of thallium has been rated higher than that of mercury or organomercurials [1]. Routine monitoring of possible thallium contamination is therefore of some importance, e.g. in liquid wastes from mines, or processing or coal-burning plants. Some of the existing procedures for traces of thallium include spectrophotometry of its ion-association compounds [2, 3], fluorimetry [3, 4], electrometry [5, 6] and atomic absorption spectrometry [7]. Many of these are insufficiently sensitive or suffer from interferences, while others require carefully controlled conditions.

The present communication describes a new spectrophotometric procedure for thallium which is based on ligand exchange at a solid surface. The exchange in aqueous samples is effected with solid bis-(2, 4, 6-tris(2-pyridyl)-s-triazine) iron(II) tetraphenylborate reagent. The solid reagent selectively exchanges its colored bis(2,4,6-tris(2-pyridyl)-s-triazine) iron(II) cation for thallium ion, and the response is linear in the range 5—40 ppm thallium.

Experimental

Reagents. The solid reagent was synthesized by mixing equal volumes of iron(II)—triazine reagent (0.01 M) and sodium tetraphenylborate (0.02 M); careful slow mixing produced a bluish white precipitate. The iron(II)—triazine reagent itself was prepared by mixing, in 1:2 proportion, equimolar iron(II) and 2,4,6-tris(2-pyridyl)-s-triazine solutions. The precipitated complex was washed liberally with deionized distilled water after it had aged for 24 h at room temperature. It was finally washed once with ethanol, dried under partial vacuum and stored in a dark-colored bottle.

All other reagents were of analytical grade or better and were employed without further purification. Deionized distilled water was used throughout. Stock solutions of thallium and other cations were prepared by accurate weighing of nitrate or sulfate salts. Working solutions were obtained by suitable dilution. Acetate buffers were employed for pH control where necessary.

Procedure. Dilute appropriately an aliquot of solution containing 0.25—2 mg of thallium and adjust the pH to 6.8 while making up the final volume to 50 ml in a standard flask. Add about 200 mg of the solid reagent and stir magnetically for about 1 h. Allow the precipitate to settle and carefully filter a 20-ml aliquot through a fine filter paper (Whatman-542). Prepare a blank in a similar manner. Fill a 10-cm cylindrical quartz end-window spectrophotometric cell and record the absorbance at 596 nm against the blank.

The Bausch and Lomb Spectronic-70 spectrophotometer used holds either rectangular or cylindrical cells for absorption measurements. The pH was measured with a Radiometer pH meter model-26.

Results and discussion

The solid reagent exchange response toward thallium was linear in the 5—40 ppm range, the corresponding absorbances being 0.03—0.335, with an average relative standard deviation of 1.2% over the range 20—40 ppm (for 5 replicate determinations at 5 concentration levels). Thallium can be determined at concentrations of 5 ppm with a relative standard deviation of 6.6% (n = 5), but quantification remains uncertain at lower levels because of the large absorbance errors. Minor changes in the acidity or alkalinity have no effect on the system; absorbances remain essentially constant in the pH range 4—8, but decrease gradually below pH 3 or above pH 9.

The proposed solid reagent is reasonably selective for thallium. When a 20-ppm thallium solution was analysed in the presence of up to 200 ppm of K^+, Rb^+, Cs^+, NH_4^+, Hg^{2+}, Ag^+, Cu^{2+}, Cd^{2+}, Co^{2+}, Fe^{3+}, VO^{2+}, Cl^-, SO_4^{2-}, CO_3^{2-}, HCO_3^-, NO_3^-, and CH_3COO^-, the absorption data were the same as in the case of a pure thallium solution.

This selective exchange behavior for thallium is significant, since some other tetraphenylborate reagents examined have shown strong reactivity towards Hg^{2+} and Ag^+ ions, in particular [8, 9]. The present results show that a selective analytical reagent can be tailored for a particular model ion by proper selection of the ion-association complex in the solid reagent, and offer further insight into the analytical chemistry of the tetraphenylborate reagents.

The analytical response of the solid reagent must result from the ion-displacement mechanism:

$$[Fe(triazine)_2(TPB)_2]_{(s)} + 2Tl^+ \rightleftharpoons [Fe(triazine)_2]^{2+}_{(soln)} + 2TlTPB_{(s)}$$

The sensitivity of the reagent depends on rapid exchange at the solid surface, on the molar absorptivity of the released iron(II) triazine cation, on the reaction of foreign ions with either of the ions in the solid reagent, and finally on the solubility of the reagent itself.

The solid reagent is remarkably insoluble in water in the pH range 4—8, even on prolonged contact with water. Surprisingly, metals such as Hg^{2+}, Ag^+, Rb^+, K^+ and Cs^+ which are known to form insoluble tetraphenylborates do not

interfere. This may be rationalized on the basis that the solubility products of these alkali metal tetraphenylborates are higher than the solubility product of the solid reagent, so that these metals cannot displace the colored iron(II)—triazine cation from the solid surface. The mercury and silver cations do form rather insoluble tetraphenylborates ($pK_{so} \simeq 32$ and 17, respectively), but these cations compete with iron for coordination with the triazine molecule, and displacement of the colored iron(II)—triazine cation as such is not observed. Hence thallium ion alone is appropriately suited to displace the iron(II) –triazine cation selectively from the solid surface. Thallium tetraphenylborate is insoluble ($pK_{so} \simeq 14.5$), so that Tl^+ combines on the solid surface with tetraphenylborate. The iron(II)—triazine complex is known to provide a sensitive determination of iron(II) in the microgram range, with maximum absorbance at 596 nm [10]. The supernatant liquid after thallium exchange shows no change in the absorption characteristics, which means that the iron(II)—triazine cation is displaced intact in the exchange reaction. These observations suggest that the lower limit of 5 ppm for thallium observed under static conditions results essentially from the rate of exchange at the solid surface. This lower limit might be improved if dynamic column operation were substituted for the static approach. The solid reagent can be converted for column operation by attaching it to an inert support [8].

When samples of drinking water, source water and sea water were spiked with 10, 20 or 30 ppm thallium, the recoveries were quantitative when the recommended method was applied.

This study thus offers a rapid and straightforward method for thallium determinations.

The authors acknowledge gratefully the financial support provided by the National Research Council of Canada and the Université de Moncton.

REFERENCES

1 V. Zitko, Sci. Total Environ., 4 (1975) 185.
2 A. G. Fogg, C. Bourgess and T. D. Burns, Talanta, 18 (1971) 1175; Analyst, 98 (1973) 347.
3 H. Onishi, Bull. Chem. Soc. Jpn., 30 (1957) 567, 827.
4 G. F. Kirkbright, T. S. West and C. Woodward, Talanta, 12 (1965) 517.
5 W. T. Foley and R. F. Pottie, Anal. Chem., 28 (1956) 1011.
6 I. Sinko and S. Gomiscek, Microchim. Acta, (1972) 163.
7 A. J. Curry, J. F. Reed and A. R. Knorr, Analyst, 94 (1969) 744.
8 M. C. Mehra and P. O'Brien, Microchem. J., 19 (1974) 387.
9 M. C. Mehra and C. Bourque, Analusis, 3 (1975) 299.
10 P. F. Collins, H. Diehl and G. F. Smith, Anal. Chem., 32 (1960) 1862.

Analytica Chimica Acta, 97 (1978) 181—184

Short Communication

SOLVENT EXTRACTION SEPARATION OF THALLIUM(III) WITH MESITYL OXIDE

S. KALYANARAMAN and S. M. KHOPKAR*

Department of Chemistry, Indian Institute of Technology, Powai, Bombay 400 076 (India)

(Received 12th July 1977)

Thallium is usually present in lead, cadmium, indium or zinc metals as a trace constituent. Thallium is often separated as an ion-pair complex with basic triphenylmethane dyes [1—4], but antimony, lead, indium and mercury usually interfere in such extractions. Extraction with 20% tributyl phosphate from 4 M hydrochloric acid is quantitative [5], but extraction with benzoylacetone or dibenzoylmethane [6] is not. Dithizone, diethyldithiocarbamate and 8-hydroxyquinoline have also been used for the extraction [7], as have Amberlite LA-1 [8] and tri-n-octylamine [9].

The method proposed here involves the extraction of thallium from hydrochloric acid with mesityl oxide and direct spectrophotometric determination in the organic phase with Brilliant green. Thallium can be separated from aluminium, gallium, indium, zinc and cadmium, as well as other metals.

Experimental

Apparatus and reagents. Perkin-Elmer model 402 and Spektromom-204 spectrophotometers with 10-mm matched quartz cells, a digital pH meter 822 ECIL, India) and a wrist-action flask shaker were used.

Mesityl oxide (B.D.H.) was distilled twice and the fraction collected at 128—130°C was used. For the stock solution of thallium(III), 0.65 g of thallium(III) oxide (Merck) was dissolved in 5 ml of (1 + 1) nitric acid and the solution was diluted to 100 ml. Standardization [10] showed that it contained 5.5 mg Tl ml^{-1}. The working solution, prepared by dilution contained 5.5 μg Tl ml^{-1}. Brilliant green (B.D.H.) was used as a 0.01% (w/v) solution in ethanol.

General procedure. To an aliquot of solution containing 2.7—16 μg of thallium, add hydrochloric acid and lithium chloride to give a final concentration of 1 M each in a total volume of 25 ml. Transfer the solution to a separatory funnel and extract with 10 ml of 40% (v/v) mesityl oxide in toluene for 30 s. Carefully withdraw the aqueous phase and discard. Shake the organic phase with 10 ml of 1 M hydrochloric acid and 0.5 ml of the Brilliant green solution for 30 s. Measure the green complex at 640 nm.

Results and discussion

The absorption spectrum of the thallium(III)—Brilliant green complex in 40% mesityl oxide—toluene against the reagent blank showed a broad maximum at 640 nm with a slight shoulder at ca. 600 nm; the reagent blank did not absorb at 520—720 nm. At 640 nm, the molar absorptivity was 1.03×10^5 l mol^{-1} cm^{-1} and the sensitivity was 0.00198 μg cm^{-2} (Sandell's definition).

Effects of reagent concentrations. The hydrochloric acid concentration was varied from 0.05 to 2.0 M and that of mesityl oxide from 20 to 100% (v/v) with toluene as the diluent, with and without salting-out agent (Fig. 1). Extraction was quantitative from 1—2 M HCl in the presence of 1 M LiCl. The composition of the extractable species was examined by means of a logarithmic plot of distribution ratio against mesityl oxide concentration at 0.05 M HCl. The slope of 3.07 indicates that the extracted species is probably $TlCl_3 \cdot 3MeO$ (MeO = mesityl oxide).

With all other factors constant, the chlorides of lithium, sodium, potassium and ammonium were tested as salting-out agents. Extraction was quantitative from 1—3 M HCl containing 1—2 M LiCl, from 2—3 M HCl with 1—2 M NaCl, from 3 M HCl with 1—2 M KCl, and from 3 M HCl with 2 M NH_4Cl as salting-out agent.

The volume of Brilliant green was varied from 0.03 to 2.0 ml of 0.01% solution; this solution was adequate for full colour development.

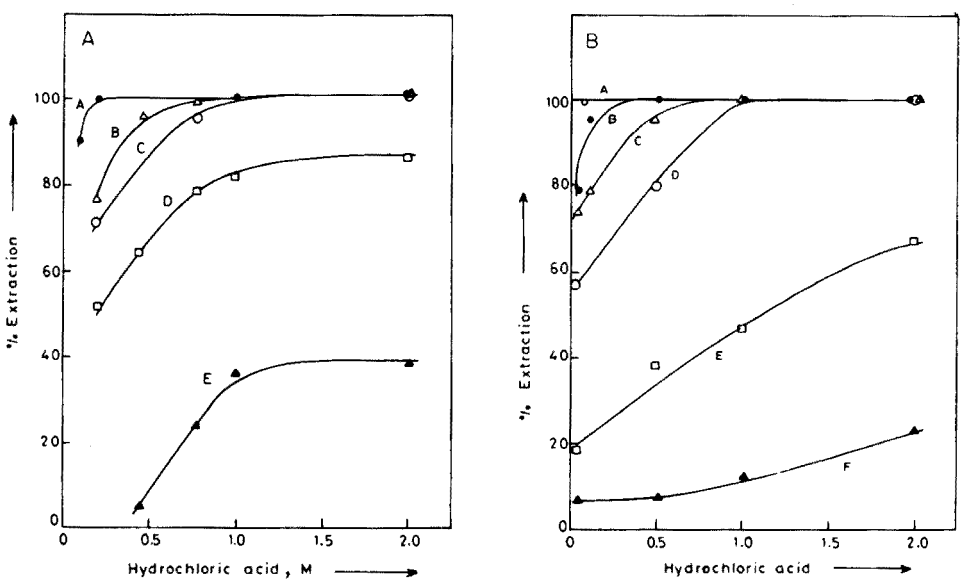

Fig. 1. Effect of HCl and mesityl oxide concentrations. (A) In the absence of lithium chloride; curve A = 100%, B = 80%, C = 60%, D = 40% and E = 30% mesityl oxide. (B) In the presence of 1 M LiCl; curve A = 100%, B = 60%, C = 50%, D = 40%, E = 30% and F = 20% mesityl oxide in toluene.

The period of equilibration was varied from 10 s to 5 min. The optimum time was 30 s for each extraction. After extraction and colour development, the absorbance was stable for 36 h.

Verification of Beer's law. Different amounts of thallium were extracted as in the recommended Procedure and the absorbance was measured at 630, 640 and 650 nm. The system conformed to Beer's law in the range 0.05 to 1.6 $\mu g\ ml^{-1}$. From a Ringbom [11] plot the effective concentration range was 0.27 to 1.6 $\mu g\ ml^{-1}$. The relative standard deviation was 0.56% ($N = 10$).

Effect of diverse ions. The tolerance limit was taken as the amount of foreign ion to cause a ±2% error in the recovery of 5.5 μg of thallium. Table 1 shows that many metals and common complexing agents can be tolerated at quite high ratios. Antimony and tin(IV) do not interfere at 200:1 ratios, but tungstate, thiocyanate, ascorbate, and thiosulphate interfere.

Sequential separation of thallium from aluminium, gallium and indium. Thallium was first extracted from the mixture with 40% mesityl oxide and determined in the organic phase with Brilliant green. Then gallium was extracted twice with 30% mesityl oxide in benzene from the aqueous phase adjusted to 5 M HCl. Indium was extracted from this 5 M hydrochloric acid with 100% mesityl oxide (3 × 20 ml). Aluminium remained unextracted in

TABLE 1

Effect of diverse ions on the determination of 5.5 μg Tl(III)

Tolerance limit (mg)	Foreign Ion	Tolerance limit (mg)	Foreign Ion
1000	Zn^{2+}, Cd^{2+}	5	Tl^{+}, Ru^{3+}, Os^{4+}, Hg^{2+}, Zr^{4+}, Hf^{4+},
100	Be^{2+}, Ca^{2+}, Mg^{2+}, Ba^{2+}, Sr^{2+}, Fe^{2+},		Ti^{4+}, VO_2^{2+}
	$Tart^{3-}$, $C_2O_4^{2-}$, $EDTA^{4-}$, CH_3COO^{-},	2.5	Ge^{4+}, TeO_3^{2-}
	Cit^{3-}, HPO_4^{2-}, F^{-}, malonate^{2-}	2	$Mo_7O_{24}^{6-}$
25	Br^{-}, I^{-}	1	Sb^{3+}, Sn^{4+}
20	Cu^{2+}	None	WO_4^{2-}, $S_2O_3^{2-}$, SCN^{-}, ascorbate
15	Co^{2+}, Ni^{2+}, Mn^{2+}, Bi^{3+}, UO_2^{2+}		
10	Ce^{3+}, Pd^{2+}, Pt^{4+}, Rh^{3+}, Ir^{3+}, Sc^{3+}, Y^{3+},		
	Cr^{3+}, As^{3+}, Rb^{+}, Cs^{+}, SeO_3^{2-}		

TABLE 2

Sequential separation of thallium from aluminium, gallium and indium

Aluminium		Gallium		Indium		Thallium	
Taken (mg)	Found (mg)	Taken (mg)	Found (mg)	Taken (mg)	Found (mg)	Taken (mg)	Found (mg)
9.74	9.71	4.32	4.32	6.31	6.31	5.5	5.5
24.4	24.1	21.63	21.6	25.3	25.0	5.5	5.4
48.7	48.2	43.3	43.6	50.5	50.2	11	10

the aqueous phase. Gallium and indium were determined complexiметrically [10] after stripping with water. Aluminium was also determined complexiметrically [10]. The recovery results are presented in Table 2.

REFERENCES

1 R. E. Van Aman and J. H. Kanzelmeyer, Anal. Chem., 33 (1968) 1128.
2 P. A. Chainani, P. Murugaiyan and Ch. Venkateswaralu, Anal. Chim. Acta, 57 (1971) 67.
3 Z. Marczenko, H. Kalowska and M. Mojski, Talanta, 21 (1974) 93.
4 B. Kominami and H. Ono, Jpn. Anal., 18 (1967) 578.
5 A. K. De and A. K. Sen, Talanta, 14 (1967) 629.
6 J. Stary and E. Hladky, Anal. Chim. Acta, 28 (1963) 27.
7 A. K. De, S. M. Khopkar and R. A. Chalmers, Solvent Extraction of Metals, Van Nostrand Reinhold, London (1970).
8 T. Suzuki and T. Sotobayashi, Jpn. Anal., 14 (1965) 414.
9 I. Tsukahara, M. Sakakibara and T. Yamamoto, Anal. Chim. Acta, 83 (1976) 251.
10 F. J. Welcher, Analytical Application of Ethylenediaminetetraacetic acid, Van Nostrand, London, 1958.
11 A. Ringbom, Z. Anal. Chem., 115 (1939) 332.

Analytica Chimica Acta, 97 (1978) 185—189

Short Communication

DETERMINATION OF RARE-EARTH ELEMENTS IN ROCKS BY NEUTRON ACTIVATION FOLLOWED BY HIGH-RESOLUTION X-RAY SPECTROMETRY OR γ-SPECTROMETRY

P. VOLDET*

Department of Mineralogy, University of Geneva, 13 rue des Maraîchers, 1211 Geneva 4 (Switzerland)

W. HAERDI

Department of Mineral, Analytical and Applied Chemistry, University of Geneva, 30 quai E. Ansermet, 1211 Geneva 4 (Switzerland)

(Received 31st August 1977)

The determination of rare-earth elements, present in parts per million in all igneous rocks, has become increasingly important in geochemistry in recent years.

The present communication extends previous work, which described the determination of europium and dysprosium in rocks [1], to the determination of other rare-earth elements.

The analysis involves separation of the rare-earth elements as described previously [1], neutron activation and measurement of the activity of the different isotopes by high-resolution x-ray spectrometry or by γ-spectrometry. The method was applied to different kinds of rocks, but particularly to basic rocks.

Experimental

Standards. Solutions (100 μg ml^{-1}) of the rare-earth elements were prepared by dissolving the appropriate weights of the oxides (Fluka p.a.) in dilute nitric acid. Mixtures of the appropriate quantities of each rare-earth element were prepared by the method described [1]; the approximate quantities were chosen so as to obtain the same matrix for the standard and the type of rock examined.

Procedure. The method of separation of the rare-earth group and the preparation of the samples for neutron activation have been described [1].

Irradiation and counting. For Eu and Dy, the conditions were as described earlier [1]. For La, Ce, Nd, Sm, Eu, Gd, Ho, Yb and Lu, samples and standards were irradiated for 10 h in the Diorit reactor (Würenlingen) at a thermal neutron flux of about 2.5×10^{12} n cm^{-2} s^{-1}. The activities were determined either by high-resolution x-ray spectrometry, or by γ-spectrometry. The x-rays and γ-rays used are described in Table 1. These activities

TABLE 1

Isotopes and selected rays used in the analysis

Product isotope	Half-life	Detector Ge photopeak (keV)	Detector Ge(Li) photopeak (keV)
^{140}La	40.2 h		329 — 487 — 751 — 816 — 867 — 1597
^{143}Ce	33 h	35.55 (Pr Kα_2) + 36.03 (Pr Kα_1)	293
^{147}Nd	11.1 d	91.25	
^{153}Sm	46.5 h	40.88 (Eu Kα_2) + 41.53 (Eu Kα_1) 47.02 (Eu Kβ_1)	
^{152m}Eu	9.3 h	39.52 (Sm Kα_2) + 40.13 (Sm Kα_1) 45.40 (Sm Kβ_1) 122	122
^{153}Gd	236 d	97.55	97.55
^{159}Gd	18 h	44.47 (Tb Kα_1)	
^{161}Tb (=Gd)	7.2 d		49
^{165}Dy	2.36 h	47.53 (Ho Kα_1) 53.87 (Ho Kβ_1) 95	
^{166}Ho	27.2 h	49.09 (Er Kα_1) 81	81
^{169}Yb	30.6 d	49.76 (Tm Kα_2) 50.72 (Tm Kα_1) 110	110
^{175}Yb	4.2 d	52.96 (Lu Kα_2) 54.07 (Lu Kα_1)	283 — 396
^{177}Lu	6.75 d	54.62 (Hf Kα_2) 113	113 — 208

were measured after a cooling time of ca. 36, 60 and 110 h. Each sample was counted for 500 s with the Ge detector and 60 s with the Ge(Li) detector. For high-resolution x-ray spectrometry, the equipment used has been described [1]. For γ-spectrometry the following equipment was used: Ge(Li) detector (Seforad, 50 cm^3, efficiency 8.6%), pre-amplifier (Seforad SR-100), amplifier (Ortec 472), and a 4096-channel Zoomax SEIN analyzer (2048 channels were used in this work). The resolution of the system for the 122-keV ^{57}Co and 1.332-MeV ^{60}Co peak was 850 and 1810 eV, respectively.

Results and discussion

This method allows the determination of 8—10 rare-earth elements in different kinds of rocks, with a precision of the order of 5—20%, limited principally by the accuracy of the measurements. The activities were calculated by a computer programme established by J. P. Blanc. No interference

TABLE 2

Description of samples analysed

Rock number	Type	Location	Rock number	Type	Location
T40, 42, 50, 52, 53	Diabase	Kizil Dağ, Turkey	T68, 69, 71, 63	Gabbro	Kizil Dağ, Turkey
T43, 44, 48, 49	Pillow lava	Kizil Dağ, Turkey	T74	Gabbro	Montgenèvre, France
			W-1	Diabase[a]	
T54	Granodiorite	Maki Deresi, Turkey	BCR-1	Basalt[a]	
T55	Granophyre	Ikizdere, Turkey	G-2	Granite[a]	
T56	Granodiorite	Ikizdere, Turkey	GSP-1	Granodiorite[a]	
T57	Porphyritic granodiorite	Ikizdere, Turkey	NIM-S	Syenite[b]	
			NIM-N	Norite[b]	
T58	Tonalite	Güneyce, Turkey	NIM-P	Pyroxenite[b]	
T59	Quartz diorite	Güneyce, Turkey	NIM-D	Dunite[b]	
T60	Tonalite	Ikizdere, Turkey	MGR-1	Gabbro[c]	Mount Royal, Montreal, Canada
T61	Granodiorite	Cimilbasköy, Turkey			

[a]U.S.G.S. International geological standards [2].
[b]NIMROC geochemical reference materials, South African Bureau of Standards [1, 2].
[c]Canadian rock sample for use as certified reference material, Geological Survey of Canada, Ottawa.

TABLE 3

Rare-earth element determinations (in ppm)

Rock number		La	Ce	Nd	Sm	Eu	Gd	Dy	Ho	Yb	Lu
T40		<10			2.1	1.0	3.9	6.4	0.6		
T42		<10		6.3	2.9	1.3	3.8	6.3	1.2		
T50		<10	<20	4.9	2.2	1.0	4.7	6.3	1.0	2.5	0.7
T52		<10	<20	4.3	2.2	1.0	3.5	6.5	0.8	2.3	0.6
T53		<10	<20	6.6	2.2	1.0	3.9	5.4	1.0	2.7	0.7
T43		<10	<20		1.7	0.7	3.6	4.7	0.9		
T44		<10	<20	6.8	1.3	0.7	4.1	3.9	0.9	2.7	0.7
T48		<10	<20	7.9	1.3	0.8	4.1	3.4	0.8	2.6	0.6
T49		<10	<20	5.5	1.3	0.7	4.1	4.5	0.9	2.5	0.7
T54		30.8	37.6	16.8	2.2	1.8	5.7	9.4	1.8	7.7	3.3
T55		16.0	40.6	16.5	5.0	1.9		11.6	3.4		2.0
T56		17.1	33.0	15.5	3.6	1.2		11.7	3.3	11.1	2.1
T57		36.4	34.7	4.8	1.9	1.2		5.7	3.1		2.0
T58		15.4	18.0	18.7	5.3	1.6		9.1	5.3	22.7	1.5
T59		8.7	15.7	7.7	3.6	1.4		5.9	4.4	8.6	1.7
T60		14.3	22.5		5.3	1.5		10.0	6.1	18.9	1.2
T61		37.8	44.4	15.1	3.6	0.7		3.1	1.6	9.7	0.9
T63		0.8	10.6		0.9	0.5		1.8	0.8	3.0	0.4
T68		0.7	16.5		0.5	0.5		2.6	0.3	1.2	0.2
T69		1.2	11.3		0.9	0.7		3.3	0.6	1.4	0.2
T71		0.7	13.5		0.7	0.5		2.7	0.7	2.2	0.3
T72		2.1	11.2		1.7	1.0		5.5	1.2	3.3	0.5
T74		0.6	7.7		1.0	0.8		4.1	1.6	2.1	
W-1	This work	14.0		10.0	3.9		4.2		1.6		0.8
	Flanagan [3]	9.8		15	3.6		4		0.69		0.35
BCR-1	This work	23.4	50.9		6.2	1.90	7.2	6.34	1.6		2.4
	Flanagan [3]	26	53.9		6.6	1.94	6.6	6.3	1.2		0.55
G-2	This work	84.9	165.9			1.24		2.48	0.4		0.25
	Flanagan [3]	96	150			1.5		2.6	0.4		0.11
GSP-1	This work	164.9	400.0			2.68		5.82			
	Flanagan [3]	191	394			2.4		5.4			
NIM-S	This work	50	14.4		6.6	0.36		0.63		2.0	0.3
	Certified value [4]	70	12			0.4		0.6		<3	0.05
NIM-D	This work	0.2	2.5		0.018	<0.1		<0.1			
	Certified value [4]	<3	10		0.018	0.06					
NIM-P	This work	2.3	8.5		0.8	0.25		1.21	0.6	1.8	0.4
	Certified value [4]	4				0.2				<3	
NIM-N	This work	3.1	15.8		0.9	0.69		1.93	0.3	2.4	0.2
	Certified value [4]	3	14			0.6				<3	0.2
MGR-1	This work	10.0	21.8	2.6	3.0	2.4		4.6	0.6	2.8	0.4
	Abbey et al. [5]	10	25	18	4.1	1.4		4.6	0.5	1?	0.06—<3

by other elements was observed; this confirms the validity of the method of separation. Of the methods proposed in the literature, this method is relatively fast.

For petrology and magmatology, this method has the advantage of being applicable to basic rocks with very low rare-earth concentrations. Table 2 gives a description of the rocks examined. Table 3 gives the results obtained for the rare-earth elements. The method was also applied to various geological standards; the data obtained (Table 3) are generally in good agreement compared with previous results.

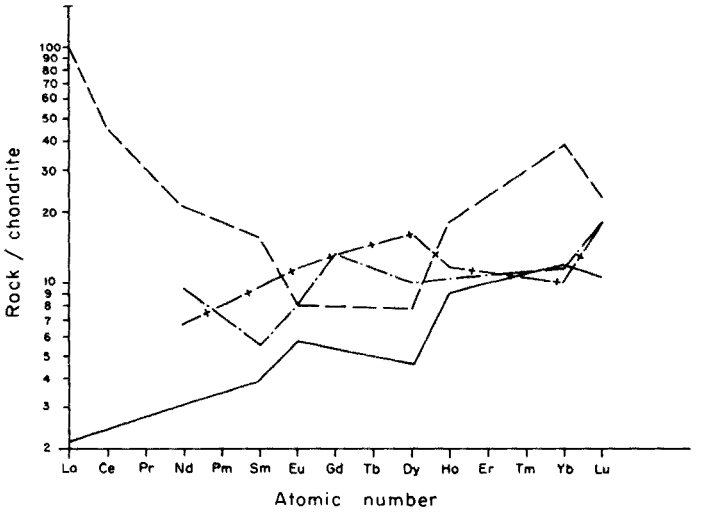

Fig. 1. Rare-earth abundances in the rocks analysed, normalized to chondrite Leedey [6]. —+—+— diabase; —·—·— pillow lava; ——— granodiorite; —— gabbro.

TABLE 4

Ratio of content of rare earth elements in rock to that in chondrite Leedey

REE	Rock type (Number)			
	Diabase (T50)	Pillow lava (T44)	Gabbro (T63)	Granodiorite (T61)
La			2.116	100.000
Ce				45.491
Nd	6.843	9.487		21.089
Sm	9.565	5.652	3.913	15.652
Eu	11.547	8.083	5.773	8.083
Gd	13.181	13.183		
Dy	16.153	10.000	4.615	7.948
Ho	11.520	10.368	9.216	18.433
Yb	10.040	10.843	12.048	38.955
Lu	18.087	18.087	10.335	23.255

As an example of the use of data for rare-earth elements in petrology to establish the lanthanide distribution in rocks, the data for four different rocks are plotted against atomic number in Fig. 1. Conventionally, each rare-earth value is given as a ratio to its equivalent value of chondrite (Table 4). The curve pattern, and the depletion or enrichment in some of the rare-earth elements, are useful tools in studies of the origin and history of the magmas.

We thank Professor R. Beeler (reactor AGN-201-P of the Faculty of Sciences, University of Geneva) and Mr. H. Aebersold (reactor Diorit of the EIR, Würenlingen) for neutron activations. We are also grateful to Mr. J. P. Blanc (Department of Analytical Chemistry, University of Geneva) for a computer programme for the calculation of activities.

REFERENCES

1 P. Voldet and W. Haerdi, Anal. Chim. Acta, 87 (1976) 227.
2 P. Voldet and W. Haerdi, Anal. Chim. Acta, 72 (1974) 111.
3 F. J. Flanagan, Geological Survey Professional Paper, 840 (1976) 171.
4 Certificate of Analysis, SARM 1—6 (1974).
5 S. Abbey, A. H. Gillieson and G. Perrault, Report MPR/MSL 75-132 (TR) and Canmet Report 76-36.
6 A. Masuda and N. Nakamura, Geochim. Cosmochim. Acta, 37 (1973) 239.

Analytica Chimica Acta, 97 (1978) 191—193

Short Communication

SEPARATION OF PYRETHRINS BY HIGH-PRESSURE LIQUID CHROMATOGRAPHY

D. MOUROT*, J. BOISSEAU and G. GAYOT

Laboratoire National des Médicaments Vétérinaires de Fougères, Direction de la Qualité, Ministère de l'Agriculture, Javené — 35300 Fougères (France)

(Received 19th September 1977)

The insecticidal properties of "pyrethrins", the active components of pyrethrum extracted from *Chrysanthemum cinerariaefolium* have been studied for many years [1]. Many analytical methods [2] including a variety of chromatographic procedures, mainly gas-liquid chromatography [3], have been reported for the separation of these compounds. However, the separations of the six active constituents of "pyrethrins": jasmolin (I) and (II), cinerin (I) and (II) and pyrethrin (I) and (II) are difficult and the results obtained are seldom satisfying. Moreover, the thermal instability — components pyrethrin (I) and (II) are particularly labile — and the poor stability of these six esters in the presence of air and light make any quantitative estimation very hazardous.

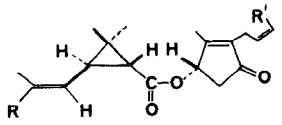

	R	R'
Jasmolin I	CH_3	C_2H_5
Cinerin I	CH_3	CH_3
Pyrethrin I	CH_3	$CH{=}CH_2$
Jasmolin II	$COOCH_3$	C_2H_5
Cinerin II	$COOCH_3$	CH_3
Pyrethrin II	$COOCH_3$	$CH{=}CH_2$

Thus, it was necessary for this laboratory, concerned with control analysis, to develop a rapid and efficient method for their separation. This report describes a method for the complete separation of "pyrethrins" by h.p.l.c. on a silica column at ambient temperature after a simple dilution of the sample.

EXPERIMENTAL

Chromatographic system. A Varian LC 8500 high-pressure liquid chromatograph with a u.v. detector operating at 254 nm and a Lichrosorb Si60 column (15 cm × 4.7 mm i.d.), particle size 5 μm, was used. The flow-rate was maintained at 100 ml h^{-1}. The column pressure was 1500 psi.

Chemicals. The reference sample of pyrethrins was Pestanal (Riedel de Haen, Seelze, Hannover). Pyrethrins (I) and (II) were present in equal proportions by weight at a concentration of 2 g l^{-1} in cyclohexane. All the solvents were analytical-reagent grade.

Analytical method. The mixture of "pyrethrins" was separated by isocratic elution with the solvent, composition hexane—ethyl acetate (90:10). The individual peaks were identified provisionally by analogy with results obtained by t.l.c. of this mixture on silica gel with the same solvents [4]. Final confirmation of identity must await the availability of pure components whose retention times can be obtained individually and/or by mass spectrometric identification of the eluted peaks.

RESULTS AND DISCUSSION

Figure 1 shows a typical chromatogram of the pyrethrin mixture. The order of elution is jasmolin (I), cinerin (I), pyrethrin (I), jasmolin (II), cinerin (II), pyrethrin (II). Total separation of the six compounds takes less than 10 min.

This simple, rapid separation allows the presence of pyrethrins in commercially available insecticidal preparations to be ascertained. The analysis is unaffected by the presence of the synergist (piperonyl butoxide) used most frequently. In order to determine the amount of "pyrethrins" in such formulations, quantitative analyses with internal standards and peak area measurements are now being carried out.

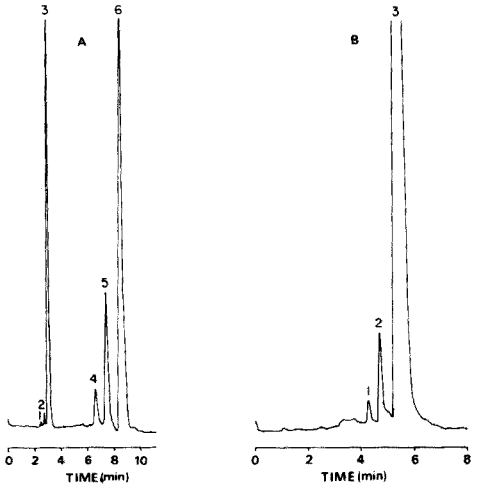

Fig. 1. Chromatogram showing the separation of pyrethrins on a Lichrosorb Si60 (Merck) microparticulate column with isocratic elution. 1 = jasmolin I; 2 = cinerin I; 3 = pyrethrin I; 4 = jasmolin II; 5 = cinerin II; 6 = pyrethrin II. A: solvent composition, hexane—ethyl acetate (90:10); flow rate, 100 ml h^{-1}; detector sensitivity, 0.64 AUFS. B: solvent composition, hexane—ethyl acetate (92:8); flow rate, 100 ml h^{-1}; detector sensitivity, 0.16 AUFS.

The authors are grateful for the technical assistance of Bernard Delépine.

REFERENCES

1 J. E. Casida, (Ed.), Pyrethrum, the natural insecticide, Academic Press, New York, 1973.
2 S. W. Head, in J. E. Casida (Ed.), Pyrethrum, the natural insecticide, (Chapter 3), Academic Press, New York, 1973.
3 S. W. Head, Pyrethrum Post, 7 (4) (1964) 12; 8 (4) (1966) 3; 9 (1) (1967) 12.
4 E. Stahl, (Ed.), Thin Layer Chromatography, Springer-Verlag, Berlin, 1969, p. 645.

Analytica Chimica Acta, 97 (1978) 195—198

Short Communication

THE DETECTION LIMIT OF ANODIC STRIPPING COULOMETRY AT MERCURY-FILM GLASSY CARBON ELECTRODES

RUEDI EGGLI

Institute of Inorganic Chemistry, University of Zürich, CH-8001 Zürich (Switzerland)

(Received 14th September 1977)

In direct anodic stripping coulometry [1], the metal concentration C in a sample solution of volume V is calculated from the charge Q required to strip the metal from the working electrode after an exhaustive pre-electrolysis step: $C = (Q/V) \cdot (1/n\,F)$, where n is the number of electrons used in the stripping reaction and F is the Faraday constant. Thus, the limit of detection with respect to metal concentration, C_{det}, depends on the charge detection limit and the sample volume and is conveniently expressed by

$$C_{det} = q_{det} \cdot (A/V) \cdot (1/n\,F) \qquad (1)$$

where q_{det} is the lowest detectable charge per electrode area A. The ratio A/V is related to the pre-electrolysis time and q_{det} is determined by the nature of the electrode and the electrolyte used. As the charge Q of a stripping peak is measured from the difference between sample and blank anodic stripping signals, the magnitude of q_{det} depends only on the reproducibility of the blank stripping signal and can be defined [2] as $q_{det} = 3 \cdot s_{bl}$, where s_{bl} is the standard deviation of the blank charge accumulated in a potential interval corresponding to the base width of a metal stripping peak.

In this communication, values for s_{bl} are given for anodic potential sweeps performed at rotating thin-film mercury electrodes in acetate buffer, and the detection limit of direct anodic stripping coulometry is evaluated.

Experimental

Apparatus. A glass cell (Metrohm E 880-20) was used, fitted with a rotating electrode [1], a platinum wire counter electrode and a saturated calomel electrode, which was separated from the working electrode compartment by a double junction (fine glass frits) filled with supporting electrolyte. Merck Suprapur reagents and doubly-distilled water were used to prepare the 0.05 M acetic acid—0.05 M sodium acetate supporting electrolyte. Deaeration was performed with prepurified nitrogen. A potentiostat (Amel 551), driven by a linear sweep generator (Amel 566) was used and charges were measured with a PAR 379 digital coulometer, fitted with a PAR 4101 transient recorder.

Electrodes. The preparation of the glassy carbon disk electrodes (Tokay GC-A, Tokay Carbon Co., diameter 6 mm; and Sigradur-K, Sigri Elektrographit GmbH, diameter 8 mm) has been described [1]. Mercury films were preformed by deposition at −1 V vs. SCE from 2×10^{-4} M $Hg(NO_3)_2$ in acetate buffer. The deposition was monitored coulometrically and terminated at a charge of 0.12 C cm^{-2} of electrode area.

Procedure. Each preplated electrode was first conditioned by five polarization cycles, each consisting of a 10-min period at −1 V, followed by a potential sweep to 0 V at a rate of 20 mV s^{-1}. Then, potential scans from −1 to 0 V were run to determine blank charges for a given scan rate, each scan being preceded by a 3-min period at −1 V. All measurements were carried out at ambient temperature (25°C) under continuous electrode rotation (45 rps) in 20 ml of well deaerated supporting electrolyte.

Results and discussion

Electrodes. The polished surfaces of the two brands of glassy carbon were morphologically different. Sigradur-K had large irregularly formed pores (diameter 10—50 μm); the pores on Tokay GC-A were circular and smaller (diameter 5—15 μm) but the pore density was about twice as high as that on the Sigradur-K surfaces. However, the appearance of the mercury deposit was the same on both electrode materials and similar to that described by Štuliková [3] for much the same plating conditions.

Reproducibility of blank charge. Blank charges were determined by direct current integration over two potential intervals of 200 mV, one centred at −300 mV and the other at −800 mV, for scan rates between 5 and 50 mV s^{-1}. The choice of the integration interval was based on the results of preliminary stripping experiments with very small amounts of cadmium and lead, which showed that the peak base widths scatter considerably, their average values ranging between 110 and 180 mV for scan rates rising from 5 to 50 mV s^{-1}.

Of each type of glassy carbon, four different electrodes were prepared, and the standard deviation of each electrode was obtained from five consecutively measured blank charges. Table 1 shows the average values $\bar{s}_{bl}$, with their standard deviations. The results show that the blank noise is independent of potential and that differences between the two sorts of glassy carbon are not significant, except that the reproducibility of s_{bl} is lower for Sigradur-K electrodes. There is, however, a dependence of noise on scan rate, indicated by the sharp increase of $\bar{s}_{bl}$ between 10 and 5 mV s^{-1}; this increase of noise with rising integration time is probably due to faradaic currents, resulting from slow reactions of functional groups located at the glassy carbon surface [4].

From the variations observed, two overall noise figures can be calculated by averaging all $\bar{s}_{bl}$ values obtained for 5 mV s^{-1} and all those in the range 10—50 mV s^{-1}. The respective values are 2.8 and 0.6 μC cm^{-2}, and the corresponding charge detection limits, as defined above, are therefore 8.4 and 1.8 μC cm^{-2}.

TABLE 1

Noise of blank anodic stripping signals at mercury covered glassy carbon electrodes (Electrolyte, 20 ml of 0.05 M acetate buffer; glassy carbon disk electrodes preplated at −1 V vs. SCE with 6.2×10^{-7} mol cm^{-2} of Hg; electrode rotation rate, 45 rps.)

Scan rate ($mV\ s^{-1}$)	Standard deviations of net charges ($\mu C\ cm^{-2}$)[a,b,c]							
	Tokay GC-A				Sigradur-K			
	−800 mV		−300 mV		−800 mV		−300 mV	
	$\bar{s}_{bl}$	s	$\bar{s}_{bl}$	s	$\bar{s}_{bl}$	s	$\bar{s}_{bl}$	s
5	2.0	0.8	2.0	0.3	3.4	2.5	3.7	2.0
10	0.6	0.2	0.6	0.1	0.8	0.3	1.1	0.8
20	0.6	0.1	0.5	0.2	0.5	0.3	0.7	0.5
50	0.4	0.2	0.4	0.3	0.5	0.5	0.5	0.4

[a]Charge per geometrical electrode area, accumulated in a potential interval of 200 mV.
[b]$\bar{s}_{bl}$ = mean, calculated from s_{bl} of four different electrodes; each s_{bl} was obtained from five charge values.
[c]s = standard deviation of $\bar{s}_{bl}$; this represents the reproducibility for a given type of electrode material.

Limit of detection. For a given q_{det}, the detection limit of concentration can be calculated from the geometrical cell constant A/V. For a diffusion-controlled pre-electrolysis at a rotating disk electrode, A/V is given by

$$A/V = -(1/t_d) \times (0.62\, D^{2/3}\, \nu^{-1/6}\, \omega^{1/2})^{-1} \times \ln\beta \qquad (2)$$

(t_d = deposition time, D = diffusion coefficient of the metal ion, ν = kinematic viscosity of the solution, ω = angular viscosity of the disk, β = fraction of metal left undeposited at the time t_d). For an electrode rotation rate of 45 rps, the average value of the hydrodynamic factor ($0.62\, D^{2/3}\, \nu^{-1/6}\, \omega^{1/2}$), calculated from the observed deposition rate constants of cadmium and lead, is 0.006 cm s^{-1} [1]. Thus, for a deposition time of 15 min, a cell with $A/V = 1.3$ cm^{-1} is required to achieve a sample exhaustion of 99.9%, and the respective detection limit, calculated from eqn. (1) with $n = 2$ and $q_{det} = 1.8$ $\mu C\ cm^{-2}$, is 1.2×10^{-8}M. This is a high concentration and it is obvious that with respect to the detection limit, the coulometric method cannot compete with the conventional d.c. voltammetric procedure with non-exhaustive pre-electrolysis and calibration by standard addition. For equal hydrodynamic conditions and given values of t_d and q_{det}, the ratio of the detection limits of the two methods is equal to the ratio of the logarithms of the respective values of β. As β is typically 0.001 for coulometry and 0.95 for voltammetry, the detection limit of the voltammetric stripping procedure is about two orders of magnitude lower than that of the coulometric method.

REFERENCES

1 R. Eggli, Anal. Chim. Acta, 91 (1977) 129.
2 H. Kaiser, Anal. Chem., 42 No. 4 (1970) 26 A.
3 M. Štuliková, J. Electroanal. Chem. Interfacial Electrochem., 48 (1973) 33.
4 W. J. Blaedel and R. A. Jenkins, Anal. Chem., 46 (1974) 1952.

Analytica Chimica Acta, 97 (1978) 199—202

Short Communication

CACOTHELINE AS AN OXIDIZING REAGENT FOR THE PHOTOMETRIC TITRATION OF TIN(II), IRON(II) AND VANADIUM(III)

N. KRISHNAMURTY* and Y. PULLA RAO

Department of Chemistry, Andhra University, Waltair (India)

(Received 16th May 1977)

Cacotheline of unspecified purity has often been used as a redox indicator, and for the detection and colorimetric determination of tin(II), iron(II) and vanadium(III) [1—3]. The preparation of highly-pure cacotheline and its use as an oxidimetric reagent have been reported [4]. This pure reagent has now been studied for the photometric titration of tin(II), iron(II) and vanadium(III); the method is suitable for the analysis of tin plate, solder and pharmaceutical preparations.

Experimental

Apparatus. A Hilger Uvispek spectrophotometer with 10-mm cells, and a Klett-Summerson photoelectric colorimeter with a green filter (maximum transmission 500—560 nm) were used. The rectangular titration cell (2 × 4 × 8 cm) had a light path of 2 cm.

Reagents. All solutions were prepared from boiled-out de-ionized water. Cacotheline solution (0.005 M) in 0.02 M HCl was standardized as described earlier [4]. Iron(II) ammonium sulphate solution (0.1 M) in 0.25 M H_2SO_4 was standardized by the potassium dichromate method and used after suitable dilution.

Tin(II) chloride solution (0.025 M) in 1 M HCl was standardized conventionally [5]. Vanadium(III) sulphate solution (0.05 M) was standardized as described earlier [6].

Preliminary tests showed that the most suitable acid conditions for the reduction of cacotheline by tin(II), iron(II) and vanadium(III) are, respectively, 0.75—2 M HCl, 9—10 M H_3PO_4 and 4—8 M acetic acid.

Procedure. Place 38 ml of 1 M HCl (for tin(II)), 10 M H_3PO_4 (for iron(II)), or 6 M acetic acid (for vanadium(III)) in the 50-ml titration cell. Pass CO_2 through the solution for 10—15 min via a capillary tube placed out of the light path. Then add an aliquot of tin(II), iron(II) or vanadium(III) solution, dilute to 40 ml, and set the zero of the photometer. Titrate with 0.005 M cacotheline solution in 0.1-ml portions while continuing to pass CO_2, except during the reading of absorbances. Apply the usual volume corrections for plotting the titration curves.

Analysis of tin plate. Wash the sample with benzene or carbon tetrachloride, and dry. Use a ca. 0.1-g sample, place 10 ml of 11 M HCl in a 50-ml conical flask fitted with a three-holed stopper, which carries a gas inlet tube extending to the bottom of the flask, and a vertical 15—20 cm condenser; the third hole is stoppered. Pass CO_2 for about 10 min, add the sample through the third hole, and heat while continuing to pass CO_2. Heat until the sample dissolves and then for a further 20 min (this is necessary for consistent results). Cool and transfer the solution to the titration cell with about 30 ml of 0.5 M HCl (deoxygenated with CO_2). Then titrate as described above. A sample of tin plate gave a result of 0.86% tin with a relative standard deviation of about 0.5% (n = 6).

Analysis of solder. Remove grease from a 0.4-g sample as described above. Place 2 ml of 15.5 M HNO_3 and 10 ml of 11 M HCl in a 50-ml conical flask fitted as above, add the sample and heat until the alloy has dissolved. Then add 10 ml of 11 M HCl and heat for about 30 min to expel nitrous fumes. Cool and filter to remove lead chloride. Return the solution to the conical flask and pass CO_2 for about 5 min. Add about 1 g of aluminium wire clippings. Heat to dissolve, and continue heating for 20 min. Cool and dilute to 500 ml with deoxygenated 1 M HCl. Store this solution under an inert atmosphere. Transfer an aliquot (1—3 ml) of the solution to the titration cell, and titrate tin(II) as described above. A sample of solder gave a result of 39.92% tin with a relative standard deviation of 0.3% (n = 6).

Determination of iron in pharmaceutical preparations. For iron tablets, powder one tablet finely and extract 6 times with 1 M HCl, transferring the extracts to a 100-ml volumetric flask. Dilute to the mark with 1 M HCl acid and titrate 0.5 ml of this solution as described above.

For dumasules capsules, transfer the powder to a beaker, and dissolve the iron as in the case of iron tablets, diluting to 100 ml. Titrate 0.25 ml of this solution as described above.

Results and discussion

The absorption spectra of the product obtained by the reduction of cacotheline with tin(II), iron(II) or vanadium(III) at the recommended acidities showed a maximum at 530 nm. To ascertain the reaction stoichiometry, known amounts of cacotheline were titrated photometrically with tin(II), iron(II) and vanadium(III) under the recommended conditions. The course of the reactions was the same whether the reagent or the metal ion served as the titrant: one mole of cacotheline reacted with one mole of tin(II), two moles of iron(II) or two moles of vanadium(III) for its reduction to the pink product. The reaction mechanism has already been discussed [4].

The results obtained for the photometric titrations of pure solutions are shown in Table 1. Various foreign coloured ions such as Ni(II), Cr(III) and U(IV) had no significant effect on the results. Sb(III), As(III), Al(III), Mn(II), Mg(II), Zn(II), Cl^-, Br^-, oxalate and citrate did not interfere. Notably ascorbic acid and copper(II) did not interfere in the iron(II) titration.

TABLE 1

Photometric determination of tin(II) or iron(II) or vanadium(III) with cacotheline

Metal	Taken (mg)	Found (mg)	Error (%)
Tin(II)	0.1535	0.1543	0.5
	0.461	0.458	0.5
	0.799	0.804	0.7
Iron(II)	0.424	0.419	1.0
	0.777	0.773	0.5
	1.018	0.993	0.5
Vanadium(III)	0.064	0.0635	0.2
	0.255	0.254	0.4
	0.5093	0.5087	0.2

TABLE 2

Photometric determination of iron(II) in pharmaceutical preparations

	Iron, mg		Deviation (%)
	Proposed method	B.P. method	
Iron tablets (Rallis India Ltd.)	70.30[a]	71.35	−1.47
Damasules capsules (Pfizer Ltd., India)	97.02[a]	98.50	−1.50

[a]Each value is an average of six determinations.

The results obtained for the determination of iron in tablets and capsules are shown in Table 2; the samples were also analyzed by the standard B.P. method [8]. The advantage of the present method compared with the earlier method [3] is that the method is highly selective for iron(II); also reduced cacotheline is much more stable in phosphoric acid medium than in buffer solutions.

An advantage of cacotheline is that the reagent keeps its titre unaltered even after 15 days if prepared in 0.02 M hydrochloric acid and kept in an amber-coloured bottle.

The authors gratefully acknowledge the keen interest and advice of Prof. G. Gopala Rao, and thank the C.S.I.R. (India) for the award of a Senior Research Fellowship to Y. P. Rao.

REFERENCES

1 See, e.g. F. J. Welcher, Organic Analytical Reagents, Vol. 4, Van Nostrand, New York, 1948, p. 217.
2 F. Feigl, Qualitative analysis by spot tests, 2nd English edn., Nordmann, New York, 1939, p. 69.
3 G. Gopala Rao, V. Narayana Rao and G. Somidevamma, Z. Anal. Chem., 166 (1958) 11.
4 G. Gopala Rao, N. Krishnamurty and V. Narayana Rao, Talanta, 12 (1965) 243.
5 I. M. Kolthoff and R. Belcher, Volumetric Analysis III, 1957, p. 622.
6 G. Gopala Rao and P. Kanta Rao, Talanta, 13 (1966) 1335.
7 G. Gopala Rao and V. Narayana Rao, Talanta, 1 (1958) 169.
8 The British Pharmacopœia, Pharmaceutical Press, London, 1968, pp. 420, 412, 413.

Analytica Chimica Acta, 97 (1978) 203—206

Short Communication

DIE FÄLLUNG UND ABTRENNUNG VON KUPFER UND ZINK MIT DL-α-AMINO-n-CAPRONSÄURE

R. PIETSCH*

Institut für anorganische und analytische Chemie der Universität Graz, A-8010 Graz (Österreich)

(Eingegangen den 17. August 1977)

In der Literatur wird hingewiesen, dass gewisse α-Aminosäuren zur Fällung und Bestimmung von Metallionen Verwendung finden können. Nach Vergleichsuntersuchungen wurden die Möglichkeiten der Bestimmung von Kupfer und Zink mit DL-α-Amino-n-capronsäure (Norleucin; NL) einer näheren Untersuchung unterzogen. Hinweise auf diese Möglichkeit geben schon Kudielka [1], Kober und Sugiura [2], Lyle et al. [3] und Feigl [4]. Allerdings beziehen sich alle erwähnten Hinweise nur auf qualitative Bearbeitungen, zum Teil zur Isolierung und Kennzeichnung von Aminosäuren.

Bei der Ueberprüfung des pH-Gebietes der Fällung der Metallionen mit Norleucin ergab sich, dass unter gleichen Arbeitsbedingungen das Kupferion bei pH 2,0 zu fallen beginnt und bei pH 3,5 quantitativ gefällt ist; Zinkion erst bei pH 3,0 zu fallen beginnt und bei pH 5,5 quantitativ gefällt ist. Eine gewisse Verschiebung dieser Bereiche tritt natürlich durch Aenderung des vorliegenden Reagensüberschusses ein. Immer aber fällt Kupfer etwas saurer. Beide Fällungen sind seidig, feinkristallin und hydrophob, legen sich an den Glaswänden nicht an, sind leicht filtrierbar und gut auszuwaschen. Sie zeigen auch keine Tendenz zur Adsorption von Fremdionen.

Bei der Untersuchung der Fällungen auf ihre Zusammensetzung ergab sich ein Verhältnis von Metall: NL = 1:2. Wasser war in den Niederschlägen in beiden Fällen nicht vorhanden.

Die IR-Vermessungen zeigten eine deutliche Verschiebung der NH-Banden des Natriumsalzes von Norleucin bei 3360 cm^{-1} und 3280 cm^{-1} zu 3280 cm^{-1} und 3220 cm^{-1} bei der Kupferverbindung und zu 3300 cm^{-1} und 3220 cm^{-1} bei der Zinkverbindung, was teilweise schon aus der Literatur bekannt war [5]. Den Verbindungen kann daher die Formel I zugeordnet werden.

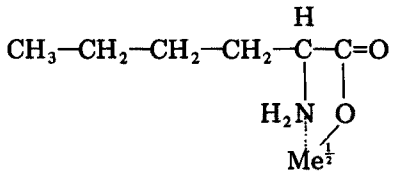

(I, Me = Cu, Zn)

Die mengenmässige Bestimmung der Fällungen kann auf verschiedene Weise erfolgen. Es kann nach Filtration aus Weissbandfilter zum Oxyd verglüht werden. Nach Trocknen bei 110°C können die Fällungsgewichte mit den stöchiometrischen Faktoren (0,19617 für $Cu(NL)_2$ auf Kupfer und 0,20071 für $Zn(NL)_2$ auf Zink) umgerechnet werden. Schliesslich bleibt noch die Möglichkeit einer Titration mit Aethylendiaminotetraessigsäure. Bei Zink kann der erhaltene Niederschlag nach Aufschlämmen in Wasser direkt gegen Indikatorpuffertabletten oder Eriochromschwarz T titriert werden, nur ist der Umschlag am Endpunkt etwas verlangsamt. Bei der Kupferverbindung ist eine einfache direkte oder indirekte Titration nicht möglich; das Kupfer ist aber nach kurzer Mineralisation ebenfalls leicht titrierbar.

Fällungsmethode

Die sauren Lösungen von Kupfer bzw. Zink werden in einem Volumen von 150—200 ml mit einem 2—5-fachen äquivalenten Ueberschuss an Norleucin (als 0,0% ig wassrige Lösung) versetzt. Ein grösserer Ueberschuss schadet nicht. Gegebenenfalls nach Lösen des Norleucin wird entweder schon in der Kälte oder nach Erwärmen auf 80°C mit verdünntem Ammoniak bei Kupfer auf einen pH über 4 und bei Zink auf einen pH über 5 gebracht, wobei man eine Glaselektrode verwendet. Der gewünschte pH ist leicht einstellbar. Kalt, oder falls man erwärmt hatte nach Abkühlung, wird wahlweise auf Weissbandfilter oder auf einen Glasfrittentiegel G 4 filtriert, wobei man den Niederschlag mit kaltem destillierten Wasser aus dem Fällungsglas ins Filter spült. Nach kurzem Nachwaschen mit wenig kaltem Wasser wird die Fällung in beliebiger Weise bestimmt; Tabelle 1 demonstriert die Brauchbarkeit der Methode.

Abtrennungen

Nach der angegebenen Einzelfällungsvorschrift, eventuell mit erhöhten Ueberschuss an Norleucin, sind Kupfer und Zink fällbar neben K, Na, Ammonium, Ag, Ca, Mg, Cr, Nitrat, Chlorid, Sulfat, Acetat und Tartrat.

TABELLE 1

Einzelfällungsergebnisse von Kupfer und Zink

Kupfer			Zink		
gegeb. (mg)	gef. (mg)	Bestimmungs-methode	gegeb. (mg)	gef. (mg)	Bestimmungs-methode
19,95	19,95	Trocknen	20,18	20,18	Titrieren
32,00	32,10	CuO	30,28	30,39	Titrieren
40,10	40,20	CuO	50,46	50,40	Titrieren
40,10	40,10	Trocknen	50,46	50,37	ZnO
48,10	48,10	Trocknen	60,55	60,49	ZnO
60,15	60,06	Trocknen			

Kupfer lässt sich weiters auch neben Phosphat fällen, während dies bei Zink infolge Fällung von Zinkphosphaten nicht möglich ist. Bemerkenswert ist die Tatsache der Fällbarkeit neben Weinsäure, die einige weitere Trennungsmöglichkeiten eröffnet.

Die Abtrennung der beiden Metalle von Mangan ist möglich, wenn man die pH-Einstellung durch eine Hydrolysenmethode, etwa die Zugabe von Harnstoff, vornimmt.

Von Ferrieisen, Uranylion und Beryllium ist die Trennung beider Metalle bie Anwesenheit von entsprechenden Mengen Weinsäure in der Fällungslösung möglich. Kupfer kann in analoger Weise auch noch von Aluminium abgetrennt werden, nicht hingegen das Zink.

Aus verschiedenen Gründen ist die Abtrennung der Metalle Kupfer und Zink von Chromiionen, Indium, Wismut, Kobalt, Nickel, Blei und Cadmium nicht möglich, zumindest wenn diese in grösseren Mengen vorliegen, sowie die Trennung von Kupfer und Zink voneinander.

TABELLE 2

Ergebnisse der Kupfer- und Zinkabtrennung von verschiedenen Begleitmetallen

Begleition	(mg)	Cu (gegeb. 40,10 mg)	Zn (gegeb. 50,46 mg)
		Cu gefunden (mg)	Zn gefunden (mg)
Ca^{2+}	159,6	39,97	50,40
Mg^{2+}	177,0	40,15	50,50
Ag^{+}	255,0	39,95	50,33
Fe^{3+}	103,7	40,04	50,33
Mn^{2+}	152,4	39,94	50,23
U als UO_2^{2+}	98,8	40,09	50,66
Be^{2+}	53,5	40,20	50,69
Cr als CrO_4^{2-}	65,8	40,03	50,59
Al^{3+}	97,7	40,00	
PO_4^{3-}	94,9	40,10	

TABELLE 3

Bestimmung von Kupfer oder Zink in Legierungen und Mineralien

Substanz	Metallgehalt (%) nach Normalanalyse	Sonstige enthalt. Bestandteile	Metallgehalt (%) nach NL-Methode
Zinnmetall	Cu 3,5	Sn, Sb, As, Pb	Cu 3,0
Aluminiummetall	Cu 4,5	Al, Fe, Si, Mn, Ti	Cu 4,4
Arndt'sche Leg.	Cu 58,3	Mg	Cu 58,2
Optisches Glas	ZnO 8,9	SiO_2, B_2O_3, Al_2O_3, BaO	ZnO 8,6
Schwefelkies	Zn 2,4	S, Fe, Pb, Cu	Zn 2,1
Zinkofen-Flugstaub	Zn 66,6	SiO_2, CaO, MgO, C	Zn 66,6

Die Tabelle 2 zeigt die Ergebnisse einer Reihe von durchgeführten Trennungen; desgleichen wurden Testanalysen von verschiedenen festen Analysenproben vorgenommen (Tabelle 3).

LITERATUR

1 H. Kudielka, Monatsh. Chem., 29 (1908) 351.
2 P. A. Kober und K. Sugiura, J. Am. Chem. Soc., 35 (1913) 1584.
3 W. G. Lyle, L. Curtman und J. T. Marshall, J. Am. Chem. Soc., 37 (1915) 1471.
4 F. Feigl, Chemistry of Specific, Selective and Sensitive Reactions, Academic Press, New York, 1949, S. 219.
5 J. F. Jackovitz und J. L. Walter, Spectrochim. Acta Part A, 22 (1966) 1393.

Analytica Chimica Acta, 97 (1978) 207—211

Short Communication

DISSOCIATION CONSTANTS OF *m*-NITROANILINIUM ION IN 1,2-DIMETHOXYETHANE—WATER MIXTURES AT 25°C BY SPECTROPHOTOMETRIC MEASUREMENTS

RABINDRA N. ROY*, JAMES J. GIBBONS and CHARLES H. TILLMAN, Jr.
Department of Chemistry, Drury College, Springfield, Missouri 65802 (U.S.A.)
(Received 5th July 1977)

The effect of changing solvent composition on the pK_a (the dissociation constant) of a weak acid or base is a useful means of inferring changes in the pattern of ion—solvent interactions in binary solvent systems (such as water—non-aqueous solvent mixtures). The dissociation constants of a weak acid of the charge type A^+B^0 (expressed by an isoelectric process, $BH^+ \rightleftarrows B + H^+$), such as *m*-nitroanilinium ion, have been spectrophotometrically studied in many water—dipolar aprotic solvents, such as water—acetone [1], water—tetrahydrofuran [2], water—dioxane [3], water—dimethylsulfoxide [4], and water—sulfolane [5]. As a continuation of previous thermodynamic studies of hydrochloric acid [6] and hydrobromic acid [7] in THF—water mixtures and 1,2-dimethoxyethane—water mixtures [8, 9], the dissociation constants of *m*-nitroanilinium ion in 1,2-dimethoxyethane—water solvent mixtures have been investigated, since pK_a data for this acid in this media were not available for comparison with those obtained in the afore-mentioned mixed solvents. These data have been collected at 25°C for 0, 10, 30, 50, and 70 mass % 1,2-dimethoxyethane. Some physical properties of these solvent mixtures are summarized in Table 1.

The advantage of using this cationic acid, *m*-nitroanilinium ion, is that for other studies of this kind (such as *p*-nitrophenol [10]), accurate values for the pH of these buffers in the mixed solvents should be known, whereas for *m*-nitroanilinium ion (with $pK_a = 2.465$ in water at 25°C) [2], the dissociation constants can be conveniently determined in solutions whose H^+ concentrations are directly known by HCl content.

Experimental

Reagents. 1,2-Dimethoxyethane (dimethyl Cellusolve; glyme; Fisher Certified Reagent Grade) was stored over sodium metal for 1 d, after which the solvent was refluxed over anhydrous calcium sulfate for 2 d and then vacuum-distilled before use. For purification, *m*-nitroaniline was recrystallized once from benzene and twice from methanol.

TABLE 1

Properties of the 1,2-dimethoxyethane—water mixtures at 25°C

Mass % glyme	Mole fraction glyme	Density (g cm^{-3})	Dielectric constant	Dissociation constant (pK_a)
0	0.0000	0.9971	78.3	2.47
10	0.02173	0.9922	92.3	2.23
30	0.07891	0.9852	93.1	2.19
50	0.1666	0.9673	49.5	1.50
70	0.3181	0.9332	28.5	1.39
90	0.6427	0.8887	13.2	—
100	1.0000	0.8621	7.2	—

1,2-Dimethoxyethane—water stock solution. The 1,2-dimethoxyethane (doubly-distilled) and conductivity-grade water were weighed to make up all of the various percentages of the mixed solvent.

Hydrochloric acid stock solution. Stock solutions of hydrochloric acid, obtained from the middle fractions of the twice-distilled constant boiling hydrochloric acid solution, were prepared in the various experimental compositions.

Indicator stock solution. The *m*-nitroaniline stock solution was added to the respective mixed solvent system after the latter two stock solutions had been combined.

Four to seven different concentrations of hydrochloric acid at each mass % were prepared by weighing appropriate amounts of the three stock solutions, so that the molality of each different solution could be calculated. All these weighings were vacuum-corrected.

Apparatus. All solutions were thermostated to 25.00 ± 0.05°C (Lauda K-2 type Constant Temperature Bath) before two 1-cm optical silica cells (one containing the buffer, the other a blank containing the same solution without the indicator) were filled. The temperature of the room was kept very close to 25°C. The spectral measurements were made with a Beckman Model B Spectrophotometer at 352, 352, 368, 366, and 375 nm for 0, 10, 30, 50, and 70 mass % glyme, respectively. These wavelengths were selected because they were very close to the determined maximum absorption of *m*-nitroaniline.

Procedure. The absorbance of the protonated form of *m*-nitroaniline, A_a, was obtained in water and in the mixed solvent by direct measurement in solutions of 6 M HCl. The absorbance of the pure basic form of *m*-nitroaniline, A_b, was also obtained directly by measuring a solution in which about 0.4 g of sodium carbonate had been dissolved. The absorbance A refers to a buffer solution in which *m*-nitroaniline is present partly in its molecular form and partly in its ionized form.

Results and discussion

The isoelectric dissociation process of *m*-nitroaniline is expressed as $BH^+ \rightleftarrows B + H^+$, and the dissociation constant, K_a, is obtained (after proper simplification of the activity expression) as

$$pK_a = -\log m_{H^+} - \log (\alpha/1-\alpha) - \log (\gamma_B \gamma_{H^+}/\gamma_{BH^+}) \quad (1)$$

in which α is the degree of dissociation, and is given by the expression $\alpha = (A - A_a)/(A_b - A_a)$, where A_a and A_b have already been defined, and A is the absorbance of the buffer (i.e., the partially transformed form of *m*-nitroaniline). For dilute solutions, the activity coefficients can be assumed to be small, and eqn. (1) then becomes

$$pK_a = -\log m_{H^+} - \log (A - A_a)/(A_b - A) \quad (2)$$

The true equilibrium value of m_{H^+} was calculated from

$$m_{H^+} = m_{HCl} - m(A_b - A)/(A_b - A_a) \quad (3)$$

where m_{HCl} is the stoichiometric molality of HCl, and m is the molality of the indicator (i.e., *m*-nitroaniline).

The values of the parameters needed to calculate the pK_a' with eqn. (2) for 0, 10, 30, 50, and 70 mass % 1,2-dimethoxyethane, as well as the ranges of the molalities of the indicator and those of HCl, are given in Table 2. The variations of pK_a' with m_{H^+} for each experimental solvent composition are random and insignificant; hence, the average data of pK_a' in each solvent mixture was taken as the pK_a. In order to test the reliability of our technique, the pK_a of *m*-nitroanilinium ion in water was also determined. A value at 25°C of 2.468, in good agreement with previous data, e.g. 2.465 [2], 2.461 [11], or 2.461 [4], was obtained.

Table 2 gives the experimental results (pK_a) on the molal scale. The factors which influence the dissociation of a weak acid such as *m*-nitroanilinium ion in aqueous, non-aqueous or mixed solvent are as follows: (a) the dielectric constant of the solvent system; (b) the acid—base strength of the solvent; and (c) the solvating power of each of the ionic species present (e.g. *m*-nitroaniline, *m*-nitroanilinium ion, and a proton in this investigation).

The dissociation of *m*-nitroanilinium ion studied here in 1,2-dimethoxyethane—water is an isoelectric process (i.e. one with no net gain or loss of charge). Thus, the dielectric constant (which is responsible for electrostatic effects of the Born type) is not expected to have a major role in the change of pK with alterations in the solvent composition. The only contributing factor arising from the effect of the dielectric constant may result from the differences in the ion sizes of these ions involved in the dissociation process. That the dielectric constant plays such a minor role is confirmed by the graphs in Fig. 1(A) where pK_a is plotted as a function of the reciprocal of the dielectric constant (ϵ). Here, instead of an increasingly monotonic function with the lowering of ϵ, a minimum of pK_a is observed for all systems except for THF—H_2O [2], where the solvent composition did not

TABLE 2

Dissociation constants of *m*-nitroanilinium ion in different media at 25°C

$\times 10^{-3}$ m_{HCl} (mol kg^{-1})	$-\log m_{H^+}$	$\log \frac{A - A_a}{A_b - A}$	pK_a	Average pK_a
In pure water (λ = 352 nm; *indicator* = 6.1—6.4 $\times 10^{-4}$ *mol kg*$^{-1}$)				
1.539	2.866	0.4105	2.456	
3.080	2.682	0.2092	2.472	
5.354	2.302	−0.1707	2.473	
6.098	2.243	−0.2276	2.471	2.468 ± 0.008
In 10 mass % 1,2-dimethoxyethane—water (λ = 352 nm; *indicator* = 3.0 $\times 10^{-4}$ *mol kg*$^{-1}$)				
2.326	2.646	0.4068	2.239	
3.093	2.521	0.2824	2.239	
4.368	2.324	0.1040	2.220	
5.423	2.274	0.05337	2.221	
6.204	2.216	0.00314	2.213	2.226 ± 0.012
In 30 mass % 1,2-dimethoxyethane—water (λ = 368 nm; *indicator* = 1.5 $\times 10^{-4}$ *mol kg*$^{-1}$)				
1.535	2.825	0.4771	2.348	
2.280	2.650	0.3951	2.255	
3.059	2.522	0.3101	2.211	
3.808	2.425	0.3010	2.124	
4.574	2.386	0.3565	2.030	2.19 ± 0.09
In 50 mass % 1,2-dimethoxyethane—water (λ = 366 nm; *indicator* = 1.6 $\times 10^{-4}$ *mol kg*$^{-1}$)				
1.480	2.832	1.299	1.533	
2.240	2.652	1.144	1.508	
2.941	2.534	0.9294	1.605	
3.685	2.435	1.026	1.409	
5.149	2.290	0.8669	1.423	1.50 ± 0.03
In 70 mass % 1,2-dimethoxyethane—water (λ = 375 nm; *indicator* = 2.3 $\times 10^{-4}$ *mol kg*$^{-1}$)				
1.655	2.784	1.380	1.404	
2.443	2.615	1.195	1.420	
3.267	2.489	0.8934	1.596	
4.915	2.311	0.9542	1.356	
5.813	2.237	1.081	1.156	1.39 ± 0.09

extend high enough to locate the minimum. In methanol—water [12], it is found at 70 mass % methanol. The data at 90 mass % 1,2-dimethoxyethane is based on unpublished measurements from this laboratory.

Two other factors, e.g. base strength of the solvent and the amount of solvation of the free base (*m*-nitroaniline) and other ions, will play primary roles in bringing about changes of pK_a with varying solvent composition. In Fig. 1(B), the pK_a is plotted as a function of these solvent compositions. The relative positions of the curves on this graph indicate that *m*-nitroaniline has the strongest preference for THF. The interactions between dimethylsulfoxide (DMSO) and *m*-nitroaniline are stronger than those of 1,2-dimethoxyethane for 30 mass % DMSO and beyond. The *m*-nitroaniline is poorly solvated at higher percentage compositions, thus becoming almost identical

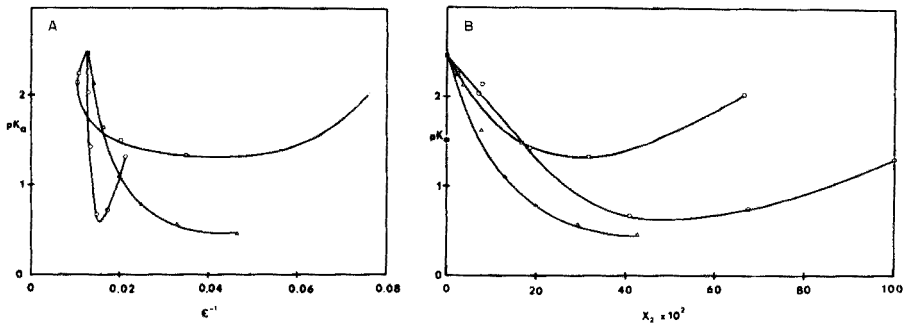

Fig. 1. pK_a for *m*-nitroanilinium ion (on the molal scale) as (A) a function of the reciprocal of the dielectric constant ϵ, and (B) a function of the mole fraction x of the organic component, in three different binary mixed solvent systems. □ 1,2-Dimethoxyethane. ○ Dimethylsulfoxide. △ Tetrahydrofuran.

below 30 mass %. The above conclusions concerning solute—solvent interactions are drawn from the equation:

$$RT \ln 10\ (\Delta pK_a) = \Delta G_t^0\ (m\text{-nitroaniline}) - [\Delta G_t^0\ (m\text{-nitroanilinium ion}) - \Delta G_t^0\ (H^+)] \quad (4)$$

in which the first part of the right-hand side indicates the Gibbs energy changes associated with the transfer of the neutral molecule (i.e., *m*-nitroaniline) from pure water to the solvent mixture, whereas the second part refers to the difference between the Gibbs energies of transfer of *m*-nitroanilinium ion and the proton. The first part explains the stabilization or destabilization of the base when additional organic solvent is added to water. The second part deals with the selective solvation (by either water or glyme) of H^+ and *m*-nitroanilinium ion in the mixed solvent medium.

The authors wish to thank Mr. T. White and Ms. L. Brown for making some of the preliminary measurements.

REFERENCES

1 K. P. Ang, J. Solution Chem., 4 (1975) 949.
2 R. A. Robinson, J. Res. Nat. Bur. Stand., 74A (1970) 495.
3 K. A. Boni and H. A. Strobel, J. Phys. Chem., 70 (1966) 3771.
4 R. G. Bates, L. Johnson and R. A. Robinson, Chem. Anal. (Warsaw), 17 (1972) 479.
5 K. P. Ang, J. Solution Chem., 4 (1975) 369.
6 R. N. Roy and B. Sen, J. Chem. Eng. Data, 12 (1967) 584; J. Chem. Eng. Data, 13 (1968) 79.
7 R. N. Roy, E. E. Swensson and G. LaCross, Jr., J. Chem. Thermodyn., 7 (1975) 1015.
8 D. A. Johnson and B. Sen, J. Chem. Eng. Data, 13 (1968) 376.
9 R. N. Roy, E. E. Swensson, G. LaCross, Jr. and C. W. Krueger, Thermodynamic Behavior of Electrolytes in Mixed Solvents, W. F. Furter (Ed.), in Advances in Chemistry Series, no. 155, Ch. 13, 1976.
10 R. A. Robinson and A. I. Biggs, Trans. Faraday Soc., 51 (1955) 901.
11 A. I. Biggs and R. A. Robinson, J. Chem. Soc., (1961) 388.
12 E. E. Sager, R. A. Robinson and R. G. Bates, J. Res. Nat. Bur. Stand., 68A (1965) 305.

Analytica Chimica Acta, 97 (1978) 213—217

Short Communication

POLYETHYLENE DISPENSING BOTTLES — A GRAVIMETRIC ALTERNATIVE TO VOLUMETRIC WARE

T. D. RICE

Chemical Laboratory, New South Wales Department of Mines, P.O. Box 76, Lidcombe 2141 (Australia)

(Received 19th May 1977)

Preparation of solutions with concentrations expressed as weight/weight has been recommended for greater analytical accuracy [1] and is conveniently done by a top-pan balance, with taring capacity, weighing to the nearest 0.01 g or better. A top-pan balance has been used [2] in a gravimetric technique for high-precision titrimetry and, with a polyethylene wash-bottle, has been used for gravimetric titrations [3].

The polyethylene dispensing bottles described here resemble the widely-used polyethylene wash-bottles and when used with a top-pan balance calibrated against standard weights, provide an alternative to volumetric ware in many analytical procedures. Any low-density polyethylene bottle with a self-sealing linerless cap and of capacity not greater than 1100 ml is suitable for conversion to a dispensing bottle. A novel feature of these bottles (Fig. 1) is the easily applied closure for the dispensing tube.

Over the past six years in this laboratory, such bottles have been increasingly used in the wet-chemical analysis of geological materials, especially when high precision and accuracy are sought. A more detailed description than previous ones [4, 5] is therefore warranted.

Experimental

Method of assembly. This has been adequately described [5], except for the technique found most convenient for making a hole in the bottle cap, which is as follows. With the squarely ground shank of a 2.08-mm diameter drill fitted in the chuck of a pedestal drill, a hole is punched through the centre of the cap, which is held securely by a specially made die (Fig. 2). This allows a set of caps to be holed cleanly and quickly.

Preliminary treatment. New dispensing bottles are about one-third filled with 0.5 M hydrochloric acid and left for a few days with occasional shaking. To prevent acid leakage, the dispensing tube must be sealed with its closure. Treatment of new polyethylene bottles with dilute hydrochloric acid has been recommended by Riley [6].

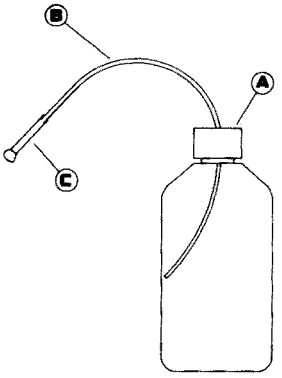

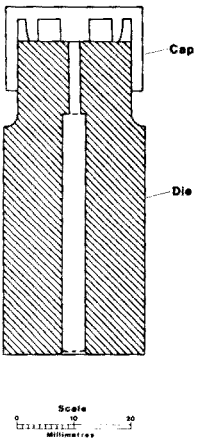

Fig. 1. Main features of polyethylene dispensing bottle: (A) holed polyethylene cap, self-sealing and linerless; (B) polyethylene dispensing tube, Portex ref. no. PP205, bore 1.57 mm, ext. diam. 2.08 mm; (C) closure made of polyethylene tubing (Portex ref. no. PP270, bore 2.00 mm, ext. diam. 3.00 mm) heat-sealed at one end.

Fig. 2. Cross-section of the brass die on top of which a self-sealing polyethylene cap is held for punching. The central stump beneath the cap promotes effective sealing of the dispensing bottle.

Previously used dispensing bottles are prepared for re-use by removing the closure and rinsing the whole unit three times with tap water followed by four times with deionized water. The weight of the dry empty bottle (including the cap, tube and closure) is often required and is found after drying overnight at 60—65°C.

Preparation of a given weight of solution. Unlike the case of a solution diluted to the mark in a volumetric flask, thorough mixing of the final weight of solution in a dispensing bottle is possibly not achieved merely by shaking the sealed bottle, because of the solution trapped in the bottom of the dispensing tube. Therefore, after the sealed bottle has been shaken, the cap is loosened and the bottle squeezed somewhat; the cap is then re-tightened, and the closure of the dispensing tube is removed, so that the tube is cleared by air entering the bottle. The closure is then replaced, the bottle shaken and loosening of the cap, etc., is repeated.

Solution storage and dispensing. Solutions in sealed dispensing bottles are stored away from direct sunlight and other sources of heat, and preferably with the bottle walls slightly depressed, so as to prevent build-up of pressure. Without these precautions, solution may leak through the dispensing tube as soon as the closure is removed. Before solution is dispensed, it may be necessary to shake the sealed bottle and to squeeze out several ml of solution into a spare container so as to condition the tube.

In the preparation of, say, ten-fold diluted solutions for measurement by

atomic absorption, it is convenient to weigh, from a dispensing bottle, w ($\leqslant 5$) g of initial sample solution into a dry, 60-ml polyethylene bottle tared on a top-pan balance and then to add the appropriate diluent from another dispensing bottle until the final solution weighs $10 \times w$ g.

Weight burettes. If the dispensing bottle is to be used as a weight burette (or as a wash bottle), the dispensing tube can be readily fitted with a fine tip made of drawn-out PP205 tubing joined to about 8 mm of PP270 tubing. (The most satisfactory technique for drawing out polyethylene tubing seems to be to heat momentarily in a fairly strong Meker burner flame and, after 5—10 s, to draw out in the same way as for glass tubing.) A fine tip giving a drop size of 0.01 g can be readily made. However, a fine tip is unnecessary if a drop size of 0.04 g enables sufficiently precise end-point detection.

Gravimetric titrations are carried out by a procedure similar to that of Swift and Butler [3]: the dispensing bottle, containing titrant and with closure removed, is weighed on a top-pan balance before and after titration.

Results and discussion

Rather than make many dispensing bottles, it may be convenient to fit a tube to only one cap of a set of polyethylene bottles and to use this as a "movable dispenser" by fitting it to each bottle as required.

Evaporation losses. Owing to the permeability of polyethylene to solvents, solutions gradually increase in concentration when stored in polyethylene bottles, provided that there are no adsorption effects. The magnitude of the increase can be determined by periodically weighing the tightly capped bottle. Table 1 gives typical results for the loss in weight of aqueous solutions stored in the recommended bottles and in identical bottles with unmodified caps; evaporation losses from dispensing bottles are not much higher than from ordinary polyethylene bottles.

The results in Table 1 were found to be independent of the amount of solution contained; this agrees with the findings of Curtis et al. [7]. Therefore, in the absence of wall effects, the increase in solution concentration with time is inversely proportional to the volume of solution stored. For example, after one year, 500 ml of solution stored in a 570-ml dispensing bottle will increase in concentration by 0.24% while the concentration

TABLE 1

Weight loss, in milligrams per year, of aqueous solutions stored in tightly sealed, low-density polyethylene bottles (Australian Consolidated Industries Ltd.)

Bottle capacity (ml)	Weight loss (mg/year)	
	Without dispensing tube	With dispensing tube and closure
285	550	580
570	1100	1200

increase would be 2.4% with only 50 ml of solution stored in the same bottle.

Exchange processes between solutions and bottles. Exchange processes between solutions and vessels ("wall effects") have been reviewed by Tölg [8]. The formation of ion-exchanging sites, e.g. carboxyl and carbonyl groups, on plastic surfaces under the influence of oxygen, heat or light, has been suggested [6] as a possible cause of adsorption of ions from solutions. The weights of the dispensing bottles described here have not varied by more than 0.02 g during 4 years of repeated use. Hence the formation of ion-exchanging sites on these bottles has not been on a scale large enough to cause a detectable increase in weight.

A solution of 0.05 N potassium dichromate, stored in a 570-ml dispensing bottle used as a weight burette for the determination of iron(II) in rocks and minerals, underwent only a slight increase in dichromate concentration in one year, caused by evaporation loss.

The concentrations of usually determined elements in dilute acid solutions — stored in dispensing bottles — of silicate rock or coal ash samples, were found to be constant over a 12-month period after correction for evaporation losses.

A decrease in concentration of some constituents of dilute solutions in polyethylene bottles may occur if the bottles are not dried at 60—65°C before use: loss of phosphate from water samples stored in polyethylene has been attributed to its uptake by bacteria growing on the polyethylene [6]; a recent ASTM publication [9] mentions the possibility of heat treatment having a significant effect on the resistance of plastics to fungi and bacteria.

Conclusions

Experience suggests that polyethylene dispensing bottles can be re-used indefinitely in the wet-chemical analysis of geological materials. Investigations of possible "wall effects" are being continued.

Use of these bottles in conjunction with a top-pan balance raises the question of the feasibility of automated gravimetric dilutors. An automated computer-controlled solution-handling system measuring weights rather than volumes of solution has recently been described [10].

Permission to publish this communication was given by the Under Secretary, New South Wales Department of Mines. The author thanks J. Davis and T. Stewart, both of the New South Wales Department of Mines, for help with the die and the diagrams.

REFERENCES

1 K. Eckschlager, Errors, Measurements and Results in Chemical Analysis, Van Nostrand-Reinhold, London, 1969, p. 34.
2 R. W. Perry and H. J. Scullion, Analyst (London), 94 (1969) 801.

3 E. H. Swift and E. A. Butler, Quantitative Measurements and Chemical Equilibria, W. H. Freeman, San Francisco, 1972, pp. 335—339.
4 T. D. Rice, Proc. Roy. Aust. Chem. Inst., 40 (1973) 320.
5 T. D. Rice, Anal. Chim. Acta, 91 (1977) 221.
6 J. P. Riley, in J. P. Riley and G. Skirrow (Eds.), Chemical Oceanography, Vol. 2, Academic Press, New York, 1965, pp. 301—303.
7 G. J. Curtis, J. E. Rein and S. S. Yamamura, Anal. Chem., 45 (1973) 996.
8 G. Tölg, Talanta, 19 (1972) 1489.
9 Annual Book of ASTM Standards, Part 30, American Society for Testing and Materials, 1916 Race St., Philadelphia, Pa. 19103, 1971, pp. 1319, 1324.
10 B. W. Renoe, K. R. O'Keefe and H. V. Malmstadt, Anal. Chem., 48 (1976) 661.

Analytica Chimica Acta, 97 (1978) 219

ANNOUNCEMENTS

12th FEBS Meeting
Dresden, July, 2—8, 1978

The 12th FEBS-Meeting will be held in Dresden, July 2—8, 1978. The meeting is organized by the Biochemical Society of the German Democratic Republic. Following the traditions of FEBS meetings, the Scientific Program will include plenary lectures, symposia, colloquia, round table discussions and poster sessions. There will be also be a full Social Program.

Symposia will be arranged on the following themes:
DNA—Protein Interactions, Gene Expression, Protein Structure and Assembly, Structure and Function of Enzymes, Bioenergetics, Processing and Turnover of Proteins and Organelles in the Cell, Cyclic Nucleotides in Cell Regulation, and Regulation of Secondary Plant Product and Hormone Metabolism.

Colloquia will be organized on:
Technology of Genetic Engineering, Molecular Immunology, Molecular Diseases, Macromolecular Changes and Neuronal Function, Technical Enzymology, Investigation of Biopolymers with Scattering Methods, Cytochrome P-450, and Biochemical Education.

Further information from: 12. FEBS Meeting Dresden, D.D.R. — 806 Dresden, P.O.B. 313.

8th Annual Symposium on the Analytical Chemistry of Pollutants
Geneva, Switzerland, April 5—7, 1978

The 1978 symposium of the series of symposia on the "Analytical Chemistry of Pollutants" will be held in Geneva, Switzerland (April 5—7). This annual symposium, which is already well known in professionally interested circles, has previously been held in Halifax (Canada), Athens (Georgia, U.S.A.), Basel (Switzerland), Jekyll Island (Georgia, U.S.A.), Vienna (Austria) and Lake Lanier Island (Georgia, U.S.A.).

Once again scientists from many countries will be presenting plenary lectures, research papers and poster sessions in the field of inorganic and organic trace analysis of pollutants. An exhibition of instruments and literature in this field is also planned. As a new feature one day (April 6) will be set aside to treat a very clearly defined topic from an interdisciplinary angle. The topic chosen for Geneva is "Atmospheric Particles from Nonstationary Combustion Sources; Implications for Analytical Chemistry". A fuel chemist, an engine designer, a medical scientist, a botanist and several analytical chemists will set out the problem in detail and present their views. With the aid of plenary and panel discussions it is hoped to reach some constructive conclusions on: "What do you want from Analytical Chemistry and what can it actually do".

Further information from: Congress Secretariat, P.O. Box 182, CH-4013 Basel, Switzerland.

(continued from outside of cover)

Short Communications

Printed in The Netherlands

VOL. 97 No. 1 ANALYTICA CHIMICA ACTA MARCH 1, 1978

CONTENTS

(continued on inside page of the cover)